Short- and long-term influence of chronic variable stress (Cvs) on the regulation of the glucose and lipid metabolism

Inaugural-Dissertation

zur Erlangung des Doktorgrades
der Mathematisch-Naturwissenschaftlichen Fakultät
der Heinrich-Heine-Universität Düsseldorf

vorgelegt von

Matthias Dille
aus Willich

Düsseldorf, Juni 2020

aus dem Institut für Klinische Biochemie und Pathobiochemie
des Deutschen Diabetes-Zentrums
Leibniz-Zentrum für Diabetes-Forschung
an der Heinrich-Heine-Universität Düsseldorf

Gedruckt mit der Genehmigung der
Mathematisch-Naturwissenschaftlichen Fakultät der
Heinrich-Heine-Universität Düsseldorf

Berichterstatter:
1. Prof. Dr. Hadi Al-Hasani
2. Prof. Dr. Michael Feldbrügge

Tag der mündlichen Prüfung: 27. Mai 2020

ZUSAMMENFASSUNG

In Industrie- und Schwellenländern steht Fettleibigkeit nicht nur in Zusammenhang mit dem Konsum von hochkalorischer Nahrung und geringerer körperlicher Aktivität, sondern auch mit vermehrtem Stress. Chronische Stressbelastung ist verantwortlich für die Entwicklung von Angststörungen, Depressionen und posttraumatischer Belastungsstörung (PTBS). Trotz der akuten positiven Wirkung eines erhöhten Glucocorticoidspiegels (GC) durch Stress zur Aktivierung des Stoffwechsels für die Bereitstellung von Energie für den Fluchtreflex, sind die Langzeitfolgen, wenn Stresszustände chronisch werden, ein massives negatives Risiko für die metabolische Homöostase. Metabolische Erkrankungen wie Fettleibigkeit, Typ 2 *Diabetes mellitus* (T2DM) und die Nichtalkoholische Fettlebererkrankung (NAFLD) weisen daher eine erhöhte Prävalenz in Menschen auf, die an PTBS leiden. Der zugrunde liegende molekulare Mechanismus der metabolischen Regulierung nach chronischem Stress ist derzeit noch nicht komplett aufgedeckt.

Das Ziel der vorliegenden Arbeit war die Klärung des Einflusses einer PTBS auf die metabolische Anpassung des Energiestoffwechsels in metabolisch aktiven Geweben. *In vivo* als auch *ex vivo* Analysen wurden durchgeführt, um mögliche kurzzeitige und langfristige metabolische oder zelluläre Anpassungsmechanismen aufzudecken. Hierfür wurden zwölf Wochen alte C57BL/6-Mäuse einem 15-tägigen Protokoll für chronisch variablem Stress (Cvs) unterzogen. Analysen mittels hyperinsulinämisch-euglykämischer-Clamp-Technik ergaben, dass diese Mäuse eine akute hepatische Insulinresistenz aufgrund des gesteigerten Corticosteronspiegels entwickeln. Nach dreimonatiger Erholungsphase sind die GC-Spiegel normalisiert und die Mäuse entwickelten eine verbesserte Insulinsensitivität kombiniert mit einer erhöhten Glukoseaufnahme ins weiße Fettgewebe und einer erhöhten Fettoxidation im Skelettmuskel bei einem gesteigerten Plasmaspiegel des Wachstumsfaktors *Fibroblast growths factor 21* (FGF21). Darüber hinaus wiesen diese Mäuse eine Fettleber auf, wobei der Lipidgehalt eine signifikante Korrelation mit der FGF21 Plasmakonzentration zeigte. Um diesem Befund nachzugehen, wurden FGF21-*knockout* (FGF21KO) Mäuse dem Cvs Protokoll unterzogen. Interessanterweise zeigten diese nach Stress keine langfristige Verbesserung der Insulinsensitivität. *Ex vivo* Analysen von primären Hepatozyten ergaben nach Cvs allerdings eine Reduktion der *de novo* Lipidsynthese (DNL). Damit einher gingen Stress-bedingte Änderungen der hepatischen Glukoneogenese und eine gesteigerte Fettsäureaufnahme in Hepatozyten. Die stress-induzierte Veränderungen der hepatischen Deacetylase- und Methyltransferase-Aktivität deuten auf eine langfristige Modulation der Transkription hin, die zu metabolischen Anpassungen führen könnte.

Diese Befunde unterstreichen die Rolle von FGF21 bei der metabolischen Anpassung nach chronischem Stress und verdeutlichen die klinische Relevanz bei der Prognose und Behandlung von T2DM oder NAFLD bei Patienten, die an einer ernsten Stresserkrankung leiden.

ABSTRACT

In industrialized and emergent countries obesity is not only related to high consumption of high caloric food and decreased physical activity, but also to increased stress. Chronic stress exposure is responsible for the development of anxiety, depression and post-traumatic stress disorder (PTSD). Beside beneficial acute stress effects responsible for the fight or flight reaction, chronic high exposure to circulating glucocorticoids (GC) have severe impact on the metabolic homeostasis. Metabolic complication, like obesity, type 2 diabetes mellitus (T2DM) and non-alcoholic fatty liver disease (NAFLD) show high prevalence in people suffering from PTSD. However, the underlying mechanism of metabolic regulation after chronic stress is still unclear.

To investigate metabolic adaptations in a post-stress situation and examine possible adaptive mechanisms twelve weeks old C57BL/6 mice underwent an established 15-day protocol of chronic variable stress (Cvs) and both *in vivo* and *ex vivo* analyses were performed. Hyperinsulinemic-euglycemic clamps analyses revealed a hepatic insulin resistance due to the rise in corticosterone levels of these mice. After three-month recovery, corticosterone levels are normalized. Nevertheless, stressed mice showed an improved insulin sensitivity combined with an increased glucose uptake in the white adipose tissue (WAT) and an enhanced fatty acid oxidation in the skeletal muscle. The plasma levels of the fibroblast growths factor 21 (FGF21) rose simultaneously. In addition, stressed mice exhibit a fatty liver and the lipid content shows a significant correlation to FGF21 plasma levels. To investigate this results, FGF21 knockout mice underwent the same Cvs protocol. Interestingly, FGF21KO mice showed no improvement in long-term insulin sensitivity after stress. *Ex vivo* analyses of primary hepatocytes reveal a decreased *de novo* lipogenesis (DNL) after Cvs. Along with that an increase in hepatic fatty acid uptake and changes in gluconeogenesis were observed in hepatocytes. Stress-induced alterations of the hepatic deacetylase and methyltransferase activity indicate a long-term modulation of gene transcription, which can lead to metabolic adaptations.

These results highlight FGF21 as a potential modulator of the long-term metabolic adaptation after chronic stress. These findings underline the possible clinical relevance for the prediction of T2DM or NAFLD in individuals with a severe past of chronic stress.

TABLE OF CONTENT

LIST OF FIGURES

LIST OF TABLES

LIST OF ABBREVIATIONS

11B-HSD1	11β-Hydroxysteroid dehydrogenase type 1
ACAD	Acyl-CoA dehydrogenase
ACTH	Adrenocorticotropic hormone
ADP	Adenosine diphosphate
AGRP	Agouti-related peptide
AKT	Protein kinase B
AP-1	Activator protein 1
ATP	Adenosine triphosphate
AUC	Area under the curve
BAT	Brown adipose tissue
CBG	Corticosteroid-binding globulin
CCL	Chemokine (C-C motif) ligand
ChIP	Chromatin immunoprecipitation
CORT	Corticosterone/Cortisol
CRH	Corticotropin-releasing hormone
CS	Citrate synthase
Ctrl	Control
Cvs	Chronic variable stress
DNL	De novo lipogenesis
ECAR	Extracellular acidification rate
EDL	Extensor digitorum longus
EE	Energy expenditure
EGP	Endogenous glucose production
ELISA	Enzyme-linked immunosorbent assay
ER	Endoplasmic reticulum
F1,6BP	Fructose 1,6-bisphosphate
F6P	Fructose 6-phosphate
Fabp4	Fatty acid binding protein 4
FAO	Fatty acid uptake
FAT/CD36	Fatty acid translocate / Cluster of differentiation 36
FBP1	Fructose-1,6-bisphosphatase 1
FCCP	Carbonyl cyanide-4-(trifluoromethoxy)phenylhydrazone
FFA	Free fatty acid

FGF21	Fibroblast growth factor 21
FGF21KO	Fibroblast growth factor 21 knockout
FGFR	Fibroblast growth factor receptor
FKBP51 & 52	FK506 binding protein 51 & 52
FOXO1	Forkhead box protein O1
G6P	Glucose 6-phosphate
GC	Glucocorticoid
G-CSF	Granulocyte-colony stimulating factor
GIP	Gastric inhibitory polypeptide
GIR	Glucose infusion rate
GLP-1	Glucagon-like peptide-1
GLUT1 & 4	Glucose transporter 1 & 4
GM-CSF	Granulocyte-macrophage colony-stimulating factor
GR	Glucocorticoid receptor
GRE	Glucocorticoid receptor response element
GTT	Glucose tolerance test
gWAT	Gonadal white adipose tissue
Hadh	Hydroxyacyl-coenzyme A dehydrogenase
HAT	Histone acetyltransferase
HDAC	Histone deacetylase
HPA	Hypothalamic–pituitary–adrenal axis
HSP90 & 70	Heat shock protein 90 & 70
IFNγ	Interferon γ
IL	Interleukin
IR	Insulin receptor
IRS1	Insulin receptor substrate 1
ITT	Insulin tolerance test
KC	Chemokine (C-X-C motif) ligand 1
KHB	Krebs–Henseleit buffer
KRH	Krebs-Ringer-HEPES buffer
LIF	Leukemia inhibitory factor
MCP-1	Monocyte chemoattractant protein 1
M-CSF	Macrophage colony-stimulating factor
MIG	Monokine induced by Gamma-Interferon
MIP	Macrophage inflammatory protein
MTase	Methyltransferase
mTOR	Mammalian target of Rapamycin
NAD / NADH	Nicotinamide adenine dinucleotide
NADP / NADPH	Nicotinamide adenine dinucleotide phosphate
NAFLD	Non-alcoholic fatty liver disease
NEFA	Non-esterified fatty acids
NF-κB	Nuclear factor 'kappa-light-chain-enhancer' of activated B-cells
NMR	Nuclear magnetic resonance
NPY	Neuropeptide Y
OCR	Oxygen consumption rate

p38MAPK	p38 mitogen-activated protein kinases
PAI-1	Plasminogen activator inhibitor-1
PC	Pyruvate carboxylase
PCK1	Phosphoenolpyruvate carboxykinase 1
PDGF-BB	Platelet-derived growth factor
PEP	Phosphoenolpyruvate
PFK1	Phosphofructokinase 1
Pnpla2 + 3	Patatin-like phospholipase domain-containing protein 2 & 3
POMC	Proopiomelanocortin
PTSD	Post-traumatic stress disorder
PTT	Pyruvate tolerance test
PVN	Paraventricular nucleus
Rd	Glucose disposal rate
RER	Respiratory exchange ratio
SIRT	Sirtuin
SNS	Sympathetic nervous system
SPA	Spontaneous physical activity
T1DM	Type 1 Diabetes Mellitus
T2DM	Type 2 Diabetes Mellitus
TAG	Triglyceride
TCA	Tricarboxylic acid cycle
TNFα	Tumor necrosis factor α
UCP1	Uncoupling protein 1
VEGF	Vascular endothelial growth factor
VLDL	Very low-density lipoprotein
VO_2 / VCO_2	Volume of Oxygene / Carbon dioxide
WAT	White adipose tissue
WT	Wildtype

1. INTRODUCTION

1.1 Obesity

Overweight and obesity are defined as abnormal or excessive fat accumulation that may impair health (WHO, 2018). The prevalence of obesity is nearly tripled between 1975 and 2016 (WHO, 2018). In 2016, more than 1.9 billion adults were overweight (BMI > 25); out of these over 650 million people were obese (BMI > 30). In industrialized and emergent countries obesity is not only related to consumption of high caloric food but also to decreased physical activity and increased stress (Tamashiro et al., 2007; WHO, 2018). Lifestyle interventions like physical activity, eating behavior and a work life balance therefore can reduce body weight and prevent obesity related diseases. Further, pharmacological treatments or bariatric surgery can improve body weight and energy metabolism to counteract overweight (Leitner et al., 2017; WHO, 2018). The major health risk of obesity is that it is the main pathophysiology leading to Type 2 Diabetes Mellitus, cardiovascular and musculoskeletal disorders (WHO, 2018) and is a crucial risk factor for developing non-alcoholic fatty liver disease (NAFLD) (Bellentani, 2017; Jelenik et al., 2017a; WHO, 2018).

1.1.1 Type 2 Diabetes Mellitus and insulin resistance (IR)

Nowadays diabetes is one of the biggest world-wide health problems. By 2017, the number of deaths due to diabetes was 4 million worldwide and more than 425 million people (age 18+ years) were living with diabetes (IDF, 2017; WHO, 2018).

Diabetes is mainly classified in the etiopathogenetic categories of type 1 and type 2 diabetes mellitus (T1DM and T2DM). T1DM results from the destruction of the insulin secreting pancreatic β-cells by the immune system. Based on the genetic susceptibility, T1DM cannot be prevented at present (IDF, 2017). In contrast, around 90% of all diabetes cases belong to T2DM (IDF, 2017) which is caused by environmental as well as genetic factors. During diabetes progression, initially the pancreas compensates the decreased insulin sensitivity by increasing insulin release to a certain extent, but this may lead to pancreatic exhaustion and β-cell mass lost as peripheral insulin resistance progresses (IDF, 2017; Leney and Tavare, 2009; WHO, 2018). The most relevant risk factors associated with T2DM are overweight, unhealthy diet, physical inactivity and genetic susceptibility (IDF, 2017; WHO, 2018). Life style interventions, like physical activity or healthy diet can delay or even prevent the onset of T2DM (IDF, 2017).

1.1.2 Non-alcoholic fatty liver disease (NAFLD)

NAFLD is the most common cause of chronic liver disease in western countries and its development is related to diabetes and further to obesity as a central factor. 70% of patients suffering from T2DM also show the development of NAFLD and this may be linked to an unhealthy lifestyle, mainly overnutrition (Blachier et al., 2013). On the other hand, NAFLD in turn increases the risk for T2DM, cardiovascular diseases and chronic kidney disease. The progression of NAFLD starts with the excessive accumulation of lipids in liver caused by risk factors like insulin resistance, obesity, T2DM or higher age (Anstee et al., 2013; Hyysalo et al., 2014). Ectopic fat accumulation, high levels of circulating lipids and insulin, adipose tissue inflammation associated with altered adipokine secretion are present in T2DM as well as obesity and lead to the development or progression of NAFLD (Byrne and Targher, 2015). One characteristic of NAFLD is the hepatic steatosis, the rise of intracellular hepatic lipids. The progression of NAFLD could cause hepatic inflammation and fibrosis, described as non-alcoholic steatohepatitis (NASH), a serious liver dysfunction (Fabbrini et al., 2010). Approximately 30 – 40% of people with NAFLD develop NASH and 40 – 50% of people with NASH develop liver fibrosis and hepatic cancers (Ekstedt et al., 2006).

The development of NAFLD were studied intensively. However, an exact molecular mechanism is currently still unknown. The hepatic lipid homeostasis is strict regulated by different metabolic regulators and the inter-organ crosstalk. Initially, in 1998 the 'two hit' hypothesis were proposed by Day and James explaining the development of NASH by two successive events transforming NAFLD to NASH (James and Day, 1998). First, the accumulation of intrahepatic fatty acids associated with insulin resistance and an increased susceptibility of hepatocytes to the second hit consisting of oxidative stress, mitochondrial dysfunction and inflammation, leading fibrosis. At present, a multifactorial theory acquire an increased importance, where the progression of NAFLD and NASH is developed by several hepatic and systemic metabolic alterations as well as genetic susceptibility and environmental factors (Buzzetti et al., 2016; Fang et al., 2018; Tilg and Moschen, 2010). Metabolic alterations in adipose tissue and liver play the main role in developing NAFLD, but also a genetic origin was described. For example, variations of the gene for patatin-like phospholipase domain-containing protein 3 (PNPLA3) contributes to differences in hepatic fat content and the susceptibility to NAFLD (Romeo et al., 2008). Nevertheless, the underlying molecular mechanism consists of several factors. High levels of fatty acids released by the adipose tissue and enhanced hepatic DNL together with reduced hepatic fatty acid oxidation causes an excessive lipid accumulation in the liver (Cobbina and Akhlaghi, 2017). Hepatic fat accumulation is strongly related to the development of hepatic insulin resistance (Birkenfeld and Shulman, 2014). Patients with both, NAFLD and hepatic insulin resistance show higher risk for T2DM and hepatocellular carcinoma (Birkenfeld and Shulman, 2014; Fabbrini et al., 2010)

1.1.3 Metabolic crosstalk of lipid and glucose metabolism in health and disease

Metabolic active tissues and organs, like adipose tissue, skeletal muscle and liver are working in a strict balance to maintain whole body energy homeostasis. Disruption in energy metabolism by e.g. chronic over-nutrition, pharmacological treatments but also by psychological disorders disturb this equilibrium. Metabolic active tissues are strongly associated and interact via different metabolic or hormonal pathways. Figure 1 shows the metabolic crosstalk and the development of insulin resistance in liver, adipose tissue and skeletal muscle.

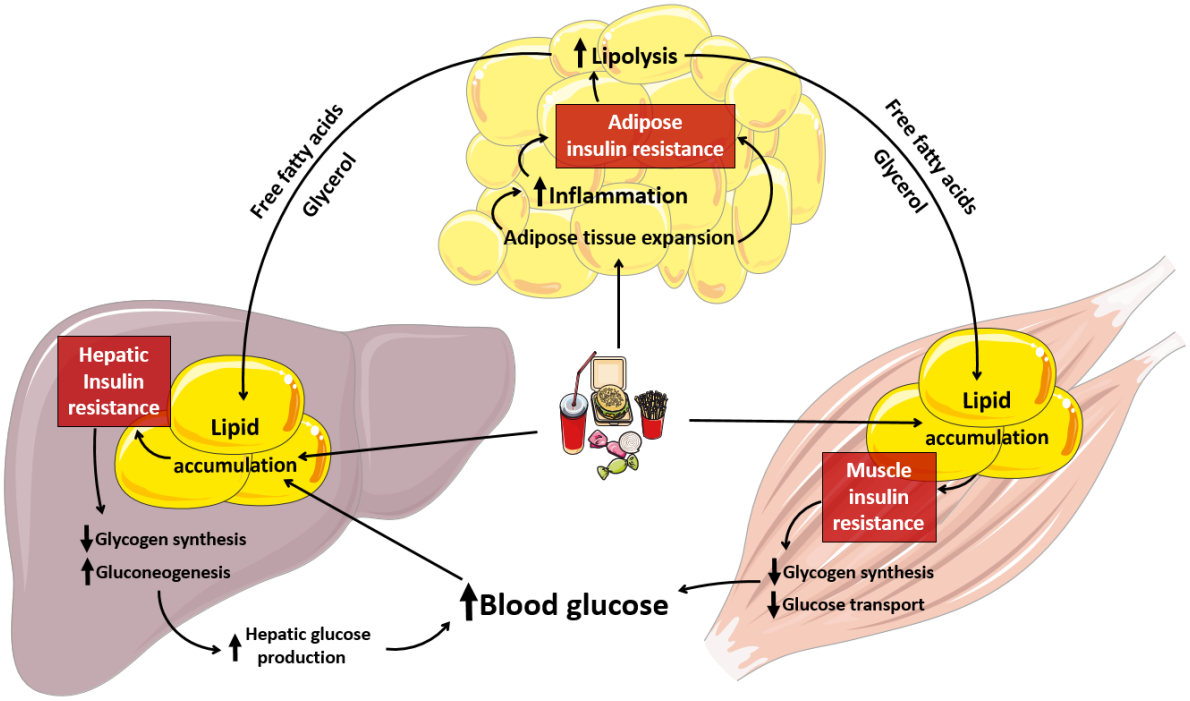

Figure 1: Influence of high caloric diet of metabolic tissues and blood glucose levels. Consumption of high caloric diet and the development of obesity influences adipose tissue, liver and skeletal muscle by inducing insulin resistance in each tissue. Adipose tissue expansion in obesity is associated with infiltration of macrophages and secretion of pro-inflammatory cytokines. Inflammation of the adipose tissue leads to insulin resistance and increased lipolysis due to inhibited insulin action. Following, free fatty acids and glycerol serve lipid accumulation in liver and skeletal muscle. Hepatic lipid accumulation leads to hepatic insulin resistance causing less glycogen synthesis and increased gluconeogenesis. The enhanced hepatic glucose production increases blood glucose levels. Lipid accumulation in skeletal muscle causes muscle insulin resistance followed by less glycogen synthesis and decreased glucose transport also causing rise in blood glucose. High blood glucose levels then promote further hepatic lipid accumulation and the development of NAFLD. Adapted from Petersen and Shulman (Petersen and Shulman, 2018).

1.1.3.1 Regulation of metabolism by insulin and metabolites

Obesity is the main risk factor for developing insulin resistance caused by elevated plasma levels of free fatty acids (Petersen and Shulman, 2018). Insulin is the main hormonal regulator of metabolic pathways in all tissues and organs. The main physiological actions of insulin under healthy conditions is the suppression of hepatic glucose production (gluconeogenesis) and fatty acid oxidation as well as promoting *de novo* lipogenesis (DNL), glycolysis and glycogen synthesis. In parallel glucose uptake and glycogen synthesis is induced in skeletal muscle and lipolysis in adipose tissue decreased (Dimitriadis

et al., 2011; Petersen and Shulman, 2018). Under conditions of insulin resistance or T2DM, the metabolic active tissues and organs fail to respond to insulin and blood glucose levels further rise. Insulin then is unable to suppress hepatic glucose production along with failure in insulin-induced glucose uptake in skeletal muscle and adipose tissue, which consequences hyperglycemia. Pancreatic β-cells try to compensate the high glucose levels by increasing the insulin production and secretion, which lead to hyperinsulinemia and finally to the collapse and the loss of β-cell mass (IDF, 2017; Kahn and Flier, 2000; Templeman et al., 2017). Hyperinsulinism in insulin resistant conditions further induces the hepatic DNL and reduces lipolysis leading to the secretion of very low density lipoproteins (VLDL) and free fatty acids promoting hepatic lipid accumulation and hypertriglyceridemia (Czech, 2017; Lotta et al., 2017).

However, other hormones or growth factors as well as metabolites itself also regulate the intracellular energy metabolism. In healthy conditions the body is affected by two metabolic states, the fasted and the fed state. In both states metabolic tissues regulate the energy homeostasis and supply the body with metabolites or store energy for later use. During fasting, lipolysis in the adipose tissue provide fatty acids as source for energy production by mitochondrial respiration. Fatty acids were oxidized in the liver to ketone bodies, which are essential for the brain and to produce energy in skeletal muscle during times of starvation (Hue and Taegtmeyer, 2009). Initial studies and hypotheses described the role of fatty acids in the regulation of glucose metabolism and its function in insulin resistance. These studies show, that fatty acids oxidation inhibits several glycolytic steps, like glucose transport and phosphorylation of glucose and/or pyruvate, which leads to increased intracellular glucose levels in skeletal muscle, leading to insulin resistance (Randle, 1998; Randle et al., 1963). However, studies in the 1990s reveal the contrary, intracellular glucose levels decrease after acute lipid-induced insulin resistance (Dresner et al., 1999; Roden et al., 1996). These studies were in line with the elucidation of the link between insulin receptor activation and glucose transporter 4 (GLUT4) translocation as induced glucose transport were defective in insulin resistance and T2DM (Cline et al., 1999; Garvey et al., 1998). Nevertheless, currently no evidence indicates, that the glucose-fatty acid cycle is responsible for the impairment in insulin-stimulated glucose uptake in muscle or for the development of insulin resistance in obesity (Boden et al., 1994; Petersen and Shulman, 2018; Rahimi et al., 2014; Roden et al., 1996). Nevertheless, the glucose-fatty acid cycle is a physiologically relevant process for the regulated selection of substrates for energy production (Frayn, 2003; Petersen and Shulman, 2018). Overall, these findings reveal a strict balanced equilibrium between fatty acids and glucose metabolism and a regulated utilization under specific conditions.

1.1.3.2 Adipose tissue

In periods of increased food intake and low physical activity the body stores energy in the form of triglycerides in the adipose tissue. In contrast, situations of increased energy demands like stress, fasting or exercise cause the breakdown of triglycerides (lipolysis) in three fatty acids and a glycerol molecule and their release into the circulation (Peckett et al., 2011), whereas these lipolysis products indirectly influence the hepatic gluconeogenesis (Lewis et al., 1997; Rebrin et al., 1996). Another aspect, which has influence on metabolic active tissues are hormonal or circulating factors derived from adipose tissue. The white adipose tissue (WAT) is not only a tissue for energy storage but also a high active endocrine or paracrine organ. Besides the lipid storing adipocytes, the adipose tissue consists of other different cell types like preadipocytes, endothelial cells (blood supply) and macrophages (immune system). Hundreds of so called adipokines are identified in the last years. These adipocyte derived factors may associate obesity to the development of metabolic diseases like T2DM, NAFLD and insulin resistance (Fasshauer and Bluher, 2015; Horbelt et al., 2018; Jelenik et al., 2017a; Leal Vde and Mafra, 2013). Furthermore, the WAT is a highly vascularized immune tissue and its expansion during obesity is associated with tissue inflammation and macrophage infiltration. Specifically, a combination of cellular stress, adipocyte enlargement (hypertrophy) and hypoxia causes adipose tissue inflammation with the subsequent expression and secretion of pro-inflammatory cytokines, like interleukin-1 (IL-1), interleukin-6 (IL-6) and tumor necrosis factor-alpha (TNFα) contributing to insulin resistance and the development of T2DM (Sell et al., 2012; Trayhurn and Wood, 2005). Adipokines and cytokines play a crucial role in the intra-organ cross talk and regulating the energy metabolism. In contrast, brown adipose tissue (BAT), a specific fat depot characterized by enhanced energy expenditure and heat production, also influences both glucose and lipid metabolism (Harms and Seale, 2013). Enlargement and/or activation of the BAT can protect against diet-induced obesity (Cui and Chen, 2016). So called beige adipocytes are white adipocytes with some typical characteristics of brown adipocytes, like mitochondria content and expression of thermogenic markers. These characteristics can be induced in white adipocytes (Cousin et al., 1992). Studies have shown a difference between brown and beige adipocytes. Classical brown adipocytes differentiate from precursor cells in the embryonic mesoderm (Kajimura et al., 2015; Seale et al., 2008). Few studies have shown, that beige adipocytes originate from transformation of mature white to beige adipocytes (Barbatelli et al., 2010; Himms-Hagen et al., 2000), while other studies describe the *de novo* differentiation from precursors (Wang et al., 2013). Browning of adipose tissue together with enhanced thermogenesis are inversely related to insulin resistance (Lo and Sun, 2013) and might protect from obesity and lipid-mediated impairments of glucose metabolism (Cohen and Spiegelman, 2016; Vitali et al., 2012).

1.1.3.3 Skeletal muscle

The metabolism of skeletal muscle plays a crucial role in maintaining glucose homeostasis in fasted and fed state. Myocytes utilize glucose to produce ATP for contraction through an anaerobic or aerobic pathway depending on the fiber type (Talbot and Maves, 2016; Zierath and Hawley, 2004). But skeletal muscle are also able to store glucose in form of glycogen to provide energy by glycogenolysis, when glucose supply is not sufficient. Furthermore, skeletal muscles provide other energy substrates like amino acids for all organs during prolonged starvation or extreme energy deficits (Argiles et al., 2016; Wolfe, 2006).

Impaired glucose metabolism and insulin resistance of skeletal muscle is associated with an excessive lipid accumulation and disturbed lipid oxidation in the skeletal muscle cells (Turcotte and Fisher, 2008). An increased lipid accumulation and a reduced fat oxidation can cause lipotoxicity associated with increased levels of diacylglycerols and ceramides in skeletal muscle (Adams et al., 2004; Goodpaster and Kelley, 2002; Krssak et al., 1999; Moro et al., 2008). These metabolites are able to impair insulin signaling via different mechanism, such as enhanced serine phosphorylation of the insulin receptor (IR) and insulin receptor substrate (IRS) 1 or reduced AKT phosphorylation (Cooney et al., 2002; Morino et al., 2006). Several studies have shown, that key enzymes of the fatty acid oxidation pathways are affected in obesity and T2DM (Blaak et al., 2000; Hulver et al., 2003; Ortenblad et al., 2005; Simoneau and Kelley, 1997). Beside these effects on lipid metabolism in skeletal muscle it is described multiple times, that free fatty acids promote insulin resistance through the activation of inflammatory pathways (Boden, 2001; Itani et al., 2002) and via downregulating glucose transport (Roden et al., 1996).

1.1.3.4 Liver

The hepatic glucose release is pending of glycogenolysis and gluconeogenesis. Postprandially, the liver stores glucose in form of glycogen, whereas during fasting the liver produces glucose to maintain euglycaemia and provide glucose for cell types, which solely consume glucose (Rizza, 2010). The liver reacts to high blood glucose levels by decreasing the glucose output involving the suppression of gluconeogenesis and glycogenolysis (Moore et al., 2012). The postprandial mechanism, which suppresses both gluconeogenesis and glycogenolysis are crucial for understanding hyperglycemia in insulin resistance and T2DM. Hepatic glucose production is influenced and regulated by direct and indirect factors. The central metabolic hormone insulin inhibits the gluconeogenesis via the phosphorylation and nuclear exclusion of the transcription factor Forkhead box O1 (FOXO1), which in absence of insulin promotes gluconeogenic gene transcription (O. Sullivan et al., 2015). Under fed conditions, insulin stimulates hepatic glycogen synthesis (Dent et al., 1990). Further gluconeogenic precursors like lactate derived from the Cori cycle or amino acids from protein degradation promote

the hepatic glucose production (Katz and Tayek, 1998). These precursors are converted to pyruvate, which is shuttled into the mitochondria and there further carboxylated to oxaloacetate by pyruvate carboxylase (PC). The oxaloacetate is converted to malate, which is shuttled to the cytoplasm via the malate/citrate shuttle where it is converted back to oxaloacetate. Afterwards oxaloacetate is catalyzed to phosphoenolpyruvate (PEP) by phosphoenolpyruvate carboxykinase (PCK1), which then enters the gluconeogenic pathway (Kuo et al., 2015). A mitochondrial form of PCK1 can also directly convert oxaloacetate to PEP, which is then transported to the cytoplasm where it enters the gluconeogenesis (Méndez-Lucas et al., 2013). The next five enzymatic steps are required for the reverse glycolysis resulting in the conversion of PEP to fructose-1,6-phosphate (F1,6BP). The bifunctional activity of phosphofructokinase 2/fructose bisphosphatase 2 (PFKFB1) is the main regulatory step between glycolysis and gluconeogenesis. The glycolytic activity of PFKFB1 is inhibited by glucagon due to e.g. fasting and starvation. Consequently, the production of fructose 2,6 bisphosphate (F2,6BP) an allosteric stimulator of the glycolytic enzyme phosphofructokinase 1 (PFK1) is inhibited, resulting in an enhanced gluconeogenesis. F1,6BP is converted by fructose 1,6-bisphosphatase (FBP1) to fructose-6-phosphate (F6P), which is then converted to glucose-6-phosphate (G6P). The enzyme glucose-6-phosphatase (G6PC) converts finally G6P to glucose in the endoplasmic reticulum (ER).

All in all, adipose tissue dysfunction or an excessive lipid exposition in over-nutrition contribute to the deposition of ectopic fat depots in tissues relevant for glucose metabolism like liver and skeletal muscle (Grundy, 2015).

1.2 Stress

Stress is initiated by intrinsic or extrinsic adverse stimuli called stressors and leads to a disturbance of the organism homeostasis (Kyrou and Tsigos, 2007). To maintain of either psychological or physical homeostatic equilibrium after stress, the body responses with different physiological and behavioral adaptations involving nervous, immune and endocrine systems as well as the energy metabolism (Bose et al., 2009; Smith and Vale, 2006). The reaction of these processes causes several physical changes that have both short- and long-term effects on the organism. Evolutionarily, the physiological stress response ensures an enhanced energy supply, cardiovascular tone and respiratory rate to provide glucose and fatty acids required by tissues and organs for the fight-or-flight response (Kyrou and Tsigos, 2009; Smith and Vale, 2006; Tsigos and Chrousos, 2002). During acute stress phases the metabolic adaptations, needed for energy mobilization for organism survival become impaired during chronic stress (Kaur, 2014; Kyrou and Tsigos, 2009). The so called eustress is in many situations a protective reaction, which helps the organism to survive in difficult situations and environments and has positive influence on the organism`s performance (Lazarus, 1974). In contrast, distress is a non-specific basis of diseases and disorders of the organism. Negative stressors are stimuli, which were felt as threatening and overcharging. Stress is only negative, when it is appears frequently and no compensation takes place. Also negative effects occur, when the organism has no possibility to cope the stress situation (McEwen, 2017). In human, chronic stress and tension lead to permanent changes in neurotransmitter and hormone secretion and finally to the development of psychological diseases like burn out or depression (Bianchi et al., 2015; Hammen et al., 2010).

Another form of severe stress is the so called post-traumatic stress disorder (PTSD), a mental disorder not caused by acute stress. PTSD can develop in persons, who were exposed to a traumatic event, like sexual assault, living in a war zone or other threats in life (Merikangas et al., 2010). War veterans, police officers or victims of natural disasters show high prevalence for PTSD (Atwoli et al., 2015; Hoge et al., 2006). Approximately 70% of people worldwide experience a traumatic event during their life and around 7 – 8% of the world population will have PTSD at some point in their lives (Gradus, 2017; Merikangas et al., 2010; NIH, 2019; Shalev et al., 2017). Numerous studies identify different biological parameters, which are associated with the development of PTSD including genes, epigenetic regulation, neuroendocrine factors and inflammatory markers (Pitman et al., 2012; Shalev et al., 2017). Moreover, epidemiological studies reveal PTSD as a risk factor for diabetes, obesity and the metabolic syndrome (Goodwin and Davidson, 2005; Hall et al., 2015; Maslov et al., 2009). Patients suffering from PTSD show an overall increase in stress hormone levels (van Leijden et al., 2018). Chronic raised levels of stress hormones lead to the development of metabolic complications like central obesity, insulin resistance and T2DM (Mezuk et al., 2008).

1.2.1 Sympathetic nervous system (SNS)

The SNS is one part of the stress response. The SNS mediates rapid physiological responses to provide the muscle and brain with fast energy in threatening situations (Patterson and Abizaid, 2013). The hypothalamus sends signals through sympathetic nerves to peripheral tissues and leads to the release of catecholamines (adrenaline and noradrenaline) from the adrenal medulla (Habib et al., 2001; Tsigos and Chrousos, 2002). Different from glucocorticoids, which regulate gene expression through its receptor, adrenaline and noradrenaline bind to G-protein coupled receptors called adrenergic receptors. These receptors consist of two main groups, α-and β-receptors which present different subtypes (α1, α2, β1, β2, β3,) (Patterson and Abizaid, 2013). Over-activation of this system like in chronic stress situations can develop pathophysiological conditions like insulin resistance, disrupted glucose and lipid metabolism, mitochondrial dysfunction and cardiac diseases (Berthelsen and Pettinger, 1977; Ciccarelli et al., 2013; Wehrwein et al., 2016). In addition to neuroendocrine pathways, the hypothalamus regulates the hepatic glucose output as well as glucose uptake and utilization in skeletal muscle via the autonomic nervous system and therefore controlling the body glucose homeostasis (Bisschop et al., 2015; Han et al., 2016; Wehrwein et al., 2016). Moreover, catecholamines induce BAT activity and stimulate beige adipocytes, which is inversely related to obesity (Nguyen et al., 2011; Wang et al., 2011b).

1.2.2 Hypothalamus-pituitary-adrenal (HPA) axis and glucocorticoids

The organism reacts similar to psychological or physical stress through the activation of the HPA axis and the final release of glucocorticoids (Habib et al., 2001). In detail, stress leads to the activation of neuroendocrine neurons in the paraventricular nucleus (PVN) of the hypothalamus and the secretion of corticotropin-releasing hormone (CRH), which subsequently stimulates the release of the adrenocorticotropic hormone (ACTH) from the pituitary gland. ACTH acts on the adrenal cortex, where is stimulate the release of glucocorticoid (GC) hormones like cortisol in humans or corticosterone in rodents. GCs suppress CRH and ACTH secretion from the hypothalamus through a negative feedback loop (Smith and Vale, 2006; Tsigos and Chrousos, 2002) (Figure 2).

GCs are cholesterol-derived corticosteroids, belonging to the class of steroid hormones, which are secreted from the adrenal glands. In the *zona fasciculate* of the adrenal glands GCs are synthesized from cholesterol by cleavage into pregnenolone by cholesterol side-chain cleavage enzymes. Pregnenolone can be further transform to 17-OH pregnenolone or progesterone which are converted via different enzymatic steps to cortisol in humans or corticosterone in rodents (CORT) (Hanukoglu, 1992; Miller, 1988). Target tissues take up the GCs from the circulation via the plasmatic transport protein corticosteroid-binding globulin (CBG) (Gagliardi et al., 2010). Further, the tissue specific activity

of 11β-hydroxysteroid dehydrogenase (11β-HSD1) reduces inactive cortisone to active cortisol/corticosterone by using nicotinamide adenine dinucleotide phosphate (NADPH) as a co-substrate (Seckl, 2004; Stomby et al., 2014).

The intracellular signal of GCs is transmitted by binding to the glucocorticoid receptor (GR), which leads to its nucleus translocation and enhanced transcriptional activity (Clark and Belvisi, 2012; Kadmiel and Cidlowski, 2013). In the nucleus the complex GC ligand-bound GR activates or represses gene transcription. Under basal conditions, the GR is member of a multi-protein complex along with the heat shock proteins 90 and 70 (HSP90 and HSP70) and the immunophilin FK506-binding proteins 51 and 52 (FKBP51 and FKBP52) (Grad and Picard, 2007). After the binding of GC to the GR in the cytosol, the GR dissociates from the protein complex and is translocated to the nucleus, where it creates GR dimers. These GR dimers bind to specific glucocorticoid response elements (GRE) in the regulatory regions of target genes (Schaaf and Cidlowski, 2002; Schoneveld et al., 2004; Sinclair et al., 2013). Alternatively, the GR is able to regulate other transcription factors by direct interaction such as the activator protein-1 (AP-1) or the nuclear factor-kappa B (NF-κB), mediators of the cellular inflammatory response (Barnes et al., 1998; Reddy et al., 2012; Schoneveld et al., 2004). However, the GR has also influence on relevant enzymes of lipid and glucose metabolism in skeletal muscle, adipose tissue and liver (Rose et al., 2010). For example, GR regulates hepatic gluconeogenesis and glycogen storage as well as adipose tissue lipid breakdown and skeletal muscle glucose uptake and protein degradation (Rose et al., 2010).

1.2.3 Influence of GCs on glucose and lipid metabolism

Increased levels of GCs under stress conditions have influence on multiple aspects of the glucose and lipid homeostasis (Figure 2). Chronic high GC levels like in patients with the Cushing syndrome or prolonged GC treatment lead to central obesity and peripheral insulin resistance (Chanson and Salenave, 2010; Shibli-Rahhal et al., 2006). On the other hand, activation of the GR reduces inflammation and ameliorates the insulin action in adipose tissue by modulating the cytokine secretory profiles (de Guia et al., 2014; Ouchi et al., 2011). In general, GCs regulate blood glucose levels by promoting hepatic gluconeogenesis and reduce the glucose uptake in skeletal muscle and white adipose tissue (WAT). Furthermore, GCs stimulate the protein degradation to provide amino acids as precursors for the hepatic gluconeogenesis (Kuo et al., 2013). These processes maintain the blood glucose levels under stress and fasting conditions to provide glucose for brain function. Insulin, secreted by pancreatic beta cells counteract the GC actions by inhibiting gluconeogenesis and promoting glycogen synthesis as well as stimulating peripheral glucose uptake (Kuo et al., 2015). Apart from the enhanced energy demand in stress situations, chronic high GC levels like in patients suffering from Cushing syndrome promotes abdominal obesity, hyperglycemia and insulin resistance (Chanson

and Salenave, 2010; Shibli-Rahhal et al., 2006). This circumstance shows the influence of GCs in central obesity and focus the visceral adipose tissue in the development of metabolic diseases.

1.2.3.1 GCs and glucose metabolism

The liver is primarily responsible for maintaining normal blood glucose levels by storing glucose as glycogen or produce glucose from glycogen degradation or from gluconeogenic precursors (Roden and Bernroider, 2003). GCs regulate both the hepatic gluconeogenesis and the glycogen synthesis. Hepatic glycogen storage is induced by GC administration in mice by stimulating the activity of glycogen synthase (De Wulf and Hers, 1967; Ray et al., 1964; Stalmans and Laloux, 1979). The inducing influence of GCs on hepatic gluconeogenesis is well studied. Here, the regulatory promoter elements, GREs, have been identified in *Pck1*, *Pfkfb1*, and *G6p* genes (Kuo et al., 2015).

Beside the liver, the skeletal muscles and WAT are the two major insulin sensitive tissues which utilize glucose. The action of GCs in skeletal muscle and WAT is different than in the liver. GCs counteract the function of insulin in these tissues by reducing glucose uptake and glucose oxidation (Pasieka and Rafacho, 2016). The resulting increase in blood glucose is beneficial during stress phases. Different studies in human and mouse myotubes show, that the reduction in insulin stimulated glucose uptake is driven by a decreased GLUT4 translocation to the plasma membrane (Dimitriadis et al., 1997; Morgan et al., 2009; Weinstein et al., 1998). Both high fed diet-induced and genetically obese mice show increased levels of circulating GCs together with an associated insulin resistance (Morgan et al., 2009; Ohshima et al., 1989). Adrenalectomy improves the insulin sensitivity and the skeletal muscle glucose utilization in these animals (Haluzik et al., 2002). The GC/GR-axis is a key regulator in insulin resistance and T2DM. A studies describes, that mice lacking liver specific GR expression show hypoglycemia under fasting conditions and display a down-regulation of gluconeogenic gene expression (Opherk et al., 2004).

1.2.3.2 GCs and lipid metabolism

Beside the adipose tissue, the liver plays a crucial role in the regulation of the lipid metabolism in stress phases. The balanced lipogenesis and lipolysis is important for the organisms' lipid homeostasis. Especially GCs play a critical role in the triglyceride metabolism. Increased circulating GC levels during fasting and starvation induce lipolysis in adipocytes, where triglycerides are hydrolyzed to fatty acids and glycerol. The secretion of free fatty acids in the blood flow provides energy for liver and skeletal muscles, where the fatty acids are oxidized. The glycerol is used as precursor for hepatic gluconeogenesis. These tight regulated adaptations are essential for the body in fasting or starvation.

Under fed conditions GCs regulate the fat distribution and the DNL efficiency after fasting periods (Wang et al., 2012).

In a heathy situation GCs are important for the regulation of the lipid homeostasis under fasted or fed conditions, but chronic increased circulating GC levels cause lipid disorders, abdominal obesity, dyslipidemia and fatty liver (Arnaldi et al., 2010; Macfarlane et al., 2008). Moreover, the chronic increase of circulating GCs lead to the disruption of the lipid homeostasis and induce insulin resistance. Most likely the chronic raised GC levels causes increased circulating fatty acids, which is associated with ectopic lipid accumulation in skeletal muscle and liver and induces insulin resistance (Petersen and Shulman, 2006; Samuel et al., 2010). However, the inactivation of the GC activating enzyme 11β-HSD1 leads to hepatic improvements in insulin sensitivity and reduced high-fed diet induces obesity in mice (Kershaw et al., 2005; Morton et al., 2001; Taylor et al., 2009).

GCs induce hepatic DNL by activating the expression of gene encoding enzymes for triglyceride or fatty acid synthesis like Acetyl-CoA carboxylase (ACC) and fatty acid synthase (FAS) (Gathercole et al., 2011a; Sul and Wang, 1998). Especially in murine hepatocytes it was shown, that GCs and insulin have an additive or synergistic effect on DNL (Amatruda et al., 1983; Kirk et al., 1976; Macfarlane et al., 2008). Diglyceride acyltransferase (DGAT), responsible for triglyceride synthesis are upregulated by GCs (Dolinsky et al., 2004).

For lipolysis it was shown by chromatin immunoprecipitation (ChIP) analyses of cultured murine 3T3-L1 adipocytes that GCs induce nearly all genes involved in the lipolytic pathway in adipose tissue. Genes encoding for lipolytic enzymes like *Pnpla2*, *Lipe* and *Mgll* are affected directly by the activity of the GR (Campbell et al., 2011; Chakrabarti and Kandror, 2009). Intriguingly, insulin represses the expression or the activity of Pnpla2 and Lipe, which is in contrast to the additive or synergistic function of GC and insulin in regulating DNL (Kershaw et al., 2006; Lampidonis et al., 2011). Beside the effects of GC on hepatic DNL they also affect hepatic fatty acid oxidation. Enzymes involved in hepatic β-oxidation like acyl-CoA dehydrogenases (ACADs) are downregulated in mice by GCs (Letteron et al., 1997; Magomedova and Cummins, 2016). It was shown, that lipid transporter like fatty acid translocase (FAT/CD36) and fatty acid binding protein (Fabp4) are upregulated in GC treated mice (Koorneef et al., 2018; Yu et al., 2010). GCs promote lipolysis in adipocytes associated with high levels of circulating fatty acids and in parallel induce hepatic DNL and fatty acid uptake together with lowering the hepatic β-oxidation, leading to an ectopic lipid accumulation and the development of hepatic insulin resistance. So, GCs interfere in all processes involved in the development and progression of hepatic steatosis which is a result of the combination of enhanced DNL, a decreased β-oxidation and a higher fatty acid uptake (Lemke et al., 2008; Vegiopoulos and Herzig, 2007).

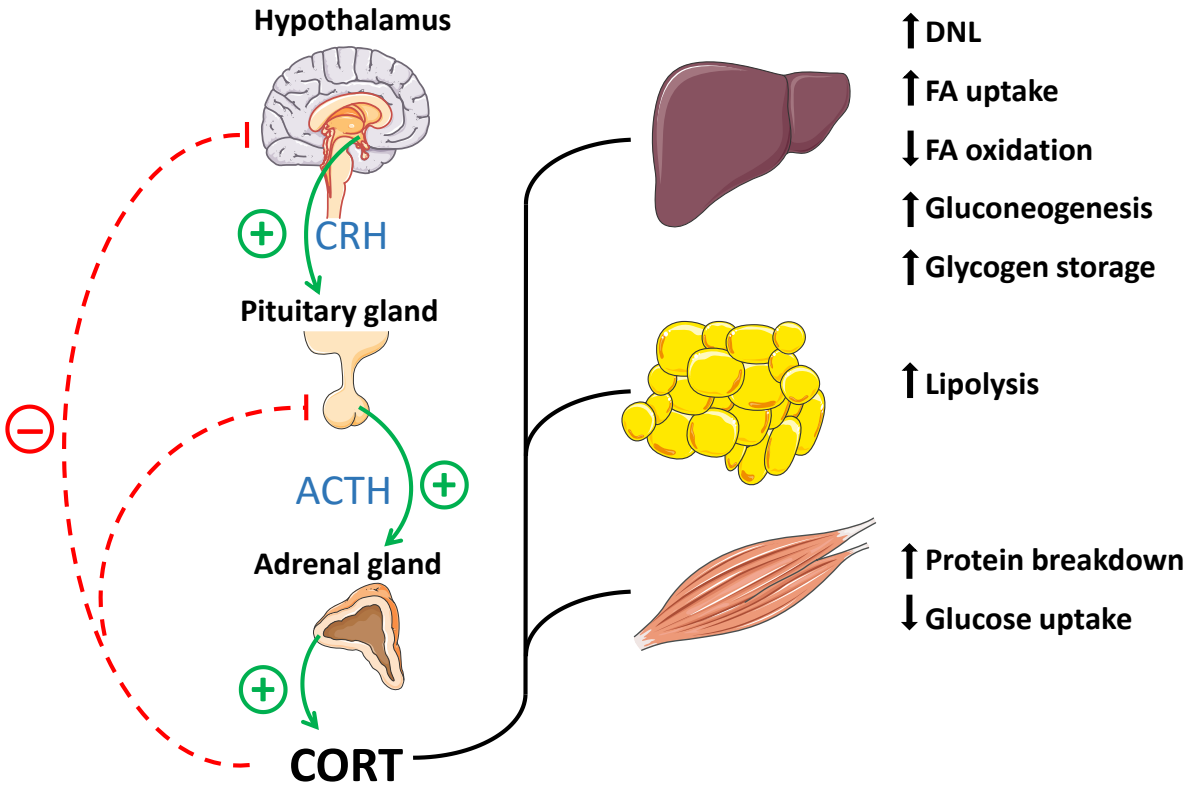

Figure 2: Schematic illustration of hypothalamus pituitary adrenal (HPA) axis and its influence on energy metabolism. The HPA axis reacts to stress stimulus through the release of corticotropin releasing hormone (CRH) from the hypothalamus. CRH has a positive influence on the secretion of adrenocorticotropin (ACTH) from the pituitary gland. In turn, ACTH stimulates the secretion of cortisol (human) or corticosterone (rodent) (CORT) from the adrenal gland cortex. CORT inhibits the release of CRH and ACTH via a feedback mechanism. Shown on the right side, the influence of CORT on metabolic active tissues and the CORT induced metabolic adaptations in liver, white adipose tissue (WAT) and skeletal muscle. DNL: *De novo* lipogenesis; FA: Fatty acid. Adapted from Magomedova and Cummins (Magomedova and Cummins, 2016).

1.2.3.3 GCs and adipose tissue inflammation

GCs increase visceral adiposity as observed in the Cushing syndrome (Chanson and Salenave, 2010; Shibli-Rahhal et al., 2006). Rapid WAT expansion causes a chronic inflammatory response via the production and release of cytokines from adipose tissue associated with the activation of pro-inflammatory signaling pathways (Bastard et al., 2006; Greenberg and Obin, 2006). The cellular inflammatory response is mediated by the transcription factors NF-κB and AP-1 which regulate the action of pro-inflammatory cytokines such as IL-1 and TNFα (Barnes, 1998; Liu et al., 2017).

A typical feedback regulation of the body's response to inflammation is the activation of the HPA-axis by different cytokines like IL-1, IL-6 and TNFα to maintain the homeostasis (De Bosscher et al., 2003; Dunn, 2000; Turnbull and Rivier, 1999). GCs have an anti-inflammatory action by activating the GR to reduce inflammation through the recruitment of several coactivator complexes and the transcription of anti-inflammatory genes like IL-10 (Barnes, 1998; De Bosscher et al., 2003; Schaaf and Cidlowski, 2002) or the trans-repression of NF-κB and AP-1 by direct protein-protein interaction (Coutinho and

Chapman, 2011; Rao et al., 2011; Schoneveld et al., 2004). In addition, pro-inflammatory cytokines induce the expression of the 11β-HSD1 in human adipocytes via NF-κB (Lee et al., 2013).
Intracellular pathways activated by inflammation underline the role of cytokines in the development of insulin resistance and type 2 diabetes mellitus (T2DM) in obesity (Marette, 2002; Shoelson et al., 2006). In contrast to the anti-inflammatory effects of GCs in acute stress which increase the immunity (Dhabhar et al., 2010), chronic stress or chronic exposure to GCs leads to a switch towards a pro-inflammatory state (Dhabhar, 2000). It is possible that chronic stress promotes inflammation through the reduction of the immune system's sensitivity to hormonal signals that normally terminate the inflammatory cascade (Miller et al., 2002) or through glucocorticoid receptor resistance and therefore the loss of down-regulation of the pro-inflammatory response (Cohen et al., 2012). Summarizing, GCs could contribute to fast adipose tissue expansion leading to increased circulating pro-inflammatory cytokines (Jiang et al., 2019) and insulin resistance (de Luca and Olefsky, 2008).

1.2.3.4 GC regulation of insulin sensitivity

Chronic GC treatment is an efficient tool to treat several human illnesses, like autoimmune diseases, cancer or therapy after transplantation, but on the other hand prolonged GC exposure lead to obesity, insulin resistance and diabetes (Chanson and Salenave, 2010; Shibli-Rahhal et al., 2006). It is known, that GCs influence several enzymes in the insulin signaling pathway, by different mechanisms. Usually, insulin binds to its receptor, which leads to an enhanced kinase activity and a number of different protein phosphorylation of downstream targets like insulin receptor substrate (IRS) and protein kinase B (AKT). GCs causes insulin resistance in skeletal muscle by downregulating the transcription of IRS-1 and enhancing transcription of the insulin counteracting enzyme p38 mitogen-activated protein kinase (p38MAPK) (Almon et al., 2005; Giorgino et al., 1993). Similarly, a GC induction of p38MAPK transcription is detected in liver (Almon et al., 2007). In addition, a reduced IR and IRS-1 phosphorylation were observed in rat hepatocytes after treatment with dexamethasone, a synthetic GC (Saad et al., 1993). Aside from that, adipose tissue show no different IRS-1 and IRS-2 abundance (Buren et al., 2008). Dexamethasone induced insulin resistance in cultured murine 3T3-L1 cells exhibit an upregulation of MAPK phosphatases associated with a reduced p38MAPK phosphorylation in (Bazuine et al., 2004). Paradoxically, several studies could show, that chronic GC exposure can lead to improvements in insulin sensitivity of human subcutaneous adipose tissue (Gathercole et al., 2007; Gathercole et al., 2011b; Hazlehurst et al., 2013; Tomlinson et al., 2010).
Many mechanism concerning GCs-induced development of hepatic insulin resistance are described. GCs potentiate the insulin-induced hepatic lipogenesis by upregulating ACC and FAS in isolated rat hepatocytes and human HepG2 cells (Amatruda et al., 1983; Zhao et al., 2010). Moreover, hepatic insulin resistance through increased lipid accumulation is induced by indirect factors including

expansion and lipolysis of visceral WAT, leading to high levels of circulating fatty acids. The associated systemic hyperinsulinemia and hyperglycemia in turn induced hepatic DNL (Geer et al., 2014; Schwarz et al., 2003). Beside, GCs also stimulate the hepatic gluconeogenesis via induction of PCK1 and G6PC, which induce hepatic insulin resistance. In a mouse model for hepatic steatosis it is demonstrated, that the specific ablation of hepatic GR leads to decrease in triglyceride accumulation (Lemke et al., 2008). These results indicate, that chronic high GC levels affect directly or indirectly the insulin sensitivity of metabolic tissues, particular the role of the liver and the crosstalk with the adipose tissue is important in metabolic influence of GCs.

1.2.3.5 Influence of stress on the hormonal regulation of hepatic energy metabolism

One of the most prominent regulator of hepatic glucose and lipid metabolism is insulin, which induces hepatic lipogenesis and glycogen synthesis. In parallel it inhibits gluconeogenesis and activates glycolysis in the liver (Dimitriadis et al., 2011). Glucagon, the other prominent regulator, counteract insulin action by promoting gluconeogenesis and glycogen breakdown (Ramnanan et al., 2011). Further, it reduces DNL in liver and adipose tissue as well as stimulates lipolysis in these tissues. Glucagon is secreted by pancreatic alpha cells and is affected by glucose and lipid concentrations in the blood flow (Scott and Bloom, 2018). Another factor which affects the hepatic energy metabolism is the adipose tissue derived hormone adiponectin. Adiponectin enhances insulin sensitivity by increasing glucose utilization in skeletal muscles together with reducing hepatic gluconeogenesis and enhanced fatty acid oxidation in the liver (Meier and Gressner, 2004; Whitehead et al., 2006). Adiponectin levels are reduced in obesity and T2DM (Fumeron et al., 2004; Hotta et al., 2001; Yamauchi et al., 2003). Adiponectin and GCs show opposing effect on glucose and lipid metabolism. GCs induce insulin resistance in liver, skeletal muscle and WAT, whereas adiponectin act as an insulin-sensitizer. Studies analyzing the effect of GCs on adiponectin reveal contradictory results. Pharmacological treatment in cell culture and animal models show no clear function of GCs on adiponectin expression or secretion (Sukumaran et al., 2012). Leptin a further adipose tissue derived hormone act in the hypothalamus by activating pro-opiomelanocortin (POMC) neurons and thus reduce food intake and increase energy expenditure. Levels of leptin are increased in obesity and T2DM. It has a bidirectional action on hepatic energy metabolism by inhibiting hepatic DNL and stimulating fatty acid oxidation resulting in decreased hepatic triglyceride content, but it also act as an inflammatory and fibrogenic factor (Polyzos et al., 2015). Studies have shown, that *in vitro* and *in vivo* treatment with dexamethasone induce leptin levels and expression in adipocytes from rodents and human (Hardie et al., 1996; Russell et al., 1998).

1.3 Research aim

Chronic stress is associated with continuing high stress hormone levels leading to metabolic complications such as obesity or T2DM. The influence of GCs itself on metabolic processes is well established. Chronic GC exposure is linked to metabolic impairments, which are involved in the development of metabolic disorders like insulin resistance or hepatic lipid accumulation. However, most of the studies were performed with synthetic GCs and studies are often limited to acute effects. The mechanism behind the metabolic adaptations on exogenous stress especial in the long term are not completely understood. There is a lack of studies investigating the long-term metabolic regulations after chronic stress exposure and the relation to cellular and hormonal adaptations in a physiological model.

This thesis aims the molecular effects of short- and long-term metabolic adaptation after chronic stress exposure. The impact of chronic stress was evaluated in a mouse model following an established PTBS protocol. The focus of this thesis is the:

I. short- and long-term metabolic changes after chronic stress on the regulation of the glucose and lipid metabolism,
II. tissue specific analyses to investigate adaptations in metabolic active organs and to identify relevant modulators of post-stress metabolic regulation,
III. detailed analyses of major findings of the impact of chronic stress on the hepatic glucose and lipid metabolism to reveal metabolic adaptations and to investigate the role of possible molecular regulators.

The investigations were focused on *in vivo* and *in vitro* analyses on insulin sensitivity and hepatic energy metabolism. Molecular biological investigations of cellular signaling pathways and transcriptional regulation were determined to detect possible mechanistic regulation after chronic stress exposure. The experiments should identify possible mechanisms or regulators of the energy metabolism after chronic stress.

2. MATERIAL & METHODS

2.1 Material

2.1.1 Experimental animals

In the first section, twelve weeks old C57BL/6 mice were analyzed. Animals were conducted from Janvier Labs (Clermont-Ferrand, France) with an age of 8 weeks for adaptations to a new environment. *Fgf21* knockout (FGF21KO) mice, analyzed in the second section of this script, were bred in the Oskar-Minkowski-Lab at the DDZ. Initial breeding pairs of these conventional KO mice were obtained from the Department of Genetic Biochemistry, Kyoto in Japan. Starting form heterozygous offspring, FGF21KO were obtained by interbred. Resulting homozygous wildtype mice were recruited as control mice. All mice were group housed (max. 5 mice per cage) under a 12:12 hour light-dark cycle (6 pm dark) with ad libitum access to standard chow (58% carbohydrates, 9% fat, 33% protein, R/M-H Extrudat, ssniff Spezialdiäten GmbH, Soest, Germany) for up to 14 or 26 weeks and tap water.
The mice show no breeding abnormalities or other diseases. The initial publication from 2009 describing these *Fgf21* knockout mice show an increased lean mass together with a higher lipolytic activity in the adipose tissue due to the knockout (Hotta et al., 2009).
All animal protocols were approved by the *Landesamt für Natur, Umwelt und Verbraucherschutz (LANUV)*, NRW, Germany (81-02.04.2017.A421).

2.1.2 Experimental design

In the initial work, published in 2018, C57BL/6 mice were separated in age-matched control and stressed groups. One cohort were analyzed for stress-related short-term effects after a chronic variable stress (Cvs) intervention and one cohort, consisting of a control and stressed group were kept on a standard diet for three months for long-term analyses. Similar to the initial study, for the second part of this work, in total eight groups out of two cohorts, short- (15 days) and long-term (3 months), were analyzed. Each cohort consists of a control, non-stressed (Ctrl) and a stressed group (Cvs) containing WT and FGF21KO animals, respectively. At the end points the mice were euthanized and utilized for liver perfusion and hepatocyte isolation or insulin/saline injection and following tissue dissection (Figure 3). Animals passing the recovery phase (dashed bars) were analyzed in *in vivo* experiments like indirect calorimetry or tolerance tests directly after Cvs and at the end of recovery phase. During the whole experimental time the body weight and food intake were monitored.

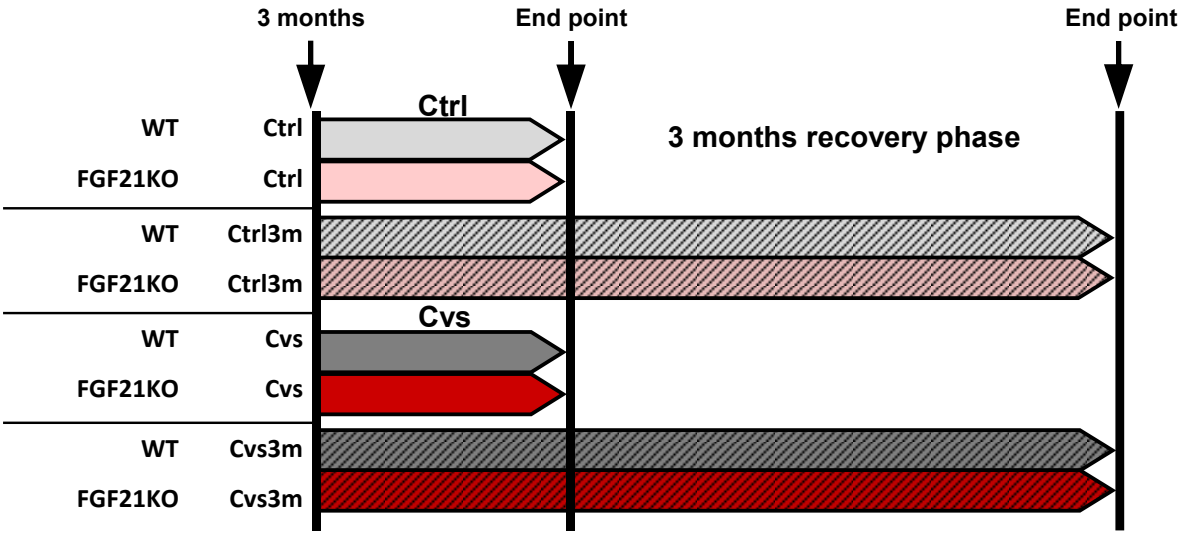

Figure 3: Experimental design. Three months old, age matched mice were exposed to a 15 days protocol for Cvs and analyzed directly after the intervention or after a three-month recovery phase. Cvs: Chronic variable stress; Ctrl: non-stressed control; WT: wildtype; FGF21KO: FGF21 knockout.

2.1.3 Instruments and disposables

Conventional instruments belonging to the standard laboratory equipment are not listed in the Table below.

Table 1: Instruments and devices.

Instruments	Manufacturer (name, location)
AE31 Trinocular inverted microscope	Motic, Wetzler, Germany
Analytical Balance	Sartorius, Göttingen, Germany
Beckman Coulter LS 6000LL/LS 6000IC	Beckman Coulter, Krefeld, Germany
Bioplex 200 suspension array system	Bio-Rad, Munich, Germany
Bioruptor pico	Diagnode, Belgium
ChemidocTM XRS+ System	Bio-Rad, Munich, Germany
Combs for SDS gels (15 well)	Bio-Rad, Munich, Germany
Electronic Precision Balance U4100	Sartorius, Göttingen, Germany
Electrophoresis Chamber Mini-PROTEAN ® Tetra Cell	Bio-Rad, Munich, Germany
FeedTime system	TSE systems, Bad Homburg, Germany
Filter papers	Oehmen, Essen, Germany
Fridge Sanyo Labcool MPR-1410R	Sanyo, Moriguchi, Japan
Gas chromatograph 6890N Network GC System	Agilent Technologies, Santa Clara, CA, USA
Glucometer and glucose test stripes	Bayer, Leverkusen, Germany
Heracell™ 240i CO_2 incubator	Thermo Fisher Scientific, Darmstadt, Germany
Heraeus LaminAir HB 2448 S GS	Thermo Fisher Scientific, Darmstadt, Germany

Instruments	Manufacturer (name, location)
Heraeus™ Multifuge™ X3 Zentrifuge	Thermo Fisher Scientific, Darmstadt, Germany
Infinite® M200 plate reader	Tecan Trading AG, Switzerland
Mini PROTEAN Tetra System	Bio-Rad, Munich, Germany
Multiplex Bio-Plex™ Protein Immunoassay System	Bio-Rad, Munich, Germany
NanoDrop™ 2000/2000c spectropmeter	Thermo Fisher Scientific, Darmstadt, Germany
Neubauer counting chamber	BRAND®, Wertheim, Germany
NMR Whole Body Composition Analyzer Echo	Echo MRI, TX, USA
Orbital shaker	Assistent GmbH, Altnau, Switzerland
Peristaltic pump	Gilson's MINIPULS® 3, Middleton, USA
Phenomaster	TSE systems, Bad Homburg, Germany
Pipettes	Eppendorf, Wesseling-Berzdorf, Germany
Power Pac Basic power supply	Bio-Rad, Munich, Germany
PURA water bath	Julabo, Seelbach, Germany
QuantStudio 7 Flex Real-Time PCR System	Thermo Fisher Scientific, Darmstadt, Germany
Short plates for SDS gels	Bio-Rad, Munich, Germany
Spacer plates (1.5 mm) for SDS gels	Bio-Rad, Munich, Germany
Spacer plates for SDS gels	Bio-Rad, Munich, Germany
Speedvac centrifuge	Eppendorf, Hamburg, Germany
T100™ thermal cycler	Bio-Rad, Munich, Germany
Table centrifuge 5417 R	Eppendorf, Wesseling-Berzdorf, Germany
Tankblot Eco Mini	Biometra, Göttingen, Germany
Thermomix	Eppendorf, Wesseling-Berzdorf, Germany
Thermomixer comfort	Eppendorf, Wesseling-Berzdorf, Germany
Tissue Lyser II	QIAGEN, Hilden, Germany
XFe96 extracellular flux analyzer	Agilent Technologies, Santa Clara, CA, USA

Table 2: Disposals.

Disposables	Manufacturer (name, location)
96-well high-binding assay plates	Sarstedt, Nümbrecht, Germany
Cell culture plates, sterile (6-, 12-, 24-, 48-, 96-well)	Greiner Bio-One, Frickenhausen, Germany
Cell scraper	Sarstedt, Nümbrecht, Germany
Chromatography column FS-FFAP-CB-0.25; Cat. No: 23208330	CS- Chromatographie Service GmbH, Langerwehe, Germany
ClearLine® cell strainers, 70 µm	Kisker Biotech, Steinfurt, Germany
Falcon® cell culture dishes, sterile	VWR, Darmstadt, Germany
Injekt®-F syringe, 1 ml B.	Braun, Hessen, Germany
MicroAmp® Fast Optical 96-Well Reaction Plate	Thermo Fisher Scientific, Darmstadt, Germany
MicroAmp® Optical Adhesive Film	Thermo Fisher Scientific, Darmstadt, Germany
Rotlabo®-syringe filter, sterile, P666.1	Carl Roth, Karlsruhe, Germany

Disposables	Manufacturer (name, location)
Stainless Steel Beads, 5 mm	QIAGEN, Hilden, Germany
Standard laboratory, normal-caloric chow	Ssniff, Soest, Germany
Sterican® cannula G 26 / ø 0,45 x 25 mm B.	Braun, Hessen, Germany
Steritop™ filter unit	Merck Chemicals GmbH, Darmstadt, Germany
Surgical blades	VWR, Darmstadt, Germany
Whatman Nitrocellulose membrane	Oehmen, Essen, Germany

2.1.4 Chemicals

Table 3: Chemicals used in the study.

Chemicals	Manufacturer (name, location)
(+)-Etomoxir, sodium salt hydrate, ≥98%, (HPLC), powder	Merck KGaA , Darmstadt, Germany
[^{14}C]-acetate	PerkinElmer Cellular Technologies GmbH, Hamburg, Germany
[^{14}C]-palmitic acid	PerkinElmer Cellular Technologies GmbH, Hamburg, Germany
[9,10-3H(N)]-Palmitic Acid	PerkinElmer Cellular Technologies GmbH, Hamburg, Germany
10% formalin, neutral buffered	Sigma-Aldrich, Darmstadt, Germany
2-Deoxy-D-glucose (2-DG)	Sigma-Aldrich, Darmstadt, Germany
4-(2-Hydroxyethyl)piperazine-1-ethanesulfonic acid (HEPES) Buffer Solution (1M)	Gibco®, Thermo Fisher Scientific, Darmstadt, Germany
Acrylamide 30%	AppliChem GmbH, Darmstadt, Germany
Ammonium persulfate (APS)	MP Biomedicals, Solon, USA
Antibiotic-Antimycotic Solution (100x)	Gibco®, Thermo Fisher Scientific, Darmstadt, Germany
Antimycin A from Streptomyces sp.	Merck KGaA , Darmstadt, Germany
Bovine serum albumin (BSA) Fraction V, fatty acid free	Carl Roth, Karlsruhe, Germany
Bromphenol Blue	AppliChem GmbH, Darmstadt, Germany
BSA Fraction V	Sigma-Aldrich, Steinheim, Germany
BSA Fraction V, very low endotoxin	Carl Roth, Karlsruhe, Germany
Carbonyl cyanide 4-(trifluoromethoxy)phenylhydrazone (FCCP, ≥98% (TLC), powder)	Merck KGaA , Darmstadt, Germany
Chloroform	Carl Roth, Karlsruhe, Germany
Collagen I, rat tail	Advanced BioMatrix, Inc., California, USA
Collagenase type IV	Worthington Biochemical Corp., Lakewood, NJ, USA
Complete Protease Inhibitor Cocktail	Roche, Mannheim, Germany
Dexametasone, ≥98% (HPLC), powder	Sigma Aldrich, St Louis, MO, USA
D-glucose	AppliChem GmbH, Darmstadt, Germany
Dimethyl sulfoxide (DMSO)	Sigma-Aldrich, Darmstadt, Germany

Chemicals	Manufacturer (name, location)
Disodium hydrogen phosphate dihydrate ($Na_2HPO_4•2H_2O$)	Sigma-Aldrich, Darmstadt, Germany
Dithiothreitol (DTT)	Sigma-Aldrich, Steinheim, Germany
DMEM, low glucose	Gibco®, Thermo Fisher Scientific, Darmstadt, Germany
DMEM, without glucose, L-glutamine, phenol red, sodium pyruvate and sodium bicarbonate, powder, suitable for cell culture	Sigma Aldrich, St Louis, MO, USA
DMEM/F-12, GlutaMAX™ Supplement	Gibco®, Thermo Fisher Scientific, Darmstadt, Germany
DMEM/F-12, HEPES, no phenol red	Gibco®, Thermo Fisher Scientific, Darmstadt, Germany
Dulbecco's modified Eagle's medium (DMEM), low glucose, pyruvate, HEPES	Gibco®, Thermo Fisher Scientific, Darmstadt, Germany
Dulbecco's Phosphate Buffered Saline (PBS), 10x without $CaCl_2$ and $MgCl_2$	Gibco®, Thermo Fisher Scientific, Darmstadt, Germany
Easycoll Separating Solution (Density 1.077 g/ml)	Biochrome GmbH, Berlin, Germany
Ethylene diamine tetraacetic acid (EDTA)	Serva, Heidelberg, Germany
Fetal calf serum (FCS)	Biochrom GmbH, Berlin, Germany
GlutaMAX™ (100x)	Gibco®, Thermo Fisher Scientific, Darmstadt, Germany
Glycine	Applichem, Darmstadt, Germany
Hydrochloric acid (HCl)	Carl Roth, Karlsruhe, Germany
Insulin from porcine pancreas	Sigma-Aldrich, Darmstadt, Germany
L-carnitin	Sigma-Aldrich, Darmstadt, Germany
L-glutamine	Sigma-Aldrich, Darmstadt, Germany
Methanol	Carl Roth, Karlsruhe, Germany
Molecular weight marker Dual Color	Bio-Rad, Munich, Germany
Nonidet P-40 (NP-40)	Sigma-Aldrich, Darmstadt, Germany
Oligomycin A, ≥95% (HPLC)	Merck KGaA , Darmstadt, Germany
Percoll gradient (Easycoll)	Biochrom GmbH, Berlin, Germany
PhosSTOP Phosphatase Inhibitor	Roche, Mannheim, Germany
Potassium chloride (KCl)	Merck, Darmstadt, Germany
Precision Plus Protein™ Standard	Bio-Rad, Munich, Germany
Rat tail type-I collagen stock (4 mg/ml)	CellSystems®, Troisdorf, Germany
Rotenone, ≥95%	Merck KGaA , Darmstadt, Germany
Rotiszint® eco plus	Carl Roth, Karlsruhe, Germany
Sodium acetate	AppliChem GmbH, Darmstadt, Germany
Sodium bicarbonate ($NaHCO_3$)	Merck Chemicals GmbH, Darmstadt, Germany
Sodium chloride (NaCl)	Carl Roth, Karlsruhe, Germany
Sodium deoxycholate	AppliChem GmbH, Darmstadt, Germany
Sodium dihydrogen phosphate monohydrate ($NaH_2PO4•H_2O$)	Sigma-Aldrich, Darmstadt, Germany
Sodium dodecyl sulfate (SDS)	AppliChem GmbH, Darmstadt, Germany
Sodium lactate	AppliChem GmbH, Darmstadt, Germany

Chemicals	Manufacturer (name, location)
Sodium palmitate, ≥98.5%	Merck Chemicals GmbH, Darmstadt, Germany
Sodium pyruvate (100 mM)	Gibco®, Thermo Fisher Scientific, Darmstadt, Germany
Tetramethylethylenediamine (TEMED)	Carl Roth, Karlsruhe, Germany
Tris(hydroxymethyl)aminomethane (TRIS)	Carl Roth, Karlsruhe Germany
Tris-HCl	AppliChem GmbH, Darmstadt, Germany
Triton X-100	Roche Diagnostics, Mannheim, Germany
Trypan blue solution (0.4%)	Sigma Aldrich, St Louis, MO, USA
Tween® 20	AppliChem GmbH, Darmstadt, Germany
Tween® 20	MP Biomedicals, Solon, USA
Western Lightning ECL Pro and Ultra	Perkin Elmer, Waltham, MA, USA
β-Mercaptothanol	Thermo Fisher Scientific, Darmstadt, Germany

2.1.5 Buffers and solutions

Table 4: Buffers and solutions

Name	Composition	Final concentration/volume
Blocking solution	TBS-T	1x
	BSA	5% (w/v)
Electrophoresis running Buffer (10x)	Tris	250 mM
	Glycine	1.92 M
	SDS	1% (w/v)
Hanks balanced salt solution (HBSS) pH adjusted to 7.4 with NaOH	KCl	5.33 mM
	KH_2PO_4	0.44 mM
	Na_2HPO_4	0.34 mM
	NaCl	138 mM
	$NaHCO_3$	4.17 mM
	Glucose	5.56 mM
	EGTA	0.5 mM
	HEPES	25 mM
Krebs-Ringer-HEPES (KRH) pH adjusted to 7.4 with NaOH	NaCl	136 mM
	KCl	4.7 mM
	$MgSO_4$	1.25 mM
	$CaCl_2$	1.25 mM
	HEPES	10 mM
Laemmli sample buffer (4x)	Tris-HCl (pH 6.8)	250 mM
	EDTA	10 mM
	SDS	8% (v/v)
	Glycerol in dH_2O	50% (v/v)
	DTT	400 mM
	Bromphenol blue	1% (v/v)
Lysis buffer (RIPA)	Tris-HCl (pH 8.0)	50 mM
	NaCl	150 mM

Name	Composition	Final concentration/volume
	NP-40	1 % (v/v)
	Sodium deoxycholate	0.1 % (v/v)
	SDS	0.1 % (v/v)
		+ Complete proteinase inhibitor
		+ PhosStop phosphatase inhibitor
Lysis buffer (NP-40)	NP-40	1% (v/v) NP-40 in 1x PBS
		+ Complete proteinase inhibitor
		+ PhosStop phosphatase inhibitor
Percoll gradient 90%	Percoll	90%
	10x PBS	10%
Tris-buffered saline with Tween® 20 (TBS-T)	Tris (pH 7.5)	20 mM
	NaCl	150 mM
	Tween® 20	0.1% (v/v)
Transfer buffer (10x)	Tris	250 mM
	Glycine	1.92 M
Seahorse lysis buffer	Tris-HCl	10 mM
	Na_2HPO_4 $2H_2O$	10 mM
	NaH_2PO_4 H_2O (pH 7.5)	10 mM
	NaCl	130 mM
	$Na_4P_2O_7$ $10H_2O$	10 mM
	Triton X-100	1% (v/v)
Separating buffer	Tris	1.5 M
pH adjusted to 8.8 with NaOH	SDS	0.4% (w/v)
Separating gel (10%)	dH_2O	3.66 ml
	Separating gel buffer	2.34 ml
	Acryamide (30%)	2.4 ml
	APS (ammonium persulfate)	18 µl
	TEMED	9 µl
Stacking buffer	Tris	0.5 M
pH adjusted to 6.8 with NaOH	SDS	0.4% (w/v)
Stacking gel	dH_2O	1.83 ml
	Stacking gel buffer	780 µl
	Acryamide (30%)	390 µl
	APS	6 µl
	TEMED	3 µl

2.1.6 Cell culture and assay medium

Table 5: Used cell culture and assay media.

Name/Basis	Composition	Final concentration
Collagenase medium	1x Antibiotic-Antimycotic mix	2% (v/v)
DMEM, low glucose	Collagenase IV	100 U/ml

Name/Basis	Composition	Final concentration
FAO assay medium	BSA Fraction V fatty acid free	10 µM
DMEM/F-12, GlutaMAX™ Supplement	1x Antibiotic-Antimycotic mix	2% (v/v)
	Sodium pyruvate	1 mM
	L-Carnitine	1 µM
	^{14}C-palmitate	2.6 µM
FAU transport buffer	Palmitat-BSA	5 µM
1x KRH	BSA Fraction V fatty acid free	2.5 µM
	^{3}H-palmitate	8.5 nM
Glucose production medium	1x Antibiotic-Antimycotic mix	2% (v/v)
DMEM, without glucose, L-glutamine,	L-Glutamine	2.5 mM
phenol red, sodium pyruvate and	HEPES	15 mM
sodium bicarbonate, powder	NaHCO3	3.7 g/ml
pH adjusted to 7.4 with NaOH		
Glycolysis stress assay medium	Glutamine	2 mM
DMEM, without glucose, L-glutamine, phenol red, sodium pyruvate and sodium bicarbonate, powder pH adjusted to 7.4 with NaOH		
Isolation medium	FCS	10% (v/v)
DMEM, low glucose	1x Antibiotic-Antimycotic mix	2% (v/v)
	Sodium pyruvate	1 mM
	Porcine insulin	0.1 µM
	Dexamethasone	1 µM
Mito stress assay medium (Seahorse)	Glutamine	2 mM
DMEM, without glucose, L-glutamine, phenol red, sodium pyruvate and sodium bicarbonate, powder pH adjusted to 7.4 with NaOH	Pyruvate	1 mM
	Glucose	10 mM
Plating medium	FCS	10% (v/v)
DMEM/F-12, GlutaMAX™ Supplement	1x Antibiotic-Antimycotic mix	2% (v/v)
	Sodium pyruvate	1 mM
	Porcine insulin	0.1 µM
	Dexamethasone	1 µM
Secretome medium	BSA Fraction V	0.2% (v/v)
DMEM/F-12, HEPES, no phenol red	1x Antibiotic-Antimycotic mix	2% (v/v)
	Sodium pyruvate	1 mM
Serum starvation medium	BSA Fraction V	0.2% (v/v)
DMEM/F-12, GlutaMAX™ Supplement	1x Antibiotic-Antimycotic mix	2% (v/v)
	Sodium pyruvate	1 mM

2.1.7 Commercial kits

Table 6: Used commercial reaction kits.

Kits	Manufacturer (name, location)
Bio-Plex Pro™ Mouse Cytokine Group 1 23	Bio-Rad, Munich, Germany
Bio-Plex Pro™ Mouse Diabetes 8-plex	Bio-Rad, Munich, Germany
Corticosterone Parameter Assay Kit	R&D Systems, Minneapolis, MN, USA
Glucose (GO) Assay Kit	Sigma-Aldrich, Darmstadt, Germany
GoScript™ Reverse Transcription System	Promega, Heidelberg, Germany
GoTaq® qPCR Master Mix	Promega, Heidelberg, Germany
HAT Activity Assay Kit II	PromoCell GmbH, Heidelberg, Germany
HDAC-Glo™ I/II Assays	Promega, Heidelberg, Germany
MILLIPLEX MAP Phosphoprotein 11-Plex	Merck KGaA , Darmstadt, Germany
MILLIPLEX MAP total protein 11-Plex	Merck KGaA , Darmstadt, Germany
miRNeasy RNA mini kit	QIAGEN, Hilden, Germany
Mouse/Rat FGF-21 Quantikine ELISA Kit	R&D Systems, Minneapolis, MN, USA
MTase-Glo™ Methyltransferase Assay	Promega, Heidelberg, Germany
NAD/NADH-Glo™ Assays	Promega, Heidelberg, Germany
Pierce™BCA Protein Assay Kit	Thermo Fisher Scientific, Darmstadt, Germany
SIRT-Glo™ Assay	Promega, Heidelberg, Germany
Randox Triglycerides	RANDOX Laboratories, Antrim, United Kingdom

2.1.8 Antibodies and oligonucleotides

Table 7: Antibodies for western blot.

Antibody, origin	Manufacturer, Cat. No.	SDS-PAGE acrylamide %	Transfer time	Dilution[1] (v/v)
Actin, rabbit	Cell Signaling, #12262	(respective)	(respective)	1:10.000
AKT, rabbit	Cell Signaling, #9272	10%	2 h	1:1000
AMPK, rabbit	Cell Signaling, #2532	10%	2 h	1:1000
FGF21, rabbit	Abcam, #ab171941	14%	0.5 h	1:1000
GAPDH, rabbit	Cell Signaling, #5174	(respective)	(respective)	1:5000
Glut1, rabbit	Dr. A. Schürmann, Potsdam	10%	2 h	1:1000
GR, rabbit	Cell Signaling, #12041	10%	2 h	1:1000
phoshpo-AMPK (Thr172), rabbit	Cell Signaling, #2531	10%	2 h	1:1000
phospho-AKT (Ser473), rabbit	Cell Signaling, #9271	10%	2 h	1:1000

Antibody, origin	Manufacturer, Cat. No.	SDS-PAGE acrylamide %	Transfer time	Dilution[1] (v/v)
phospho-AKT (Thr308), rabbit	Cell Signaling, #4056	10%	2 h	1:1000
phospho-GR (Ser211), rabbit	Cell Signaling, #4161	10%	2 h	1:1000
SIRT1, rabbit	Cell Signaling, #2028	10%	2 h	1:1000
UCP1, rabbit	Abcam, #ab10983	10%	2 h	1:1000
Secondary antibody				
Anti-rabbit IgG, HRP-linked, Goat	Jackson ImmunoResearch, #111-035-003	-	-	1:10.000

[1]All antibodies were diluted in 5% bovine serum albumin (BSA) in 1x TBS-T.

All designed oligonucleotides were purchased from Eurogentec (Cologne, Germany). Before use oligonucleotides were reconstituted to 10 nmol in H_2O.

Table 8: Oligonucleotides for RT-PCR

Target	Accession	Forward 5'->3'	Reverse 5'->3'
Acaca	NM_133360	ATGGGCGGAATGGTCTCTTTC	TGGGGACCTTGTCTTCATCAT
Acacb	NM_133904	CCTTTGGCAACAAGCAAGGTA	AGTCGTACACATAGGTGGTCC
Bmp7	NM_007557	ACGGACAGGGCTTCTCCTAC	ATGGTGGTATCGAGGGTGGAA
CD36	NM_001159556	CCTAGTAGGCGTGGGTCTGA	ACGGGGTCTCAACCATTCATC
Cidea	NM_007702	TGACATTCATGGGATTGCAGAC	GGCCAGTTGTGATGACTAAGAC
Cpt1a	NM_013495	CTCAGTGGGAGCGACTCTTCA	GGCCTCTGTGGTACACGACAA
Cpt1b	NM_009948	CAGCGCTTTGGGAACCACAT	CACTGCCTCAAGAGCTGTTCTC
Cs	NM_026444	CGGGAGGGCAGCAGTATCGG	ACCACCCTCATGGTCACTATGGATG
Dio2	NM_010050	AATTATGCCTCGGAGAAGACCG	GGCAGTTGCCTAGTGAAAGGT
Egr1	NM_007913	TCGGCTCCTTTCCTCACTCA	CTCATAGGGTTGTTCGCTCGG
Fabp4	NM_024406	AAGGTGAAGAGCATCATAACCCT	TCACGCCTTTCATAACACATTCC
Fasn	NM_007988	TTGCTGGCACTACAGAATGC	AACAGCCTCAGAGCGACAAT
Fgf21	NM_020013	CTGCTGGGGGTCTACCAAG	CTGCGCCTACCACTGTTCC
Fgfr1	NM_001079908	ACCAAGAAGAGCGACTTCCA	AACCAGGAGAACCCCAGAGT
Fgfr1b	NM_001079909	GAGTAAGATCGGGCCAGACA	TCACATTGAACAGGGTCAGC
Fgfr1c	NM_001079908	GACTCTGGCCTCTACGCTTG	TCGTCGTCGTCATCATCTTC
Fgfr4	NM_008011	ACTCCATCGGCCTTTCCTAC	TGTTGTCCACGTGAGGTCTT
Gapdh	NM_008084	CCAGGTTGTCTCCTGCGACT	ATACCAGGAAATGAGCTTGACAAAGT
Hadha	NM_178878	TGACGCTGGTTATCTTGCTG	ATCAGGGCCTTCGATTCTTT
Hprt	NM_013556	AAGCTTGCTGGTGAAAAGGA	TTGCGCTCATCTTAGGCTTT
Klb	NM_031180	ACACTGTGGGACACAACCTG	AGAGCCAACCCTTCTGATGA
Lipe	NM_010719	GGTGACTCTAACGCGACTCC	CCCCCAAACCATCCAATCCT
Pnpla2	NM_001163689	CATGATGGTGCCCTATACTC	GTGAGAGGTTGTTTCGTACC
Ppargc1a	NM_008904	CTCTCCTTGCAGCACCAGAA	CAATGAATAGGGCTGCGTGC
Prdm16	NM_027504	CAGCACGGTGAAGCCATTC	GCGTGCATCCGCTTGTG
Rpl32		GCCCAAGATCGTCAAAAAGA	ATTGTGGACCAGGAACTTGC
Scd1	NM_009127	CTTCAAGGGCAGTTCTGAGG	CAATGGTTTTCATGGCAGTG

Target	Accession	Forward 5'->3'	Reverse 5'->3'
Scd2	NM_009128	TGTACTATGTAATCAGCGCCC	ATACACGTCATTCTGGAACGC
Slc17a5	NM_172773	TGTGTGTGAAGGAACCTGGA	ACCCGGACAACTTTGTGAAG
Slc2a1	NM_011400.3	CCTGTCTCTTCCTACCCAACC	GCAGGAGTGTCCGTGTCTTC
Slc2a4	NM_009204	GTCCTGGGGGACCGGATTCCAT	CCCTGATGTTAGCCCTGAGTAGGCG
Ucp1	NM_009463.2	GGGCCCTTGTAAACAACAAA	GTCGGTCCTTCCTTGGTGTA

2.1.9 Software

Table 9: Software

Software	Version	Distributor
GraphPad Prism	8.2.0	GraphPad software Inc, San Diego, CA, USA
Image Lab™	6.0.1	Bio-Rad, Munich, Germany
Microsoft Office Professional Plus	2013	Microsoft Corporation, Redmond, WA, USA
QuantStudio™ Real-Time PCR Software	1.1	Thermo Fisher Scientific, Darmstadt, Germany
Wave	2.4.0	Agilent Technologies, Santa Clara, CA, USA

2.2 Methods

The methods in paragraph 2.2.1 to 2.2.5 are adopted from the methods section of Jelenik*, Dille* et al. (2018) (*shared first author).

2.2.1 Hyperinsulinemic-euglycemic clamp

Mice underwent hyperinsulinemic-euglycemic clamps with deuterated glucose to determine whole-body and hepatic insulin sensitivity as described previously (Jelenik et al., 2017b; Jelenik et al., 2014). In brief, a silicon catheter (Silastic laboratory tubing, Dow Corning, Midland, MI) was placed into the right jugular vein under Isoflurane (CP Pharma, Burgdorf, Germany) anaesthesia. Mice were allowed to recover for 4–5 days and fasted for 6 h on the day of the experiment (03:00–09:00a.m.). To assess basal whole-body glucose disposal, D-[6,6-$^{2}H_2$]glucose (98% enriched; Cambridge Isotope Laboratories, Andover, MA, USA) was infused at a rate of 4 µmol/kg/min for 120 min. The hyperinsulinemic-euglycemic clamp was performed with a primed (40 mU/kg)-continuous infusion (4 mU/kg/min; Huminsulin, Lilly, Giessen, Germany) for 180 min. Euglycemia was maintained by periodically adjusting a variable 20% glucose infusion. D-[6,6-$^{2}H_2$]glucose was co-infused together with insulin solution (0.4 µmol/kg/min) and variable glucose infusion to obtain stable tracer concentrations during varying glucose infusion rates. Blood samples were taken at 10-min intervals during the last 30 min of basal, and hyperinsulinemic-euglycemic clamps.

2.2.2 Insulin-stimulated glucose uptake by white adipose cells (WAC)

Isolation of primary WAC and glucose uptake were performed as described previously (Chadt et al., 2015). Epididymal WAT was excised and pooled in 4 ml of Krebs Ringer bicarbonate HEPES (KRBH) buffer-5% (w/v) BSA with 2 mg/ml type I collagenase (Worthington Biochemical Corporation, Lakewood, NJ, USA). The fat pads were minced and the suspension was shaken in a water bath at 160 rpm for 50 min at 37°C. The cells were strained through a 200 µm sterile mesh and washed twice with KRBH buffer with 5% BSA. After aspirating the wash buffer, the cells were gently re-suspended in KRBH buffer with 5% BSA to make a 10% cell suspension for glucose uptake assay. 200 µl of cell suspension was distributed into vials containing 200 µl KRBH buffer with 5% BSA with/without insulin and then incubated for 30 min at 37°C in a gyratory bath. One hundred µl of hot medium with D-[U-^{14}C] glucose were added (final concentration 0.06 µCi/ml), and the cells were incubated for another 30 min at 37°C. After that, glucose uptake was terminated by transferring 250 µl of the cell suspension to 100 µl of dinonyl phthalate (Merck, Darmstadt, Germany) in a microcentrifuge tube. The cells were centrifuged for 10 min at 14,000 rpm. The cells (top layer) were cut away from the buffer (bottom layer) and put in scintillation tubes for radioactivity determination. Each condition was assayed in four replicates. An

aliquot of the cell suspension of each group was taken before glucose uptake assay and total lipid in these cells was extracted as follow: cell suspension was firstly mixed with 2.7 ml extraction solution (80% 2-propanol, 20% N heptane, 2% sulfuric acid vol/vol), then 1.2 ml N heptane and 0.8 ml distilled water was added, after mixing by vortex, the mixture was centrifuged at 22°C 1,000 rpm for 5 min. One ml of organic phase was taken to a pre-weighed tube and dried with nitrogen. Afterwards the tube with lipid was weighed again and total lipid weight from adipocytes could be calculated. The DPM values were normalized to the corresponding lipid weight.

2.2.3 Insulin-stimulated glucose uptake and AICAR-stimulated fatty acid oxidation (FAO) in skeletal muscles

Isolation of skeletal muscles, measurements of glucose uptake and FAO were performed as described previously (Chadt et al., 2015). *Extensor digitorum longus* (EDL) muscles were removed from anesthetized mice and incubated for 30 min at 30°C in vials containing pre-oxygenated (95% O_2/5% CO_2) Krebs-Henseleit buffer (KHB) containing 5 mM HEPES and supplemented with 5 mM glucose and 15 mM mannitol. All incubation steps were conducted under continuous gassing (95% O_2/5% CO_2) at 30°C and slight agitation. After recovery, muscles were transferred to new vials and incubated for 30 min in KHB with 5 mM HEPES, 15 mM mannitol and 5 mM glucose under basal condition or in the presence of 120 nM insulin (Actrapid, Novo Nordisk, Mainz, Germany) throughout the duration of the experiment. Muscles were then transferred to new vials containing pre-oxygenized KHB supplemented with insulin and 15 mM mannitol and incubated for 10 min. Thereafter, muscles were transferred to new vials containing pre-oxygenized KHB supplemented with 1 mM [^{3}H]2-deoxy-glucose (2.5 mCi/ml) and 19 mM [^{14}C]mannitol (0.7 mCi/ml) for 20 min. Muscles were immediately frozen in liquid nitrogen and stored at −80°C. Cleared protein lysates were used to determine incorporated radioactivity by scintillation counting. To assess palmitate oxidation, soleus muscles were incubated in pre-gassed KHB containing 15 mM mannitol, 5 mM glucose, 3.5% fatty acid-free BSA, 4 mCi/ml [^{3}H]palmitate and 600 µM unlabeled palmitate with or without 2 mM AICAR (5-Aminoimidazole-4-carboxamide ribonucleotide) at 30°C for 2 h. After absorption of fatty acids to activated charcoal, FAO was determined by scintillation measurement of tritiated water.

2.2.4 Muscle mitochondrial respiration and reactive oxygen species (ROS) emission

Ex vivo mitochondrial respiration and ROS emission was measured in freshly permeabilized soleus muscle using the Oxygraph-2k (Oroboros Instruments, Innsbruck, Austria) according to the method described previously (Jelenik et al., 2017a; Jelenik et al., 2014). Defined respiratory states were obtained by employing the following protocols: (i) tricarboxylic acid cycle (TCA)-linked respiration using

2 mM malate, 10 mM pyruvate (state 2, complex I), 2.5 mM ADP, 10 mM glutamate and (state 3, complex I), 10 mM succinate (state 3, complex I + II), 10 µM cytochrome c (mitochondrial membrane integrity check) and carbonyl cyanide-p-trifluoromethoxyphenylhydrazone (FCCP) (stepwise increments of 0.25 µM up to the final concentration of max. 1.25 µM, state u) and (ii) ß-oxidation-linked respiration using 2 mM malate, 1 mM octanoyl-carnitine (state 2, complex I + II), 2.5 mM ADP (state 3, complex I + II), 10 µM cytochrome c (mitochondrial membrane integrity check) and FCCP (stepwise increments of 0.25 µM up to the final concentration of max. 1.25 µM, state u). Addition of cytochrome c did not increase oxygen consumption indicating integrity of the outer mitochondrial membrane after saponin permeabilization.

Furthermore, the rate of ROS production was assessed simultaneously with respiration by measuring the H_2O_2 levels fluorometrically (O2k-Fluorescence Modul, Oroboros Instruments). In the presence of horse radish peroxidase (Sigma–Aldrich, MO, USA), Amplex Red (Amplex® Red, Invitrogen, Darmstadt, Germany) reacts with H_2O_2 to produce the red-fluorescent oxidation product resorufin (excitation/emission maxima of 571/585 nm, respectively). The same protocols were used as for respiration except for the addition of 5 nM oligomycin instead of cytochrome C and FCCP, to induce state 4°C.

2.2.5 Real-time quantitative polymerase chain reaction (qPCR)

Total RNA was extracted from frozen tissues with the RNeasy Mini Spin Kit (Qiagen, Hilden, Germany). RNA was quantified with Nanodrop 2000 (Thermo Scientific, Wilmington, USA). cDNA templates for qPCR were synthesized from 1 µg of total RNA using the GoScript Reverse Transcription System (Promega, Madison, WI, USA). qPCR was performed using Quantifast SYBR Green PCR Kit (Promega, Madison, WI, USA). Gene expression was evaluated using the ΔΔ-Ct method and Hprt, Rpl32 or Gapdh were used as housekeeping genes. Primer sequences are listed in Table 8.

2.2.6 Chronic variable Stress (Cvs)

The protocol for Cvs consists of five different stressors (warm swim, cold exposure, shaking, restraint and overnight isolation) applied in a random manner 2 per day for 15 days (Table 10). The stressors were applied in the morning between 8 – 10 a.m. and in the afternoon between 15 – 17 p.m. The protocol provides a varied stress exposure to avoid adaptations. Following, the list of stressors:

Stressors:	
Warm swim	20 min swimming in 30°C warm water
Cold exposure	1 h cold exposure at 4°C in individual cages without bedding
Shaking	1 h shaking at 100 rpm
Restraint	30 min restrain in a 50 ml tube with a hole to enable breathing
Overnight isolation	individual o/n isolation in large cages with ad libitum access to food and water

Table 10: Time schedule of Cvs protocol

Day 1 **am:** Cold exposure **pm:** Restraint	**Day 2** **am:** Warm swim **pm:** Shaking	**Day 3** **am:** Warm swim **pm:** Restraint	**Day 4** **am:** Cold exposure **pm:** Shaking & o/n isolation	**Day 5** **am:** Shaking **pm:** Warm swim
Day 6 **am:** Cold exposure **pm:** Restraint	**Day 7** **am:** Warm swim **pm:** Shaking	**Day 8** **am:** Cold exposure **pm:** Restraint & o/n isolation	**Day 9** **am:** Shaking **pm:** Warm swim	**Day 10** **am:** Cold exposure **pm:** Restraint
Day 11 **am:** Shaking **pm:** Cold exposure & o/n isolation	**Day 12** **am:** Warm swim **pm:** Restraint	**Day 13** **am:** Shaking **pm:** Warm swim	**Day 14** **am:** Cold exposure **pm:** Restraint	**Day 15** **am:** Warm swim **pm:** Cold exposure & o/n isolation

2.2.7 Genotyping of mice

Genotyping PCR were conducted with DNA from the tail tip. DNA were isolated with the Invisorb Genomic DNA Kit II (Invitek, Freiburg, Germany) according to manufacturer's instructions. PCR were performed with the use of Dream Taq Green DNA Polymerase Kit (Thermo Fisher Scientific, Darmstadt, Germany). Primer1 (5' GACTGTTCAGTCAGGGATTG 3') and Primer3 (5' ACAGGG TCT CAG GTT CAA AG 3') produced a 541 bp fragment of the wildtype *Fgf21* locus. Primer2 (5' CCCGTGATATTGCTGAAGAG 3') and Primer3 produced a 243 bp fragment of a mutant *Fgf21* locus (Figure 4).

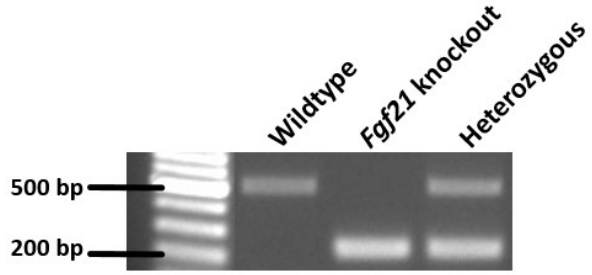

Figure 4: PCR products of wildtype, FGF21KO and heterozygous mice. Example of the PCR products of the FGF21 genotyping. The fragment of the wildtype locus has 541 base pairs and the fragment of the mutant Fgf21 locus has 243 base pairs.

2.2.8 *In vivo* analyses

Beside the daily control of the health status of each animal during the Cvs phase the body weight and food intake were measured, too. In the recovery phase the control by the experimentalist were conducted weekly. All *in vivo* analyses were performed in different cohorts directly after the Cvs intervention (short-term) or after three months of recovery (long-term).

2.2.8.1 Nuclear magnetic resonance (NMR)

Body composition was analyzed with nuclear magnetic resonance (NMR), (Whole Body Composition Analyzer, Echo MRI, TX, USA) to determine the fat and lean mass before, after 15 days following the end of the Cvs intervention and after the three months recovery phase. Body composition measurements are done by a sequence of radio pulses followed by recording of nuclear magnetic resonance responses (NMR Echos). The sequence contains several periodic Carr-Purcell-Meiboom-Gill parts (CPMG segments) separated by pauses of different duration. The characteristic (relaxation) time scales of the NMR responses (transverse, “T2” and longitudinal, “T1”, relaxation) which is specific for fat mass, lean mass or free water is analyzed. The final values of these parameters are calculated by linear regression due to the signal’s linear combination of fat mass, lean mass and free water signals and their respective relaxation rate (Kovner et al., 2010).

2.2.8.2 Intraperitoneal glucose tolerance test (i. p. GTT)

To analyze an impaired glucose metabolism an i.p. GTT was performed. 6 hours fasted WT and FGF21KO mice were injected intraperitoneally with glucose solution (2 g glucose/kg body weight). During the experiment the animals were single housed in fresh cages with *ad libitum* access to water. The blood glucose was monitored before and 15, 30, 60, and 120 minutes after glucose injection. The individual blood glucose was determined with a commercially available glucometer (Contour, Bayer AG, Leverkusen, Germany). The area under the curve (AUC) were calculated by the sum of all trapezoid areas. Each trapezoid between each time point were calculated by the formula for calculating

$$\text{area of a trapezoid} = (\text{Sum of 2 vertical sides}) / 2 \times (\text{Base of trapezoid}).$$

Accordingly, calculation of the AUC of an i. p. GTT were done by

$$\text{AUC} = \sum (\text{Sum of 2 blood glucose values}) / 2 \times (\text{timespan between these measuring point}).$$

2.2.8.3 Intraperitoneal insulin tolerance test (i. p. ITT)

To evaluate the integrity of hypothalamic-pituitary-adrenal (HPA) axis an i. p. ITT was performed. For this test, nonfasted WT and FGF21KO mice were injected intraperitoneally with insulin (1 IU/kg body weight) and blood glucose was measured from the tail tip at the time point 0, 15, 30, 60, 120 min. During the experiment the animals were single housed with *ad libitum* access to water. The food was removed during the 120 min of measurements. Calculation of AUC for i. p. ITT is described in 2.2.8.2.

2.2.8.4 Intraperitoneal pyruvate tolerance test (i. p. PTT)

The i. p. PTT is a variant of the i. p. GTT to assess gluconeogenesis. WT and FGF21KO mice were fasted for 16 hours to clear all glucose and glycogen storages. After fasting a pyruvate solution (1.5 g pyruvate/kg body weight) was injected and at the time point 0, 15, 30, 60, 120 min the blood glucose was measured from the tail tip. During the experiment the animals were single housed with *ad libitum* access to water. Calculation of AUC for i. p. PTT is described in 2.2.7.2.

2.2.8.5 Indirect calorimetry

In one cohort of mice the individual respiratory exchange ratio (RER) and spontaneous physical activity (SPA) were determined via a customized calorimetric system (TSE PhenoMaster, TSE systems, Bad Homburg, Germany). Measurements were conducted every 30 minutes for a 3 days period. SPA measurements were taken with a non-invasive infra-red based light beam system and the RER measurements through O_2 consumption (VO_2) and CO_2 production (VCO_2) quantification. The RER were automatic calculated by the system with the following formula:

$$RER = VCO_2 / VO_2$$

Energy expenditure (EE) were calculated from the VO_2 normalized by body surface:

$$EE = VO_2 / kg^{0.75}$$

Shown mean ± SD in results were calculated from the individual 12 hours mean of light or dark cycle respectively.

2.2.9 Analysis of hepatic triglyceride content

Triglyceride content in tissues was analyzed by using Triglycerides TRIGS-Kit (Randox Triglycerides with a range of 0.02 – 11.4 mmol/l, RANDOX Laboratories, Antrim, United Kingdom) according to the manufacturer's protocol. For triglyceride isolation, frozen tissues were (20-30 mg) were added to 1.5 ml of a 2:1 (v/v) chloroform/methanol mix and subsequently lysed for 4 min at 25,000 rpm via TissueLyser (Qiagen, Hilden, Germany). To extract the triglycerides samples were horizontal inverted for 2h at RT. Afterwards, 200 µl of ddH_2O were added to the samples, mixed and centrifuged for 15

min at 3,300 x g in order to separate the upper aqueous phase from the lower organic phase. Subsequently, 500 µl of the organic phase were transferred to a new vial and the chloroform was evaporated by centrifugation in a Speedvac centrifuge (Eppendorf, Hamburg, Germany) for 1h at RT. The obtained pellet was re-suspended in 1 ml chloroform, mixed well and duplicates of 25µl of the suspension were transferred to two new tubes. The chloroform was evaporated again. The detection solutions from the kit were prepared and 150µl were added to the samples and incubated for 10 min at RT. After incubation, 130 µl were transferred to a 96-well plate and measurement of the duplicates was performed photometrically at a wavelength of 490 nm with Tecan Infinite 200 reader. Subsequently, values were normalized by introduced amount of tissue.

2.2.10 Primary hepatocyte isolation, purification and cultivation

Primary hepatocytes of each experimental group were isolated from mouse liver via two-step perfusion. The isolation procedure was initially describes by Akie and Cooper, 2015 (Akie and Cooper, 2015). After scarification of mice by CO_2 asphyxiation the superior *vena cava* was clamped to avoid pressure lost and perfusion of thoracical parts. Subsequently, a needle was inserted in the inferior *vena cava* and the liver were perfused with 5 ml/min of HBSS perfusion buffer (2.1.5) for approximately 3 - 4 minutes. To release the perfusion buffer, the portal vein was cut. After complete blood depletion the liver tissue turns from red to beige and the liver was digested via perfusion with collagenase medium (2.1.6) containing 100 U/ml collagenase for approximately 4 - 5 minutes. Afterwards, the liver appears swollen and pinkish. Following, the liver was dissected from the mouse and the gall bladder was removed. The dissected liver was covered with isolation medium (2.1.6) and scraped with a blade until the whole liver was transferred into a cell suspension. The hepatic cell suspension was filtered with a 70 µm cell strainer and the centrifuged at 50x g, 5 min, 4°C. Subsequently, the pellet was washed by centrifugation with plating medium (2.1.6). To isolate viable hepatocytes from non-viable cells, a density separation with a 90% Percoll gradient (2.1.5) (50x g, 10 min, 4°C) with low acceleration and deceleration was performed. After a final washing step cell number and viability was evaluated through trypan blue staining and using a Neubauer chamber for cell counting. Isolated hepatocytes were seeded in assay specific densities on rat tail type-I collagen coated plates and cultured in serum-free medium (2.1.6) over night at 37°C and 5% CO_2.

2.2.11 *Ex vivo* experiments in murine primary hepatocytes

All *ex vivo* experiments were conducted in primary hepatocytes from all groups directly after the Cvs intervention and after a three months recovery phase. Depending on the assay, after overnight

incubation in serum-free medium the assay was conducted in the serum-free medium or specific assay medium.

2.2.11.1 Glucose production assay

For analyzing the production of glucose in primary hepatocytes the cells were seeded in a 12-well plate with a density of $2.5x10^5$ cells/well. To determine the short- and long-term effects of Cvs on the glucose secretion from hepatocytes of WT and FGF21KO mice the serum-free medium was replaced by a glucose production medium (2.1.6). Half of the primary hepatocytes were pre-treated 1 hour with 10 nM insulin before they were treated with or without 2mM sodium lactate/pyruvate for further 4 hours (37°C, 5% CO_2). Afterwards, cell culture supernatants were collected and glucose concentration was determined by an enzymatic, colorimetric glucose assay kit (2.1.7) according to manufactures instructions.

2.2.11.2 *De novo* lipogenesis (DNL) assay

The short- and long-term consequences of Cvs on lipogenesis of WT and FGF21KO mice were evaluated by analyzing the DNL in primary hepatocytes. Cells were seeded in a 24-well plate with a density of $9x10^4$ cells/well according to Akie et al. and Jelenik et al. (Akie and Cooper, 2015; Jelenik et al., 2017b) cells were incubated overnight with or without 100 nM insulin in serum-free medium (37°C, 5% CO_2). Following, 0.5 µCi ^{14}C-acetate in 10 µM acetate solution was added to the medium. After four hours treatment (37°C, 5% CO2) cells were washed two times with 1x PBS and lysed in 120 µl 0.1 M HCl by scraping. To extract lipids from the lysates a 2:1 chloroform/methanol solution were used for 5 minutes. After adding 250 µl H_2O the mixture was centrifuged (3,000x g, RT, 10 min). The lower lipid containing phase were taken with a syringe and transferred to 3 ml liquid scintillation fluid (Rotiszint®, Roth) to analysing the incorporated ^{14}C into lipids of hepatocytes.

2.2.11.3 Fatty acid oxidation (FAO) assay

The impact of Cvs on the FAO in primary hepatocytes from WT and FGF21KO mice was assessed by analyzing the release of radioactive $^{14}CO_2$. Briefly, cells were seeded in a 48-well plate with a density of $3x10^4$ cells/well and after overnight serum starvation cells were treated with or without 40 µM etomoxir to inhibit the mitochondrial FAO. A filter paper soaked with 50 µl 1 M NaOH with a surface of 4 cm^2 was placed next to each cell well. The cell wells and their corresponding filter wells are connected via a tube for gas exchange. Afterwards, cells were exposed to a FAO working solution containing 0.3 µCi ^{14}C-palmitic acid, 57 µM fatty acid free BSA and 9 µM L-carnitin in an appropriate volume of serum-starvation medium. Then, the cell culture plate was clamped in an oxidation chamber

at 37°C, 5% CO_2. After 4 hours incubation HCl with a final concentration of 0.5 M were added into the cell wells to release all CO_2 from the supernatant and oxidation chamber were then incubated overnight at 37°C, 5% CO_2. Due to the soaked filter the released CO_2 reacts with the NaOH to sodium carbonate which is bound in the filter paper. On the next day, each filter was transferred to 3 ml liquid scintillation fluid (Rotiszint®, Roth) and the radioactive counts were analyzed.

2.2.11.4 Fatty acid uptake assay

To investigate the fatty acid uptake in primary hepatocytes from WT and FGF21KO mice after Cvs and after three months recovery the cells were seeded in a 24 well plate with a density of $1x10^5$ cells/well. After overnight incubation the cells were washed 3 times with pre-warmed KRH/0.1% fatty acid free BSA (2.1.4) and once with BSA free KRH. Afterwards cells were incubated in 1ml KRH/40 µmol/l fatty acid free BSA. For starting the palmitate uptake assay 1 ml transport buffer (2.1.6) containing ^{3}H-palmitate was added to the cells for 15 minutes at 37°C, 5% CO_2. To stop the uptake the medium were aspirated and the cells were washed three times with ice cold KRH/0.1% BSA. Then the cells were lysed in 120 µl 0.1 M HCl and 100 µl of the lysate were transferred to 3 ml liquid scintillation fluid (Rotiszint®, Roth). The incorporated ^{3}H-palmitate were analyzed by radioactive counting.

2.2.11.5 Investigation of mitochondrial respiration and glycolysis

The cellular mitochondrial respiration and glycolysis were evaluated by using the Seahorse XF^{e}96 extracellular flux analyzer (2.1.3) as previously described (Blumensatt et al., 2017). This technology enables the recording of the oxygen consumption rate (OCR) and extracellular acidification rate (ECAR) in living cells. To analyze the impact of Cvs on primary hepatocytes from WT and FGF21KO mice the cells were seeded in a density of $1x10^4$ cells/well in an XF^{e}96 cell culture well plate. To examine the mitochondrial respiration from OCR, cell medium was switched to DMEM based unbuffered Seahorse mitochondrial respiration assay medium (2.1.6) (pH 7.4 at 37°C) after overnight serum starvation and cells were incubated in a CO_2-free incubator at 37°C, 1h before starting the experiment. After basal OCR measurements successive injections of 1 µM oligomycin, 0.5 µM FCCP and 1 µM of antimycin A and rotenone were conducted automatized by the Seahorse XFe96 extracellular flux analyzer. OCR measurements were taken in a cycle of 3 for basal condition and after each injection.

For measuring ECAR for evaluating glycolysis of hepatocytes, the medium was changed to unbuffered Seahorse glycolysis assay medium (2.1.6) after overnight serum starvation. ECAR was measured under basal conditions and after injection of 10 mM glucose in 3 cycles respectively. Each reading point contains 3 minutes mixing and 3 minutes measurement. Recorded data were evaluated with wave software (2.1.9). After all OCR and ECAR measurements the cells in each XF^{e}96 cell culture well plate

was lysed and the protein content were determined with Pierce BCA Protein Assay Kit. OCR and ECAR of each well were normalized by total protein content.

2.2.12 Insulin stimulation and sample collection

One cohort of including WT and FGF21KO mice either stressed or not were used for tissue and blood collection. For tissue harvesting the mice were fasted 5 hours and one half of the mice were injected intraperitoneally with insulin (1 IU/kg body weight) the other half with saline respectively. After 10 minutes animals were sacrificed by CO_2 asphyxiation and blood were collected by cardiac puncture in 0.1 M EDTA coated tubes. Afterwards liver, gonadal white adipose tissue (gWAT), *gastrocnemius* muscle and brown adipose tissue (BAT) were dissected, snap frozen in liquid nitrogen and stored on -80°C. Blood samples were centrifuged for 10 min at 2,000x g at 4°C in EDTA tubes (0.1M). The resulting plasma (supernatant) were collected, aliquoted in 100 µl and stored at -80°C for further analyses.

2.2.13 Plasma biochemistry analyses

Blood samples were collected immediately after CO_2 asphyxiation by cardiac puncture in EDTA tubes (0.1 M) and stored on ice. After liver perfusion and dissection, blood samples were centrifuged at 2,000x for 10 min at 4°C. The resulting plasma in the supernatant were collected, aliquoted in 100µl and stored in -80°C until further analyses.

2.2.13.1 Enzyme-linked Immunosorbent Assay (ELISA)

To analyze the short- and long-term impact of Cvs associated with the knockout of FGF21 on plasma levels of the stress hormone corticosterone and the metabolic active growth factor FGF21 specific ELISA for each molecule were performed according to manufacturer's instructions.

2.2.13.2 Determination of tri-acylglycerides (TAG) in plasma

Triglyceride content in plasma was determined by kit-colorimetric based assays according to the manufacturer's instructions (Randox Triglycerides with a range of 0.02 – 11.4 mmol/l, RANDOX Laboratories, Antrim, United Kingdom).

2.2.13.3 Analysis of fatty acid composition in plasma

Fatty acid composition in plasma were analyzed by gas chromatography. For sample preparation, 25 µl of 1 µg/µl C15:0 fatty acid was added to 100 µl of EDTA plasma. Afterwards, samples were mixed with 0.5 ml extraction solution containing of 2-Propanol/ 0.5 M H_2SO_4 [40:1 (v/v)]. After mixing, 4 ml of n-hexan were added and mixed again. Subsequently, samples were centrifuged for 5 min at 1,400x

g. The resulting organic phase was transferred in a new reaction tube and completely evaporated by nitrogen. Then 100 µl of MeOH/CH_3COCl [100:7 (v/v)] was added dropwise to avoid dehydration of the sample and then boiled for 30 minutes at 90°C without drying the samples. Afterwards, samples were again completely evaporated by nitrogen at 50-60°C and the residue was solubilized in 100 µl n-hexan. Then samples were analyzed by gas chromatography (Gas chromatograph 6890N Network GC System, Agilent Technologies, Santa Clara, CA, USA).

2.2.13.4 Measurement of metabolic hormones and cytokines in plasma

A commercially available multiplex bead-based immunoassay (Bio-Plex Pro™ Mouse Diabetes 8-plex; Bio-Rad Laboratories, Bio-Rad, Munich, Germany) was used to determine plasma levels of leptin, resistin, glucagon, PAI-1, glucagon-like-peptide 1 (GLP-1), gastric inhibitory peptide (GIP), ghrelin and insulin. Furthermore, two analogous bead based immunoassays (Bio-Plex Pro™ Mouse Cytokine Group 1 23-plex and Group 2 9-plex; Bio-Rad Laboratories, Bio-Rad, Munich, Germany) were utilized to measure plasma levels of interleukin (IL)1a, IL1b, IL2, IL3, IL4, IL5, IL6, IL9, IL10, IL12(p40), IL12(p70), IL13, IL15, IL17, IL18, eotaxin (CCL11), granulocyte colony stimulating factor (G-CSF), granulocyte macrophage colony stimulating factor (GM-CSF), interferon gamma (IFN-γ), platelet-derived growth factor-inducible protein (KC), monocyte chemotactic protein-1 (MCP-1), macrophage inflammatory protein alpha (MIP-1α), macrophage inflammatory protein 1 beta and 2 (MIP-1β and 2), RANTES (CCL5), tumor necrosis factor alpha (TNF-α), Basic fibroblast growth factor (FGF basic), Leukemia inhibitory factor (LIF), macrophage colony-stimulating factor (M-CSF), monokine induced by Gamma-Interferon (MIG), Platelet-derived growth factor two B subunits (PDGF-BB) and vascular endothelial growth factor (VEGF). Analyses were performed using a Bioplex 200 suspension array system (Bio-Rad, Munich, Germany) according to the manufacturer's instructions. Cell lysates were handed to the Proteomics facility at the ICB for the MilliPlex immunoassay measurement. Analyses raw data were returned for analyses. Protein concentrations were calculated from the appropriate optimized standard curves using Bio-Plex Manager software version 6.0 (Bio-Rad, Munich, Germany).

2.2.14 Cell and tissue lysis and protein determination

Before analyzing protein abundance primary hepatocytes or dissected tissue were lysed in corresponding lysis buffer (2.1.5). Hepatocytes were lysed in assay specific lysis buffer including protease and phosphatase inhibitors for determining protein abundance via bead based MilliPlex immunoassay (Cell Signaling Multiplex Assay; Merck, Darmstadt, Germany). Dissected tissues from mice either treated with saline or insulin (1U/kg body weight) before sacrification were lysed in RIPA buffer containing protease and phosphatase inhibitors.

For protein abundance analyses frozen hepatocytes or tissues were homogenized in corresponding lysis buffer with a pestle in a 1.5 ml reaction vial and then incubated in an overhead roller for 30 min at 4°C. Afterwards, cell homogenates were lysed by ultra-sonic exposure with the Bioruptor® pico sonicator (Diagenode, Seraing, Belgium). Finally, lysates were centrifuged for 10 min at 20,000x g and 4°C. Supernatant were transferred in a new reaction vial and protein concentration was determined with the Bicinchoninic (BCA)-assay (Thermo Scientific, Schwerte, Germany) according to the manufacturers' instructions.

2.2.15 Cell based activity assays of primary hepatocytes

To evaluate the short- and long-term influence of Cvs in WT and FGF21KO mice as well as the effect of FGF21 knockout per se on sirtuin, methyltransferase, histone acetyl transferase (HAT) and histone deacetylase (HDAC) activity as well as the NAD^+/NADH ratio in hepatocytes, cells were incubated overnight in serum-free medium (2.1.6) (37°C, 5% CO_2). Afterwards, cells were scraped in ice cold 1x PBS, transferred in a 1.5 ml reaction vial, short centrifuged and after 1x PBS aspiration stored in -20°C until lysis. Frozen pellets of primary hepatocytes were lysed in 1% NP40 in 1x PBS in a 1.5 ml reaction vial and incubation for 15 minutes on ice. After homogenization with a pestle all samples were rotated for 30 min at 4°C. Then homogenates were centrifuged (10 min, 4°C, 14,000x g). The resulting supernatant were transferred in a new 1.5 ml reaction vial and the protein content was evaluated via BCA-assay (2.2.14). Samples were stored at -20°C until further measurements. All assays were conducted in opaque-walled 96-well plates.

2.2.15.1 Analysis of sirtuin (SIRT) activity

Sirtuins belong to the NAD^+-dependent histone deacetylases class III. After lysis (2.2.15) 5 µg of protein used to analyzing SIRT activity via the commercially luminescence-based SIRT-Glo™ assay system (Promega, Heidelberg, Germany). According to manufacturer's instructions luminescence was measured 15 min after adding the protease and luciferase mixture to the lysates by the Tecan Infinite 200 reader. The luminescence is directly proportional to deacetylase activity.

2.2.15.2 Analysis of methyltransferase activity

Methyltransferase activity were measured in whole cell lysates from primary hepatocyte (2.2.15) by MTase-Glo™ Methyltransferase assay (Promega, Heidelberg, Germany) according to manufacturer's instructions. For the luminescence-based assay 1 µg of total protein from each sample were used and luminescence were measured by using Tecan Infinite 200 reader. The luminescence is directly proportional to methyltransferase activity.

2.2.15.3 Analysis of histone acetyltransferase (HAT) and histone deacetylase (HDAC) activity

The activity of HAT and HDAC were measured by luminescence-based HAT Activity Assay Kit II (PromoCell GmbH, Heidelberg, Germany) and HDAC-Glo™ I/II Assays and Screening System (Promega, Heidelberg, Germany). For both assays 5 µg of total protein from previously described hepatocyte lysates (2.2.15) were utilized, respectively. Luminescence were measured by using Tecan Infinite 200 reader. The luminescence is directly proportional to HAT or HDAC activity.

2.2.15.4 Analysis of nicotinamide adenine dinucleotide (NAD) content

The ratio of oxidized NAD^+ and reduced NADH were determined by NAD^+/NADH-Glo™ Assay (Promega, Heidelberg, Germany) by separated measurements of each molecule. The assay benefits from the heat stability of NAD^+ in acid solutions and NADH in basic solutions. In both measurements 5 µg of total protein lysate were utilized and either pre-treated with 0.4 M HCl for NAD^+ or with a 1:1 HCl/Tris (v/v) solution for NADH examination. NAD^+/NADH detection was performed according to manufacturer´s instructions and luminescence were measured by using Tecan Infinite 200 reader.

2.2.16 Bead based MilliPlex Akt/mTOR total and phosphor immunoassay

With the bead based MilliPlex immunoassay technology is it possible to analyze a distinct signalling pathway in one well. The Akt/mTOR total immunoassay quantifies the protein abundance of the following enzymes: Akt: Protein kinase B, GSK3α + β: Glycogen synthase kinase 3α + β, IGF1R: Insulin growths factor 1 receptor, IR: Insulin receptor, IRS1: Insulin receptor substrate 1, mTOR: mammalian target of rapamycin, p70S6K: Ribosomal protein S6 kinase, PTEN: Phosphatase and tensin homolog, RPS6: Ribosomal protein S6, TSC2: Tuberous Sclerosis Complex 2. The Akt/mTOR phospho immunoassay quantify the phosphorylation status of the following enzymes: Akt (Ser473), GSK3α (Ser21), GSK3β (Ser9), IGF1R (Tyr1135/Tyr1136), IR (Tyr1162/Tyr1163), IRS1 (Ser312), mTOR (Ser2448), p70S6K (Thr412), PTEN (Ser380), RPS6 (Ser235/Ser236), TSC2 (Ser939). Tissue or hepatocytes were lysed in assay specific lysis buffer containing protease and phosphatase inhibitors According to manufacturer's instructions (2.2.14). For each measurement 10 µg of total protein lysate were utilized. Cell lysates were handed to the Proteomics facility at the IKBP for the MilliPlex immunoassay measurement. Analyses raw data were returned for analyses. After the abundance analysis the ratio of phosphorylation to total protein were calculated.

2.2.17 Detection of membrane bound proteins by Western blot

Tissue lysates were diluted in ddH_2O and mixed with 4x Laemmli buffer (2.1.5) containing SDS (8%, v/v) and dithiothreitol (DTT) (400 mM) to a final protein concentration of 1µg/µl. This mixture is boiled for 5 minutes at 95°C to denature the proteins and then 20 µg of protein were loaded on a polyacrylamide gel for sodium dodecyl sulfate–polyacrylamide gel electrophoresis (SDS-PAGE). According to the molecular weight of the target protein the percentage of acrylamide content in the separating gel (10 – 14%) were chosen (2.1.8). The gel was applied to a constant voltage until the required resolution was reached. To control the running conditions and the expected protein size a pre-stained marker (2.1.4) was loaded in an individual well. After SDS-PAGE the proteins were transferred from the acrylamide gel to a nitrocellulose membrane via tank blotting technique. A constant current of 0.2 A was applied to the tank and the transfer times were chosen according to the molecular weight of the proteins of interest (2.1.8). Following blotting, the membrane was briefly washed in TBS-T and then blocked in 5% BSA/TBS-T. For protein detection epitope specific primary antibodies and species-specific IgG horse radish peroxidase (HRP)-linked secondary antibodies were used for staining and detection of the respective proteins. The respective concentrations of the primary antibodies were diluted in 5% BSA/TBS-T and incubated overnight at 4°C. Secondary antibodies were diluted 1:10.000 in 5% BSA/TBS-T and incubated 1 hour at RT. The antibody concentration depends on the target protein (2.1.8). The protein detection was carried out in accordance to manufacturer's instructions with enhanced chemiluminescence (ECL) Pro or Ultra (PerkinElmer, Waltham, MA, USA) and a ChemiDoc System (Bio-Rad, Munich, Germany). The light sensitive camera of the ChemiDoc System detects the chemiluminescent light that results from a HRP catalyzed reaction of the reagents, the intensity is finally quantified with Image Lab analysis software (Bio-Rad, Munich, Germany).

2.2.18 Statistical analyses and software

All data are presented as mean ± standard deviation (SD). Values were analyzed for statistically significant differences applying two-tailed unpaired t-tests or ANOVA analyses, $p<0.05$ was considered significant using GraphPad Prism Version 8.2 (GraphPad Software, San Diego, CA, USA). The applied statistical test for each data set is indicated in the figure legend.

3. RESULTS

3.1 Association of FGF21 and metabolic regulation after chronic variable stress (Cvs)

As long as not noted elsewhere, the following results of this work from 3.1.1 to 3.1.6 were adopted word by word from the results section of the publication Jelenik*, Dille* et al. (2018; *shared first author), which was published 2018 in Molecular Metabolism. Results and data sets performed and analyzed by co-authors are marked and cited in the respective figure legend and in Table 15. If changes to the original text were necessary to facilitate readability, these changes are highlighted as underlined.

3.1.1 Plasma corticosterone levels increase while body weight and lean mass decrease post Cvs exposure, but not three months post-Cvs intervention

Twelve weeks old male C57BL/6 mice were exposed to a random series of stressors for 15 days (Cvs) whereas corresponding unstressed mice served as controls (Ctrl) (Figure 5A). Cvs substantially increased plasma corticosterone levels (Figure 5B), decreased body weight and lean mass (Figure 5C, D) but unchanged fat mass (Figure 5E), mRNA expression of hypothalamic neuropeptide *Npy*, *Pomc* and *Agrp* (Supplementary Figure 1C) and plasma adrenaline (Supplementary Figure 1D). Adrenal weight was increased after Cvs (Supplementary Figure 1E). From 23 analyzed plasma cytokines, anti-inflammatory IL10 was increased while pro-inflammatory cytokines eotaxin and RANTES were decreased in Cvs (Supplementary Table 2). In contrast, three months post Cvs, plasma corticosterone, body weight, body composition (Figure 5F–I), expression of hypothalamic neuropeptides and plasma adrenaline (Supplementary Figure 1C) were not different between stressed mice (Cvs3m) and age-matched non-stressed controls (Ctrl3m). Colony-stimulating factor 3 in plasma was elevated, all other cytokines were not different between Cvs3m and Ctrl3m (Supplementary Table 2).

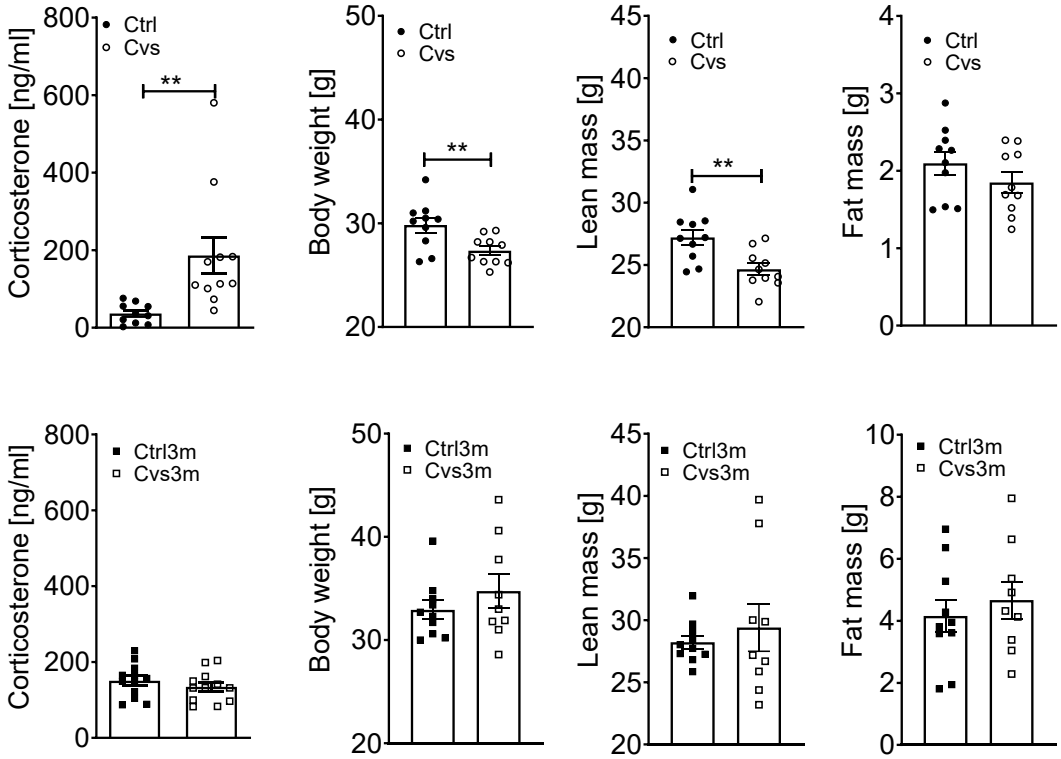

Figure 5: Plasma corticosterone and body composition analysis from Cvs and three months post Cvs mice. Experimental protocol: C57BL/6 male mice were exposed to chronic variable stress (Cvs) for 15 days or to no intervention (Ctrl) (A). Mice underwent respective *in vivo* and *ex vivo* analyses right after Cvs intervention or three months post Cvs intervention (Cvs3m) and compared to the age-matched controls (Ctrl and Ctrl3m, respectively). Corticosterone levels in plasma from mice fasted for 4 h (B) n = 10–12. Body weight, lean and fat mass data from Cvs (C–E) and Cvs3m mice (F–H) n = 9–12. Data presented as means ± s.e.m. Statistical analyses were done by two-tailed unpaired Student's t-test (B–G). ***p < 0.01*.

3.1.2 Cvs leads to long-term improvements in whole-body glucose disposal

Fasted plasma glucose was decreased while insulin was unchanged upon Cvs (Supplementary Figure 2). Steady-state blood glucose levels (~120 mg/dl) during hyperinsulinemic-euglycemic clamps were similar among all groups (Figure 6A, D). Basal endogenous glucose production (EGP) was lower after Cvs (Figure 6B) in line with lower fasting blood glucose levels (Supplementary Figure 2A). Whole-body insulin-stimulated glucose disposal, expressed as glucose infusion rate (GIR), was comparable between both groups. However, insulin-mediated suppression of EGP was lower, indicating hepatic insulin resistance, while insulin-stimulated peripheral glucose disposal (Rd) was higher in Cvs compared to Ctrl mice (Figure 6C).

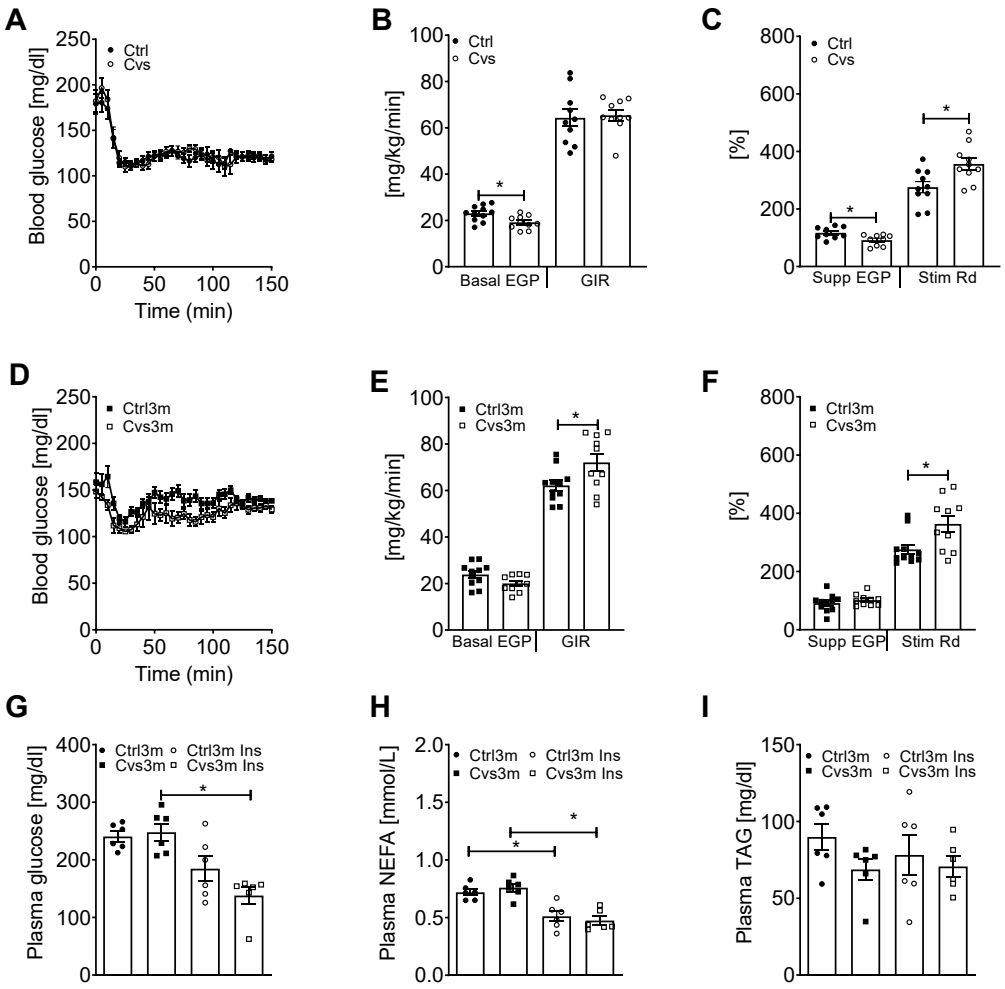

Figure 6: *In vivo* insulin sensitivity analysis from Cvs and three months post Cvs mice. Blood glucose levels before and during the hyperinsulinemic-euglycemic clamp (A, D) n = 10–11, endogenous glucose production (EGP) and glucose infusion rate (GIR) under basal conditions (B, E) n = 9–11, as well as insulin-mediated suppression of EGP and stimulation of glucose disposal (Rd) (C, F) in mice post Cvs (A–C) and three months post Cvs (Cvs3m) (D–F) compared to the age-matched controls (Ctrl and Ctrl3m, respectively) n = 9–11. Blood biochemical parameter after bolus injection of insulin to Cvs3m and Cvs3m mice; plasma blood glucose (G), plasma NEFA (H) and plasma triglyceride (I) n = 6. Data presented as means ± s.e.m. Statistical analyses were done by two-tailed unpaired Student's t-test (A–F) or by Two-Way ANOVA followed by Bonferroni post hoc (G–I). *$p < 0.05$, **$p < 0.01$, ***$p < 0.001$. Experiments and analyses of A-F were performed by Dr. Tomas Jelenik.

Three months post Cvs, fasted plasma insulin and glucose levels were comparable between Cvs3m and Ctrl3m (Supplementary Figure 2). Basal EGP tended to be lower in Cvs3m mice ($p = 0.055$, Figure 6E). Surprisingly, GIR was higher in the Cvs3m mice (Figure 6E). This was accounted for the persistent increase in insulin-stimulated Rd (Figure 6F), while the suppression of EGP was unchanged in Cvs3m (Figure 6F). These results indicate enhanced insulin sensitivity in peripheral insulin responsive tissues, such as skeletal muscle and adipose tissue, even three months post Cvs intervention. Also intraperitoneal insulin injection led to a more pronounced decrease in plasma glucose in Cvs3m mice (Figure 6G), while the decrease in plasma NEFA was similar between Cvs3m and Ctrl3m (Figure 6H). Plasma triglycerides were not affected by insulin and were similar between Cvs3m and Ctrl3m mice (Figure 6I).

3.1.3 Cvs enhances basal fatty acid oxidation, but has no effect on the insulin-stimulated glucose uptake in skeletal muscle

Next glucose and lipid metabolism were determined in *extensor digitorum longus* (EDL) skeletal muscle. Both basal and insulin-stimulated glucose uptake were similar between the Cvs and Ctrl mice (Figure 7A). Three months post Cvs exposure, both basal and insulin-stimulated glucose uptake were reduced in EDL muscle to a similar extent, but no differences were observed between muscles from Cvs3m mice and Ctrl3m animals (Figure 7B). Analysis of insulin signalling proteins revealed induction of pAKT^{Ser473} in response to insulin but no differences between Cvs3m and Ctrl3m (Figure 7C, D). However, no differential activation of pAMPK^{Thr172} upon insulin stimulation was observed between the different conditions (Figure 7C, E).

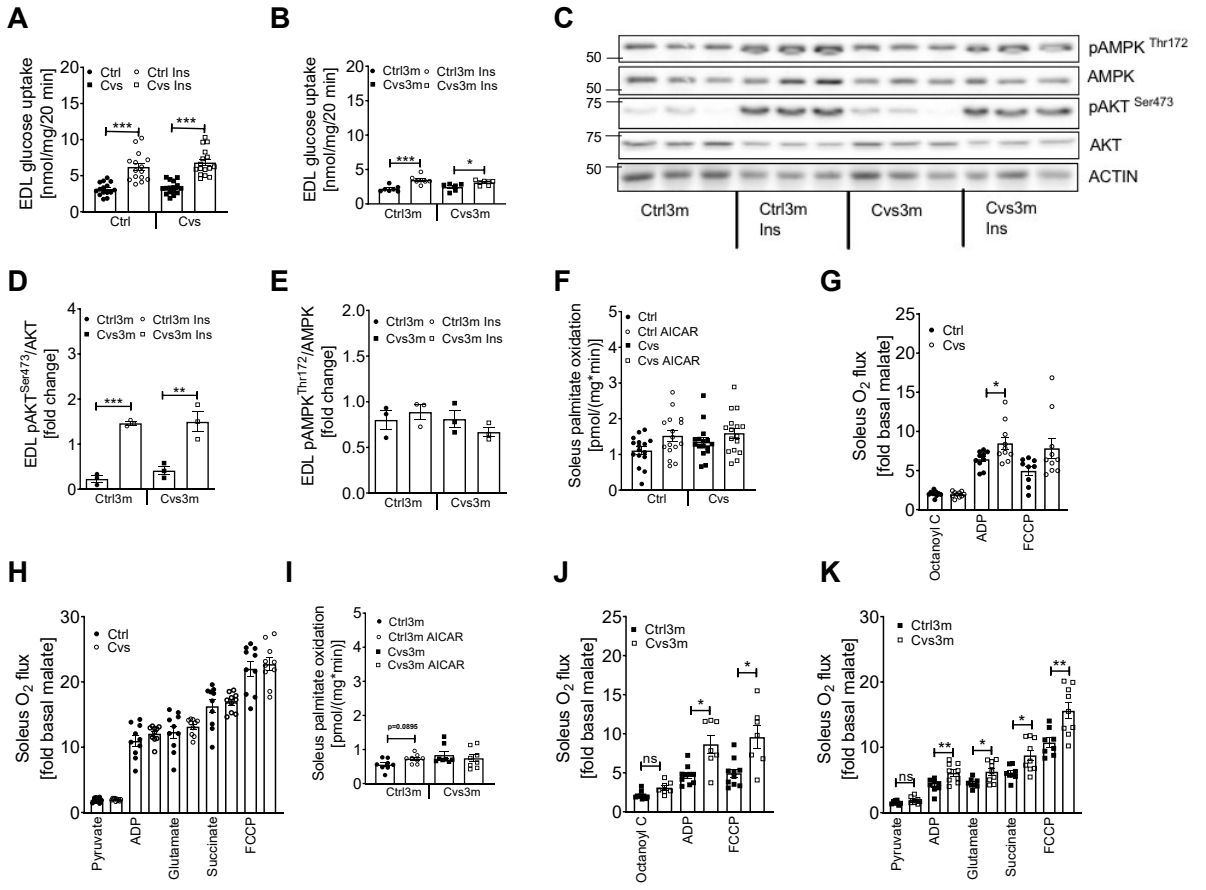

Figure 7: Effect of Cvs and long-term effects of Cvs intervention on muscle metabolism. *Ex vivo* glucose uptake under basal and insulin-stimulated conditions in intact isolated EDL muscle from Cvs (A) and three months post Cvs (Cvs3m) mice (B) compared to the age-matched controls (Ctrl and Ctrl3m, respectively). Representative western blot of insulin stimulated pAKT and pAMPK from EDL muscle obtained from 3 Cvs3m and Ctrl3m mice collected after *ex vivo* glucose uptake assay (C) and representative densitometric analysis (D, E). *Ex vivo* FAO in intact isolated Soleus muscle under basal and AICAR-stimulated conditions (F, I), ß-oxidation-linked respiration (G, J), TCA-linked respiration (H, K) in Soleus muscle. Data presented as mean ± s.e.m; two-tailed unpaired Student's t-test or by Two-Way ANOVA followed by Bonferroni post hoc (A-B, D-F and I) *$p < 0.05$, **$p < 0.01$, ***$p < 0.001$, FAO and mitochondrial respiration n = 7–18, n = 6–16 in EDL muscle glucose uptake and n = 3 for western blot analysis. Experiments and analyses of G, H, J and K were performed by Dr. Tomas Jelenik. Experiments in A, B, F and I were conducted by Dr. Zhou Zhou and Dr. Sabrina Müller-Lühlhoff.

Further lipid catabolism in skeletal muscle were explored by measuring [3H]-palmitate oxidation in the soleus muscle. Only subtle changes in AICAR-stimulated fatty acid oxidation in the soleus from Cvs (Figure 7F) as well as Cvs3m mice (Figure 7I) were observed. On the other hand, state 3 (ADP) ß-oxidation-linked respiration in soleus from Cvs mice was increased (Figure 3G), while no changes in TCA cycle-linked respiration were observed (Figure 7H). Moreover, triglycerides were unchanged in gastrocnemius muscle (Supplementary Figure 1A). Furthermore, both ß-oxidation-linked respiration as well as TCA-cycle-linked respiration were increased in soleus from Cvs3m mice (Figure 7J, K). In line with these observations, triglycerides in gastrocnemius muscle were decreased in Cvs3m mice (Supplementary Figure 1B). Mitochondrial mass, assessed as citrate synthase activity as well as TCA-cycle- and ß-oxidation-linked H_2O_2 production from permeabilized soleus muscle were not different among the groups (Supplementary Figure 3).

3.1.4 Enhanced insulin-stimulated glucose uptake and browning markers in white adipose cells/tissue from mice three months post Cvs intervention

In white adipose cells (WAC), basal and insulin-stimulated glucose uptake was not different after Cvs (Figure 8A). Conversely, three months post Cvs insulin-stimulated glucose uptake was increased in WAC from Cvs3m compared to Ctrl3m (Figure 8B). Higher glucose uptake in WAC from Cvs3m mice was accompanied by the enhanced insulin signalling. Insulin-stimulated $pAKT^{Ser473}$ was markedly elevated in adipose tissue from Cvs3m mice (Figure 8C,D) in parallel with the higher GLUT1 protein (Figure 8F) and mRNA (Figure 8G) levels, while $pAMPK^{Thr172}$ (Figure 8E) and *Slc1a4* mRNA expression (Figure 8H) was unchanged. Moreover, in epididymal white adipose tissue (eWAT) from Cvs3m mice, the genes regulating adaptive thermogenesis were substantially induced, including uncoupling protein 1 (*Ucp1*), PR domain containing 16 (*Prdm16*), bone morphogenetic protein 7 (*Bmp7*), PPARG coactivator 1 alpha (*Pgc1a*), a key regulator of mitochondrial gene expression and carnitine palmitoyltransferase 1b (*Cpt1b*), a rate-limiting enzyme for fatty acid oxidation (Figure 8I).

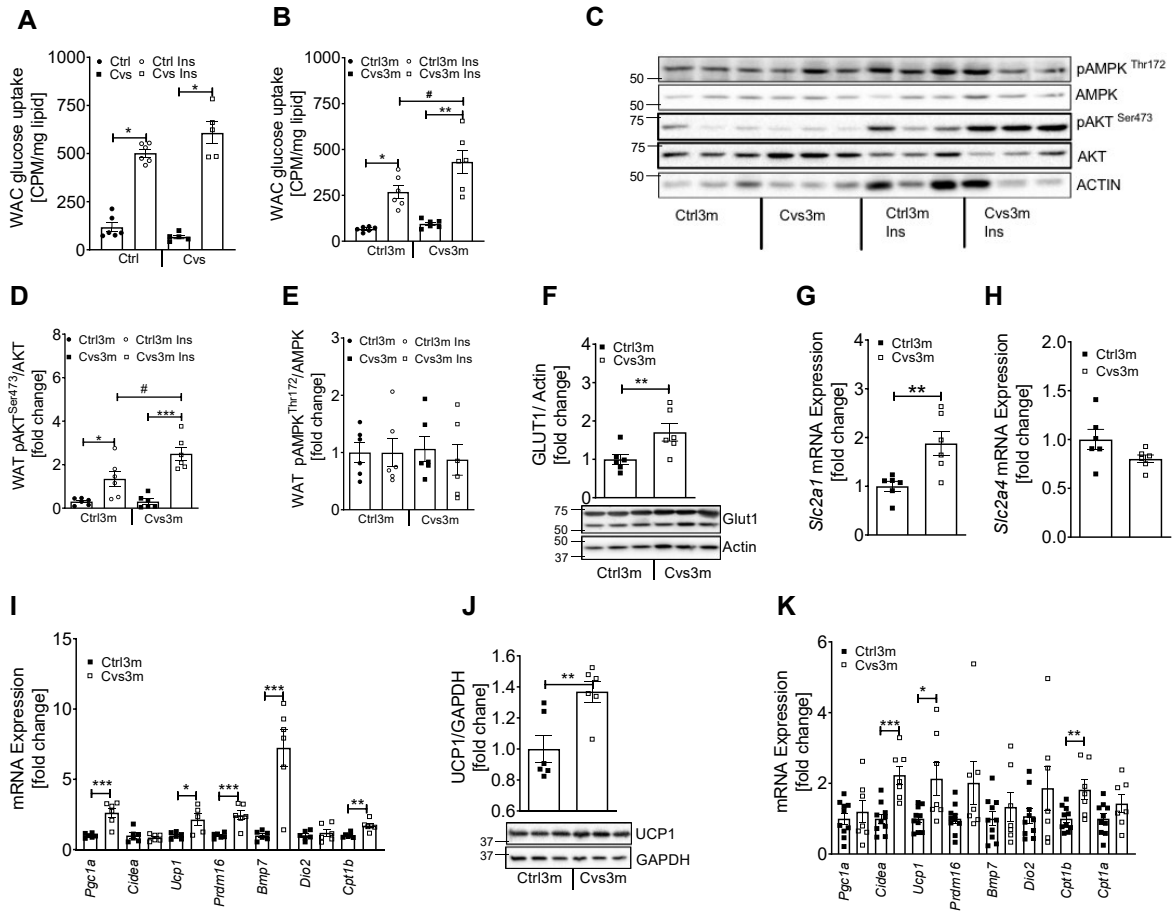

Figure 8: Effect of Cvs and long-term effects of Cvs intervention on fat metabolism. *Ex vivo* glucose uptake under basal and insulin-stimulated conditions in primary adipose cells from Cvs (A) and three months post Cvs (Cvs3m) mice (B) compared to the age-matched controls (Ctrl and Ctrl3m, respectively) n = 5–6. Representative white adipose tissue western blot of insulin stimulated pAKT and pAMPK (C) obtained from Cvs3m and Ctrl3m mice injected with insulin for 10 min and representative densitometric analysis of (D and E) n = 6. Representative western blot and densitometry analysis of GLUT1 (F) n = 6, mRNA expression analysis of *Slc2a1* (Glut1) (G), *Slc2a4* (Glut4) (H) n = 6 and browning and thermogenic marker from eWAT following 3-month post Cvs and control mice (I) n = 6. Representative western blot and densitometry analysis of UCP1 (J) n = 6 and mRNA analysis of browning and thermogenic marker from BAT from Cvs3m and Ctrl3m mice (K) n = 7–10. Values are means ± s.e.m. Statistical analyses were done by two-tailed unpaired Student's t-test (F–K) or by Two-Way ANOVA followed by Bonferroni post hoc (A-B, D-E). **p < 0.05, **p < 0.01, ***p < 0.001.* Experiments in A-B were conducted by Dr. Zhou Zhou and Dr. Sabrina Müller-Lühlhoff.

Protein and mRNA levels of *Ucp1* were markedly increased also in brown adipose tissue (BAT) from Cvs3m mice (Figure 8J, K). Moreover, *Cpt1b* and cell death-inducing DFFA-like effector a (*Cidea*) mRNA expression were significantly increased in BAT (Figure 8K) of Cvs3m, whereas other markers of BAT activity, such as *Pgc1a*, *Bmp7*, *Cpt1a*, *Prdm16* and iodothyronine deiodinase 2 (*Dio2*) only tended to be increased (Figure 8K). Corticosterone can regulate expression of inflammatory markers, but only marginal changes in the cytokines of eWAT from Cvs and Cvs3m mice were found (Supplementary Table 3).

3.1.5 Early exposure to Cvs leads to late onset increase in hepatic lipid content and elevation of plasma FGF21

Hepatic triglycerides were unchanged post Cvs but markedly increased three months post Cvs in Cvs3m mice (Figure 9A). Genes involved in lipogenesis including fatty acid synthase (*Fasn*), acetyl-CoA carboxylase (*Acc1*, *Acc2*), stearoyl-Coenzyme A desaturase (*Scd1*, *Scd2*) did not change in Cvs3m mice (Figure 9B). However, hepatic fatty acid translocase FAT/*Cd36* was highly upregulated in Cvs3m mice, while solute carrier family 27 (fatty acid transporter) member 5 (*Fatp5*) and fatty acid binding protein 4 (*Fabp4*) were unchanged (Figure 9C). Interestingly, also increased expression of patatin like phospholipase domain containing 2 (*Pnpla2*) were observed, which catalyses the initial step of triglyceride hydrolysis in lipid droplets (Figure 9D). Moreover, there was increased expression of *Cpt1a*, a rate limiting enzyme in fatty acid oxidation (Figure 9E).

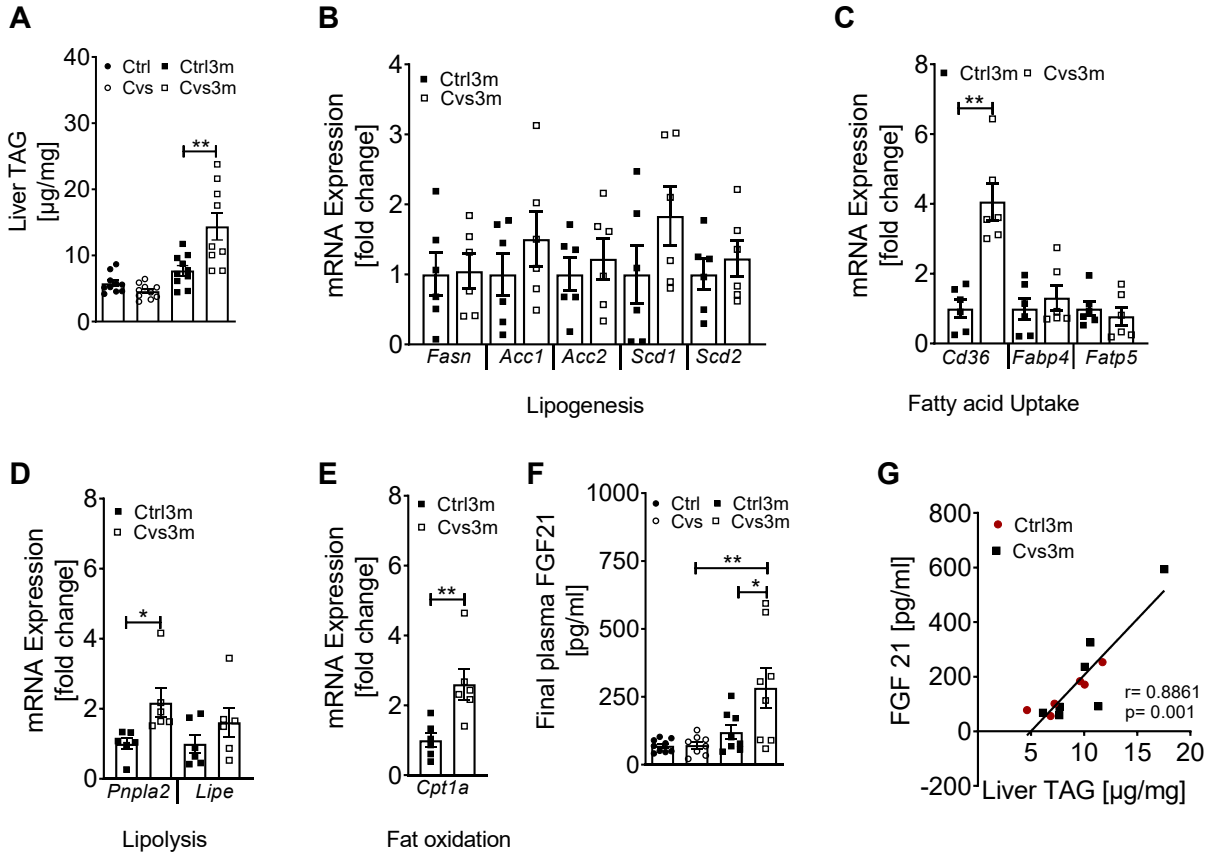

Figure 9: Enhanced liver triglyceride (TAG) content positively correlates with FGF21 secretion in mice three months post Cvs. Liver TAG content from Cvs and three months post Cvs (Cvs3m) mice (A) compared to the age-matched controls (Ctrl and Ctrl3m, respectively) n = 9–10. mRNA expression of gene associated with lipogenesis (B), fatty acid uptake (C), lipolysis (D) and fat oxidation (E) from Cvs3m and Ctrl3m mice n = 6. Plasma level of FGF21 (F) n = 8–9 and correlation analysis of plasma FGF21 and liver TAG content (G) n = 6–7. Values are means ± s.e.m. Statistical analyses were done by two-tailed unpaired Student's t-test (B–E) or by Two-Way ANOVA followed by Bonferroni post hoc (A and F). *$p < 0.05$, **$p < 0.01$. r is representing Pearson correlation.

Considering the pleiotropic effects of corticosterone on number of endocrine organs, circulating hormones that regulate glucose homeostasis were analysed (Supplementary Table 1). Plasma FGF21 was not different right after stress exposure but showed marked elevation three months post Cvs compared to the respective control mice (Figure 9F). Furthermore, plasma FGF21 showed a positive correlation with liver triglyceride content in both Cvs3m and Ctrl3m mice (Figure 9G). In addition, reduced level of ghrelin and glucagon in Cvs mice were found, while circulating adiponectin was lower in Cvs3m mice compared to controls (Supplementary Table 1).

3.1.6 Enhanced late onset FGF21 signalling in multiple tissues following Cvs exposure

The data indicate that early stress exposure leads to alterations in glucose and lipid metabolism in multiple tissues, where many of these changes were previously linked to FGF21 signalling. Therefore, expression of key components of FGF21 signalling in liver, skeletal muscle, BAT and WAT were analysed. FGF21 receptors and some of its downstream targets were upregulated in the liver, eWAT and BAT from Cvs3m mice, including fibroblast growth factor receptors (*Fgfr*) isoforms 4, 1 and 1c, *Pnpla2*, hydroxyacyl-CoA dehydrogenase (*Hadh*) and citrate synthase (*Cs*) (Figure 10A–D). Furthermore, elevated *Fgf21* gene expression in the liver, BAT and skeletal muscle (Figure 10E–G), indicating that these tissues are main sources of FGF21 three months post Cvs. In contrast, no changes in *Fgf21* mRNA of WAT were observed (Figure 10H).

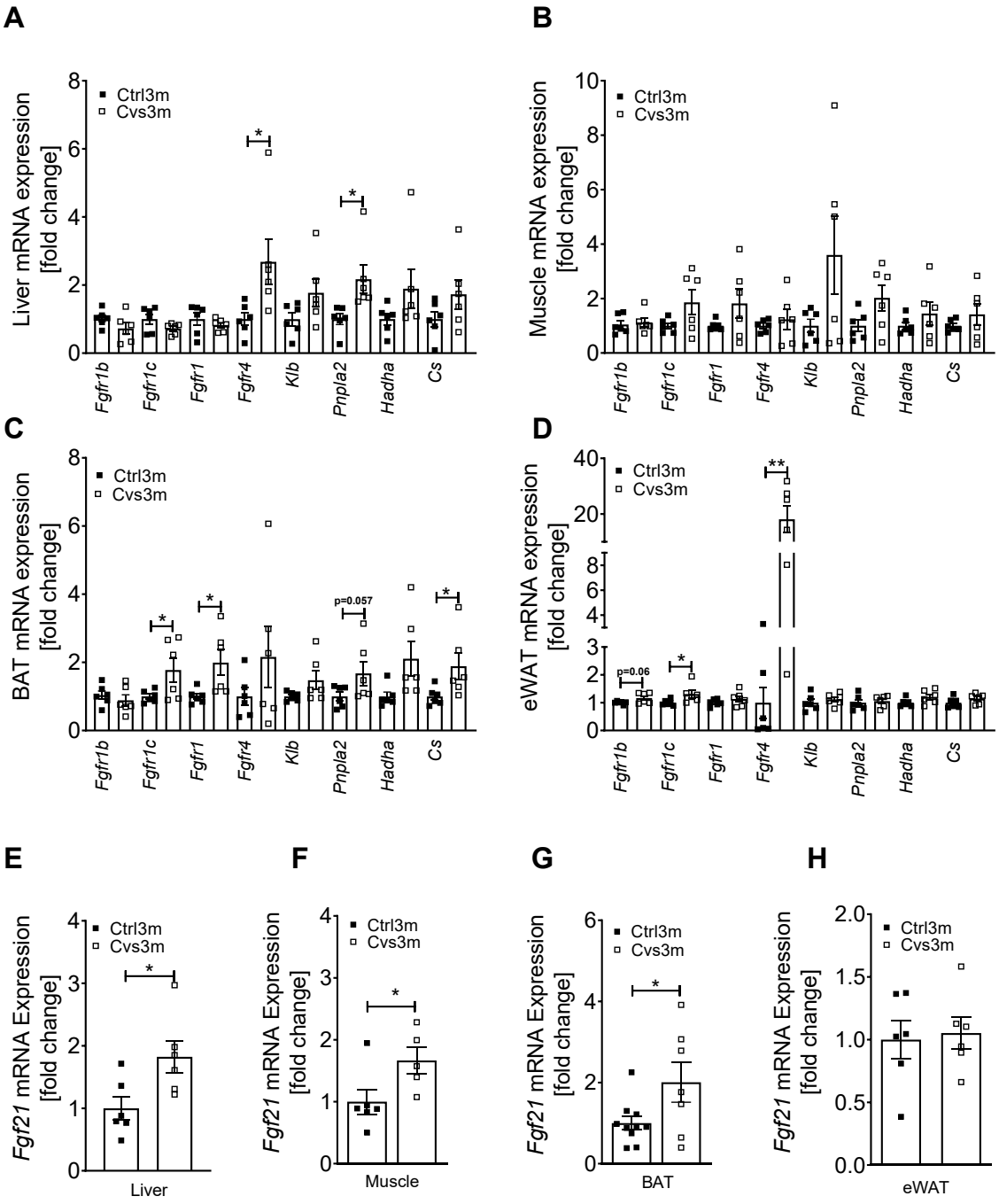

Figure 10: Induction of *Fgf21* mRNA expression along with FGF21 regulated genes in metabolic tissue from mice three months post Cvs. mRNA expression analysis of FGF21 regulated key genes from liver (A), gastrocnemius muscle (B), BAT (C) and eWAT (D) from mice three months post Cvs (Cvs3m) and age-matched control (Ctrl3m) mice n = 6. mRNA expression of *Fgf21* from liver (E), gastrocnemius muscle (F), BAT (G) and eWAT (H) from Cvs3m and Ctrl3m mice n = 5–10. Values are means ± s.e.m. Statistical analyses were done by two-tailed unpaired Student's t-test between groups (A–H). **p < 0.05, **p < 0.01.*

3.2 The role of the liver in the FGF21 regulated metabolic adaptation after Cvs

One major hypothesis derived from the previous manuscript, which can be summarized as: Early stress exposure leads to alterations in glucose and lipid metabolism, and these changes are linked to FGF21 signaling. Based on the previous results, the following section of this thesis examines the role of FGF21 in the stress affected energy metabolism utilizing *Fgf21* knockout mouse model. Beside the regulating functions of FGF21 in skeletal muscle and adipose tissue, the initial findings indicate the liver as a main source of FGF21. Furthermore, the hepatic fat accumulation is associated with the rise in plasma FGF21 levels. Therefore, the glucose and fat metabolism was investigated in isolated primary hepatocytes. Further, the impact of Cvs and the associated long-term metabolic adaptations were analyzed. Two major question should be answered by these investigations, i) are the long-term metabolic improvements abolished in *Fgf21* knockout mice after Cvs and ii) do *Fgf21* knockout mice show the same stress-related fat accumulation in the liver?

3.2.1 Metabolic physiology after Cvs and after recovery

Age-matched wildtype (WT) or whole-body knockout mice (FGF21KO) underwent the Cvs protocol with or without 3 months of recovery phase. The physiological characteristic of all mice in the study are listed in Table 11 for short-term (Cvs) and in Table 12 for long-term (Cvs3m) conditions.

After 15 days of Cvs both WT and FGF21KO mice showed either decreased body weight or lean mass as well as less fat mass, along with increased levels of corticosterone compared to the respective non-stressed control mice. Both WT and FGF21KO mice exhibit higher 6 hours fasted blood glucose levels after Cvs intervention compared to Ctrl mice. Stressed WT mice showed less hepatic triglyceride content but increased plasma free fatty acids compared to non-stressed WT mice. In FGF21KO mice both parameters were not significantly different. Moreover, plasma analyses of major metabolic active hormones revealed elevated levels of leptin, ghrelin and resistin in WT Cvs mice compared to WT Ctrl mice. Stressed FGF21KO mice show increased level of ghrelin compared to unstressed littermates. In line with the literature, FGF21KO mice show an increased lean mass compared to WT mice and decreased fat mass due to a higher lipolytic activity in the adipose tissue (Hotta et al., 2009).

Table 11: Physiological parameters of WT and FGF21KO mice after Cvs.

Parameter	WT Ctrl	WT Cvs	*p-value*	FGF21KO Ctrl	FGF21KO Cvs	*p-value*
N (male)	5-9	5-9		5-10	5-10	
Age (weeks)	14.11 ±0.61	14.00 ±0.98		14.00 ±0.00	13.19 ±0.79	
Body weight (g)	30.22 ±1.17	27.80 ±0.38	*	30.74 ±1.14	29.49 ±1.27	
Lean mass (g)	25.75 ±2.73	24.31 ±1.01		27.87 ±1.14$^{\#}$	26.10 ±1.20	*
Fat mass (g)	3.22 ±1.44	2.12 ±0.39	**	2.24 ±0.16$^{\#\#}$	1.89 ±0.26	*
Liver triglycerides (µg/mg)	19.56 ±10.27	8.49 ±3.50	*	17.14 ±6.34	11.20 ±6.28	

Parameter	WT Ctrl	WT Cvs	*p-value*	FGF21KO Ctrl	FGF21KO Cvs	*p-value*
Fasting blood glucose (mg/dl)	91.00 ±24.01	125.60 ±37.28	*	105.00 ±13.47	134.20 ±15.90	*
Corticosterone (ng/ml)	51.87 ±16.55	116.80 ±32.09	***	53.80 ±4.17	124.60 ±20.10	***
Triglycerides (mg/dl)	22.29 ±14.38	32.37 ±9.57		45.55 ±13.62	55.90 ±15.49	
Free fatty acids (µg/µl)	1.40 ±0.35	2.26 ±0.70	*	1.59 ±0.35	1.78 ±0.43	
Insulin (pg/ml)	6689 ±13859	1702 ±459		5697 ±3449	3836 ±2497	
Glucagon (pg/ml)	277 ±60	220 ±243		813 ±928	294 ±83	
Leptin (pg/ml)	645 ±353	1267 ±350	*	1124 ±180	679 ±476	
Ghrelin (pg/ml)	24755 ±15056	43024 ±12636	*	31562 ±9943	30718 ±13904	
GIP (pg/ml)	331 ±129	333 ±100		380 ±68	401 ±144	
GLP-1 (pg/ml)	33 ±24	24 ±8		100 ±97	47 ±40	
PAI-1 (pg/ml)	1965 ±1462	1009 ±321		1863 ±1013	1289 ±395	
Resistin (pg/ml)	70255 ±20740	119994 ±12969	*	90699 ±27802	140765 ±30025	*

Values are mean ± CI. Statistical analyses were done by two-way ANOVA with correction for multiple comparison using Tukey post hoc analysis. With *p < 0.05, **p < 0.01, ***p < 0.001 between the Cvs intervention and $^{\#}$p < 0.05, $^{\#\#}$p < 0.01, $^{\#\#\#}$p < 0.001 between the genotypes.

Age-matched mice were kept after Cvs for three months on a standard chow diet without further stress application. After 3 months of recovery WT mice exhibited no significant changes in body composition due to the former Cvs intervention. Stressed FGF21KO mice had less fat mass compared to non-stressed FGF21KO mice. However, stressed WT mice showed higher hepatic triglyceride content and increased plasma free fatty acids together with decreased fasted blood glucose level compared to WT Ctrl mice. These parameters were not significantly different between non-stressed and stressed FGF21KO mice. In line with the literature, FGF21KO mice showed increased liver triglycerides compared to WT mice (Hotta et al., 2009). Analyses of metabolic modulators of previous stressed FGF21KO mice showed increased levels of GIP and PAI-1 compared to the FGF21KO Ctrl3m. No changes of these parameters were observed in WT mice.

Table 12: Physiological parameters of WT and FGF21KO mice after 3 months recovery.

Parameter	WT Ctrl3m	WT Cvs3m	*p-value*	FGF21KO Ctrl3m	FGF21KO Cvs3m	*p-value*
N (male)	5-9	5-9		5-9	5-9	
Age (weeks)	26.00 ±0.65	26.00 ±1.18		26.00 ±0.60	26.14 ±1.38	
Body weight (g)	32.44 ±1.70	31.97 ±1.93		31.91 ±1.62	31.59 ±1.32	
Lean mass (g)	27.21 ±1.57	28.06 ±1.88		27.02 ±1.35	28.12 ±1.28	
Fat mass (g)	4.08 ±1.46	2.92 ±0.51		4.20 ±1.10	2.61 ±0.85	*
Liver triglycerides (µg/mg)	7.31 ±2.80	17.99 ±5.50	*	36.22 ±20.47$^{\#\#\#}$	37.19 ±14.54$^{\#\#\#}$	
Fasting blood glucose (mg/dl)	124.70 ±12.40	93.33 ±11.44	**	109.30 ±17.83	106.10 ±19.85	
Corticosterone (ng/ml)	89.90 ±13.04	74.69 ±25.58		77.41 ±15.27	89.13 ±17.46	
Triglycerides (mg/dl)	62.70 ±42.35	67.51 ±18.47		49.90 ±28.38	59.43 ±27.32	
Free fatty acids (µg/µl)	1.69 ±0.35	3.31 ±0.83	***	1.36 ±0.53	1.47 ±0.24	
Insulin (pg/ml)	8689 ±8194	5498 ±4243		2864 ±1689	7759 ±5820	
Glucagon (pg/ml)	561 ±471	327 ±410		123 ±109	371 ±319	
Leptin (pg/ml)	1561 ±790	803 ±344		1154 ±445	1031 ±453	

Parameter	WT Ctrl3m	WT Cvs3m	*p-value*	FGF21KO Ctrl3m	FGF21KO Cvs3m	*p-value*
Ghrelin (pg/ml)	20351 ±13413	25478 ±12041		13183 ±4703	12159 ±5708$^{\#}$	
GIP (pg/ml)	686 ±216	343 ±117		194 ±79	506 ±275	*
GLP-1 (pg/ml)	64 ±29	56 ±49		26 ±15	64 ±50	
PAI-1 (pg/ml)	1051 ±514	1341 ±469		457 ±102	1062 ±518	*
Resistin (pg/ml)	72877 ±40583	75815 ±44548		48742 ±9027	51492 ±12039	

Values are mean ± CI. Statistical analyses were done by two-way ANOVA with correction for multiple comparison using Tukey post hoc analysis. With *p < 0.05, **p < 0.01, ***p < 0.001 between the Cvs intervention and #p < 0.05, ##p < 0.01, ###p < 0.001 between the genotypes.

The stress-induced alterations of the body composition between Ctrl and Cvs mice due to increased levels of stress hormones are absent after recovery. Significant differences in corticosterone plasma levels due to Cvs are not visible, but the general corticosterone plasma levels are increased by age independent of FGF21. Fasting blood glucose levels were higher in WT and FGF21KO Cvs mice compared to the respective Ctrl mice directly after Cvs intervention. Three months later, WT Cvs3m mice showed lower fasting blood glucose levels compared to WT Ctrl3m mice. However, FGF21KO mice showed no stress-induced long-term changes in blood glucose. Previously stressed WT mice, both after Cvs as well as recovery show increased levels of free fatty acids compared to non-stressed WT mice, in contrast to FGF21 KO mice. Interestingly, the former observed lower hepatic triglyceride content of WT and FGF21KO mice after Cvs compared to the respective controls was increased after recovery only in WT Cvs3m mice. Stressed FGF21KO Cvs mice showed no significant stress-related changes in liver triglyceride content compared to FGF21KO Ctrl3m mice after recovery, although the overall contend was much higher in both groups compared to the respective WT mice. Despite of the changes in hepatic triglyceride content the levels of free fatty acids in the plasma did not change by age.
The mice were not fasted before scarification, which could be the reason for the high variability of the metabolic hormones levels.

3.2.2 Plasma cytokine levels after Cvs and recovery

Persisting hepatic lipid accumulation can be accompanied by increased low grade systemic inflammation (Rosso et al., 2019). The composition of plasma cytokines can give information on the inflammatory status of WT and FGF21KO mice. Analyses of plasma cytokines was performed by multiplex Bio-Plex technology (Bio-Rad, Munich, Germany) to determine the influence of Cvs on pro- and anti-inflammatory markers. No significant stress-related changes in plasma cytokine levels are observed directly after chronic stress exposure of Cvs in WT and FGF21KO mice (Table 13).

Table 13: Plasma cytokine levels after Cvs in WT and FGF21KO mice.

Parameter (pg/ml)	WT Ctrl	WT Cvs	*p-value*	FGF21KO Ctrl	FGF21KO Cvs	*p-value*
IL-1a	68,2 ± 51,5	25,1 ± 13,6		36,2 ± 11,1	39,4 ± 7,4	
IL-2	16,2 ± 3,8	11,4 ± 5,5		7,9 ± 1,1	10,4 ± 4,9	
IL-5	4,5 ± 0,8	5 ± 1,2		5,1 ± 1,9	4,5 ± 1,2	
IL-6	7,2 ± 3,1	4,6 ± 1,6		10 ± 4,1	13,6 ± 11	
IL-12(p40)	848,2 ± 359,3	410,7 ± 100,9		683,1 ± 227,4	569,5 ± 139	
IL-12(p70)	69,2 ± 33,5	91,2 ± 48,3		67,9 ± 47,9	74,2 ± 35,1	
IL-13	213,6 ± 193,4	244,8 ± 92,8		207,1 ± 197,2	202,7 ± 93,6	
IL-17	14,6 ± 11,9	7,4 ± 3,1		11 ± 1,8	8,4 ± 4,1	
G-CSF	507 ± 494,5	95,8 ± 21,5		401,9 ± 216	198,2 ± 176,6	
KC	17,6 ± 13,3	8 ± 1,2		15,7 ± 14,6	16,2 ± 14,8	
MIP-1a	5,2 ± 1,5	5,1 ± 2,6		6 ± 0,9	5,8 ± 1,6	
RANTES	123,8 ± 30,6	82,3 ± 21,6		62,7 ± 21,8	88,4 ± 14	
TNF-a	60,5 ± 36,9	61,6 ± 35,6		57,7 ± 13	46,9 ± 19,5	
IL-18	205,5 ± 67,2	240,9 ± 43		301,7 ± 110,5	273,8 ± 42,3	
M-CSF	2182,6 ± 707,9	1690,5 ± 397,9		1641 ± 156,2	1601,3 ± 198,3	
MIG	65,1 ± 33,6	69,4 ± 15,4		35,9 ± 16,7	53 ± 12,4	
MIP-2	8,3 ± 1,6	8,7 ± 1,4		6,9 ± 1,7	11,2 ± 3,5	
PDGF-bb	630,7 ± 686,7	870,8 ± 544,4		163,7 ± 141,5	231,2 ± 160	
VEGF	14224 ± 8592,3	21793,2 ± 3579,1		5170,7 ± 7495,5	12508,8 ± 9166,7	

Values are mean ± CI. Statistical analyses were done by two-way ANOVA with correction for multiple comparison using Tukey post hoc analysis. With *p < 0.05, **p < 0.01, ***p < 0.001 between the Cvs intervention and #p < 0.05, ##p < 0.01, ###p < 0.001 between the genotypes.

In addition, the cytokine levels were measured to determine if Cvs exposure persistently interfered with alterations of inflammatory markers and thereof might influence metabolic alterations observed in chronic stress response. On the long-term, some stress-related changes in cytokine levels were observed. The pro-inflammatory cytokine IL12 (p40) was increased after recovery in WT mice (Table 14). Whereas there was no further alteration in WT animals, FGF21KO Cvs3m mice show higher levels of eotaxin and MIP-1a compared to FGF21KO Ctrl3m mice. All in all, Cvs show no strong impact on cytokine plasma levels neither directly after the intervention nor after a three-month recovery phase.

Table 14: Plasma cytokine levels after 3 month recovery in WT and FGF21KO mice.

Parameter (pg/ml)	WT Ctrl3m	WT Cvs3m	*p-value*	FGF21KO Ctrl3m	FGF21KO Cvs3m	*p-value*
IL-1a	27,8 ± 5,8	22,5 ± 7,7		26,7 ± 14,2	30,5 ± 11,7	
IL-1b	430,5 ± 102,6	259 ± 123,2		236,9 ± 154,5	428,4 ± 189,3	
IL-2	26,4 ± 12,9	33,6 ± 9,1		21,8 ± 17,2	28,5 ± 16,8	
IL-3	22,5 ± 4,8	17,4 ± 7,5		19,7 ± 9,2	19,5 ± 9,6	
IL-4	7,8 ± 1,6	5 ± 1,7		6 ± 2,2	7,7 ± 3,5	
IL-5	19,1 ± 4	17,4 ± 9,6		12 ± 4,6	18,9 ± 10,6	
IL-6	26,2 ± 14,1	14,5 ± 8,8		9,6 ± 9,8	23 ± 13,7	
IL-10	157,5 ± 91	81,8 ± 38,9		43,3 ± 17,2	101 ± 25,4	
IL-12(p40)	**510,7 ± 121,2**	**767,5 ± 188,2**	*	348,6 ± 83,1	574,9 ± 87	

Parameter (pg/ml)	WT Ctrl3m	WT Cvs3m	*p-value*	FGF21KO Ctrl3m	FGF21KO Cvs3m	*p-value*
IL-12(p70)	725 ± 736,4	287,3 ± 199,5		143,7 ± 103,6	274 ± 86,5	
IL-13	511 ± 170,1	337,6 ± 114,6		283,4 ± 217,8	375,7 ± 269,9	
IL-17	62,6 ± 25,3	55,7 ± 33,8		46,1 ± 7,2	65,5 ± 37,4	
Eotaxin	1372,6 ± 444	1167,5 ± 524,7		**660,1 ± 364,4**	**1635 ± 460,7**	*
G-CSF	88,3 ± 17,7	106,5 ± 38,9		75,6 ± 18,9	272,3 ± 224,8	
IFN-g	219,9 ± 142,8	124,1 ± 54,9		62,7 ± 71,8	181 ± 60	
KC	68,7 ± 18,7	99,9 ± 12,6		57 ± 9,1	106,1 ± 69,6	
MCP-1	562,3 ± 89,1	462,5 ± 145,3		335,6 ± 123,7	662,5 ± 220,4	
MIP-1a	17,3 ± 7,2	11,8 ± 3,7		**5,8 ± 4,4**$^{\#}$	**19,1 ± 5,8**	*
MIP-1b	101,3 ± 43,2	70,7 ± 29,4		46 ± 33	100,6 ± 32,3	
RANTES	130,8 ± 65,2	118,5 ± 55,4		140 ± 58,8	111 ± 22	
TNF-a	506,5 ± 267,1	621,2 ± 711,5		1024,1 ± 1993,6	1008,6 ± 886,2	
IL-18	234,3 ± 42,4	228,6 ± 39,6		370,9 ± 161,9	302,6 ± 217,5	
M-CSF	1145,6 ± 233,5	1411,4 ± 244,2		839,6 ± 237,6	982,4 ± 337,4	
MIG	210,2 ± 54,4	199,7 ± 135,4		156,4 ± 53,3	160,2 ± 80,9	
MIP-2	13,5 ± 5	20,3 ± 2		13,1 ± 3,6	19,5 ± 3,7	

Values are mean ± CI. Statistical analyses were done by two-way ANOVA with correction for multiple comparison using Tukey post hoc analysis. With *p < 0.05, **p < 0.01, ***p < 0.001 between the Cvs intervention and #p < 0.05, ##p < 0.01, ###p < 0.001 between the genotypes.

3.2.3 Metabolic phenotyping after Cvs and recovery

For examination of the metabolic phenotype after Cvs and after three months of recovery, food intake, the individual gas exchange and the related energy expenditure were measured. In contrast to the changes in body weight, the food intake in 15 days of Cvs and during the three-month recovery phase was increased in response to Cvs. The analyses showed, that both, WT and FGF21KO mice, consumed more food during and after Cvs compared to the respective non-stressed Ctrl mice (Figure 11A-D). Despite this, both groups simultaneously lost body weight during the Cvs intervention (see Table 11). However, both stressed WT and FGF21KO mice showed enhanced food intake in the recovery phase (Figure 11C-D), but no significant body weight differences after the recovery period (see Table 12).

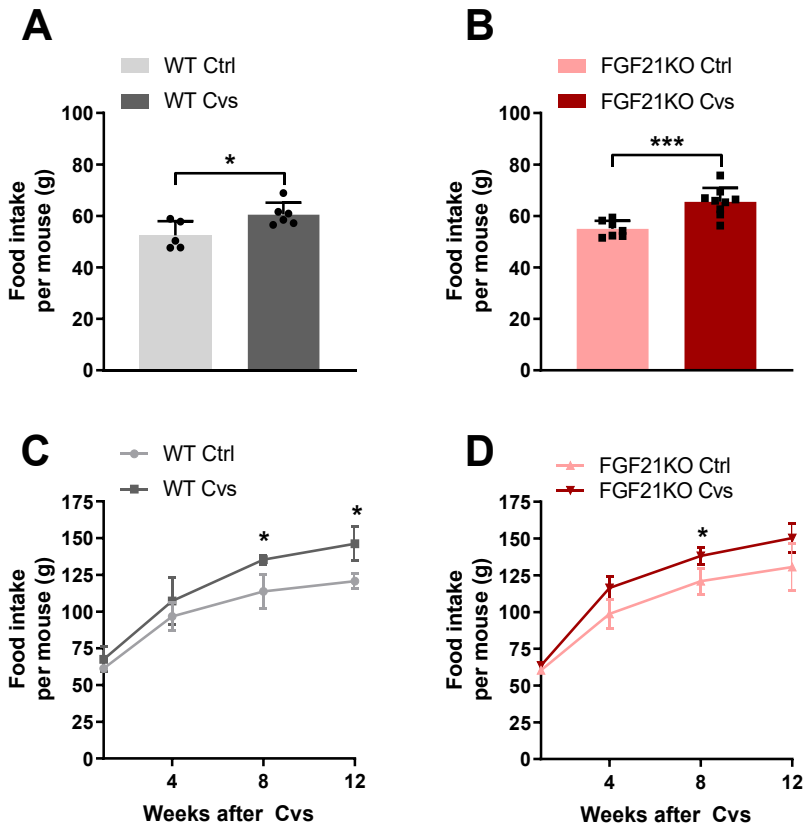

Figure 11: Food intake of WT and FGF21KO mice during and after Cvs. Food intake of stressed and non-stressed WT (A) and FGF21KO (B) mice during 15 days of Cvs. Progress of food intake in three-month recovery phase of stressed and non-stressed WT (C) and FGF21KO (D) mice. Values are mean ± SD. Statistical analyses of curves were done by Two-Way ANOVA followed by Sidek post hoc. Statistical analyses were performed by two-tailed unpaired Student's t-test between groups. N = 4 – 8; *p < 0.05, **p < 0.01, ***p < 0.001.

Based on the different body weight gain and food intake after chronic stress, changes in energy expenditure and substrate utilization were evaluated by individual indirect calorimetric measurements. Therefore, respiratory exchange ratio (RER), spontaneous physical activity (SPA) and energy expenditure, displayed as O_2-consumption in time normalized by body surface (VO_2/Bodyweight$^{0.75}$) were analyzed for 48 hours in two light and two dark phases. Experiments were conducted after the last day of Cvs and after three-month recovery.

Immediately after chronic stress WT and FGF21KO mice show similar SPA with unaltered night activity between Ctrl and Cvs mice (Figure 12A-B). Nevertheless, the RER increases due to Cvs intervention independent of FGF21 genotype (Figure 12C-D). Analyses of the RER showed that the animals had a higher RER compared to the non-stressed controls in especially in the first dark phase (Figure 12E-F). Energy expenditure of stressed WT mice were not significant different (Figure 12G). However, stressed FGF21KO show an overall significantly increased energy expenditure compared to their non-stressed control mice (Figure 12H).

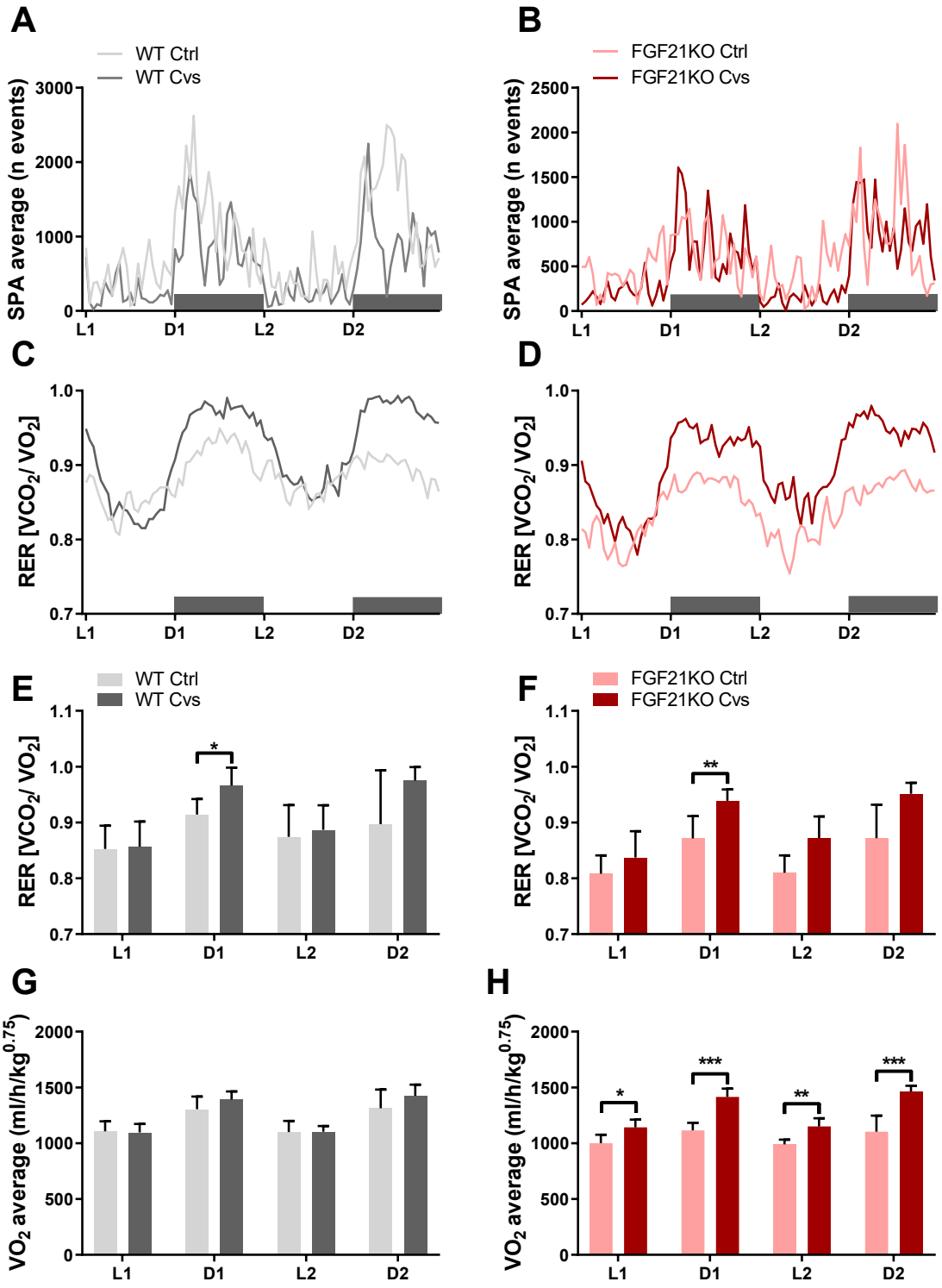

Figure 12: Calorimetric profile of WT and FGF21KO mice after Cvs intervention. Time curve of spontaneous physical activity (SPA) of stressed (Cvs) and non-stressed (Ctrl) WT (A) and FGF21KO (B) mice. 48-hour progress and analysed light/dark phases of respiratory exchange ratio (RER) after Cvs of WT (C, E) and FGF21KO (D, F) mice, respectively. Light/dark phase related energy expenditure of stressed and non-stressed control mice of WT (G) and FGF21KO (H) mice. Grey bars indicate dark phases in A-D. L: light phase; D: dark phase. Values are mean ± SD. Statistical analyses were performed by two-tailed unpaired Student's t-test between groups. N = 6 – 8; *p < 0.05, **p < 0.01, ***p < 0.001.

Next, the long-term changes after a chronic stress intervention and its influence on metabolic parameters were investigated. In individual indirect calorimetric measurements WT (Figure 13A) and FGF21KO (Figure 13B) mice showed no stress-related differences in SPA. However, WT Cvs mice exhibited an increased RER compared to non-stressed WT mice (Figure 13C, E), but with no changes in energy expenditure (Figure 13G). The long-term RER (Figure 13D, F) and energy expenditure (Figure 13G) of FGF21KO was not affected by Cvs.

The increased RER after the Cvs intervention in WT and FGF21KO mice was therefore further enhanced in the three months recovery period of WT mice. In contrast, FGF21KO mice did not show this progression, as the initial stress-induced higher RER of FGF21KO Cvs mice was even abolished over time.

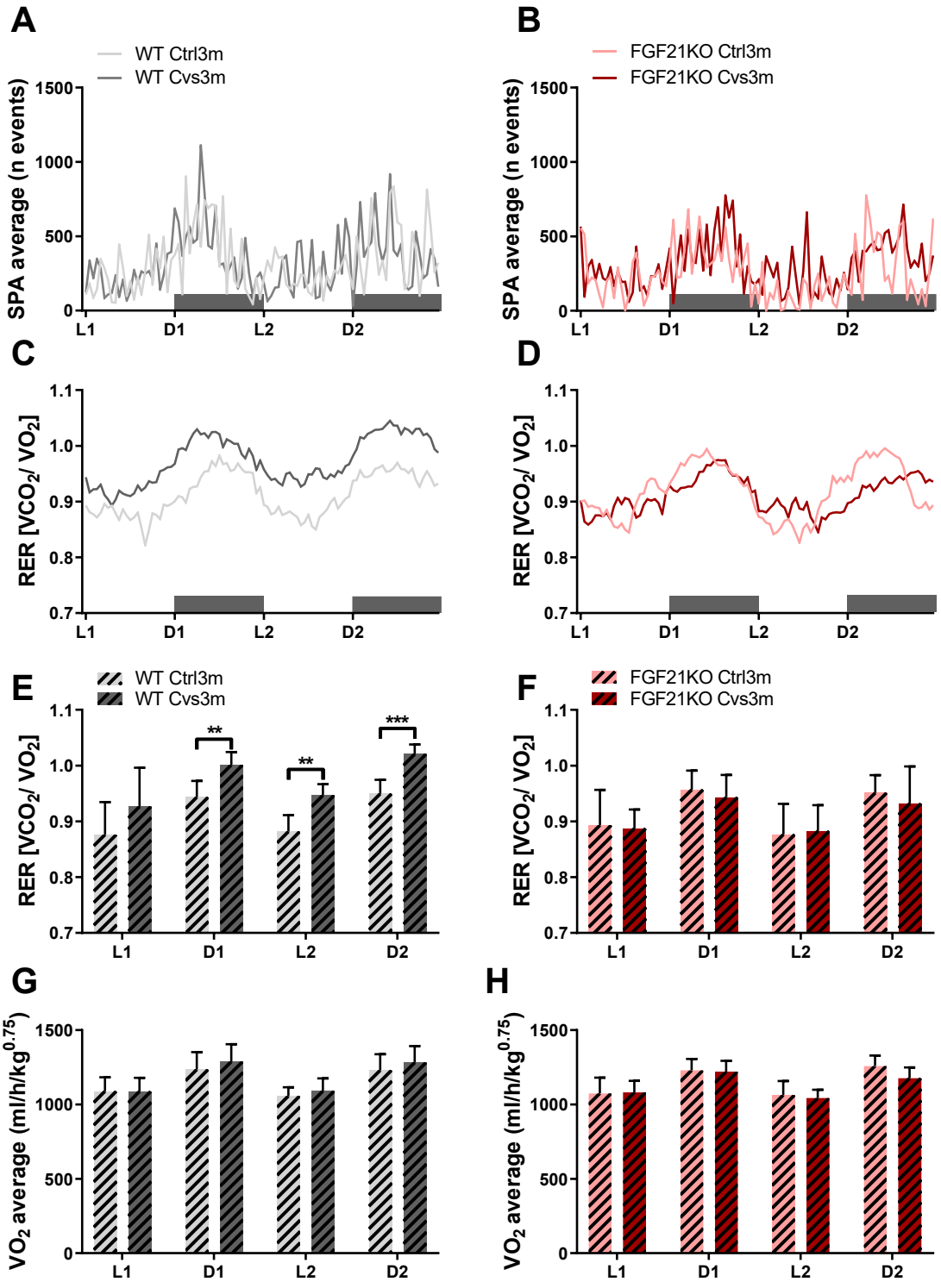

Figure 13: Calorimetric profile of WT and FGF21KO mice after three-month recovery. Time curve of spontaneous physical activity (SPA) of previous stressed (Cvs3m) and non-stressed (Ctrl3m) WT (A) and FGF21KO (B) mice. 48-hour progress and analysed light/dark phases of respiratory exchange ratio (RER) after recovery of WT (C, E) and FGF21KO (D, F) mice, respectively. Light/dark phase related energy expenditure of previous stressed and non-stressed control mice of WT (G) and FGF21KO (H) mice. Grey bars indicate dark phases in A-D. L: light phase; D: dark phase. Values are mean ± SD. Statistical analyses were performed by two-tailed unpaired Student's t-test between groups. N = 6 – 8; **p < 0.01, ***p < 0.001.

3.2.4 Tolerance tests after Cvs and recovery

To further investigate stress-induced changes in glucose metabolism and insulin sensitivity and the impact of FGF21 in the post-stress metabolic regulation, glucose, insulin and pyruvate tolerance test were performed. To analyze stress-related changes in glucose tolerance of WT and FGF21KO mice a intraperitoneal glucose tolerance test (i. p. GTT) was conducted immediately after Cvs (Figure 14A-B) and after three months recovery (Figure 14C-D). Glucose injection led to a strong and fast increase of blood glucose. Highest blood glucose levels were observed after 15 minutes to comparable levels in all conditions investigated. The further blood glucose decline indicated the glucose clearance that finally reached basal levels in all conditions. The results show, that the glucose clearance 30 minutes after injection is improved in mice which were stressed before, independent of FGF21. However, only FGF21KO mice showed a significant lower area under the curve (AUC) indicating improved over-all glucose clearance. After three months of recovery both WT and FGF21KO mice showed improved glucose tolerance if previously faced stress compared to the respective non-stressed control mice. Over the time of recovery, no changes in glucose tolerance are observed. Previous stressed WT and FGF21KO mice are less glucose tolerant compared to non-stressed mice.

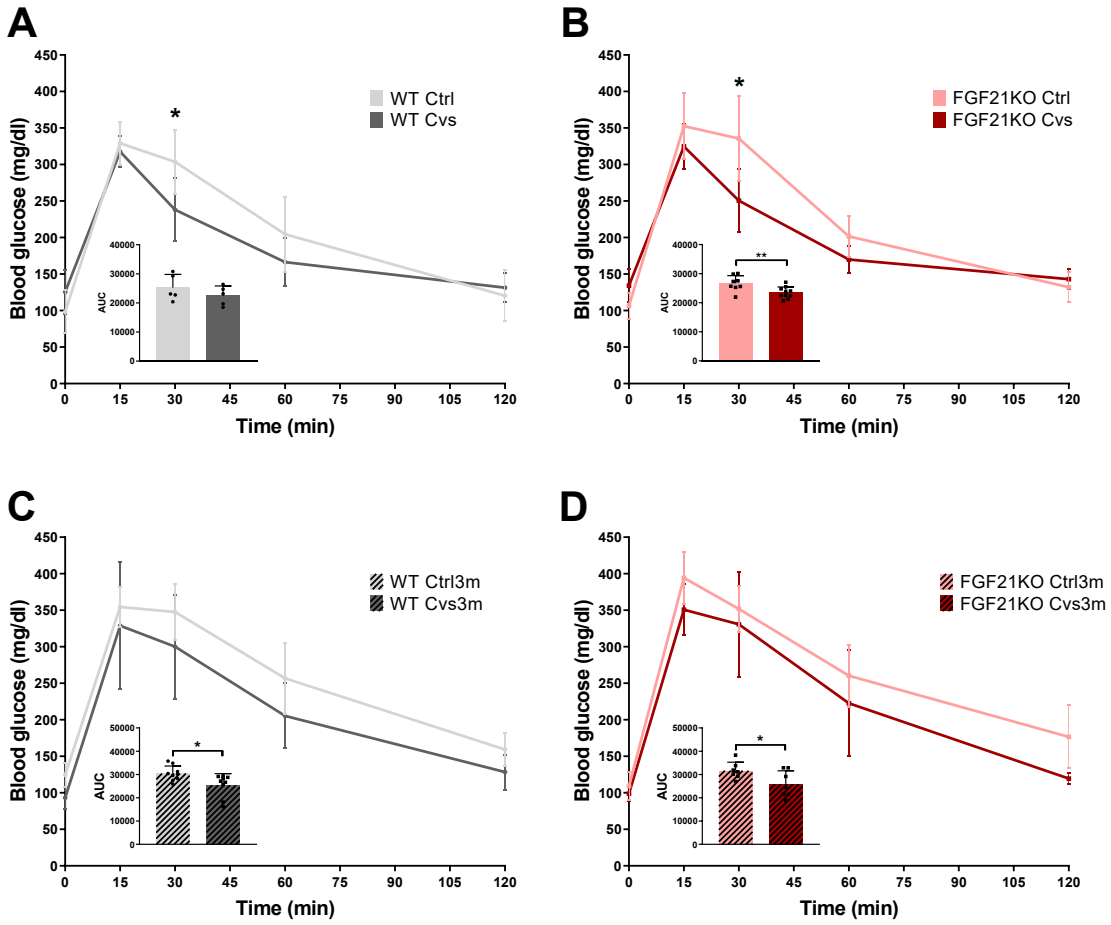

Figure 14: Intraperitoneal glucose tolerance test (i. p. GTT) after Cvs and recovery. An intraperitoneal glucose tolerance test (i. p. GTT) were performed subsequently after Cvs in WT (A) and FGF21KO (B) mice and after three months of recovery (C-D). AUC: Area under the curve. Values are mean ± SD. Statistical analyses of curves were done by Two-Way ANOVA followed by Sidek post hoc. Statistical analyses of AUC were performed by two-tailed unpaired Student's t-test between groups. N = 5-9; *p < 0.05, **p < 0.01.

The measurement of the insulin tolerance is a standard procedure to investigate the insulin sensitivity *in vivo*. Like for the i. p. GTT, the intraperitoneal insulin tolerance tests (i. p. ITT) were conducted after Cvs for short-term and after three months for long-term investigations. The injection of insulin stimulates the glucose uptake in peripheral tissues and inhibits the hepatic gluconeogenesis resulting in degreasing blood glucose levels. WT mice showed a slightly impaired insulin tolerance after Cvs compared to non-stressed control mice (Figure 15A), whereas FGF21KO mice showed no significant changes due to the Cvs intervention and increased stress hormone levels (Figure 15B). However, on the long-term the prior stressed WT mice improved insulin tolerance (Figure 15C) and showed the opposite. FGF21KO mice show no difference in insulin tolerance over time (Figure 15D).

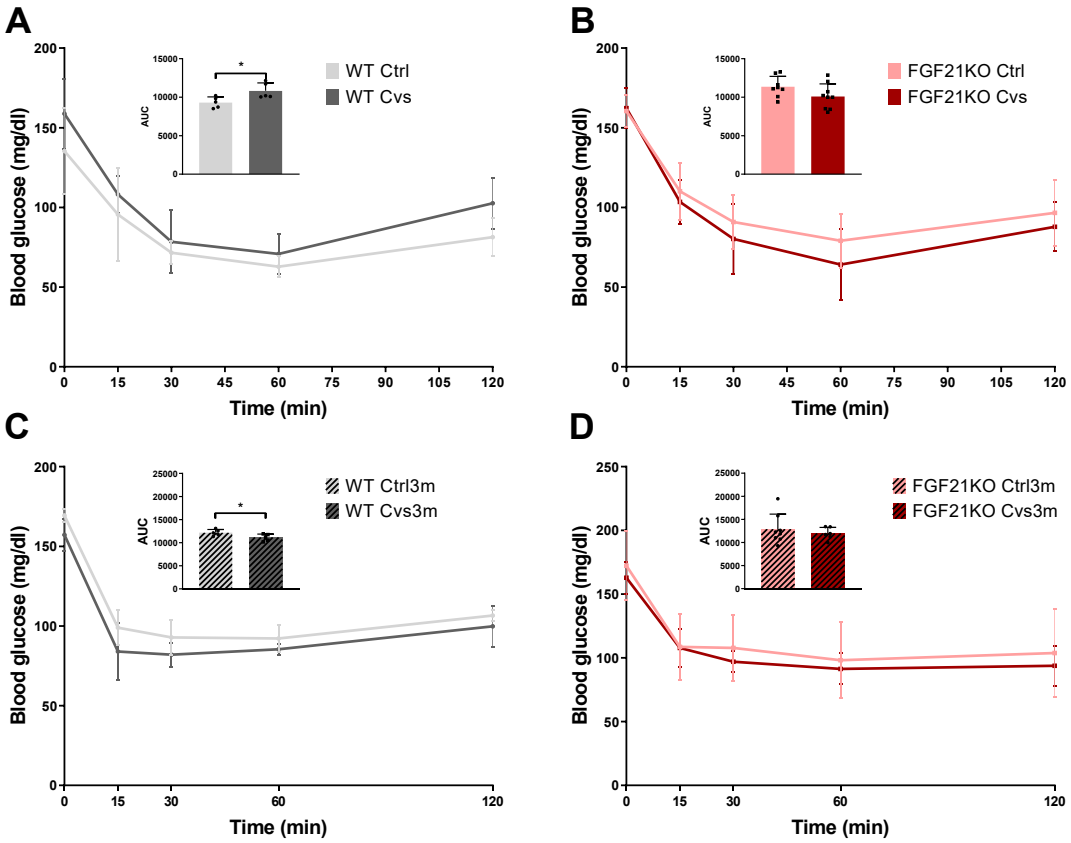

Figure 15: Intraperitoneal insulin tolerance test (i. p. ITT) after Cvs and recovery. An intraperitoneal insulin tolerance test (i. p. ITT) were performed subsequently after Cvs in WT (A) and FGF21KO (B) mice and after three months of recovery (C-D). AUC: Area under the curve. Values are mean ± SD. Statistical analyses of curves were done by Two-Way ANOVA followed by Sidek post hoc. Statistical analyses of AUC were done by two-tailed unpaired Student's t-test between groups. N = 5-9; *p < 0.05, **p < 0.01.

Next to glucose and insulin sensitivity, the capability of systemic glucose disposal by hepatic glucose production and release into the circulation plays an important role in the overall glucose homeostasis. Under fasting conditions, the liver is the crucial organ to control blood glucose levels and prevent against hypoglycaemia by gluconeogenesis and glycogenolysis. Therefore, the impact of Cvs on the hepatic gluconeogenesis was investigated directly after Cvs intervention and after three months recovery using an intraperitoneal pyruvate tolerance test (i. p. PTT). Under fasted conditions, the injection of the gluconeogenic substrate pyruvate, evokes hepatic glucose production. Consequently, an i. p. PTT reveals the hepatic capability to produce glucose from pyruvate. Interestingly, stressed WT and FGF21KO mice showed different responses to pyruvate injection. WT Cvs mice had an increased pyruvate tolerance compared to WT Ctrl mice (Figure 16A), whereas FGF21KO Cvs mice showed a decrease compared to FGF21KO Ctrl (Figure 16B). On the long-term no significant differences between WT Ctrl3m and WT Cvs3m mice were observed (Figure 16C). In contrast, FGF21KO Cvs mice showed an improvement in gluconeogenesis.

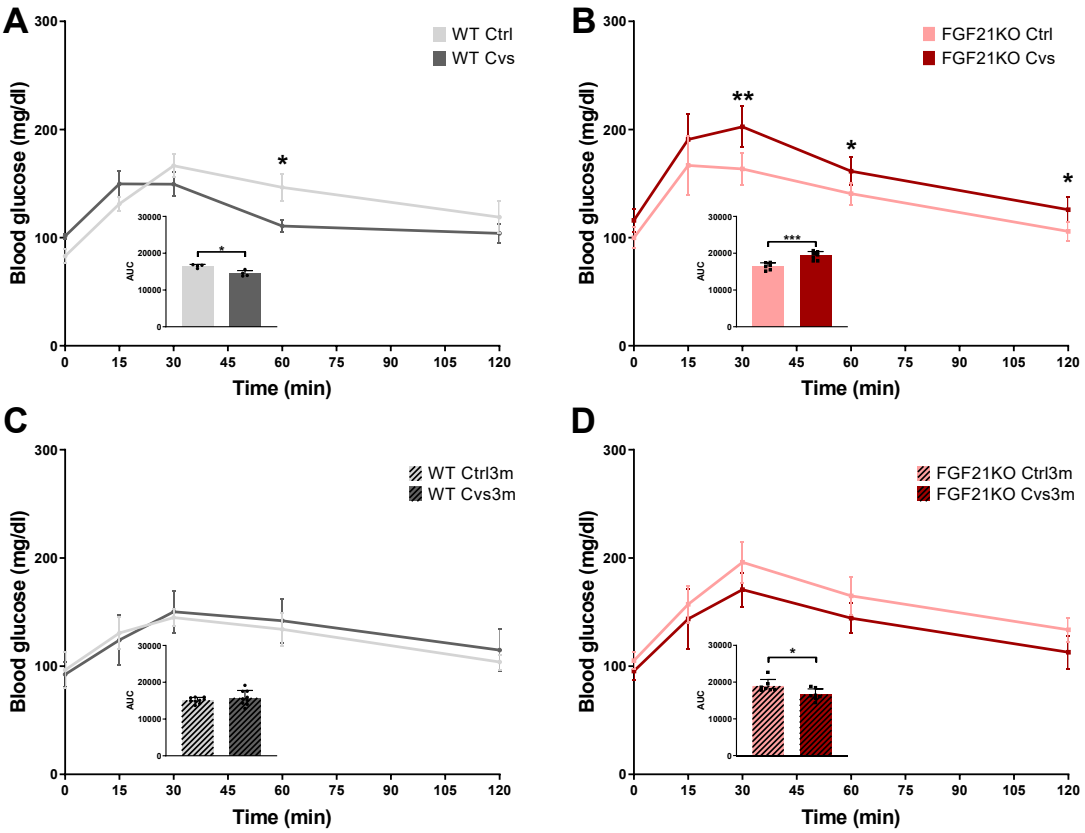

Figure 16: Intraperitoneal pyruvate tolerance test (i. p. PTT) after Cvs and recovery. An intraperitoneal pyruvate tolerance test (i. p. PTT) were performed subsequently after Cvs in WT (A) and FGF21KO (B) mice and after three months of recovery (C-D). AUC: Area under the curve. Values are mean ± SD. Statistical analyses of curves were done by Two-Way ANOVA followed by Sidek post hoc. Statistical analyses of AUC were performed by two-tailed unpaired Student's t-test between groups. N = 4-9; *p < 0.05, **p < 0.01.

3.2.5 Impact of Cvs on insulin signaling in adipose tissue and glucose clearance

The *in vivo* tolerance tests showed an enhanced glucose clearance after Cvs (Figure 14) and a FGF21-dependent improvement in insulin action after recovery of WT mice (Figure 15). These findings were in line with the previous data from the hyperinsulinemic-euglycemic clamp measurements (see 3.1.2). Also a crucial role of the gonadal white adipose tissue (gWAT) for the insulin stimulated glucose disposal in the periphery was shown (see 3.1.4) after recovery.

To determine the possible role of FGF21 on insulin sensitivity in WAT, first the integrity of the mTOR/AKT pathway was monitored by relative quantification of multiple basal phosphorylation and total pathway proteins. Cvs intervention did not result in alterations in short-term WT (Figure 17A) and FGF21KO (Figure 17B). These findings revealed that Cvs has neither an immediate influence on the basal abundance of proteins nor on their basal phosphorylation.

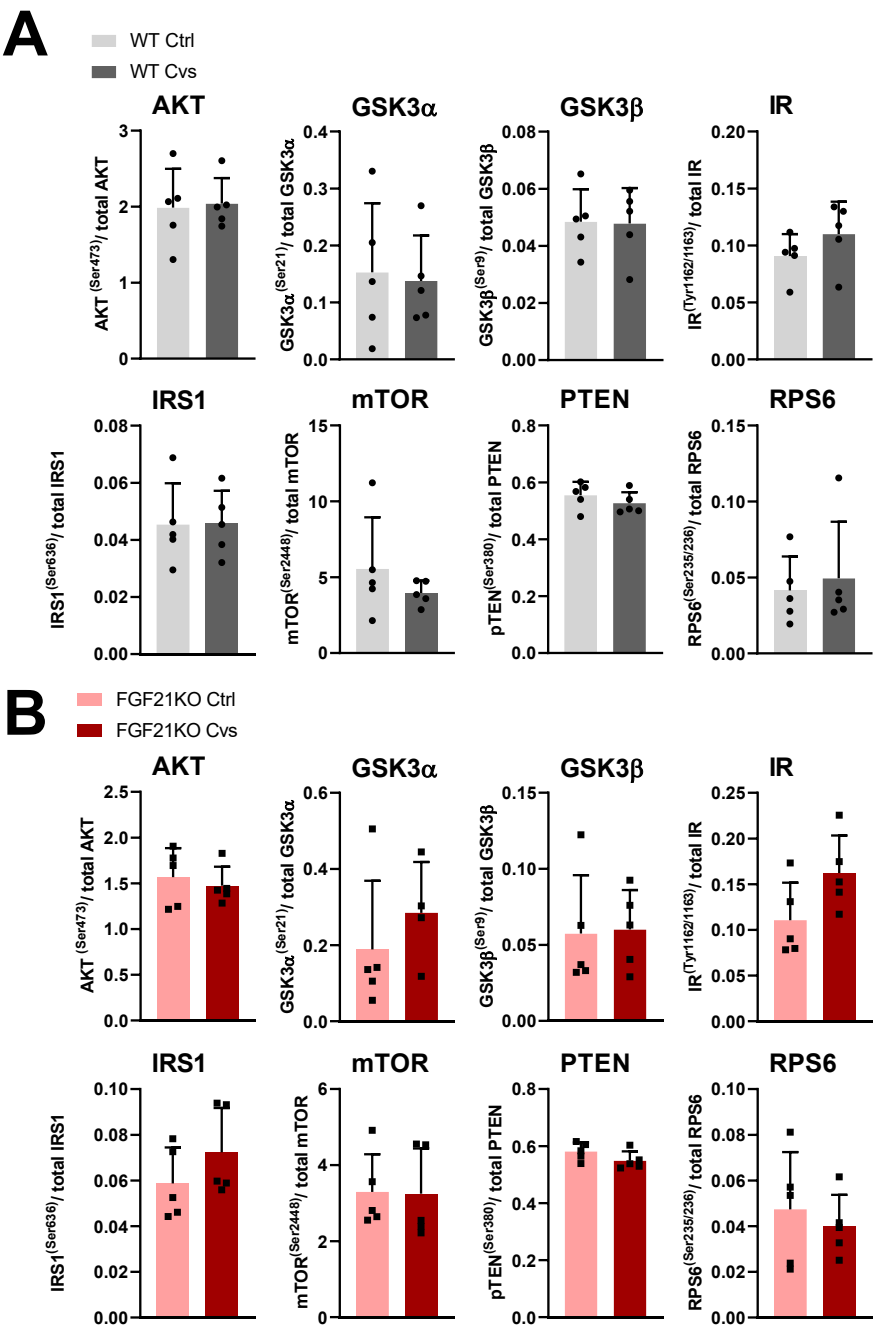

Figure 17: Relative quantification of multiple phosphorylation and total mTOR/AKT pathway proteins in the gWAT after Cvs. Analysis of multiple phosphorylation and total mTOR/AKT pathway proteins after Cvs in WT (A) and FGF21KO (B) mice. Basal protein abundance of mTOR/AKT signaling proteins in gWAT were analyzed by bead-based immunoassay. Akt = Proteinkinase B, GSK3α + β: Glycogen synthase kinase 3α + β, IR: Insulin receptor, IRS1: Insulin receptor substrate 1, mTOR: mammalian target of rapamycin, PTEN: Phosphatase and tensin homolog, RPS6: Ribosomal protein S6. Values are mean ± SD. Statistical analyses were done by two-tailed unpaired Student's t-test between groups. N = 4-5; *p < 0.05, **p < 0.01.

To test the influence of Cvs on the insulin sensitivity in gWAT, mice from each cohort received either 10 minutes bolus of saline (basal) or insulin (1 U/kg) before scarification. To monitor insulin sensitivity the protein abundance of AKT and its phosphorylation on the insulin stimulated phosphorylation site

AKT^{Ser473}, were conducted in gWAT lysates of stressed and non-stressed WT and FGF21KO mice. Immediately after Cvs, WT (Figure 18A) as well as FGF21KO mice (Figure 18B) mice showed an insulin stimulated AKT Ser^{473}-phosphorylation in non-stressed and stressed conditions. The insulin stimulated AKT^{Ser473} phosphorylation was decreased in WT Cvs compared to WT Ctrl mice. FGF21KO mice showed the opposite, as stressed FGF21KO mice had increased AKT^{Ser473} phosphorylation compared to non-stressed FGF21KO mice. However, beside the insulin activation of AKT, after three-month recovery WT Cvs3m mice showed an enhanced insulin induced AKT^{Ser473} phosphorylation compared to WT Ctrl3m (Figure 18C). FGF21KO Cvs3m mice showed a decreased insulin stimulated AKT^{Ser473} phosphorylation compared to FGF21KO Ctrl3m mice (Figure 18D) although not reaching significance. Similar to the results of the i. p. ITT (Figure 15) in WT mice, the insulin sensitivity changed during the three-month recovery from an impaired insulin action after Cvs and improved after three-month recovery (Figure 18A, C).

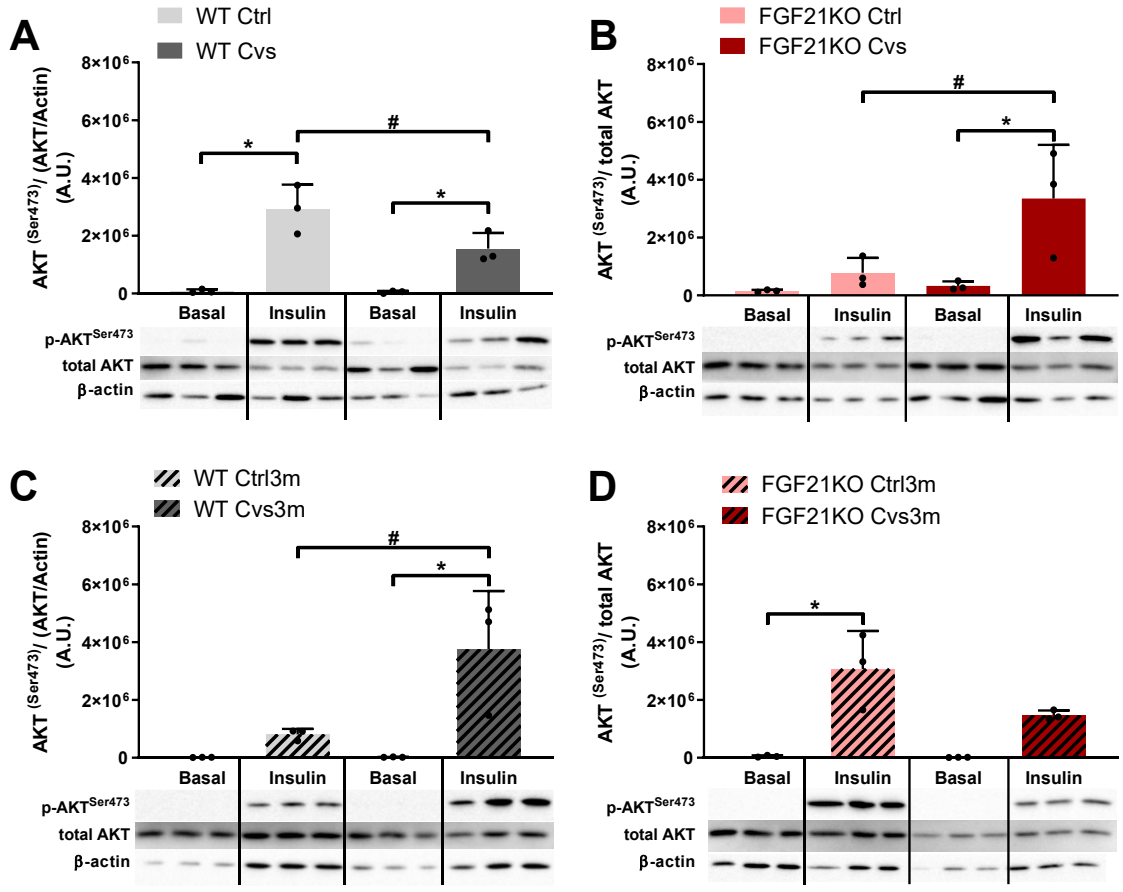

Figure 18: Analyses of insulin signalling in gWAT after Cvs and recovery. Western blot and densitometric analysis of basal and insulin stimulated pAKT^{Ser473} from gWAT obtained after a 10 min bolus of saline or insulin (1 U/kg) from Cvs and Ctrl of WT (A) and FGF21KO (B) mice as well as from Ctrl3m and Cvs3m of WT (C) and FGF21KO (D) mice after 3 months of recovery. Values are mean ± SD. Statistical analyses were done by Two-Way ANOVA followed by Tukey post hoc. N = 3; *p < 0.05, **p < 0.01 within the group; $^{\#}$p < 0.05 between the group.

3.2.6 Effect of Cvs on lipolysis in adipose tissue

Continuously high levels of stress hormones promote lipolysis in the white adipose tissue resulting in increased free fatty acid plasma levels (Xu et al., 2009a). To further investigate possible mechanisms, which affect the lipid metabolism after a chronic stress intervention the plasma levels of free fatty acids were analyzed after Cvs and after recovery. Analyses of total free fatty acids and the fatty acid pattern in plasma of non-stressed and stressed WT and FGF21KO mice revealed increased levels of free fatty acids (Figure 19A) and a higher percentage of cC18:2 fatty acids in WT Cvs mice the in WT Ctrl mice and lower percentage of cC20:4 fatty acids (Figure 19B). FGF21KO mice showed no differences in total free fatty acids (Figure 19C) and in the fatty acid composition after Cvs (Figure 19D). After the three month stress recovery phase free fatty acid levels were massively increased in WT Cvs3m mice (Figure 19E) accompanied by higher C16:0 and cC18:2 and decreased cC16:1 and cC18:1 amount compared to WT Ctrl3m mice (Figure 19F. This increase was abolished in FGF21KO mice as they showed no differences in fatty acid content (Figure 19G) and composition (Figure 19H) also under these conditions.

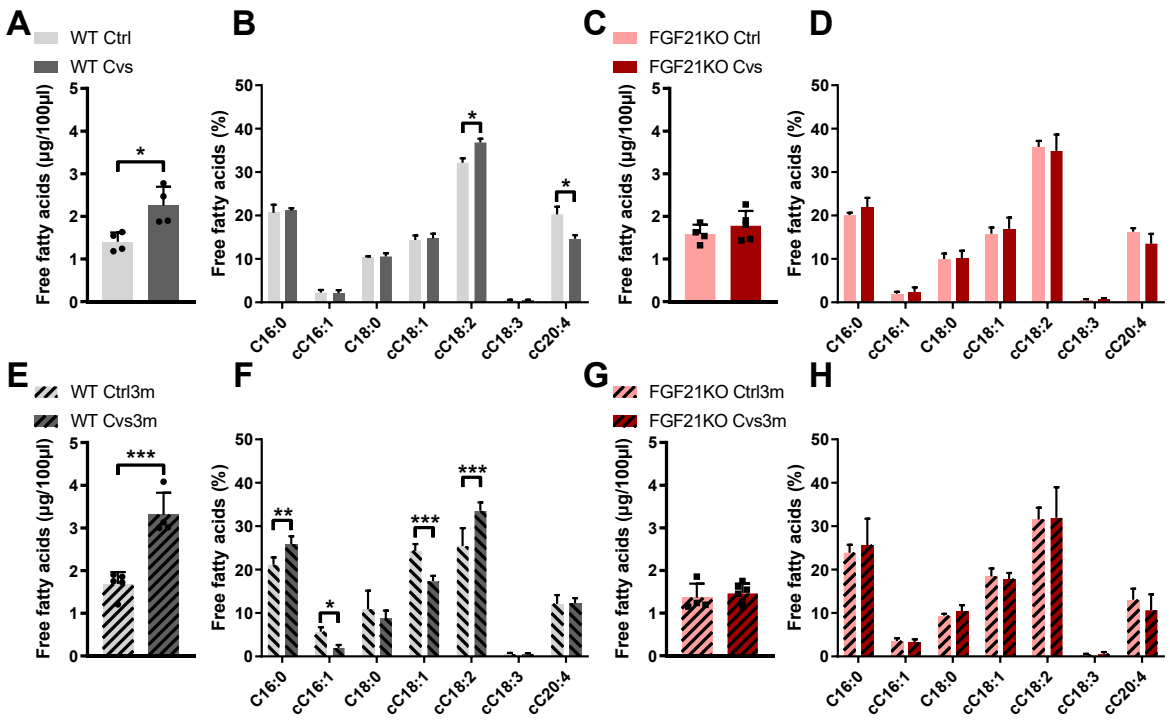

Figure 19: Measurement of free fatty acid pattern in plasma after Cvs and recovery. Analyses of total plasma free fatty acids and the fatty acid pattern after Cvs in WT (A-B) and FGF21KO (C-D) mice as well as after recovery in WT (E-F) and FGF21KO (G-H) mice. Values are mean ± SD. Statistical analyses of total free fatty acids were done by two-tailed unpaired Student's t-test between groups. Statistical analyses of fatty acid pattern were done by Two-Way ANOVA followed by Tukey post hoc. N = 5; *p < 0.05, **p < 0.01 ***p < 0.001.

3.2.7 Influence of FGF21 on lipid metabolism after Cvs and recovery in the liver

Next to the adipose tissue, the liver is a main organ in the metabolism and Cvs regulates change in the glucose and lipid metabolism. Additionally, the liver is the major organ which secretes FGF21 into the blood flow where it acts as metabolic regulator by controlling glucose metabolism, insulin sensitivity and hepatic lipid metabolism (Lin et al., 2017; Nishimura et al., 2000). Based on the results in section 3.1 the next parts of this work focuses the hepatic adaptations after Cvs and the function of FGF21 in the metabolic regulation after stress.

Based on the previous observations, there was a strong correlation between liver fat content and plasma FGF21 levels in C57Bl6 mice (see Figure 9G) (Jelenik, 2018). This observation was first verified in an independent experimental setup using non-stressed or stressed control FGF21 WT mice either directly or after the recovery period to determine plasma FGF21 levels and the amount of hepatic TG content (Figure 9). Non-stressed control (Ctrl) and stressed (Cvs) homozygous wildtype (WT) mice revealed a comparable direct correlation between liver triglycerides and FGF21 in all conditions investigated (Figure 20A). FGF21 plasma levels after Cvs and after 3 months recovery indicate, that directly after Cvs the stressed mice have decreased levels of FGF21, although not reaching significance. After 3 months recovery of the stressed mice, FGF21 levels were significantly increased in plasma. Furthermore, stressed WT mice show higher FGF21 abundance in the liver compared to the respective non-stressed mice, both directly after Cvs and after recovery (Figure 20B). Moreover, after recovery WT Cvs3m mice have increased FGF21 abundance then WT Cvs (Figure 20C). These observations together with former results support the importance of the liver in the metabolic regulation after Cvs intervention and in the adaptation processes in a three months recovery phase.

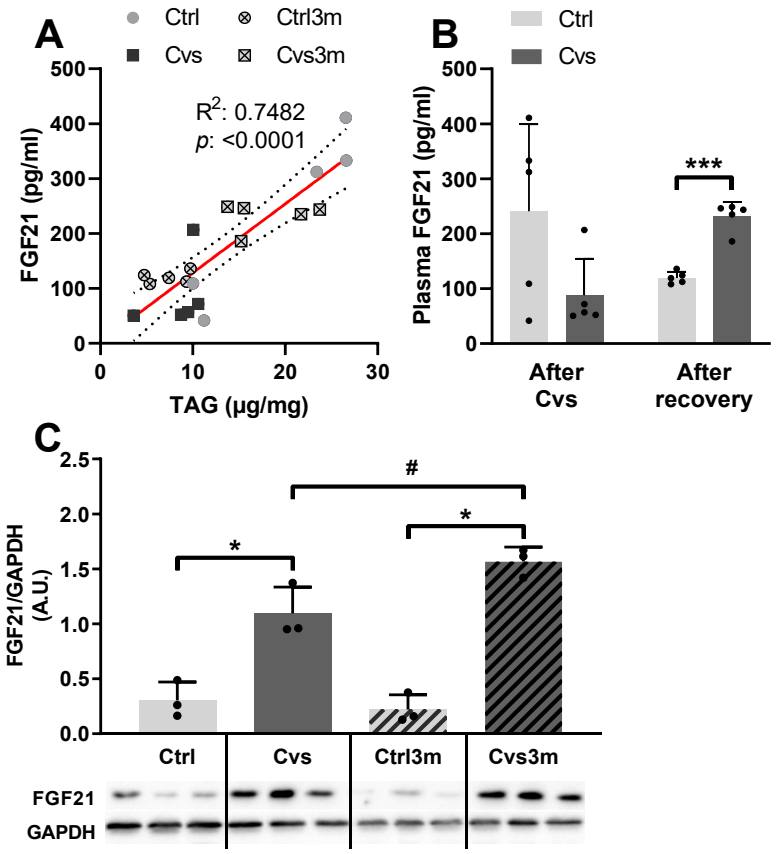

Figure 20: Increased liver triglyceride content correlates with plasma FGF21 levels. Correlation analysis of liver triglycerides (TAG) content and plasma FGF21 (A) n = 5. Plasma FGF21 levels after Cvs and after 3 months of recovery in non-stressed control (Ctrl) mice and stressed (Cvs) mice (B). Hepatic FGF21 abundance in WT mice after Cvs and after three months (3m). Values are mean ± SD. Statistical analyses were performed by Two-Way ANOVA followed by Tukey post hoc. N = 5; ***p < 0.001. r is representing Pearson correlation.

3.2.8 Cellular insulin signaling after Cvs and recovery in the liver

Free fatty acids are known to induce hepatic insulin resistance (Roden et al., 1996) and lead to higher liver triglyceride content. The increased plasma fatty acids levels and composition observed could have an influence on the liver after Cvs in WT and may lead to changes in hepatic energy metabolism, and this at least in part may be dependent on FGF21 (Figure 19). Furthermore, after the recovery period an enhanced hepatic triglyceride storage was observed (Figure 9).

To determine whether the hepatic insulin signaling cascade was affected by Cvs intervention or the resulting physiological alterations, abundance and basal phosphorylation status mTOR/AKT pathway proteins were assessed via bead-based immunoassay in liver lysates of stressed and non-stressed WT and FGF21KO mice, respectively. Short-term Cvs revealed an impact of Cvs on the basal hepatic protein phosphorylation of mTOR/AKT pathway proteins, which could be the basis of long-term alterations in hepatic insulin sensitivity. WT Cvs mice showed significantly decreased basal levels of AKT and PTEN

phosphorylation due to the Cvs intervention (Figure 21A). Moreover, FGF21KO mice showed also a stress-induced decrease in AKT and PTEN phosphorylation, together with an increased basal phosphorylation of GSK3β (Figure 21B).

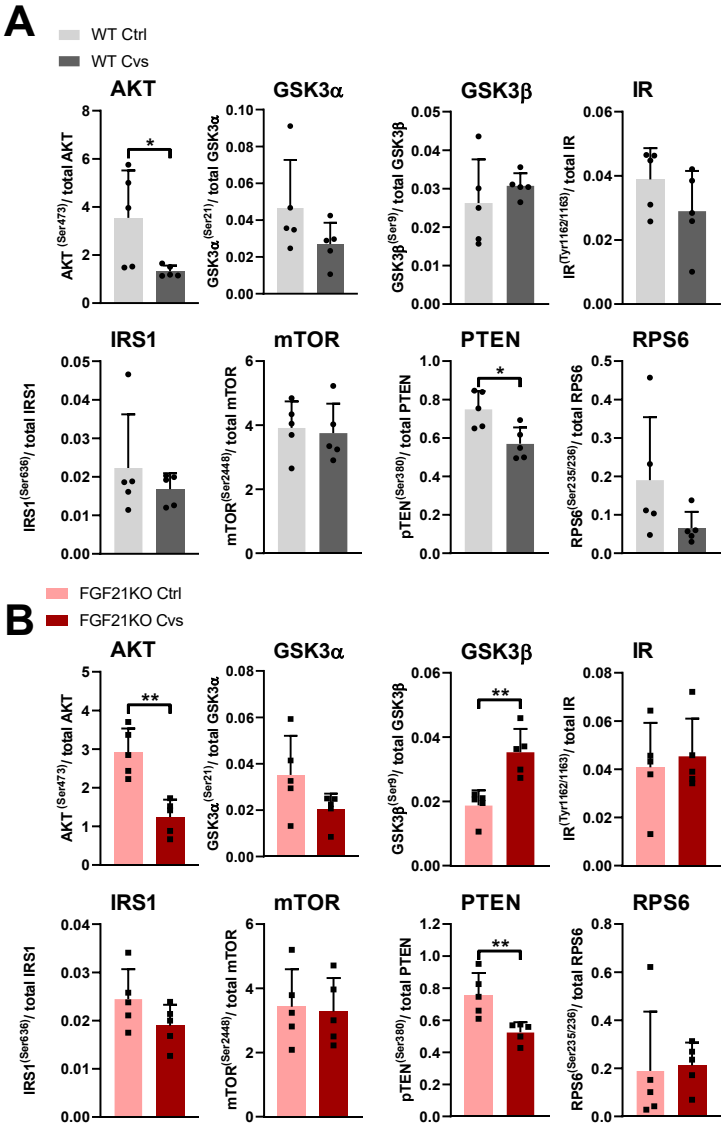

Figure 21: Relative quantification of basal multiple phosphorylation and total mTOR/AKT pathway proteins in the liver after Cvs. Analysis of multiple basal phosphorylation and total mTOR/AKT pathway proteins after Cvs in WT (A) and FGF21KO (B) mice directly after Cvs. Akt = Proteinkinase B, GSK3α + β: Glycogen synthase kinase 3α + β, IR: Insulin receptor, IRS1: Insulin receptor substrate 1, mTOR: mammalian target of rapamycin, PTEN: Phosphatase and tensin homolog, RPS6: Ribosomal protein S6. Values are mean ± SD. Statistical analyses were performed by two-tailed unpaired Student's t-test between groups. N = 4-5; *p < 0.05, **p < 0.01.

To test the influence of Cvs on the insulin sensitivity in liver, mice from each cohort received either 10 minutes bolus of saline (basal) or insulin (1 U/kg) before scarification. To monitor insulin sensitivity the protein abundance of AKT and its phosphorylation on the insulin stimulated phosphorylation site

AKT^{Ser473}, were conducted in liver lysates of stressed and non-stressed WT and FGF21KO mice. Analyses of AKT abundance revealed an insulin induced serine 473 phosphorylation due to the injection of insulin (Figure 22A-D) in all conditions. However, the focus lies on the influence of Cvs on the insulin stimulation. The results show a decreased basal and insulin stimulated serine 473 phosphorylation of WT Cvs mice compared to WT Ctrl mice (Figure 22A). This comparison did not reach significance in stressed FGF21KO mice (Figure 22B). After three months of recovery the insulin stimulated AKT^{Ser473} phosphorylation was increased in WT Cvs 3m mice compared to the respective control WT Ctrl3m mice (Figure 22C). FGF21KO mice showed no changes after recovery in basal or insulin stimulated AKT^{Ser473} phosphorylation due to the previous Cvs intervention (Figure 22D). So, also in the liver a change of the insulin action three months after the Cvs intervention is visible. The initially stress-induced reduction in insulin action shift to an enhanced insulin stimulated AKT^{Ser473} phosphorylation after the recovery. Again, this may at least in part be mediated by FGF21.

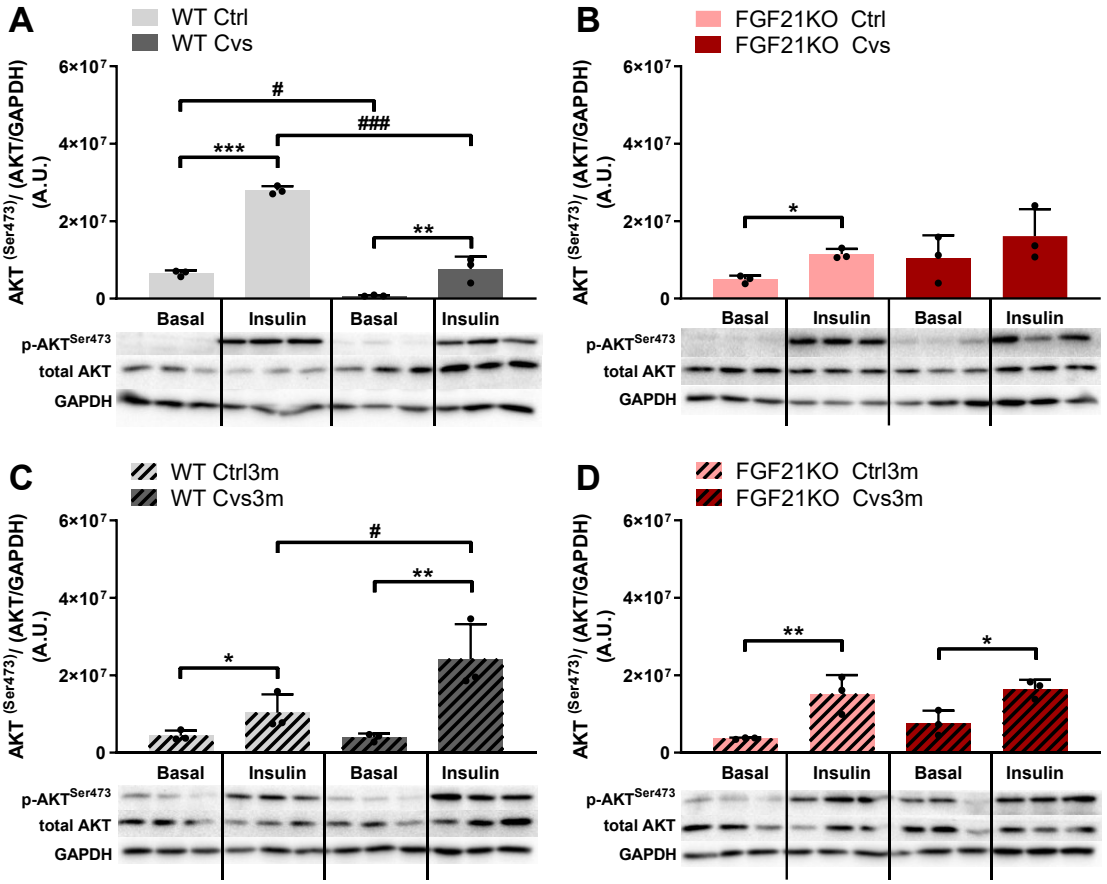

Figure 22: Analyses of hepatic insulin dependent AKT Ser473 phosphorylation after Cvs and recovery. Western blot and densitometric analysis of basal and insulin stimulated pAKT^{Ser473} from liver obtained after a 10 min bolus of saline or insulin (1 U/kg) from Cvs and Ctrl of WT (A) and FGF21KO (B) mice as well as from Ctrl3m and Cvs3m of WT (C) and FGF21KO (D) mice after 3 months of recovery. Values are mean ± SD. Statistical analyses were done by Two-Way ANOVA followed by Tukey post hoc. N = 3; *p < 0.05, **p < 0.01 within the group; #p < 0.05 between the group.

Besides the AKT activation via the phosphorylation of serine 473, AKT is also activated by a threonine 308 phosphorylation. Analyses of the AKT^{Thr308} phosphorylation in liver protein lysates exhibited an increased insulin-induced AKT^{Thr308} phosphorylation in WT Ctrl mice but not in WT Cvs mice (Figure 23A). FGF21KO deficiency resulted in no differences in basal or insulin-induced AKT^{Thr308} phosphorylation after Cvs (Figure 23B). Three months after Cvs, WT mice showed an enhanced insulin-induced AKT^{Thr308} phosphorylation, but no significant stress related changes in basal or insulin stimulated AKT^{Thr308} phosphorylation (Figure 23C). Beside the insulin-induced AKT^{Thr308} phosphorylation, FGF21KO Cvs3m mice had also a general higher phosphorylation compared to FGF21KO Ctrl3m mice (Figure 23D).

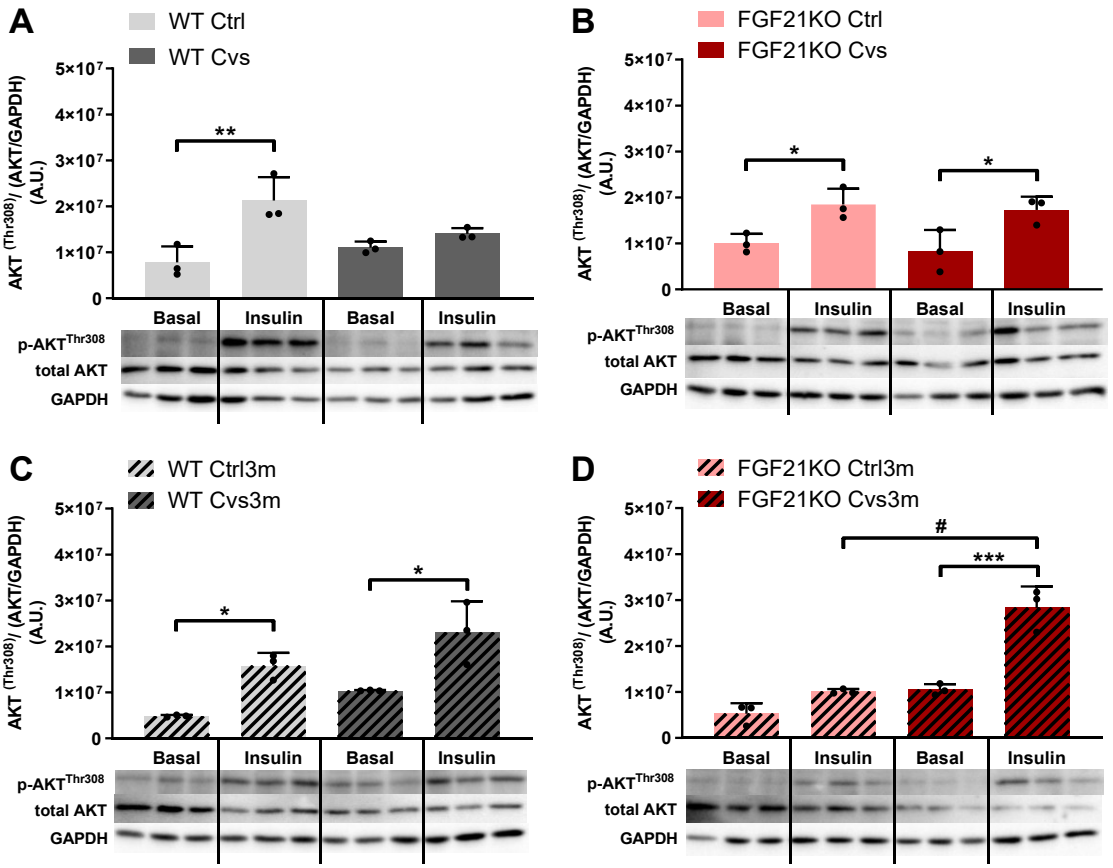

Figure 23: Analyses of hepatic insulin dependent AKT Thr308 phosphorylation after Cvs and recovery. Western blot and densitometric analysis of basal and insulin stimulated pAKT^{Thr308} from liver obtained after a 10 min bolus of saline or insulin (1 U/kg) from Cvs and Ctrl of WT (A) and FGF21KO (B) mice as well as from Ctrl3m and Cvs3m of WT (C) and FGF21KO (D) mice after 3 months of recovery. Values are mean ± SD. Statistical analyses were done by Two-Way ANOVA followed by Tukey post hoc. N = 3; *p < 0.05, **p < 0.01 within the group; #p < 0.05 between the group.

The hepatic glucose metabolism is not only regulated by insulin, but also by glucocorticoids (GC). GC can enter the cell from the blood flow or they are converted intracellularly from cortisone by the enzyme 11β-Hydroxysteroide dehydrogenase type 1 (11β-HSD1). GC bind to the glucocorticoid

receptor (GR), which becomes hyperphosphorylated and translocates into the nucleus to activate nuclear targets (Bodwell et al., 1998). The activation and nuclear translocation of the GR is featured by serine 211 phosphorylation, a key regulator of receptor transcriptional activation and repression and a biomarker for hormone activated nucleus translocation (Chen et al., 2008; Wang et al., 2002).

Cvs does not interfere with GR^{Ser211} phosphorylation in WT mice directly after the stress intervention (Figure 24A), but FGF21KO Cvs mice show an increased GR^{Ser211} phosphorylation after insulin stimulus compared to FGF21KO Ctrl mice (Figure 24

Figure 24B). Interestingly, both WT Cvs and FGF21KO Cvs mice showed an enhanced phosphorylation after insulin injection compared to basal levels. However, after three months of recovery WT Cvs3m mice had an enhanced GR^{Ser211} phosphorylation in basal and insulin treated state compared to WT Ctrl3m mice (Figure 24C), whereas FGF21KO mice showed no differences due to Cvs (Figure 24D). In WT animals, activation of the GR by phosphorylation changes over the recovery phase. The activated GR could be a possible regulator of metabolic changes after the recovery phase.

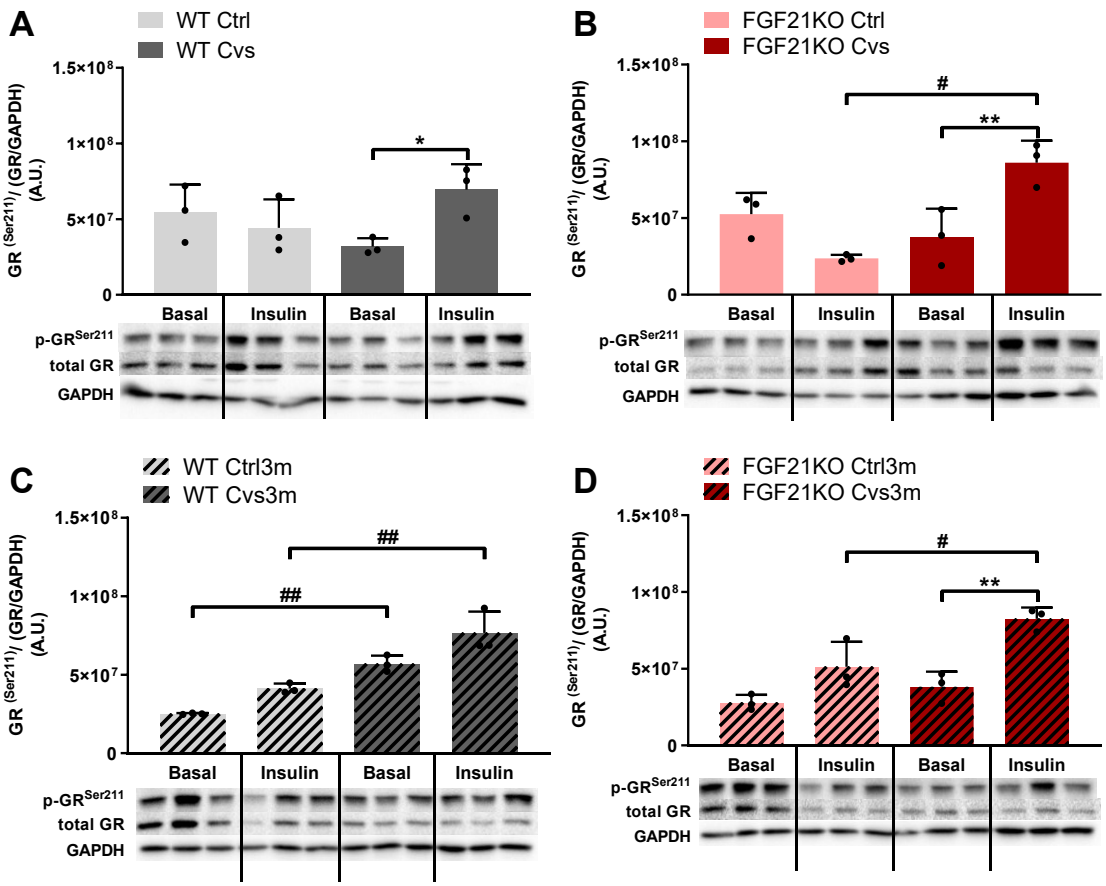

Figure 24: Analyses of hepatic GR Ser211 phosphorylation after Cvs and recovery. Western blot and densitometric analysis of basal and insulin stimulated pGR^{Ser211} from liver obtained after a 10 min bolus of saline or insulin (1 U/kg) from Cvs and Ctrl of WT (A) and FGF21KO (B) mice as well as from Ctrl3m and Cvs3m of WT (C) and FGF21KO (D) mice after 3 months of recovery. Values are mean ± SD. Statistical analyses were done by Two-Way ANOVA followed by Tukey post hoc. N = 3; *p < 0.05, **p < 0.01 within the group; #p < 0.05 between the group.

To investigate the crucial role of CG in the regulation of the hepatic glucose metabolism, and protein abundance of 11β-HSD1 as marker for intracellular conversion, and GR^{Ser211} phosphorylation were analyzed in this study.

Analyses of hepatic 11β-HSD1 protein abundance show no significant differences due to the Cvs intervention or the FGF21 deficiency (Figure24) indicating no role for intracellular conversion to increase GC concentration, thus focusing solely on GC from the circulation.

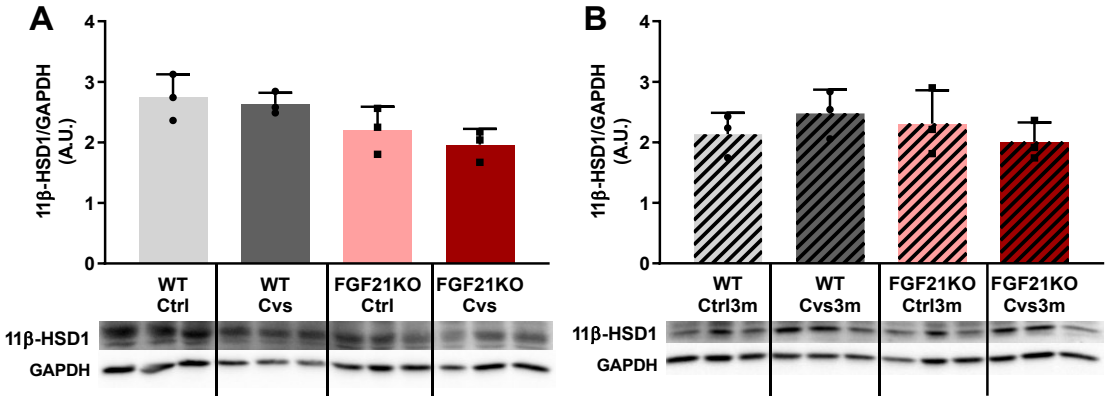

Figure 25: Analyses of hepatic 11β-HSD1 protein abundance after Cvs and recovery. Western blot and densitometric analysis of hepatic 11β-HSD1 protein abundance in short-term (A) and long-term (B) liver lysates of stressed and non-stressed WT and FGF21KO mice. Values are mean ± SD. Statistical analyses were performed by Two-Way ANOVA followed by Tukey post hoc. N = 3.

3.2.9 Impact of Cvs on insulin sensitivity in isolated hepatocytes

Insulin sensitivity was determined by analyzing the mTOR/AKT pathway proteins under basal and insulin (10 nM) treated conditions. Therefore, primary hepatocytes from all groups were treated for 10 minutes with saline or insulin. Hepatocytes isolated from WT and FGF21KO immediately after Cvs showed no significant changes, neither due to insulin stimulation, nor Cvs (Figure 26).

On the other hand, hepatocytes isolated from WT and FGF21KO after the 3 month recovery phase revealed an increased AKT^{Ser473} phosphorylation due to insulin stimulation in WT Ctrl3m and WT Cvs3m hepatocytes (Figure 27A). In addition, WT Cvs3m show a higher insulin stimulated mTOR^{Ser2448} phosphorylation compared to WT Ctrl3m. In contrast, FGF21KO hepatocytes showed no phosphorylation differences of insulin signaling proteins at all after the recovery phase (Figure 27B).

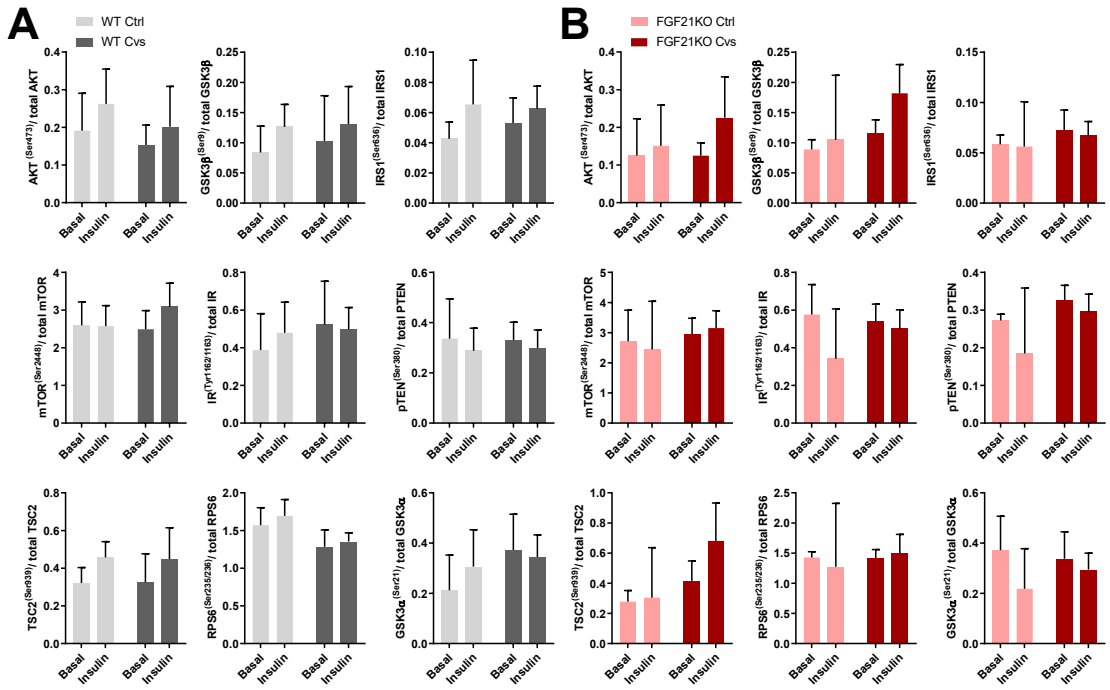

Figure 26: Relative quantification of phosphorylation and total mTOR/AKT pathway proteins in hepatocytes after Cvs. Analysis of multiple phosphorylation and total mTOR/AKT pathway proteins after Cvs in hepatocytes of WT (A) and FGF21KO (B) mice. Akt = Proteinkinase B, GSK3α + β: Glycogen synthase kinase 3α + β, IR: Insulin receptor, IRS1: Insulin receptor substrate 1, mTOR: mammalian target of rapamycin, PTEN: Phosphatase and tensin homolog, RPS6: Ribosomal protein S6. Values are mean ± SD. Statistical analyses were done by Two-Way ANOVA followed by Tukey post hoc. N = 4-5.

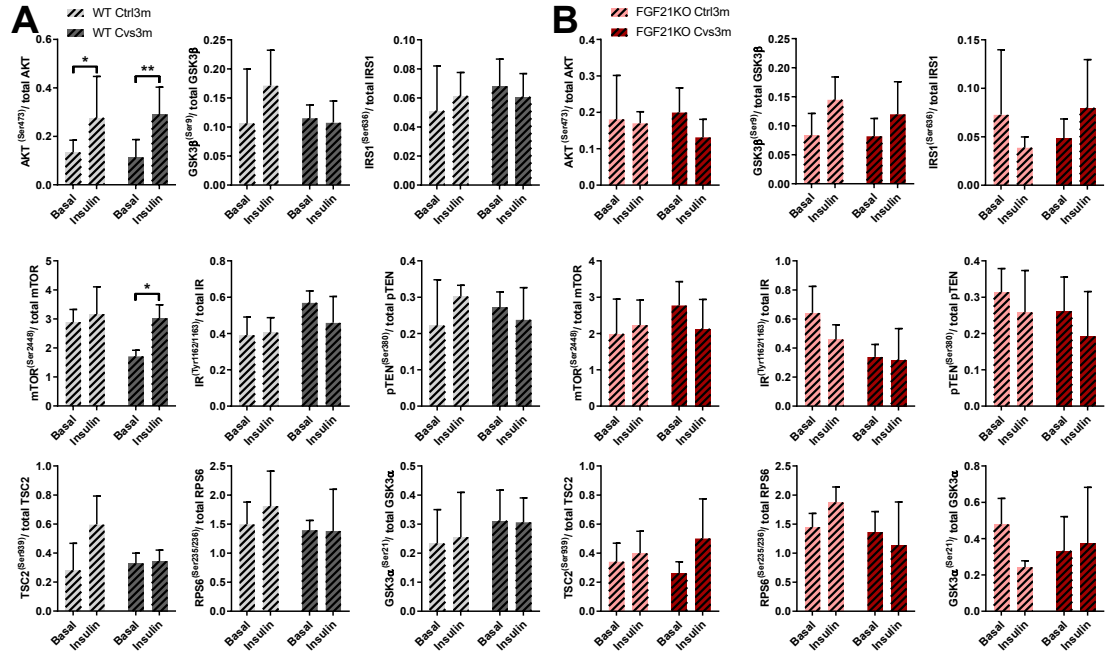

Figure 27: Relative quantification of phosphorylation and total mTOR/AKT pathway proteins in hepatocytes after recovery. Analysis of multiple phosphorylation and total mTOR/AKT pathway proteins after recovery in hepatocytes of WT (A) and FGF21KO (B) mice. Akt = Proteinkinase B, GSK3α + β: Glycogen synthase kinase 3α + β, IR: Insulin receptor, IRS1: Insulin receptor substrate 1, mTOR: mammalian target of rapamycin, PTEN: Phosphatase and tensin homolog, RPS6: Ribosomal protein S6. Values are mean ± SD. Statistical analyses were done by Two-Way ANOVA followed by Tukey post hoc. N = 4-5.

3.2.10 Glucose metabolism in isolated hepatocytes short- and long-term after Cvs

The effect of direct Cvs and three months recovery on glucose production and secretion of primary hepatocytes was investigated in WT and FGF21KO mice. To monitor glucose release, hepatocytes were incubated in glucose free medium and were treated with insulin to inhibit gluconeogenesis and pyruvate/lactate to stimulate the gluconeogenesis prior to measurement of glucose secreted into the medium. All experimental conditions responded to lactate/pyruvate induction with a maximal increase of glucose secretion, indicating functionality of the assay. Primary hepatocytes from stressed Cvs animals, either WT (Figure 28A) or FGF21KO (Figure 28B) had a higher glucose secretion, probably due to the positive influence of glucocorticoids on gluconeogenesis. Primary hepatocytes isolated from WT mice after the recovery phase only showed a marginal insulin-mediated inhibition of glucose secretion. In contrast to short-term Cvs, WT Cvs3m exhibit after three months a general decrease in glucose secretion (Figure 28C). Hepatocytes from FGF21KO show the typical insulin and pyruvate/lactate action in non-stressed and stressed hepatocytes also after three months of recovery (Figure 28D). Accordingly, Cvs had a long-term impact on glucose secretion in hepatocytes, which involved FGF21.

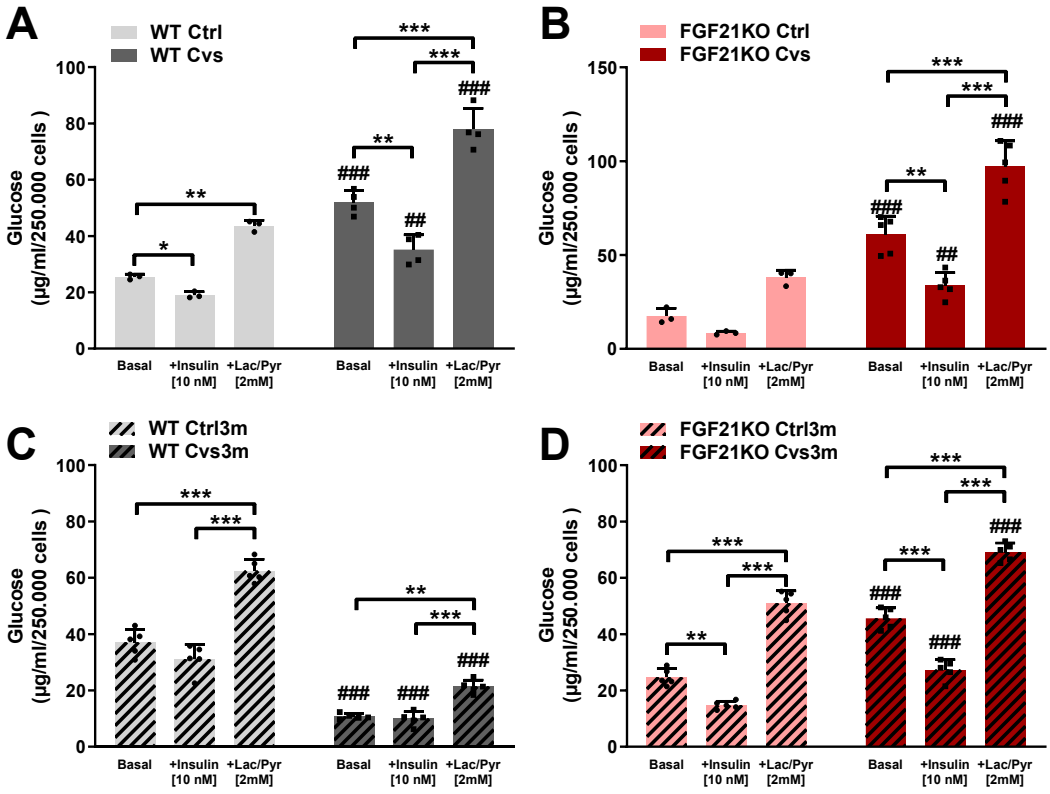

Figure 28: Glucose secretion from primary hepatocytes of WT and FGF21KO after Cvs and recovery. Measurement of released glucose from basal, insulin (10 nM) and pyruvate/lactate (2 mM) treated primary hepatocytes after Cvs and recovery in WT (A and C) and FGF21KO (B and D) mice, respectively. Values are mean ± SD. Statistical analyses were done by Two-Way ANOVA followed by Tukey post hoc. CPM: Counts per minute. N = 3-5; *p < 0.05, **p < 0.01, ***p < 0.001 within the group; #p < 0.05, ##p < 0.01, ###p < 0.001 between the group.

High levels of glucocorticoids during stress periods down-regulate the glycolysis by promoting gluconeogenesis. The glycolytic potential was determined by extracellular acidification rate (ECAR) in the seahorse® flux analyzer. ECAR was used to evaluate the glycolytic activity of hepatocytes by measuring the acidification of the medium.

In primary hepatocytes derived from all conditions an increased ECAR after glucose stimulation was observed. ECAR levels between WT Ctrl and WT Cvs hepatocytes showed no significant differences in basal and glucose stimulated conditions (Figure 29A). On the other hand, FGF21KO hepatocytes showed lower ECAR if derived from prior stressed mice compared to non-stressed conditions (Figure 29B). From these measurements the calculated glycolysis showed a lower tendency but no significance in hepatocytes received from WT mice (Figure 29C). Primary hepatocytes derived from FGF21KO Cvs had a significant lower glycolysis compared to FGF21KO Ctrl (Figure 29D). These findings are in line with the stressed-induced glucose production due to enhanced gluconeogenesis after Cvs in hepatocytes from stressed mice (see Figure 28).

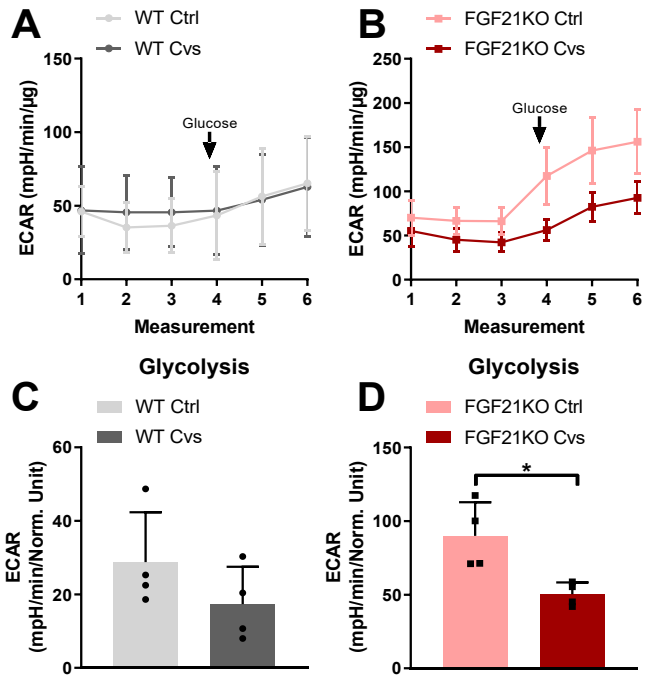

Figure 29: Measurement of glycolysis in hepatocytes of WT and FGF21KO mice after Cvs. The basal and glucose stimulated extracellular acidification rate (ECAR) were analyzed in primary hepatocytes from non-stressed (Ctrl) and stressed (Cvs) WT (A) and FGF21KO (B) mice. Calculated glycolysis rate was determined from OCR levels before and after glucose injection from WT (C) and FGF21KO (D). Values are mean ± SD. Statistical analyses were done by two-tailed unpaired Student's t-test between groups. N = 4-5; *p < 0.05.

Long-term analyses after 3 month recovery revealed an increased ECAR after glucose stimulation, but no different ECAR levels in relation to Cvs of both primary hepatocytes derived from WT (Figure 30A) and FGF21KO (Figure 30B) animals. The calculated glycolysis rate also showed no significant differences between Ctrl3m and Cvs3m after the three months recovery phase in primary hepatocytes derived

from WT (Figure 30C) and FGF21KO (Figure 30D). Hepatocytes from previous stressed mice show a high individual variability in ECAR levels.

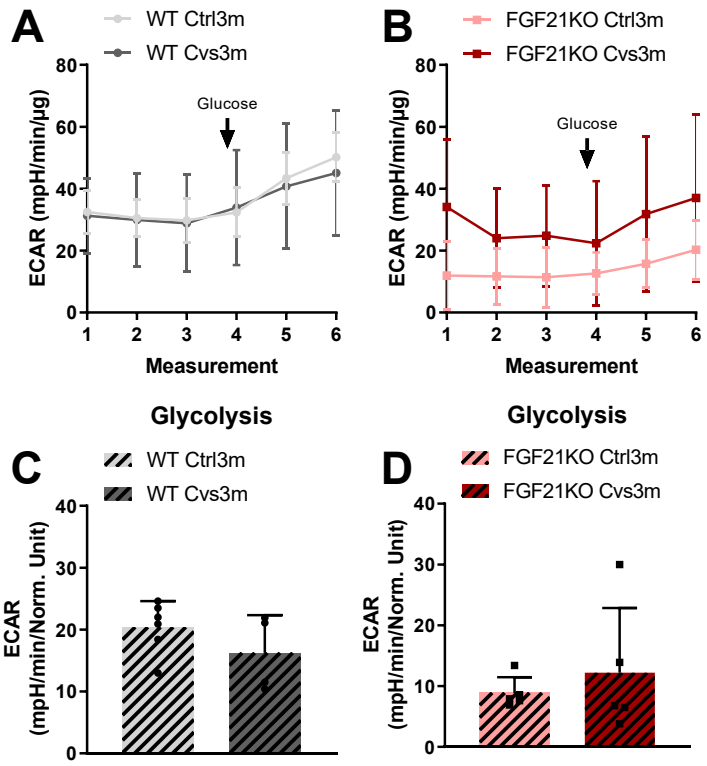

Figure 30: Measurement of glycolysis in hepatocytes of WT and FGF21KO mice after recovery. The basal and glucose stimulated extracellular acidification rate (ECAR) were analyzed in primary hepatocytes from non-stressed (Ctrl) and stressed (Cvs) WT (A) and FGF21KO (B) mice. Calculated glycolysis rate was determined from OCR levels before and after glucose injection from WT (C) and FGF21KO (D). Values are mean ± SD. Statistical analyses were done by two-tailed unpaired Student's t-test between groups. N = 4-5; *p < 0.05.

3.2.11 Lipid metabolism in isolated hepatocytes short- and long-term after Cvs

Beside the gluconeogenesis the hepatic lipid metabolism plays another crucial role in the metabolism after chronic stress and in possible adaptation processes.

Mice, which were stressed before show after three months an increase in hepatic triglyceride content (see Figure 9 and Table 12). To investigate possible mechanism which lead to these changes in hepatic fat storage, *de novo* lipogenesis (DNL), fatty acid uptake and oxidation were analyzed in isolated primary hepatocytes.

Primary hepatocytes were treated with insulin to investigate the insulin-induced DNL. The DNL was analyzed by measuring incorporated lipid precursor [C^{14}]-acetate over a defined time period. The results showed that in both, WT Ctrl and WT Cvs mice insulin stimulated DNL and Cvs did not interfere with lipogeneses (Figure 31A). In contrast, in primary hepatocytes of FGF21KO mice insulin was not able to induce DNL independent to Cvs (Figure 31B). After three months recovery, in primary

hepatocytes derived from WT mice showed also an insulin stimulated DNL independent to previous stress, respectively. However, in primary hepatocytes derived from previously stressed WT Cvs3m mice in general had a reduced DNL compared to the control condition (Figure 31C). Primary hepatocytes derived from unstressed FGF21KO mice still showed no insulin inducible DNL (Figure 31D), but if cells were isolated from stressed FGF21KO mice insulin induced DNL was reconstituted compared to its basal condition. These results show the long-term inhibitory influence of Cvs on the hepatic DNL and the protective role of FGF21 depletion in this process.

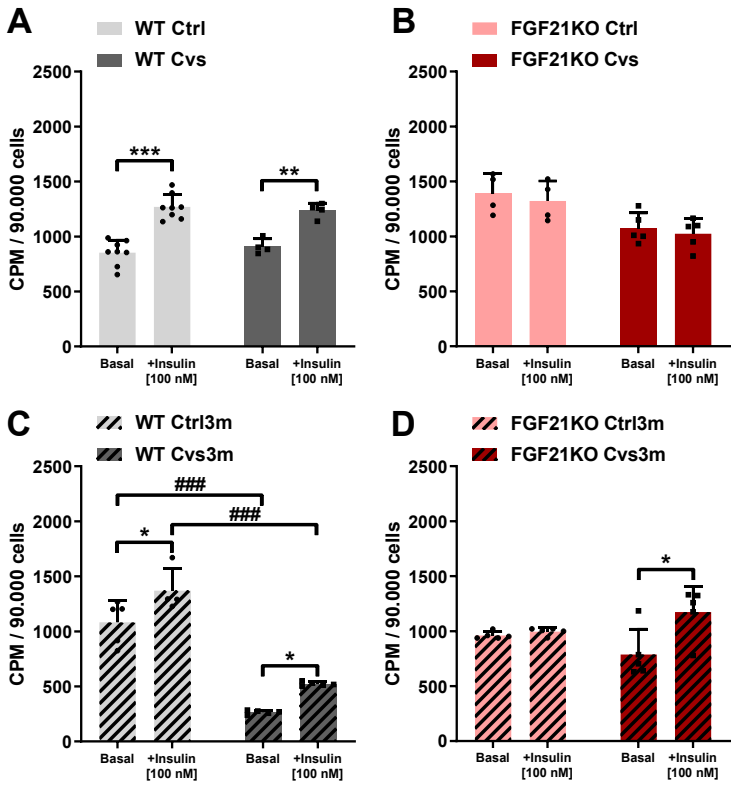

Figure 31: *De novo* lipogenesis (DNL) in primary hepatocytes of WT and FGF21KO after Cvs and recovery. Measurement of incorporated [C^{14}]-acetate in basal and insulin (100 nM) treated primary hepatocytes after Cvs and recovery in WT (A and C) and FGF21KO (B and D) mice, respectively. Values are mean ± SD. Statistical analyses were done by Two-Way ANOVA followed by Tukey post hoc. CPM: Counts per minute. N = 5; *p < 0.05, **p < 0.01, ***p < 0.001 within the group; #p < 0.05, ##p < 0.01, ###p < 0.001 between the group.

From the results of the insulin-stimulated DNL it is unlikely that DNL is the major player resulting in the higher hepatic lipid storage observed in stressed mice after the recovery phase. Alterations of the fatty acid uptake could also be the reason for the Cvs associated increased hepatic lipid storage. Fatty acid uptake was analyzed by measuring the absorbed radioactive labelled [C^{14}]-palmitate into isolated primary hepatocytes from non-stressed and stressed mice from all experimental conditions. Overall, fatty acid uptake to hepatocytes from FGF21KO mice was higher of compared to the WT littermates (Figure). The results further showed an enhanced fatty acid uptake due to Cvs intervention in WT mice

(Figure 32A) and FGF21KO mice (Figure 32B). After the recovery phase, hepatocytes from WT Cvs3m mice show still an increased fatty acid uptake then hepatocytes from WT Ctrl3m mice (Figure 32C). In contrast, hepatocytes from FGF21KO Cvs3m mice exhibit a decreased fatty acid uptake after three months compared to FGF21KO Ctrl3m (Figure 32D).

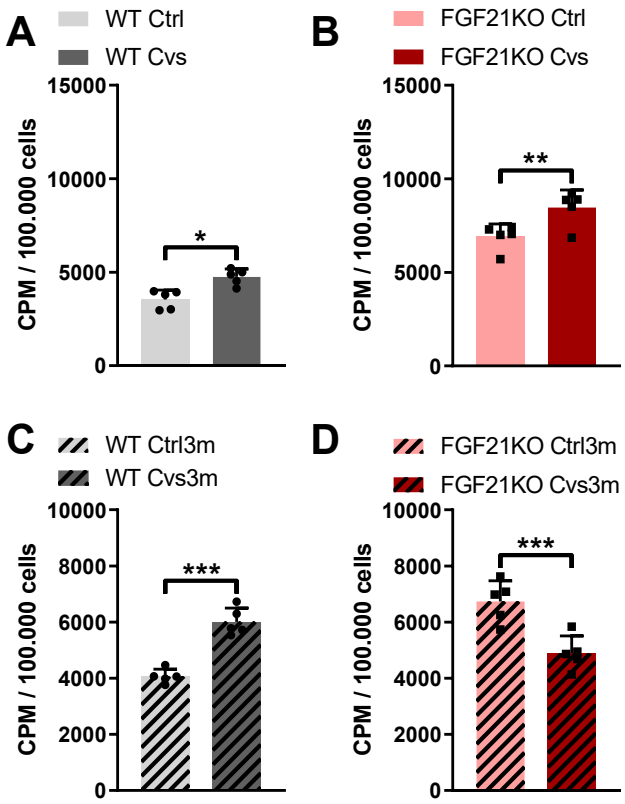

Figure 32: Fatty acid uptake in primary hepatocytes of WT and FGF21KO after Cvs and recovery. Measurement of resorbed [C^{14}]-palmitate in primary hepatocytes after Cvs and recovery in WT (A and C) and FGF21KO (B and D) mice, respectively. CPM: Counts per minute. Values are mean ± SD. Statistical analyses were done by two-tailed unpaired Student's t-test between groups. N = 5; *p < 0.05, **p < 0.01, ***p < 0.001 within the group.

Next to lipid synthesis and uptake, the degree of fatty acid degradation by oxidation can account to an increased hepatic lipid accumulation, as observed. Alterations in this process interfere with hepatic fat accumulation and changes in hepatic energy metabolism. To determine FAO, primary hepatocytes were incubated with radioactive labelled palmitate and the released [H^3]-CO_2 was captured to determine the rate of oxidized fatty acids. In primary hepatocytes derived from Cvs conditions of both WT (Figure 33A) and FGF21KO (Figure 33B) mice had higher basal fatty acid oxidation compared to hepatocytes received from Ctrl mice. After the three-month recovery hepatocytes from WT Cvs3m showed decreased basal end cellular oxidation compared to WT Ctrl3m (Figure 33C). So, the short-term increased basal fatty acid oxidation was not maintained over the recovery phase. Hepatocytes derived from FGF21KO Cvs3m mice also showed a lower basal fatty acid oxidation compared to FGF21KO Ctrl3m (Figure 33D). Furthermore, in these experiments etomoxir was used to inhibit the

mitochondrial fatty acid oxidation in primary hepatocytes. Etomoxir inhibits the transport of fatty acids into the mitochondrial intermembrane space and thus it is possible to determine the cellular, thus non-mitochondrial respiration. The analyses showed, that the non-mitochondrial fatty acid oxidation was significant lower in all experimental groups compared to the basal oxidation, and no significant alterations were observed in the conditions in relation to the respective controls (Figure 33A-D). Taken together long-term effects of stress showed a reduced fatty acid oxidation which tends to aggravate due to FGF21 deficiency.

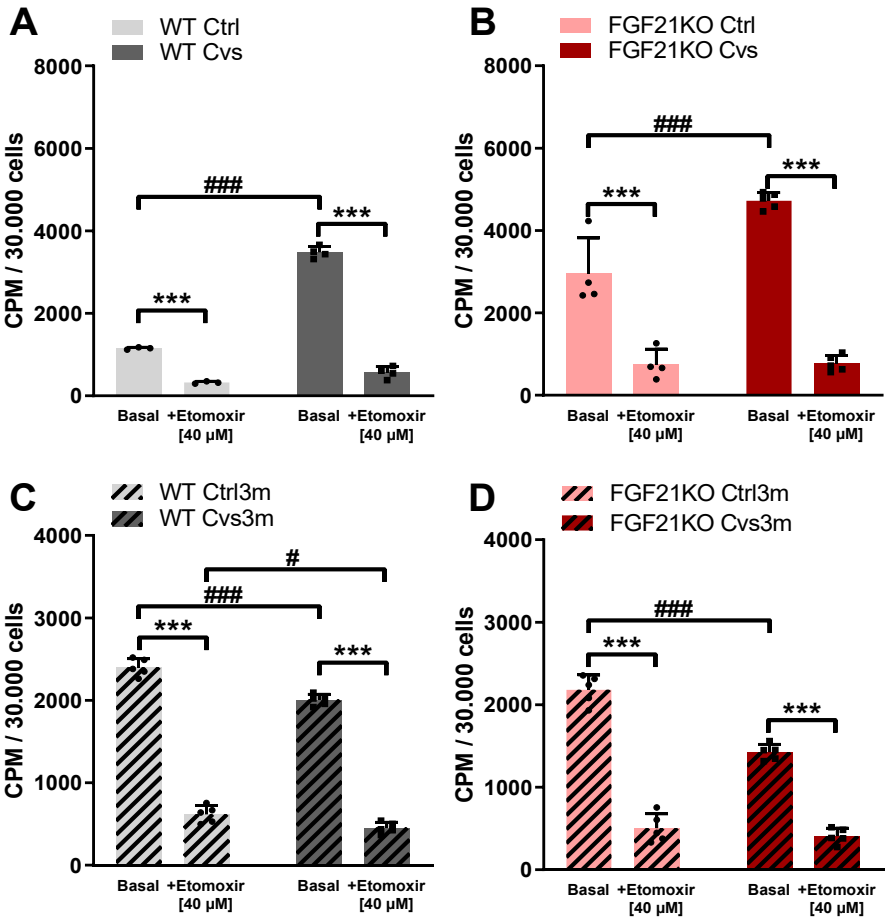

Figure 33: Fatty acid oxidation in primary hepatocytes of WT and FGF21KO after Cvs and recovery. Measurement of released [H^3]-CO_2 of basal and etomoxir (40 µM) treated primary hepatocytes after Cvs and recovery in WT (A and C) and FGF21KO (B and D) mice, respectively. CPM: Counts per minute. Statistical analyses were done by two-tailed unpaired Student's t-test between groups. N = 5; *p < 0.05, **p < 0.01, ***p < 0.001 within the group; #p < 0.05, ##p < 0.01, ###p < 0.001 between the group.

The previous results show, that the lipid uptake and change in fatty acid oxidation could be responsible for the changes in hepatic lipid accumulation three months after Cvs in WT mice and FGF21 could be protective. Based on these results, the mitochondrial respiration could be a possible regulator of the hepatic metabolic adaptations after chronic stress. The analysis of the mitochondrial function was performed using the seahorse® technology, which enables the measuring the oxygen consumption

rate (OCR). The use of specific inhibitors further narrows down the activity of the mitochondrial chain components. ATP production can be calculated by inhibiting ATP-synthase with oligomycin injection to the assay. The following injection of FCCP causes the disruption of ATP synthesis by transporting protons through the mitochondrial membrane and enables the calculation of the maximal mitochondrial respiration. In a last step, the injection of rotenone and antimycin A inhibits the entire mitochondrial respiration.

The mitochondrial function was analyzed in isolated primary hepatocytes from WT and FGF21KO mice after Cvs exposure and after the recovery of three months. Figure 34A and B show the profiles of time course of measurements. The time points of compound injections are marked with arrows.

In primary hepatocytes derived from WT mice no Cvs related differences in ATP synthesis or mitochondrial respiration or capacity as well as non-mitochondrial respiration were observed (Figure 34 grey bars). However, in FGF21 deficiency the complete OCR is reduced in stressed mice (Figure 34B). Especially after FCCP injection no marked rise was observed, resulting in reduced non-mitochondrial oxygen consumption, maximal respiration and spare respiratory capacity (Figure 34E, I, M). The computed basal respiration, ATP production and proton leak showed (Figure 34F, J, N) no significant changes because of a high sample variability.

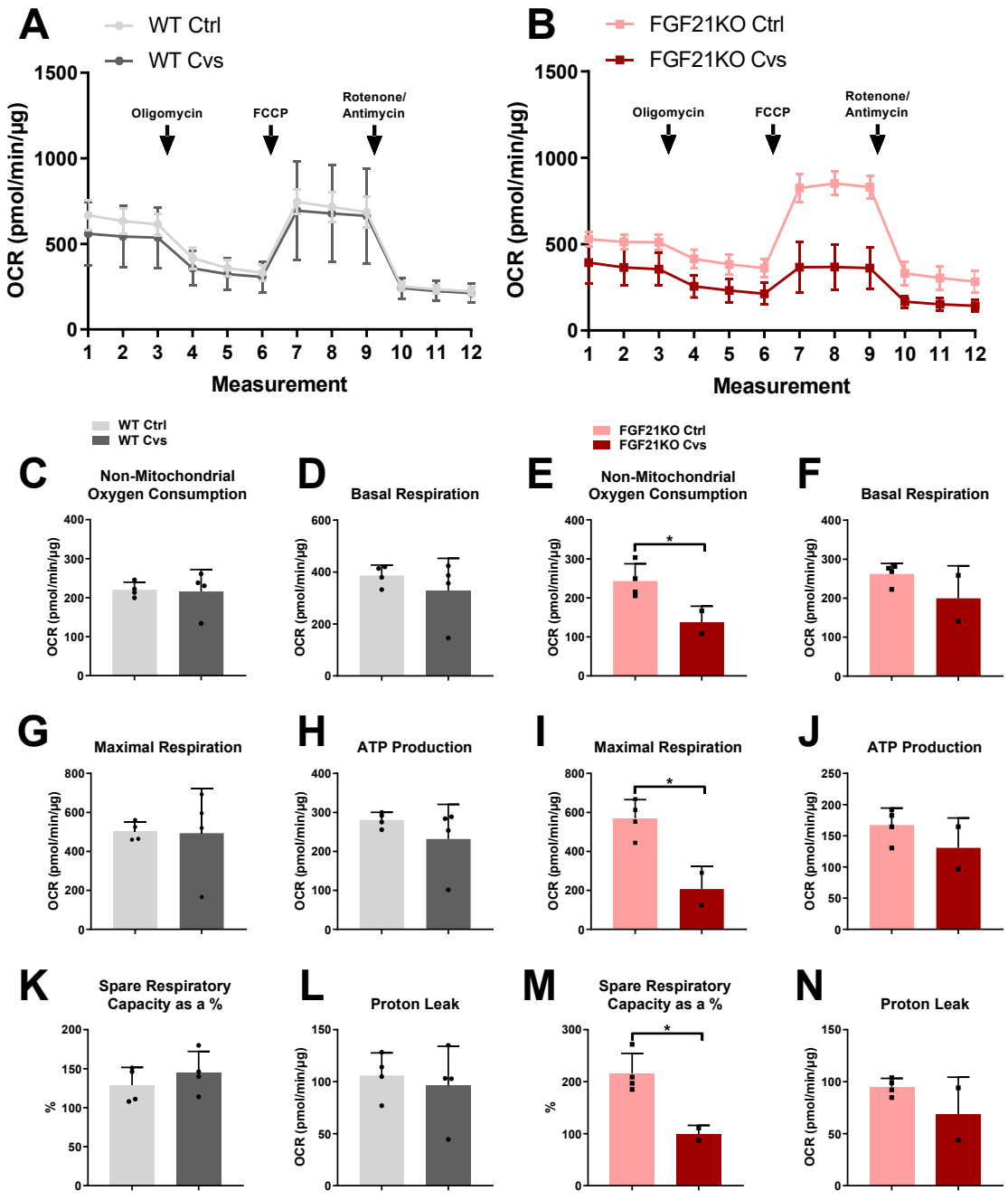

Figure 34: Analyses of mitochondrial respiration in WT and FGF21KO hepatocytes after Cvs. The OCR were measured in a cycle of 3 for basal and after each compound injection in hepatocytes from non-stressed (Ctrl) and stressed (Cvs) WT (A) and FGF21KO (B) mice. Different parameters including non-mitochondrial oxygen consumption (C, E), basal respiration (D, F), maximal respiration (G, I), ATP production (H, J), spare respiratory capacity (K, M) and proton leak (L, N) were computed from the OCR from WT (grey bars) and FGF21KO (red bars) mice, respectively. Values are mean ± SD. Statistical analyses were done by two-tailed unpaired Student's t-test between groups. N = 2-5; *p < 0.05.

After the three months recovery phase, OCR analyses of hepatocytes from WT and FGF21KO mice exposed a small overall decrease of OCR rates in hepatocytes derived from WT Cvs mice, but this was not reaching significance (Figure 35A). Like immediately after Cvs, no significant differences on

mitochondrial function was observed, too (Figure 35 grey bars). In contrast, primary hepatocytes derived from FGF21 Cvs3m showed higher OCR (Figure 35B), which resulted in increased basal and maximal respiration as well as in higher ATP production and proton leak (Figure 35F, I, J, N). Due to previous Cvs exposure, the non-mitochondrial oxygen consumption and spare respiratory capacity were not affected and showed no significant change in FGF21KO hepatocytes (Figure 35E, M).

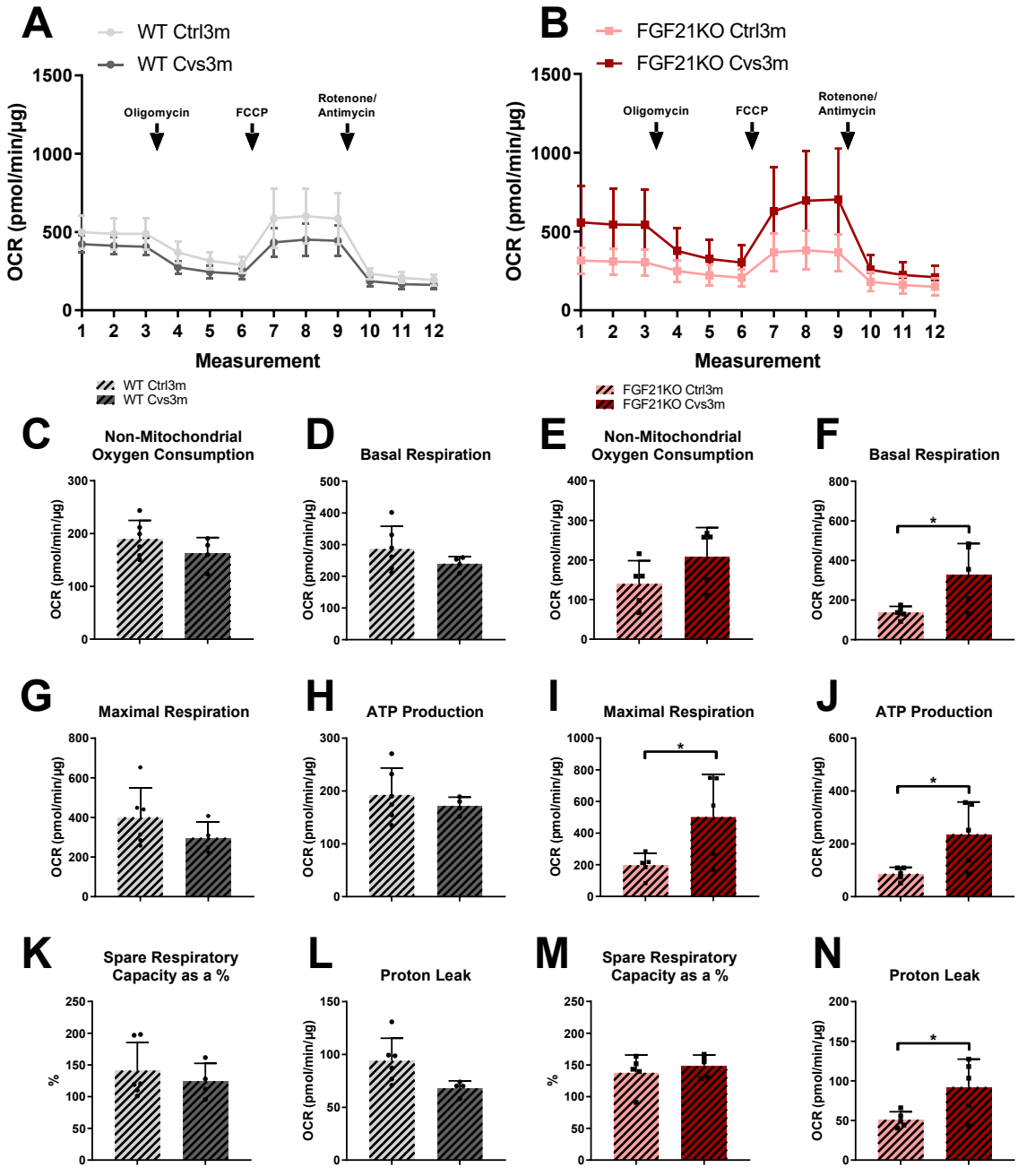

Figure 35: Analyses of mitochondrial respiration in WT and FGF21KO hepatocytes after recovery. The OCR were measured in a cycle of 3 for basal and after each compound injection in hepatocytes from previous non-stressed (Ctrl) and stressed (Cvs) WT (A) and FGF21KO (B) mice. Different parameters including non-mitochondrial oxygen consumption (C, E), basal respiration (D, F), maximal respiration (G, I), ATP production (H, J), spare respiratory capacity (K, M) and proton leak (L, N) were computed from the OCR from WT (grey bars) and FGF21KO (red bars) mice, respectively. Values are mean ± SD. Statistical analyses were done by two-tailed unpaired Student's t-test between groups. N = 4-5; *p < 0.05.

From the analyses of OCR after Cvs and recovery no influence of Cvs on WT hepatocytes was observed in hepatocytes. Neither on the short-term nor after recovery hepatocytes from WT mice showed stress induced changes in OCR.

FGF21KO deficiency and Cvs exposure lead to lower OCR levels after Cvs. However, this was opposed after recovery, resulting in an opposite activation of maximal respiration in short and long term. Furthermore, in FGF21 depletion the long-term stress effect was an activation of mitochondrial function in regard to basal respiration, proton leak and ATP-production.

3.2.12 Impact of Cvs on FGF21 secretion from isolated hepatocytes

The results of the energy metabolism analyses in isolated primary hepatocytes support the important role of FGF21 in the hepatic adaptation processes after chronic stress. After the recovery phase, hepatocytes of stressed mice showed an increased fatty acid uptake (see Figure 32) together with a decreased fatty acid oxidation (see Figure 33) and lower DNL (see Figure 31). These results were in line with the higher hepatic triglyceride content in stressed mice after recovery (Figure 20). FGF21 is a crucial regulator of hepatic lipid storage and peripheral insulin sensitivity. From the results in the study FGF21 depletion in FGF21 KO mice resulted in no stress-related improvements in insulin signaling, an unchanged glucose tolerance and secretion and no decreased DNL after recovery. To investigate if FGF21 is a direct target of Cvs and plays a direct role in the progression of the long term stress effects, the influence of Cvs on FGF21 secretion from the primary hepatocytes were determined after 24h cultivation. FGF21 measurements reveal no Cvs associated changes directly after the stress intervention. However, after three-month recovery previous stressed mice show increased FGF21 secretion compared to non-stressed control hepatocytes (Figure 36). So, the systemic rise of serum FGF21 after Cvs recovery appears most likely due to enhanced FGF21 secretion from hepatocytes. Secretome samples of FGF21KO were analyzed in parallel. Because of the absence of FGF21 in these samples the analyses were not possible. The individual values were under the limit of detection.

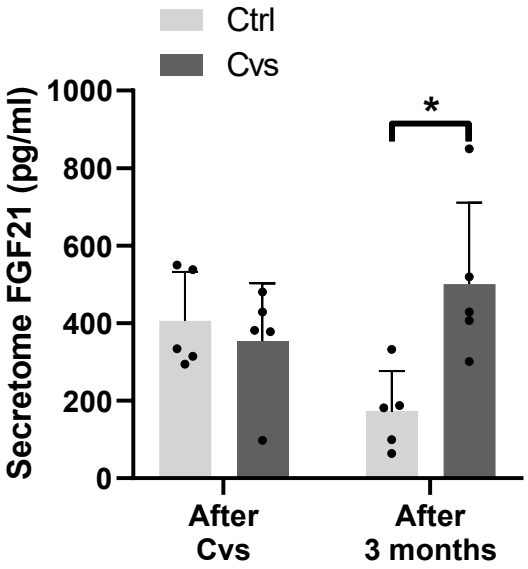

Figure 36: FGF21 determination in the secretome of WT primary hepatocytes. ELISA analyses of FGF21 in the secretome of isolated primary hepatocytes from WT mice. Values are mean ± SD. Statistical analyses were done by Two-Way ANOVA followed by Tukey post hoc. N = 5; *p < 0.05.

3.2.13 Molecular mechanisms of Cvs on energy metabolism

Dependent on the cellular status of NAD^+ the deacetylases Sirtuins (SIRT) directly regulates the glucose as well as lipid metabolism and the mitochondrial energy production (Finkel et al., 2009). Beside the metabolic regulation, SIRTs play also a role in stress response by regulating the GR by direct interactions (Suzuki et al., 2018). Based on these findings NAD^+/NADH ratio and the activity of SIRTs were assessed primary hepatocytes from Ctrl and Cvs mice after intervention and after three-month recovery.

First, the NAD^+/NADH ratio was analyzed by measuring NAD^+ and NADH independently by chemiluminescence based assay. Hepatocytes from WT Cvs mice showed a decreased NAD^+/NADH ratio thus they have higher levels of the reduced form NADH, compared to non-stressed WT Ctrl (Figure 37A). In contrast, no differences in NAD^+/NADH ratio were observed in FGF21KO hepatocytes directly after the Cvs intervention (Figure 37B). Interestingly, after three months recovery hepatocytes from WT Cvs3m mice had still a decreased NAD^+/NADH ratio compared to WT Ctrl3m (Figure 37C), whereas FGF21KO remained unaltered (Figure 37D).

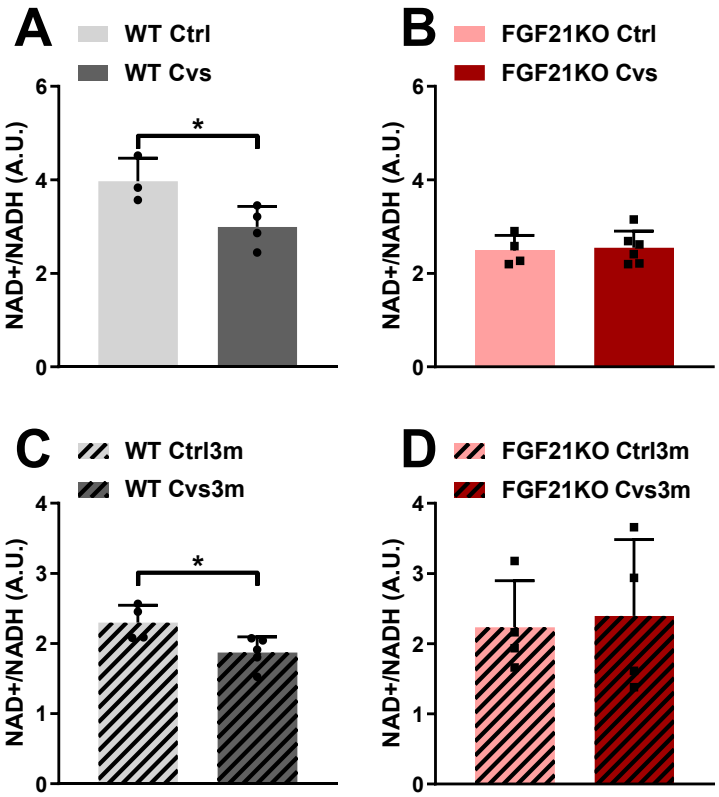

Figure 37: Influence of Cvs on NAD⁺/NADH ratio in WT and FGF21KO hepatocytes. The NAD⁺/NADH ratio were calculated from two independent measurements of NAD⁺ and NADH in hepatocytes from WT (A) and FGF21KO (B) directly after the intervention and after three months (C and D), respectively. Values are mean ± SD. Statistical analyses were done by two-tailed unpaired Student's t-test between groups. N = 3-5; *p < 0.05.

Furthermore, the protein abundance of SIRT1 was determined by western blot in liver protein lysates. WT Cvs hepatocytes showed a lower SIRT activity then WT Ctrl cells (Figure 38A), whereas Cvs had no influence on SIRT activity of FGF21KO hepatocytes (Figure 38B). Additionally, SIRT1 protein abundance was not affected by stress or FGF21 deficiency in FGF21KO conditions (Figure 38C). After three months, SIRT activity was still decreased in hepatocytes derived from WT Cvs3m compared to WT Ctrl3m animals (Figure 38D). Due to high sample variability significant stress-related differences in SIRT activity were not observed in FGF21KO hepatocytes after recovery (Figure 38E). However, hepatic SIRT1 protein abundance was reduced in hepatocytes of WT Cvs3m mice compared to WT Ctrl3m mice and FGF21KO mice showed general lower SIRT1 protein levels (Figure 38F).

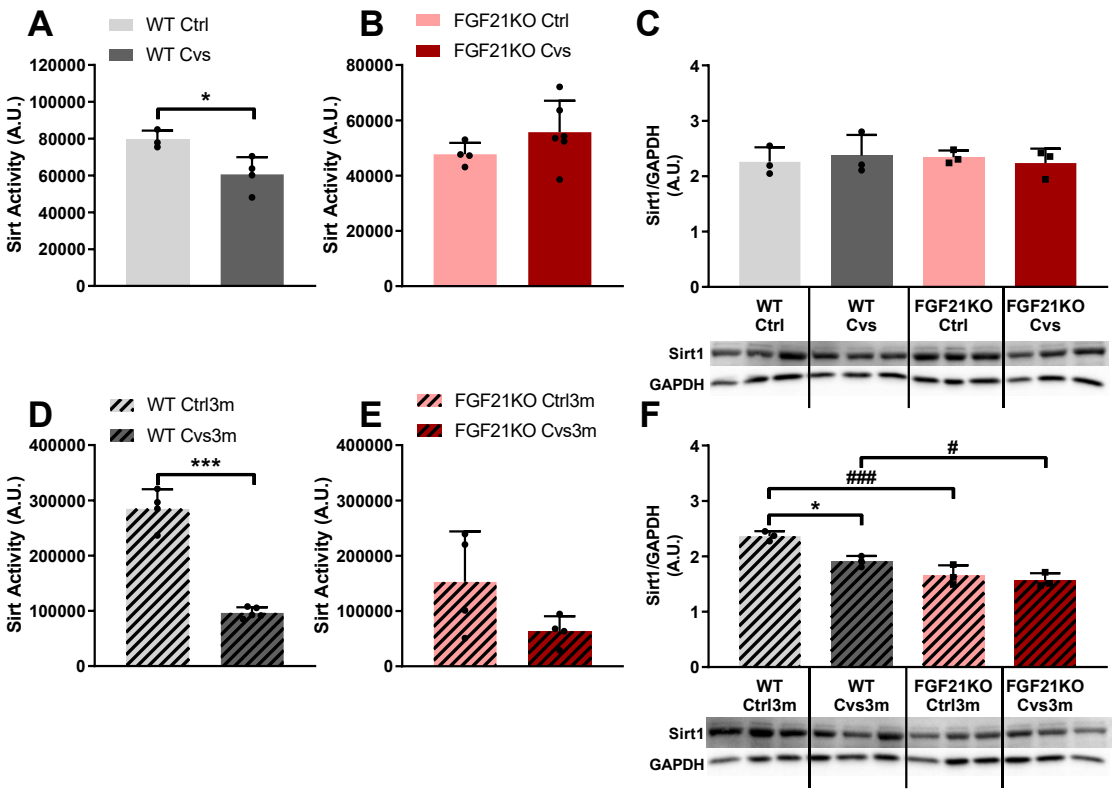

Figure 38: Hepatic SIRT activity and SIRT1 abundance after Cvs and recovery. SIRT activity in isolated primary hepatocytes were assessed after Cvs of stressed and non-stressed WT (A) and FGF21KO (B) mice. Short-term western blot and densitometric analyses of SIRT1 protein abundance in liver lysates of WT and FGF21KO mice (C). Measurement of SIRT activity after recovery in previous stressed and non-stressed WT (D) and FGF21KO (E) hepatocytes. Western blot and densitometric analyses of SIRT1 abundance in liver lysates after three months recovery (F). Values are mean ± SD. Statistical analyses of SIRT activity were done by two-tailed unpaired Student's t-test between groups. N = 3-5; *p < 0.05, ***p<0.001. Statistical analyses of SIRT1 protein abundance were done by Two-Way ANOVA followed by Tukey post hoc. N = 3; *p < 0.05, within the group; $^{\#}p < 0.05$, $^{\#\#\#}p < 0.001$ between the group.

3.2.14 Molecular mechanisms of Cvs on transcriptional regulation

The hepatic glucose and lipid metabolism is also regulated on transcriptional level by histone deacetylases (HDAC) and histone acetyltransferases (HAT) as well as methyltransferases. The HDAC activity was analyzed in hepatocytes from WT and FGF21KO mice after Cvs and after three months recovery. HDAC activity showed no significant change due to Cvs in hepatocytes derived from WT (Figure 39A) and FGF21KO (Figure 39B) mice. As for SIRT activity, the class I/II HDAC activity was also lower in hepatocytes from previously stressed WT mice compared to non-stressed mice (Figure 39C). FGF21KO hepatocytes exhibited no stress related changes after recovery (Figure 39D). After recovery, hepatocytes from stressed WT mice revealed a lower deacetylating activity indicated by less activity of HDACs.

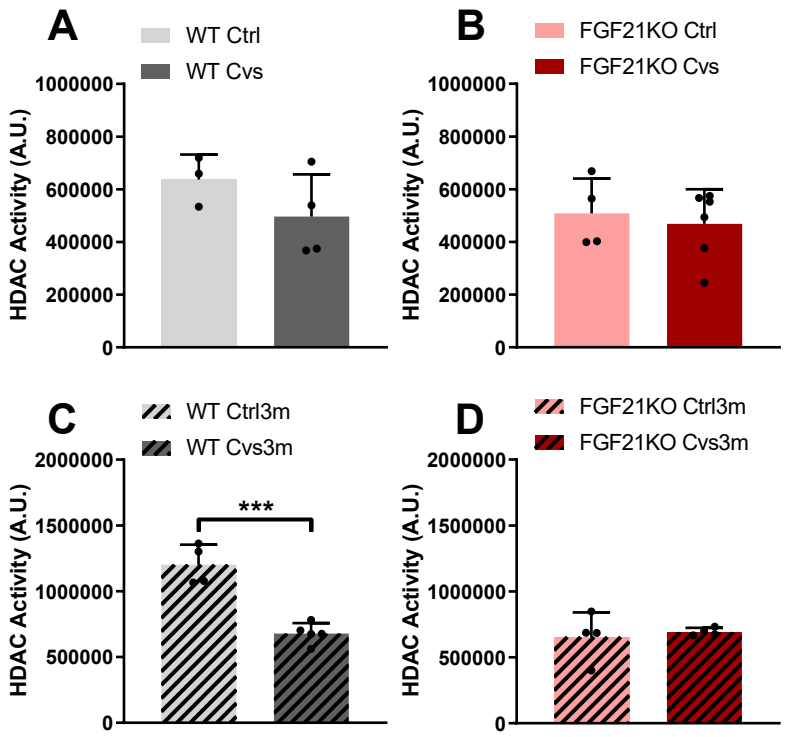

Figure 39: Measurement of hepatic HDAC activity after Cvs and recovery in primary hepatocytes. HDAC activity in isolated primary hepatocytes were assessed after Cvs of stressed and non-stressed WT (A) and FGF21KO (B) mice. Measurement of HDAC activity after recovery in previous stressed and non-stressed WT (C) and FGF21KO (D) hepatocytes. Values are mean ± SD. Statistical analyses of HDAC activity were done by two-tailed unpaired Student's t-test between groups. N = 3-5; *p < 0.05, **p<0.01.

The counterpart of HDACs are the HATs, which acetylate histones and consequently activate gene transcription. The assay quantifies fluorometrically the produced coenzyme A from the cleavage of acetly-CoA in the histone acetylating reaction. Relative HAT activity was not affected by Cvs in hepatocytes of both, WT (Figure 40A) and FGF21KO (Figure 40B). On the other hand, WT hepatocytes showed a Cvs induced HAT activity after three months recovery if compared to Ctrl3m hepatocytes (Figure 40C). In FGF21KO, chronic stress lead to a decreased HAT activity after three months (Figure 40D).

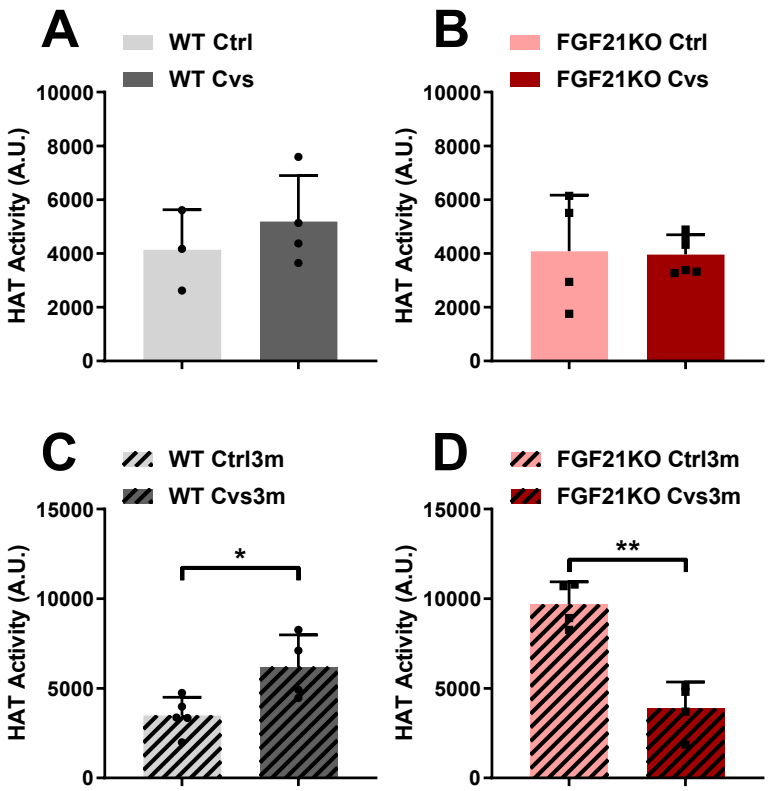

Figure 40: Measurement of hepatic HAT activity after Cvs and recovery in primary hepatocytes. HAT activity in isolated primary hepatocytes were assessed after Cvs of stressed and non-stressed WT (A) and FGF21KO (B) mice. Measurement of HAT activity after recovery in previous stressed and non-stressed WT (C) and FGF21KO (D) hepatocytes. Values are mean ± SD. Statistical analyses of HAT activity were done by two-tailed unpaired Student's t-test between groups. N = 3-5; *p < 0.05, **p<0.01.

A further modulator of transcription activity are methyltransferases, which also regulate gene transcription by DNA methylation. The assay used detects changes in activity of a broad range of methyltransferases, including DNA, protein, RNA and small molecule methyltransferases. The methyltransferase activity is proportional to the catalysed S-adenosyl methionine (SAM) to S-adenosyl homocysteine (SAH) which is used to produce ATP to measure the light from the luciferase reaction. WT hepatocytes showed a decrease methyltransferase activity due to Cvs (Figure 41A). In FGF21KO hepatocytes the methyltransferase activity was similar (Figure 41B). Both, hepatocytes from WT Cvs3m (Figure 41C) and FGF21KO Cvs3m (Figure 41D) had decreased methyltransferase activity compared to the respective Ctrl3m hepatocytes. The data showed a clear influence of Cvs on the short- and long-term methyltransferase activity in WT mice, which in short term might also be influenced by FGF21.

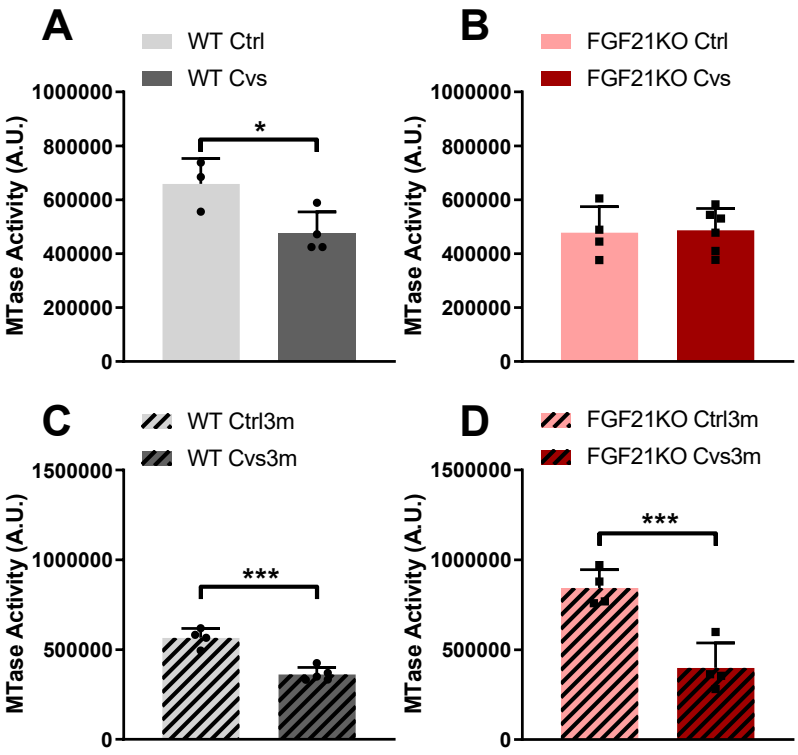

Figure 41: Measurement of hepatic methyltransferase activity after Cvs and recovery in primary hepatocytes. Methyltransferase activity in isolated primary hepatocytes were assessed after Cvs of stressed and non-stressed WT (A) and FGF21KO (B) mice. Measurement of methyltransferase activity after recovery in previous stressed and non-stressed WT (C) and FGF21KO (D) hepatocytes. Values are mean ± SD. Statistical analyses of methyltransferase activity were done by two-tailed unpaired Student's t-test between groups. N = 3-5; *p < 0.05, ***p<0.01.

4. DISCUSSION

This thesis focuses on the association of chronic stress and the development of metabolic complications. From the literature, chronic high stress hormone levels leading to metabolic diseases like as obesity or T2DM and the metabolic function of GCs are well established. Prolonged GC exposure, like in the Cushing's syndrome or in psychological disease, is linked to metabolic disorders, such as insulin resistance, NAFLD and T2DM. However, only few studies investigated influences of chronic stress exposure on the energy metabolism and the onset of metabolic complications in the long-term (Faulenbach et al., 2012; Naliboff et al., 1985; Packard et al., 2014; Pibernik-Okanovic et al., 1993; Reynolds et al., 2010). In the present work, effects of early life exposure to chronic variable stress (Cvs) and associated metabolic adaptations were examined by using a previously established mouse model for PTSD (Castaneda et al., 2011). Especially, the use of a metabolic healthy mouse model with intervention dependent chronic elevated stress hormone levels helps to investigate complicated relationships of cellular and hormonal metabolic adaptations. Tissue specific analyses helped to investigate short- and long-term metabolic changes and the general regulation of the glucose and lipid metabolism after Cvs. These investigations reveal adaptations of metabolic active organs and identify relevant modulators of post stress metabolic regulation.

4.1 Cvs leads to alterations in insulin sensitivity due to increased FGF21 plasma levels

The first part (4.1) of the discussion were adopted word by word from the publication Jelenik*, Dille* et al. (2018; *shared first author) like in the results section and necessary changes to the original text to facilitate readability were highlighted as underlined.

This study found that a history of stress exposure leads to long-term metabolic adaptations with improved insulin sensitivity, specifically in adipose tissue, which could be mediated by the tissue-specific metabolic actions of FGF21.

Consistent with previous observations, two-week exposure to Cvs intervention resulted in elevated corticosterone levels, loss of lean mass and decreased adrenal gland mass, indicating stress-induced activation of the HPA axis (Castaneda et al., 2011). Moreover, hepatic insulin sensitivity was decreased and peripheral insulin sensitivity increased as measured *in vivo* with hyperinsulinemic-euglycemic clamps. These complex stress-induced alterations in insulin sensitivity are consistent with the pleiotropic effects of corticosterone on glucoregulatory insulin responsive tissues (Hong et al., 2009; Nilsson et al., 2002; Vander Kooi et al., 2005; Yi et al., 2012). Previous pharmacological study in rats revealed that paraventricular nucleus mediates the dexamethasone-induced increase in glucose disposal rate (Rd) (Yi et al., 2012).

Three months post Cvs exposure, no differences were observed in corticosterone levels, body weight, body composition and adrenal gland weight, indicating full reversibility of the acute stress effects on HPA-axis activation. Although hepatic insulin sensitivity was unchanged, peripheral insulin sensitivity remained persistently increased, altogether leading to higher whole-body insulin sensitivity in Cvs3m animals. The *ex vivo* data indicate that skeletal muscle does not play a role in Cvs-mediated increase in Rd, as insulin-stimulated glucose uptake and AKT phosphorylation were unchanged. On the other hand, β-oxidation- and TCA cycle-linked mitochondrial respiratory capacities were elevated in the soleus muscle, which was accompanied by the lower triglyceride content. Although skeletal muscle lipid content negatively associates with insulin sensitivity and its reduction can improve glucose uptake (Ritter et al., 2015) these mechanisms do not explain the increase in insulin sensitivity three months post Cvs intervention. In contrast to skeletal muscle, insulin-stimulated glucose uptake as well as AKT phosphorylation and GLUT1 expression were increased in adipocytes from Cvs3m mice, strongly indicating that elevated glucose metabolism of adipose tissue underlies the improvements in the whole-body insulin sensitivity three months post Cvs. Moreover, WAT from Cvs3m mice showed enhanced expression of key regulators of browning and thermogenic markers. Browning of adipose tissue and increased thermogenesis have been inversely related to insulin resistance (Lo and Sun, 2013) and might protect from obesity and lipid-mediated impairments of glucose metabolism (Vitali et al., 2012). Similar mechanisms could indirectly contribute to the improved glucose metabolism also in Cvs3m mice. Furthermore, only a moderate increase of triglycerides and unchanged insulin sensitivity in the liver of Cvs3m mice were found. High levels of hepatic lipids were accompanied by induced mRNA levels of the fatty acid transporter *Cd36* but unchanged expression of genes involved in de novo lipogenesis. A previous study supports the findings by showing that chronically elevated corticosterone exacerbates hepatic steatosis via induction of *Cd36* in high-fat diet fed mice (D'Souza A et al., 2012).

The question remains, which mechanisms mediate the above-described, tissue-specific metabolic effects of Cvs three months after the exposure. The analysis of circulating metabolic hormones and cytokines, which have been linked to the regulation of glucose homeostasis, revealed a substantial increase in plasma FGF21. Previous studies identified the liver as primary source of FGF21 secretion (Badman et al., 2009; Emanuelli et al., 2014; Inagaki et al., 2007; Ohta et al., 2011) and FGF21 positively correlated with hepatic fat content in patients with non-alcoholic fatty liver disease (Li et al., 2010). Consistent with these data, increased hepatic *Fgf21* expression and a strong correlation between plasma FGF21 and hepatic triglycerides were found. Moreover, some studies have shown a strong association of glucocorticoid receptor activation with induction of FGF21 (Marino et al., 2016; Patel et al., 2015; Vispute et al., 2017). The late-onset FGF21 expression might constitute part of an adaptive mechanism for protection from glucocorticoid-induced hepatic lipid accumulation. On the other hand,

exposure to stress and PTSD have been linked to the epigenetic modifications of genes involved in various physiological pathways (Roth, 2014). Thus, epigenetic alterations in the *Fgf21* DNA could also mediate the late-onset effects of stress on FGF21 expression and insulin sensitivity, as supported by previous studies. For example, environmental changes, such as altered nutritional composition, induced Fgf21 methylation in mouse liver (Yuan et al., 2018). Recent studies showed that, in addition to liver as a source for FGF21, skeletal muscle may also secrete FGF21 under conditions of metabolic stress (Crooks et al., 2014; Guridi et al., 2015; Harris et al., 2015; Izumiya et al., 2008; Kim et al., 2013; Ost et al., 2016; Vandanmagsar et al., 2016) and adipose tissue upon cold exposure or *Ucp1* overexpression (Fisher et al., 2012; Keipert et al., 2015). These findings were extended by showing markedly increased expression of Fgf21 in skeletal muscle and brown adipose tissue three months after Cvs intervention.

FGF21 has known beneficial effects on glucose metabolism, which has been shown in various models (Emanuelli et al., 2014; Fisher et al., 2012; Li et al., 2010; Ohta et al., 2011; Potthoff et al., 2009). Multiple pathways in insulin-responsive tissues that are targets of FGF21 were affected also in Cvs3m mice. For example, expression of FGF21 receptors was induced in the liver, WAT and BAT, indicating increased FGF21-associated signaling in these tissues. Indeed, hepatic expression of downstream FGF21 targets of lipolysis and fatty acid oxidation was increased. Importantly, FGF21 could mediate the increased glucose uptake via induction of GLUT1 in WAT, as supported by previously described mechanistic link between FGF21 and GLUT1 expression in adipocytes (Ge et al., 2011). In addition to the acute effects on glucose disposal, FGF21 has been associated with WAT browning (Fisher et al., 2012). Also, Cvs3m mice showed enhanced expression of key regulators of browning, thermogenesis and fatty acid oxidation, indicating that FGF21-driven browning of WAT could contribute to the insulin-sensitizing effect in response to stress. In addition to WAT, FGF21 can regulate BAT activity and fatty acid metabolism in skeletal muscle (Fisher et al., 2012; Vandanmagsar et al., 2016), which have been changed accordingly in Cvs3m mice. Collectively, all these observations demonstrate that high circulating FGF21 levels associate with induction of multiple FGF21-regulated pathways, which could contribute to the improved insulin sensitivity following long-term chronic stress.

Summarizing, figure 41 shows that Cvs leads to a short-term increase in corticosterone levels in C57BL/6 mice. However, after three-month recovery stressed mice have higher FGF21 plasma levels along with no changes in corticosterone. FGF21 stimulates lipolysis, glucose uptake and the expression of browning markers in the WAT as well as thermogenic markers in the BAT and increases fatty acid uptake and oxidation in the skeletal muscle. These findings explain the improved insulin sensitivity of peripheral tissues found in hyperinsulinemic-euglycemic clamps analyses. Nevertheless, the mice show also a hepatic insulin resistance together with increased hepatic lipid content. Up to here, the mechanism linking FGF21 and hepatic lipid accumulation to Cvs and GC action is not revealed.

The positive effects of FGF21 on skeletal muscle and adipose tissue in the post-stress conditions is the consequence of an increased FGF21 release in the blood flow. The liver is the main organ secreting FGF21 and is therefore the target of the following investigations. Particularly, the impact of Cvs on the hepatic glucose and lipid metabolism and the role of FGF21 in their regulation after stress were analyzed.

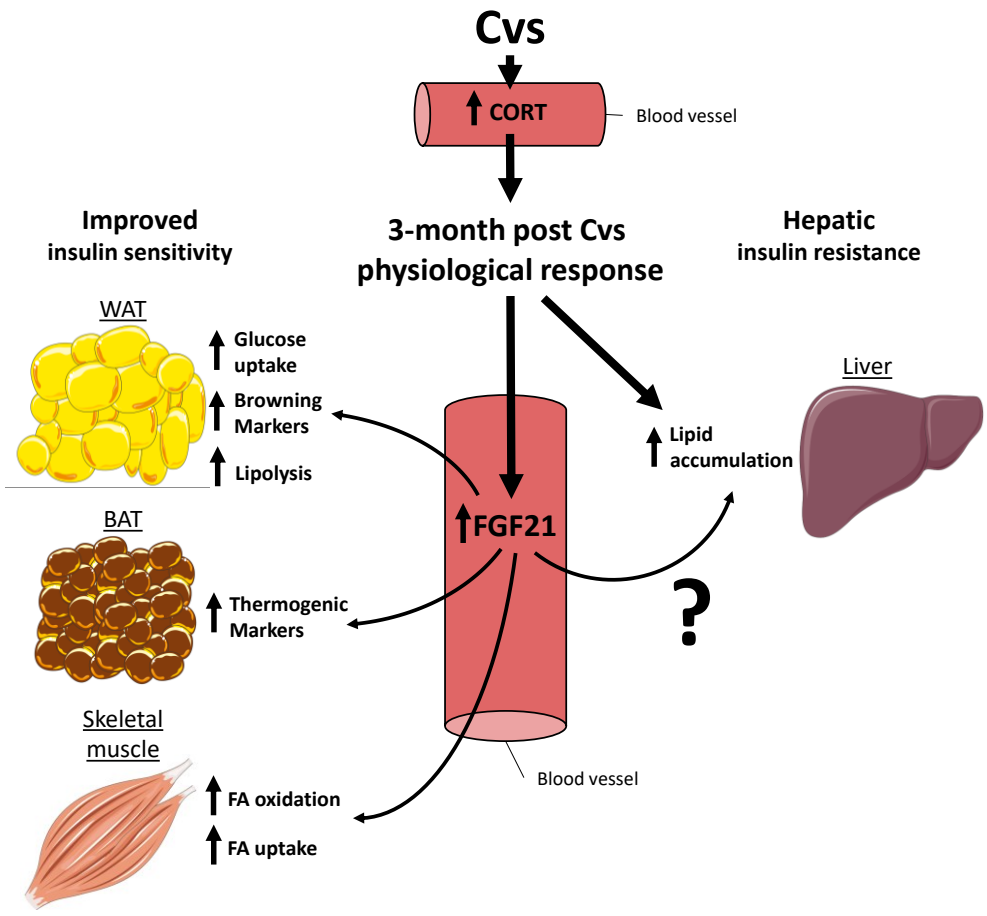

Figure 42: Long-term metabolic changes after Cvs are associated to FGF21. Chronic variable stress (Cvs) leads to the release of corticosterone (CORT) to the circulation. After three-month recovery from Cvs, stressed mice exhibit higher plasma levels of FGF21 along with an improved insulin sensitivity in peripheral metabolic tissues. In white adipose tissue (WAT) FGF21 induces glucose uptake and lipolysis along with an increased expression of browning markers. The brown adipose tissue (BAT) show an increased expression of thermogenic markers. In skeletal muscle FGF21 induces fatty acid (FA) oxidation and uptake. On the other side, previous stressed mice show a hepatic insulin resistance together with increased hepatic lipids. However, the underlying mechanism linking FGF21 and hepatic energy metabolism after Cvs is not revealed.

4.2 Improvements in insulin action are abolished in FGF21KO mice after recovery from Cvs

In continuance to the previous findings, the following section focuses the role of FGF21 in the post-stress metabolic regulations and its function in long-term metabolic improvements. Especially, it is the first time that the influence of FGF21 on hepatic energy metabolism after Cvs were investigated. This work reveals FGF21-related metabolic adaptations after chronic stress and identifies possible molecular mechanisms leading to elevated FGF21 plasma levels. To investigate the role of FGF21 in the post-stress situation a FGF21 knockout mouse model underwent the Cvs protocol. Unaffected wildtype littermates of the FGF21 KO mice were also examined, as basis of comparison for the new findings in FGF21 KO mice and to corroborate recent findings from metabolic healthy C57BL/6 mice.

FGF21 is mainly produced and secreted in the circulation by the liver. Nevertheless, under specific conditions its expression is also present in adipose tissue, pancreas and skeletal muscle (Markan et al., 2014). FGF21 is a member of the fibroblast growth factor (FGF) family and transduces its signal via the FGF21 receptor, consisting of the co-receptors FGF receptor 1 (FGFR1) and β-Klotho (BonDurant and Potthoff, 2018). It was shown, that administration of FGF21, like insulin, in obese (*ob/ob*) and obese diabetic (*db/db*) mice lowered plasma glucose levels, reduces body weight, increases energy expenditure and reduces hepatosteatosis (Coskun et al., 2008; Kharitonenkov et al., 2005). Moreover, a study from 2013 showed that the treatment of patients with obesity and type 2 diabetes with the FGF21 analog LY2405319 decreases plasma triglyceride and increases plasma adiponectin levels, but fasting glucose levels show only a lowering trend (Gaich et al., 2013). Interestingly, obese animal models like *ob/ob*, *db/db* and diet induced obese (DIO) mice has elevated plasma FGF21 levels indicating a FGF21 resistance state (Fisher et al., 2010; Zhang et al., 2008). However, it was shown, that the anti-diabetic and weight loss effects of FGF21 in obese mice are dose-dependent and repeated administration resulted in metabolic improvements (Berglund et al., 2009; Coskun et al., 2008). These studies also showed FGF21 as a critical regulator of glycemic control by improving the hepatic insulin sensitivity (Badman et al., 2007; Berglund et al., 2009; Xu et al., 2009b).

Various evidences indicate a link between the FGF21 and GC signaling pathway. The expression of genes induced by GCs, like *Pepck* and *G6pc* are induced by FGF21, too (Potthoff et al., 2009). Moreover, mice overexpressing FGF21 and mice with excessive GC treatment exhibit similar diseases (Wei et al., 2012; Weinstein, 2012). The fact, that FGF21 overexpressing mice have elevated circulating GC levels (Bookout et al., 2013) and that GC as well as FGF21 levels are increased in metabolic disorders like T2DM and obesity (Fisher et al., 2010; Hale et al., 2012) point out a strong relation of FGF21 and GCs in the metabolic regulation. For example, Cushing's syndrome patients and mice treated with synthetic GCs have elevated plasma FGF21 levels (Durovcova et al., 2010; Laskewitz et al., 2010). A link is given by the fact that GCs induce the hepatic expression and secretion of FGF21 directly by binding of the

GR in the mouse promoter of the *Fgf21* gene (Liang et al., 2014; Patel et al., 2015). Thus, the high levels of GCs could be responsible for the paradoxically increased FGF21 levels in obesity (Patel et al., 2015). In line with the previous study from 2018 not only WT but also FGF21KO mice showed elevated plasma corticosterone levels due direct effects of Cvs (Jelenik et al., 2018). These associated with a decrease body weight and lean mass, probably caused by the proteolytic action of GCs (Dardevet et al., 1995; Schakman et al., 2013). The same is true for the analyses of the mice three months after Cvs, here not only in WT but also in FGF21KO mice no stress-related changes in body composition or corticosterone levels were observed. A general higher lean mass at an age of 14 weeks was observed in FGF21KO mice compared to wildtype littermates independent of stress exposure, similar to other investigations of FGF21 deficient mice (Badman et al., 2009). Moreover, stressed mice show an overall decrease in fat mass, most likely due to an increased GC mediated lipolysis in the adipose tissue (Djurhuus et al., 2004; Krsek et al., 2006; Xu et al., 2009a). These findings were underlined by increased levels of plasma free fatty acids directly after Cvs compared to Ctrl mice. However, levels of free fatty acids are still increased after long-term recovery following Cvs in WT, but not in FGF21KO mice, confirming the observed lipolytic effect of FGF21 under normal feeding conditions (Hotta et al., 2009; Inagaki et al., 2007). So, elevated GC levels during Cvs and the following rise in FGF21 during recovery could cause the rise in circulating free fatty acids on the short- and on the long-term, respectively.

An obvious explanation for altered body composition is food intake. The literature shows various studies explaining either increased or decreased food intake in stressful situations (Harris, 2015; Jiang and Eiden, 2016; Patterson et al., 2013; Razzoli and Bartolomucci, 2016; Saegusa et al., 2011; Sanghez et al., 2013). Food intake measurements show a FGF21 independent higher food intake of stressed mice during Cvs and during the recovery phase. In further detail, individual analyzes of the respiratory exchange ratio (RER) and the energy expenditure reveal that short-term changes of RER could be associated to the rise in corticosterone, whereas the shift in RER towards a higher carbohydrate oxidation after recovery is corticosterone independent, because corticosterone levels are unchanged between WT Ctrl3m and WT Cvs3m mice. These findings could be associated to the presence of FGF21 as FGF21KO mice show no long-term difference in RER due to previous Cvs intervention.

A study from 2014 described, that FGF21 regulates fasting blood glucose levels through the activation of the HPA-axis and the upregulation of gluconeogenic genes (Liang et al., 2014). FGF21 deficient mice exhibit hypoglycemia during prolonged fasting and have impaired fasting-induced activation of the HPA-axis associated with less GC secretion. Moreover, FGF21 also reduced blood glucose in obese mouse models for T2DM by improving hepatic insulin sensitivity and increasing glucose disposal (Berglund et al., 2009; Laeger et al., 2017). Both WT and FGF21KO mice show short-term increased fasting blood glucose levels due to the stress exposure. These observations are in line with the hyperglycemic influence of chronic GC exposure (Kuo et al., 2015; Liu et al., 2014a; Perez et al., 2014).

Nonetheless, WT Cvs3m mice show lower fasting blood glucose levels then non-stressed WT Ctrl3m mice, whereas FGF21KO mice show no long-term stress-associated changes in fasting blood glucose. These findings indicate a glucose lowering role of FGF21 likely due to an induced glucose uptake in gWAT and enhanced thermogenic activity of the BAT as observed in the C57BL/6 mice. But analyses of glucose tolerance showed no FGF21 dependency, neither directly after Cvs nor after recovery. However, analyses of insulin tolerance in FGF21 WT and KO mice determined by intraperitoneal ITT indicating an improved insulin tolerance after recovery, and corroborated the insulin sensitivity measurements by the gold-standard technology i.e. hyperinsulinemic-euglycemic clamps in C57BL/6 mice. Analyses of endogenous glucose production by intraperitoneal PTT are also in line with results from hyperinsulinemic-euglycemic clamps, revealing an acutely stress-related decrease in hepatic glucose output, but no long-term impact in the presence of FGF21. Interestingly, other studies have shown, that FGF21 induces hepatic glucose output by activating the HPA-axis leading to the release of GCs, which subsequent stimulate hepatic gluconeogenesis (Liang et al., 2014; Potthoff and Finck, 2014; Wang et al., 2014). However, in the present work no direct link of FGF21 and corticosterone were observed short- or long-term after Cvs.

Initially, FGF21 was identified as a stimulator of glucose uptake in 3T3-L1 and primary human adipocytes, by upregulating the expression of GLUT1 (Kharitonenkov et al., 2005). C57BL/6 mice showing increased glucose uptake in gWAT, and in line, FGF21 WT animals show also an enhanced insulin-stimulated AKT^{Ser473} phosphorylation in gWAT and liver after recovery. These results confirm the positive effects of FGF21 on peripheral glucose disposal (BonDurant et al., 2017; Ge et al., 2012). The enhanced insulin-induced AKT activation due to previous stress intervention is abolished in FGF21KO mice. This further indicates FGF21 as a regulator of adipose tissue glucose uptake and hepatic insulin sensitivity in post-stress conditions as well as FGF21 as an insulin sensitizer as previously reported (Lee et al., 2014).

4.3 FGF21 counteracts the Cvs-induced hepatic lipid accumulation by downregulating DNL and gluconeogenesis

Consistent with previous findings, circulating FGF21 level of WT mice correlate significantly with the hepatic lipid content. FGF21KO mice show an overall higher liver triglycerides in this thesis, as reported from other studies (Badman et al., 2009; Hotta et al., 2009; Inagaki et al., 2007). Interestingly, patients with NAFLD have increased FGF21 plasma levels and show a positive correlation of FGF21 to hepatic lipid content (Dushay et al., 2010; Li et al., 2010; Yan et al., 2011; Yilmaz et al., 2010). Chronic GC exposure leads to a fatty liver and the development of NAFLD (Lemke et al., 2008; Targher et al., 2006; Woods et al., 2015). Based on these findings, analyses of the energy metabolism in isolated primary hepatocytes of WT and FGF21KO mice should reveal possible adaptive mechanism and the role of

FGF21 after chronic stress. FGF21 is an inducer of hepatic β-oxidation via the activation of the peroxisome proliferator-activated receptor gamma coactivator 1α (PGC-1α) (Potthoff et al., 2009). According to another study, FGF21 deficiency leads to an increased hepatic lipid content due to an overall increase in fatty acid uptake and decrease in fatty acid oxidation (Antonellis et al., 2016). Moreover, studies have shown a GCs-mediated increase in hepatic fatty acid uptake by upregulating the fatty acid transporter CD36 (Koorneef et al., 2018; Lemke et al., 2008; Patel et al., 2014; Yu et al., 2010). *Ex vivo* analyses demonstrate a hepatic palmitate uptake after Cvs not only in WT but also FGF21KO mice, but after Cvs recovery only WT mice show a stress-related increase in hepatic fatty acid uptake. The stress-related upregulation of *Cd36* gene expression in stressed C57BL/6 mice could elucidate the long-term enhanced fatty acid uptake in primary hepatocytes of metabolically healthy mice. In contrast, primary hepatocytes from FGF21KO mice show a general decrease in palmitate oxidation, but no further long-term stress-related changes. Interestingly, primary hepatocytes from FGF21KO mice also show a stress-related decrease in mitochondrial function after Cvs. However, after long-term recovery the respiration and ATP-production increase due to previous stress intervention in hepatocytes from FGF21KO mice. This stress-related change in mitochondrial oxidation is not observed in WT mice, which show a general higher mitochondrial respiration. These results reveal the general positive influence of FGF21 on the mitochondrial function (Potthoff et al., 2009). Furthermore, chronic stress increases the mitochondrial respiration in FGF21 deficiency after recovery to the wildtype level, which indicates a stress-related influence on mitochondrial function. The increase in lipid delivery to the liver combined with increased hepatic fatty acid uptake and reduced fatty acid oxidation could cause the stress-induced hepatic lipid accumulation of WT mice as observed after Cvs recovery. This effect may depend on FGF21, as FGF21KO mice did not respond as WT mice.

NAFLD is characterized by an abnormally increase in DNL and gluconeogenesis linked to hepatic insulin resistance (Ameer et al., 2014; Donnelly et al., 2005; Jelenik et al., 2017a; Knebel et al., 2019; Knebel et al., 2012; Kotzka et al., 2012; Sanders and Griffin, 2016). FGF21 is known to reduce liver fat and prevent NAFLD by reducing DNL (Zhang et al., 2011) and increasing β-oxidation (Potthoff et al., 2009). Interestingly, this thesis shows for the first time, that in the presence of FGF21 hepatocytes exhibit a stress-related long-term reduction in DNL after Cvs, an observation that could not made in FGF21 deficient hepatocytes. In addition, isolated hepatocytes from stressed mice show an enhanced glucose production and reduced glycolysis compared to Ctrl hepatocytes, probably due to the gluconeogenic function of stress hormones (Kuo et al., 2015; Ma et al., 2013; Pilkis et al., 1988). Interestingly, after stress recovery the glucose production shows a FGF21-dependent reduction in isolated hepatocytes from stressed WT mice, indicating a direct impact of FGF21 on the hepatic gluconeogenesis. In line, hyperinsulinemic-euglycemic clamps analyses of C57BL/6 mice show a lower EGP due to previous stress intervention. Despite hepatic lipid accumulation, stressed WT mice do not show the

pathophysiological properties of a fatty liver disease indicated by a decreased DNL and gluconeogenesis. This is supported by only minor changes in plasma cytokines observed due to Cvs and the missing evidence that stressed mice develop liver inflammation, as usually observed in fatty liver diseases (Del Campo et al., 2018; Tarantino et al., 2010). In general, the results of the initial study and the latest results do not indicate that Cvs is associated with systemic inflammation, revealed by no relevant changes in plasma cytokine levels. The results of this work suggest for the first time, that FGF21 might counteract the stress-induced hepatic lipid accumulation directly by downregulating DNL and glucose production.

Possible molecular regulators of gene transcription were analyzed to investigate long-term changes leading to increased hepatic FGF21 secretion and metabolic adaptations after Cvs. Synthetic GC treatment induce the expression of hepatic FGF21 (Vispute et al., 2017). Here, WT mice show increased FGF21 protein abundance in the liver, but no stress-induced increase in FGF21 plasma levels. In contrast, stressed WT mice show increased FGF21 plasma levels and a higher hepatic FGF21 protein abundance as well as enhanced FGF21 secretion from hepatocytes. This was despite the fact, that the corticosterone levels after recovery are comparable.

Because of the promoter of the *Fgf21* gene contains a specific GR binding sited (Cheng et al., 2014; Patel et al., 2015), one possibility is that in the liver of WT Cvs3m mice enhanced GC-mediated transcription can be activated by increased GR phosphorylation. As a result, FGF21 abundance and secretion may increase directly. Another possibility is an indirect mechanism linked to the observed metabolic alterations. Here, histone modulation due to reduced deacetylase and enhanced acetyltransferase activity may be a further plausible mechanism to possible enhanced gene transcription through binding of various transcription factors including GR. The decreased SIRT1 activity, a class III HDAC, observed in hepatocytes and lower SIRT abundance in liver tissue underline such mechanism. A study from 2014 shows, that the knockout of SIRT1 promote hepatic lipid accumulation by downregulating FGF21 plasma levels (Li et al., 2014). However, SIRTs are not restricted to direct protein interactions, they link the metabolism via NAD^+ to transcriptional regulation and cellular functions (Zhang and Kraus, 2010). Although, hepatocytes from FGF21KO mice show no changes in NAD^+/NADH ratio, a stress-related increase in ATP-production and respiration were observed. This indicates a GC-associated pathway, which influences long-term mitochondrial function in FGF21KO hepatocytes. In contrast, hepatocytes from WT mice show no changes in mitochondrial function due to Cvs, but WT mice have general higher respiration and ATP production then FGF21KO mice. Moreover, the shift in NAD^+/NADH ratio in WT mice could be responsible for the changes in SIRT activity and possible alterations in gene transcription leading to metabolic adaptations (Feige et al., 2008). Direct protein interactions of SIRT1 are associated with the development of a fatty liver disease

(Ding et al., 2017; Niu et al., 2018). Sirtuin family members like SIRT1 or SIRT3 are well known modulators of the hepatic energy and glucose metabolism, e.g. inducing hepatic gluconeogenesis (Nogueiras et al., 2012). Gene knockout of class IIa HDACs or its suppression in mice lowers blood glucose by downregulating the hepatic gluconeogenesis and protect them from adipose tissue dysfunction (Chatterjee et al., 2014; Mihaylova et al., 2011; Wang et al., 2011a). Furthermore, the inhibition of HDACs by sodium butyrate induce the expression of FGF21 in the liver (Li et al., 2012).

Taken together, figure 42A shows that in WT mice the exposure to Cvs leads to higher lipolysis and increased hepatic fatty acid uptake together with decreased fatty acid oxidation, which causes an enhanced lipid accumulation in the liver after recovery. Moreover, the relation of changes in NAD^+/NADH ratio and fatty liver disease, resulting in alterations in SIRT activity was determined and is also shown in other studies (Elhassan et al., 2017; Kendrick et al., 2011; Zhou et al., 2016). These alterations may affect the gene transcription by direct protein interactions or decreased histone deacetylase activity (Feige and Auwerx, 2008; Okabe et al., 2019) leading to enhanced FGF21 expression and subsequent higher release of FGF21 in the circulation (Patel et al., 2015; Suzuki et al., 2018; Vispute et al., 2017). Finally, circulating FGF21 may downregulate hepatic DNL and gluconeogenesis to counteract the higher fat content in the liver.

In the FGF21KO situation, illustrated in figure 42B, Cvs increases corticosterone levels as well, but no stress-related changes in lipolysis were observed. This result indicate FGF21 as possible lipolytic stimulator in the post CVS situation. Moreover, decreased hepatic fatty acid oxidation and fatty acid uptake were observed. In contrast to WT mice, Cvs and FGF21 deficiency leading to an enhanced gluconeogenesis along with no changes in hepatic DNL after recovery. Moreover, NAD+/NADH ratio is not affected by Cvs in FGF21KO mice. However, Cvs leads to an increased ATP production in FGF21KO mice.

A possible FGF21 resistance, for e.g. due to chronic high levels of FGF21 could consequently lead to an excessive hepatic lipid accumulation and causes stress-induced development of NAFLD. Obese people and patient suffering from fatty liver diseases show high levels of circulating FGF21 (Barb et al., 2019; Markan, 2018). Also, circulating FGF21 reflects the hepatic lipid accumulation in mice (Rusli et al., 2016).

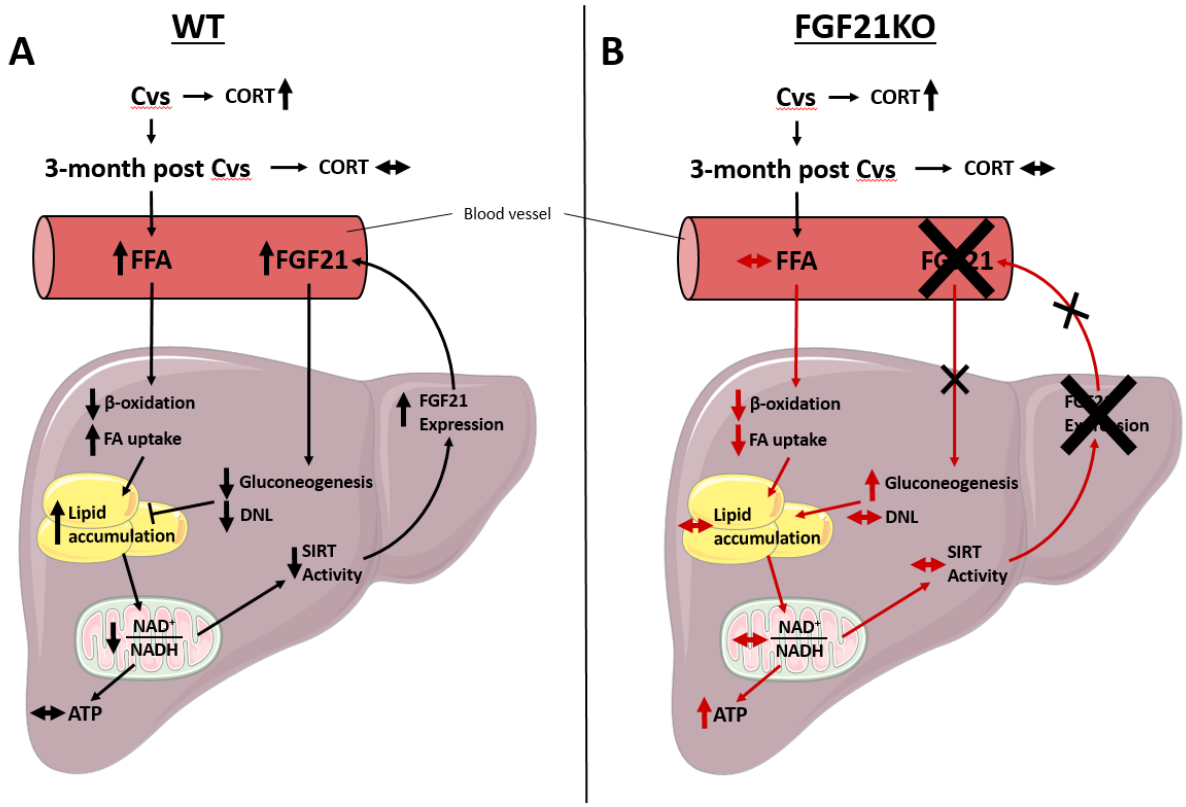

Figure 43: Putative mechanism of Cvs regulating long-term hepatic adaptations via FGF21 secretion.(A) Chronic variable stress (Cvs) exposure leads to temporary elevated corticosterone levels (CORT), which subsequent induce adipose tissue lipolysis. After three months of recovery, this results in a rise of plasma free fatty acids (FFA) and a stress-induced hepatic fatty acid (FA) uptake, which could be responsible for the increased hepatic lipid accumulation. In addition, decreased β-oxidation influences also the lipid accumulation. Changes in hepatic NAD^+/NADH ratio could be affected over a long period by the higher fat content. Due to a lower NAD^+/NADH ratio, sirtuin (SIRT) activity is downregulated, which may affect gene transcription in the liver, which could induce the transcription of specific target genes, such as *Fgf21*. Increased expression and secretion of FGF21 reduces hepatic *de novo* lipogenesis (DNL) and gluconeogenesis to counteract the enhanced hepatic lipid accumulation. (B) In FGF21KO mice Cvs also leads to the short-term release of CORT. However, no long-term changes in lipolysis were observed after recovery. Furthermore, FGF21KO mice show a long-term stress-related reduction in hepatic β-oxidation and FA uptake, leading to no changes in lipid accumulation. Along with that, no changes in NAD+/NADH ratio as well as SIRT activity were measured. However, FGF21KO mice have a stress-related increase ATP production after recovery.

4.4 Conclusion and perspective

The results in this work showed the first time a long-term improvement in insulin sensitivity after chronic stress exposure followed by long-term tissue-specific adaptations of lipid and glucose metabolism. The peripheral insulin sensitivity is improved due to increased insulin signaling and glucose uptake in WAT, adipose tissue browning and thermogenesis as well as increased fatty acid oxidation in the muscle. Investigations on WT and C57BL/6 mice reveal a strong correlation of FGF21 plasma level and hepatic fat content indicating its role in regulation of hepatic energy metabolism after chronic stress. Using FGF21KO mice in the same Cvs protocol confirm FGF21 as a potential regulator in the post-stress regulation of hepatic lipid and glucose metabolism. *In vivo* analyses of WT and FGF21KO mice show a FGF21-related influence on Cvs dependent long-term improvements in insulin-stimulated glucose disposal and decrease in fasting blood glucose levels. Moreover, *ex vivo* analyses of primary hepatocytes show enhanced fatty acid uptake and decreased fatty acid oxidation due to previous Cvs exposure. These findings are in line with other studies describing chronic stress as a risk factor for hepatic lipid accumulation and the development of NAFLD (Liu et al., 2014b; Woods et al., 2015). However, investigations indicate FGF21 as a potential counteracting modulator of hepatic lipid accumulation by downregulating DNL in the post-stress situation. First studies on transcriptional regulation show Cvs induced changes in HAT, HDAC and SIRT activity may leading to long-term enhanced transcriptional activity in the liver of previous stressed mice. The here proposed pathway links the prolonged stress-induced GR and chromatin activation to the enhanced expression and secretion of FGF21 in the liver.

Summarizing, the findings of this work link FGF21 to the metabolic adaptation after chronic stress. FGF21 may have clinical implications for the prediction for type 2 diabetes or NAFLD in individuals exposed to or having previous history of stress. Measurements of FGF21 in fatty liver disease patients may help to identify the disease progression and the FGF21 signaling pathway could be a good therapeutic target in the stress-induced development of NAFLD. Additional investigations are needed to examine the role of GR transcriptional activity in the increased expression and secretion of FGF21. Future studies could analyze the transcriptome and secretome to investigate possible co-factors and regulators of Cvs-induced FGF21 expression. Further, investigations on chromatin and histone modification could reveal transcriptional modulators and factors responsible for the stress induced upregulation of FGF21. Possible mechanism linking DNA methylation or histone modification to the Cvs-induced FGF21 rise could be evaluated in future studies as well as the role of the GR in the long-term upregulation of FGF21 expression.

REFERENCES

Adams, J.M., 2nd, Pratipanawatr, T., Berria, R., Wang, E., DeFronzo, R.A., Sullards, M.C., and Mandarino, L.J. (2004). Ceramide content is increased in skeletal muscle from obese insulin-resistant humans. Diabetes *53*, 25-31.

Akie, T.E., and Cooper, M.P. (2015). Determination of Fatty Acid Oxidation and Lipogenesis in Mouse Primary Hepatocytes. J Vis Exp, e52982.

Almon, R.R., Dubois, D.C., Jin, J.Y., and Jusko, W.J. (2005). Temporal profiling of the transcriptional basis for the development of corticosteroid-induced insulin resistance in rat muscle. J Endocrinol *184*, 219-232.

Almon, R.R., DuBois, D.C., and Jusko, W.J. (2007). A microarray analysis of the temporal response of liver to methylprednisolone: a comparative analysis of two dosing regimens. Endocrinology *148*, 2209-2225.

Amatruda, J.M., Danahy, S.A., and Chang, C.L. (1983). The effects of glucocorticoids on insulin-stimulated lipogenesis in primary cultures of rat hepatocytes. Biochem J *212*, 135-141.

Ameer, F., Scandiuzzi, L., Hasnain, S., Kalbacher, H., and Zaidi, N. (2014). De novo lipogenesis in health and disease. Metabolism *63*, 895-902.

Anstee, Q.M., Targher, G., and Day, C.P. (2013). Progression of NAFLD to diabetes mellitus, cardiovascular disease or cirrhosis. Nat Rev Gastroenterol Hepatol *10*, 330-344.

Antonellis, P.J., Hayes, M.P., and Adams, A.C. (2016). Fibroblast Growth Factor 21-Null Mice Do Not Exhibit an Impaired Response to Fasting. Front Endocrinol (Lausanne) *7*, 77-77.

Argiles, J.M., Campos, N., Lopez-Pedrosa, J.M., Rueda, R., and Rodriguez-Manas, L. (2016). Skeletal Muscle Regulates Metabolism via Interorgan Crosstalk: Roles in Health and Disease. Journal of the American Medical Directors Association *17*, 789-796.

Arnaldi, G., Scandali, V.M., Trementino, L., Cardinaletti, M., Appolloni, G., and Boscaro, M. (2010). Pathophysiology of dyslipidemia in Cushing's syndrome. Neuroendocrinology *92 Suppl 1*, 86-90.

Atwoli, L., Stein, D.J., Koenen, K.C., and McLaughlin, K.A. (2015). Epidemiology of posttraumatic stress disorder: prevalence, correlates and consequences. Curr Opin Psychiatry *28*, 307-311.

Badman, M.K., Koester, A., Flier, J.S., Kharitonenkov, A., and Maratos-Flier, E. (2009). Fibroblast growth factor 21-deficient mice demonstrate impaired adaptation to ketosis. Endocrinology *150*, 4931-4940.

Badman, M.K., Pissios, P., Kennedy, A.R., Koukos, G., Flier, J.S., and Maratos-Flier, E. (2007). Hepatic fibroblast growth factor 21 is regulated by PPARalpha and is a key mediator of hepatic lipid metabolism in ketotic states. Cell Metab *5*, 426-437.

Barb, D., Bril, F., Kalavalapalli, S., and Cusi, K. (2019). Plasma Fibroblast Growth Factor 21 Is Associated With Severity of Nonalcoholic Steatohepatitis in Patients With Obesity and Type 2 Diabetes. J Clin Endocrinol Metab *104*, 3327-3336.

Barbatelli, G., Murano, I., Madsen, L., Hao, Q., Jimenez, M., Kristiansen, K., Giacobino, J.P., De Matteis, R., and Cinti, S. (2010). The emergence of cold-induced brown adipocytes in mouse white fat depots is determined predominantly by white to brown adipocyte transdifferentiation. Am J Physiol Endocrinol Metab *298*, E1244-1253.

Barnes, P.J. (1998). Anti-inflammatory actions of glucocorticoids: molecular mechanisms. Clin Sci (Lond) *94*, 557-572.

Barnes, P.J., Pedersen, S., and Busse, W.W. (1998). Efficacy and safety of inhaled corticosteroids. New developments. Am J Respir Crit Care Med *157*, S1-53.

Bastard, J.P., Maachi, M., Lagathu, C., Kim, M.J., Caron, M., Vidal, H., Capeau, J., and Feve, B. (2006). Recent advances in the relationship between obesity, inflammation, and insulin resistance. Eur Cytokine Netw *17*, 4-12.

Bazuine, M., Carlotti, F., Tafrechi, R.S., Hoeben, R.C., and Maassen, J.A. (2004). Mitogen-activated protein kinase (MAPK) phosphatase-1 and -4 attenuate p38 MAPK during dexamethasone-induced insulin resistance in 3T3-L1 adipocytes. Mol Endocrinol *18*, 1697-1707.

Bellentani, S. (2017). The epidemiology of non-alcoholic fatty liver disease. Liver Int *37 Suppl 1*, 81-84.

Berglund, E.D., Li, C.Y., Bina, H.A., Lynes, S.E., Michael, M.D., Shanafelt, A.B., Kharitonenkov, A., and Wasserman, D.H. (2009). Fibroblast growth factor 21 controls glycemia via regulation of hepatic glucose flux and insulin sensitivity. Endocrinology *150*, 4084-4093.

Berthelsen, S., and Pettinger, W.A. (1977). A functional basis for classification of alpha-adrenergic receptors. Life Sci *21*, 595-606.

Bianchi, R., Schonfeld, I.S., and Laurent, E. (2015). Burnout-depression overlap: a review. Clin Psychol Rev *36*, 28-41.

Birkenfeld, A.L., and Shulman, G.I. (2014). Nonalcoholic fatty liver disease, hepatic insulin resistance, and type 2 diabetes. Hepatology *59*, 713-723.

Bisschop, P.H., Fliers, E., and Kalsbeek, A. (2015). Autonomic regulation of hepatic glucose production. Compr Physiol *5*, 147-165.

Blaak, E.E., Wagenmakers, A.J., Glatz, J.F., Wolffenbuttel, B.H., Kemerink, G.J., Langenberg, C.J., Heidendal, G.A., and Saris, W.H. (2000). Plasma FFA utilization and fatty acid-binding protein content are diminished in type 2 diabetic muscle. Am J Physiol Endocrinol Metab *279*, E146-154.

Blachier, M., Leleu, H., Peck-Radosavljevic, M., Valla, D.-C., and Roudot-Thoraval, F. (2013). The burden of liver disease in Europe: A review of available epidemiological data. Journal of Hepatology *58*, 593-608.

Blumensatt, M., Fahlbusch, P., Hilgers, R., Bekaert, M., Herzfeld de Wiza, D., Akhyari, P., Ruige, J.B., and Ouwens, D.M. (2017). Secretory products from epicardial adipose tissue from patients with type 2 diabetes impair mitochondrial beta-oxidation in cardiomyocytes via activation of the cardiac renin-angiotensin system and induction of miR-208a. Basic Res Cardiol *112*, 2.

Boden, G. (2001). Free fatty acids-the link between obesity and insulin resistance. Endocr Pract *7*, 44-51.

Boden, G., Chen, X., Ruiz, J., White, J.V., and Rossetti, L. (1994). Mechanisms of fatty acid-induced inhibition of glucose uptake. J Clin Invest *93*, 2438-2446.

Bodwell, J.E., Webster, J.C., Jewell, C.M., Cidlowski, J.A., Hu, J.M., and Munck, A. (1998). Glucocorticoid receptor phosphorylation: overview, function and cell cycle-dependence. J Steroid Biochem Mol Biol *65*, 91-99.

BonDurant, L.D., Ameka, M., Naber, M.C., Markan, K.R., Idiga, S.O., Acevedo, M.R., Walsh, S.A., Ornitz, D.M., and Potthoff, M.J. (2017). FGF21 Regulates Metabolism Through Adipose-Dependent and -Independent Mechanisms. Cell Metabolism *25*, 935-944.e934.

BonDurant, L.D., and Potthoff, M.J. (2018). Fibroblast Growth Factor 21: A Versatile Regulator of Metabolic Homeostasis. Annu Rev Nutr *38*, 173-196.

Bookout, A.L., de Groot, M.H., Owen, B.M., Lee, S., Gautron, L., Lawrence, H.L., Ding, X., Elmquist, J.K., Takahashi, J.S., Mangelsdorf, D.J*., et al.* (2013). FGF21 regulates metabolism and circadian behavior by acting on the nervous system. Nat Med *19*, 1147-1152.

Bose, M., Olivan, B., and Laferrere, B. (2009). Stress and obesity: the role of the hypothalamic-pituitary-adrenal axis in metabolic disease. Curr Opin Endocrinol Diabetes Obes *16*, 340-346.

Buren, J., Lai, Y.C., Lundgren, M., Eriksson, J.W., and Jensen, J. (2008). Insulin action and signalling in fat and muscle from dexamethasone-treated rats. Arch Biochem Biophys *474*, 91-101.

Buzzetti, E., Pinzani, M., and Tsochatzis, E.A. (2016). The multiple-hit pathogenesis of non-alcoholic fatty liver disease (NAFLD). Metabolism: clinical and experimental *65*, 1038-1048.

Byrne, C.D., and Targher, G. (2015). NAFLD: A multisystem disease. Journal of Hepatology *62*, S47-S64.

Campbell, J.E., Peckett, A.J., D'Souza A, M., Hawke, T.J., and Riddell, M.C. (2011). Adipogenic and lipolytic effects of chronic glucocorticoid exposure. Am J Physiol Cell Physiol *300*, C198-209.

Castaneda, T.R., Nogueiras, R., Muller, T.D., Krishna, R., Grant, E., Jones, A., Ottaway, N., Ananthakrishnan, G., Pfluger, P.T., Chaudhary, N*., et al.* (2011). Decreased glucose tolerance and plasma adiponectin:resistin ratio in a mouse model of post-traumatic stress disorder. Diabetologia *54*, 900-909.

Chadt, A., Immisch, A., de Wendt, C., Springer, C., Zhou, Z., Stermann, T., Holman, G.D., Loffing-Cueni, D., Loffing, J., Joost, H.G*., et al.* (2015). "Deletion of both Rab-GTPase-activating proteins TBC1D1 and

TBC1D4 in mice eliminates insulin- and AICAR-stimulated glucose transport [corrected]. Diabetes *64*, 746-759.

Chakrabarti, P., and Kandror, K.V. (2009). FoxO1 controls insulin-dependent adipose triglyceride lipase (ATGL) expression and lipolysis in adipocytes. J Biol Chem *284*, 13296-13300.

Chanson, P., and Salenave, S. (2010). Metabolic syndrome in Cushing's syndrome. Neuroendocrinology *92 Suppl 1*, 96-101.

Chatterjee, T.K., Basford, J.E., Knoll, E., Tong, W.S., Blanco, V., Blomkalns, A.L., Rudich, S., Lentsch, A.B., Hui, D.Y., and Weintraub, N.L. (2014). HDAC9 knockout mice are protected from adipose tissue dysfunction and systemic metabolic disease during high-fat feeding. Diabetes *63*, 176-187.

Chen, W., Dang, T., Blind, R.D., Wang, Z., Cavasotto, C.N., Hittelman, A.B., Rogatsky, I., Logan, S.K., and Garabedian, M.J. (2008). Glucocorticoid receptor phosphorylation differentially affects target gene expression. Mol Endocrinol *22*, 1754-1766.

Cheng, X., Vispute, S.G., Liu, J., Cheng, C., Kharitonenkov, A., and Klaassen, C.D. (2014). Fibroblast growth factor (Fgf) 21 is a novel target gene of the aryl hydrocarbon receptor (AhR). Toxicology and applied pharmacology *278*, 65-71.

Ciccarelli, M., Santulli, G., Pascale, V., Trimarco, B., and Iaccarino, G. (2013). Adrenergic receptors and metabolism: role in development of cardiovascular disease. Front Physiol *4*, 265.

Clark, A.R., and Belvisi, M.G. (2012). Maps and legends: the quest for dissociated ligands of the glucocorticoid receptor. Pharmacol Ther *134*, 54-67.

Cline, G.W., Petersen, K.F., Krssak, M., Shen, J., Hundal, R.S., Trajanoski, Z., Inzucchi, S., Dresner, A., Rothman, D.L., and Shulman, G.I. (1999). Impaired glucose transport as a cause of decreased insulin-stimulated muscle glycogen synthesis in type 2 diabetes. N Engl J Med *341*, 240-246.

Cobbina, E., and Akhlaghi, F. (2017). Non-alcoholic fatty liver disease (NAFLD) - pathogenesis, classification, and effect on drug metabolizing enzymes and transporters. *49*, 197-211.

Cohen, P., and Spiegelman, B.M. (2016). Cell biology of fat storage. Mol Biol Cell *27*, 2523-2527.

Cohen, S., Janicki-Deverts, D., Doyle, W.J., Miller, G.E., Frank, E., Rabin, B.S., and Turner, R.B. (2012). Chronic stress, glucocorticoid receptor resistance, inflammation, and disease risk. Proc Natl Acad Sci U S A *109*, 5995-5999.

Cooney, G.J., Thompson, A.L., Furler, S.M., Ye, J., and Kraegen, E.W. (2002). Muscle long-chain acyl CoA esters and insulin resistance. Ann N Y Acad Sci *967*, 196-207.

Coskun, T., Bina, H.A., Schneider, M.A., Dunbar, J.D., Hu, C.C., Chen, Y., Moller, D.E., and Kharitonenkov, A. (2008). Fibroblast growth factor 21 corrects obesity in mice. Endocrinology *149*, 6018-6027.

Cousin, B., Cinti, S., Morroni, M., Raimbault, S., Ricquier, D., Penicaud, L., and Casteilla, L. (1992). Occurrence of brown adipocytes in rat white adipose tissue: molecular and morphological characterization. J Cell Sci *103 (Pt 4)*, 931-942.

Coutinho, A.E., and Chapman, K.E. (2011). The anti-inflammatory and immunosuppressive effects of glucocorticoids, recent developments and mechanistic insights. Mol Cell Endocrinol *335*, 2-13.

Crooks, D.R., Natarajan, T.G., Jeong, S.Y., Chen, C., Park, S.Y., Huang, H., Ghosh, M.C., Tong, W.H., Haller, R.G., Wu, C.*, et al.* (2014). Elevated FGF21 secretion, PGC-1alpha and ketogenic enzyme expression are hallmarks of iron-sulfur cluster depletion in human skeletal muscle. Hum Mol Genet *23*, 24-39.

Cui, X.B., and Chen, S.Y. (2016). White adipose tissue browning and obesity. J Biomed Res *31*, 1-2.

Czech, M.P. (2017). Insulin action and resistance in obesity and type 2 diabetes. Nat Med *23*, 804-814.

D'Souza A, M., Beaudry, J.L., Szigiato, A.A., Trumble, S.J., Snook, L.A., Bonen, A., Giacca, A., and Riddell, M.C. (2012). Consumption of a high-fat diet rapidly exacerbates the development of fatty liver disease that occurs with chronically elevated glucocorticoids. Am J Physiol Gastrointest Liver Physiol *302*, G850-863.

Dardevet, D., Sornet, C., Taillandier, D., Savary, I., Attaix, D., and Grizard, J. (1995). Sensitivity and protein turnover response to glucocorticoids are different in skeletal muscle from adult and old rats. Lack of regulation of the ubiquitin-proteasome proteolytic pathway in aging. The Journal of clinical investigation *96*, 2113-2119.

De Bosscher, K., Vanden Berghe, W., and Haegeman, G. (2003). The interplay between the glucocorticoid receptor and nuclear factor-kappaB or activator protein-1: molecular mechanisms for gene repression. Endocr Rev *24*, 488-522.

de Guia, R.M., Rose, A.J., and Herzig, S. (2014). Glucocorticoid hormones and energy homeostasis. Horm Mol Biol Clin Investig *19*, 117-128.

de Luca, C., and Olefsky, J.M. (2008). Inflammation and insulin resistance. FEBS Lett *582*, 97-105.

De Wulf, H., and Hers, H.G. (1967). The stimulation of glycogen synthesis andof glycogen synthetase in the liver by glucocorticoids. Eur J Biochem *2*, 57-60.

Del Campo, J.A., Gallego, P., and Grande, L. (2018). Role of inflammatory response in liver diseases: Therapeutic strategies. World J Hepatol *10*, 1-7.

Dent, P., Lavoinne, A., Nakielny, S., Caudwell, F.B., Watt, P., and Cohen, P. (1990). The molecular mechanism by which insulin stimulates glycogen synthesis in mammalian skeletal muscle. Nature *348*, 302-308.

Dhabhar, F.S. (2000). Acute stress enhances while chronic stress suppresses skin immunity. The role of stress hormones and leukocyte trafficking. Ann N Y Acad Sci *917*, 876-893.

Dhabhar, F.S., Saul, A.N., Daugherty, C., Holmes, T.H., Bouley, D.M., and Oberyszyn, T.M. (2010). Short-term stress enhances cellular immunity and increases early resistance to squamous cell carcinoma. Brain Behav Immun *24*, 127-137.

Dimitriadis, G., Leighton, B., Parry-Billings, M., Sasson, S., Young, M., Krause, U., Bevan, S., Piva, T., Wegener, G., and Newsholme, E.A. (1997). Effects of glucocorticoid excess on the sensitivity of glucose transport and metabolism to insulin in rat skeletal muscle. Biochem J *321 (Pt 3)*, 707-712.

Dimitriadis, G., Mitrou, P., Lambadiari, V., Maratou, E., and Raptis, S.A. (2011). Insulin effects in muscle and adipose tissue. Diabetes Res Clin Pract *93 Suppl 1*, S52-59.

Ding, R.-B., Bao, J., and Deng, C.-X. (2017). Emerging roles of SIRT1 in fatty liver diseases. Int J Biol Sci *13*, 852-867.

Djurhuus, C.B., Gravholt, C.H., Nielsen, S., Pedersen, S.B., Moller, N., and Schmitz, O. (2004). Additive effects of cortisol and growth hormone on regional and systemic lipolysis in humans. American journal of physiology Endocrinology and metabolism *286*, E488-494.

Dolinsky, V.W., Douglas, D.N., Lehner, R., and Vance, D.E. (2004). Regulation of the enzymes of hepatic microsomal triacylglycerol lipolysis and re-esterification by the glucocorticoid dexamethasone. Biochem J *378*, 967-974.

Donnelly, K.L., Smith, C.I., Schwarzenberg, S.J., Jessurun, J., Boldt, M.D., and Parks, E.J. (2005). Sources of fatty acids stored in liver and secreted via lipoproteins in patients with nonalcoholic fatty liver disease. J Clin Invest *115*, 1343-1351.

Dresner, A., Laurent, D., Marcucci, M., Griffin, M.E., Dufour, S., Cline, G.W., Slezak, L.A., Andersen, D.K., Hundal, R.S., Rothman, D.L*., et al.* (1999). Effects of free fatty acids on glucose transport and IRS-1-associated phosphatidylinositol 3-kinase activity. J Clin Invest *103*, 253-259.

Dunn, A.J. (2000). Cytokine activation of the HPA axis. Ann N Y Acad Sci *917*, 608-617.

Durovcova, V., Marek, J., Hana, V., Matoulek, M., Zikan, V., Haluzikova, D., Kavalkova, P., Lacinova, Z., Krsek, M., and Haluzik, M. (2010). Plasma concentrations of fibroblast growth factors 21 and 19 in patients with Cushing's syndrome. Physiol Res *59*, 415-422.

Dushay, J., Chui, P.C., Gopalakrishnan, G.S., Varela-Rey, M., Crawley, M., Fisher, F.M., Badman, M.K., Martinez-Chantar, M.L., and Maratos-Flier, E. (2010). Increased fibroblast growth factor 21 in obesity and nonalcoholic fatty liver disease. Gastroenterology *139*, 456-463.

Ekstedt, M., Franzén, L.E., Mathiesen, U.L., Thorelius, L., Holmqvist, M., Bodemar, G., and Kechagias, S. (2006). Long-term follow-up of patients with NAFLD and elevated liver enzymes. Hepatology *44*, 865-873.

Elhassan, Y.S., Philp, A.A., and Lavery, G.G. (2017). Targeting NAD+ in Metabolic Disease: New Insights Into an Old Molecule. Journal of the Endocrine Society *1*, 816-835.

Emanuelli, B., Vienberg, S.G., Smyth, G., Cheng, C., Stanford, K.I., Arumugam, M., Michael, M.D., Adams, A.C., Kharitonenkov, A., and Kahn, C.R. (2014). Interplay between FGF21 and insulin action in the liver regulates metabolism. J Clin Invest *124*, 515-527.

Fabbrini, E., Sullivan, S., and Klein, S. (2010). Obesity and nonalcoholic fatty liver disease: biochemical, metabolic, and clinical implications. Hepatology *51*, 679-689.

Fang, Y.L., Chen, H., Wang, C.L., and Liang, L. (2018). Pathogenesis of non-alcoholic fatty liver disease in children and adolescence: From "two hit theory" to "multiple hit model". World journal of gastroenterology *24*, 2974-2983.

Fasshauer, M., and Bluher, M. (2015). Adipokines in health and disease. Trends Pharmacol Sci *36*, 461-470.

Faulenbach, M., Uthoff, H., Schwegler, K., Spinas, G.A., Schmid, C., and Wiesli, P. (2012). Effect of psychological stress on glucose control in patients with Type 2 diabetes. Diabetic medicine : a journal of the British Diabetic Association *29*, 128-131.

Feige, J.N., and Auwerx, J. (2008). Transcriptional targets of sirtuins in the coordination of mammalian physiology. Curr Opin Cell Biol *20*, 303-309.

Feige, J.N., Lagouge, M., Canto, C., Strehle, A., Houten, S.M., Milne, J.C., Lambert, P.D., Mataki, C., Elliott, P.J., and Auwerx, J. (2008). Specific SIRT1 Activation Mimics Low Energy Levels and Protects against Diet-Induced Metabolic Disorders by Enhancing Fat Oxidation. Cell Metabolism *8*, 347-358.

Finkel, T., Deng, C.X., and Mostoslavsky, R. (2009). Recent progress in the biology and physiology of sirtuins. Nature *460*, 587-591.

Fisher, F.M., Chui, P.C., Antonellis, P.J., Bina, H.A., Kharitonenkov, A., Flier, J.S., and Maratos-Flier, E. (2010). Obesity is a fibroblast growth factor 21 (FGF21)-resistant state. Diabetes *59*, 2781-2789.

Fisher, F.M., Kleiner, S., Douris, N., Fox, E.C., Mepani, R.J., Verdeguer, F., Wu, J., Kharitonenkov, A., Flier, J.S., Maratos-Flier, E.*, et al.* (2012). FGF21 regulates PGC-1alpha and browning of white adipose tissues in adaptive thermogenesis. Genes Dev *26*, 271-281.

Frayn, K.N. (2003). The glucose-fatty acid cycle: a physiological perspective. Biochem Soc Trans *31*, 1115-1119.

Fumeron, F., Aubert, R., Siddiq, A., Betoulle, D., Pean, F., Hadjadj, S., Tichet, J., Wilpart, E., Chesnier, M.C., Balkau, B.*, et al.* (2004). Adiponectin gene polymorphisms and adiponectin levels are independently associated with the development of hyperglycemia during a 3-year period: the epidemiologic data on the insulin resistance syndrome prospective study. Diabetes *53*, 1150-1157.

Gagliardi, L., Ho, J.T., and Torpy, D.J. (2010). Corticosteroid-binding globulin: the clinical significance of altered levels and heritable mutations. Mol Cell Endocrinol *316*, 24-34.

Gaich, G., Chien, J.Y., Fu, H., Glass, L.C., Deeg, M.A., Holland, W.L., Kharitonenkov, A., Bumol, T., Schilske, H.K., and Moller, D.E. (2013). The effects of LY2405319, an FGF21 analog, in obese human subjects with type 2 diabetes. Cell Metab *18*, 333-340.

Garvey, W.T., Maianu, L., Zhu, J.H., Brechtel-Hook, G., Wallace, P., and Baron, A.D. (1998). Evidence for defects in the trafficking and translocation of GLUT4 glucose transporters in skeletal muscle as a cause of human insulin resistance. J Clin Invest *101*, 2377-2386.

Gathercole, L.L., Bujalska, I.J., Stewart, P.M., and Tomlinson, J.W. (2007). Glucocorticoid modulation of insulin signaling in human subcutaneous adipose tissue. J Clin Endocrinol Metab *92*, 4332-4339.

Gathercole, L.L., Morgan, S.A., Bujalska, I.J., Hauton, D., Stewart, P.M., and Tomlinson, J.W. (2011a). Regulation of lipogenesis by glucocorticoids and insulin in human adipose tissue. PLoS One *6*, e26223.

Gathercole, L.L., Morgan, S.A., Bujalska, I.J., Stewart, P.M., and Tomlinson, J.W. (2011b). Short- and long-term glucocorticoid treatment enhances insulin signalling in human subcutaneous adipose tissue. Nutr Diabetes *1*, e3.

Ge, X., Chen, C., Hui, X., Wang, Y., Lam, K.S., and Xu, A. (2011). Fibroblast growth factor 21 induces glucose transporter-1 expression through activation of the serum response factor/Ets-like protein-1 in adipocytes. J Biol Chem *286*, 34533-34541.

Ge, X., Wang, Y., Lam, K.S.L., and Xu, A. (2012). Metabolic actions of FGF21: molecular mechanisms and therapeutic implications. Acta Pharmaceutica Sinica B *2*, 350-357.

Geer, E.B., Islam, J., and Buettner, C. (2014). Mechanisms of glucocorticoid-induced insulin resistance: focus on adipose tissue function and lipid metabolism. Endocrinol Metab Clin North Am *43*, 75-102.

Giorgino, F., Almahfouz, A., Goodyear, L.J., and Smith, R.J. (1993). Glucocorticoid regulation of insulin receptor and substrate IRS-1 tyrosine phosphorylation in rat skeletal muscle in vivo. J Clin Invest *91*, 2020-2030.

Goodpaster, B.H., and Kelley, D.E. (2002). Skeletal muscle triglyceride: marker or mediator of obesity-induced insulin resistance in type 2 diabetes mellitus? Curr Diab Rep *2*, 216-222.

Goodwin, R.D., and Davidson, J.R. (2005). Self-reported diabetes and posttraumatic stress disorder among adults in the community. Preventive medicine *40*, 570-574.

Grad, I., and Picard, D. (2007). The glucocorticoid responses are shaped by molecular chaperones. Mol Cell Endocrinol *275*, 2-12.

Gradus, J.L. (2017). Prevalence and prognosis of stress disorders: a review of the epidemiologic literature. Clin Epidemiol *9*, 251-260.

Greenberg, A.S., and Obin, M.S. (2006). Obesity and the role of adipose tissue in inflammation and metabolism. Am J Clin Nutr *83*, 461S-465S.

Grundy, S.M. (2015). Adipose tissue and metabolic syndrome: too much, too little or neither. Eur J Clin Invest *45*, 1209-1217.

Guridi, M., Tintignac, L.A., Lin, S., Kupr, B., Castets, P., and Ruegg, M.A. (2015). Activation of mTORC1 in skeletal muscle regulates whole-body metabolism through FGF21. Sci Signal *8*, ra113.

Habib, K.E., Gold, P.W., and Chrousos, G.P. (2001). Neuroendocrinology of stress. Endocrinol Metab Clin North Am *30*, 695-728; vii-viii.

Hale, C., Chen, M.M., Stanislaus, S., Chinookoswong, N., Hager, T., Wang, M., Veniant, M.M., and Xu, J. (2012). Lack of overt FGF21 resistance in two mouse models of obesity and insulin resistance. Endocrinology *153*, 69-80.

Hall, K.S., Hoerster, K.D., and Yancy, W.S., Jr. (2015). Post-traumatic stress disorder, physical activity, and eating behaviors. Epidemiologic reviews *37*, 103-115.

Haluzik, M., Dietz, K.R., Kim, J.K., Marcus-Samuels, B., Shulman, G.I., Gavrilova, O., and Reitman, M.L. (2002). Adrenalectomy improves diabetes in A-ZIP/F-1 lipoatrophic mice by increasing both liver and muscle insulin sensitivity. Diabetes *51*, 2113-2118.

Hammen, C., Brennan, P.A., Keenan-Miller, D., Hazel, N.A., and Najman, J.M. (2010). Chronic and acute stress, gender, and serotonin transporter gene-environment interactions predicting depression symptoms in youth. J Child Psychol Psychiatry *51*, 180-187.

Han, C., Rice, M.W., and Cai, D. (2016). Neuroinflammatory and autonomic mechanisms in diabetes and hypertension. Am J Physiol Endocrinol Metab *311*, E32-41.

Hanukoglu, I. (1992). Steroidogenic enzymes: structure, function, and role in regulation of steroid hormone biosynthesis. J Steroid Biochem Mol Biol *43*, 779-804.

Hardie, L.J., Guilhot, N., and Trayhurn, P. (1996). Regulation of leptin production in cultured mature white adipocytes. Horm Metab Res *28*, 685-689.

Harms, M., and Seale, P. (2013). Brown and beige fat: development, function and therapeutic potential. Nat Med *19*, 1252-1263.

Harris, L.A., Skinner, J.R., Shew, T.M., Pietka, T.A., Abumrad, N.A., and Wolins, N.E. (2015). Perilipin 5-Driven Lipid Droplet Accumulation in Skeletal Muscle Stimulates the Expression of Fibroblast Growth Factor 21. Diabetes *64*, 2757-2768.

Harris, R.B. (2015). Chronic and acute effects of stress on energy balance: are there appropriate animal models? American journal of physiology Regulatory, integrative and comparative physiology *308*, R250-265.

Hazlehurst, J.M., Gathercole, L.L., Nasiri, M., Armstrong, M.J., Borrows, S., Yu, J., Wagenmakers, A.J., Stewart, P.M., and Tomlinson, J.W. (2013). Glucocorticoids fail to cause insulin resistance in human subcutaneous adipose tissue in vivo. J Clin Endocrinol Metab *98*, 1631-1640.

Himms-Hagen, J., Melnyk, A., Zingaretti, M.C., Ceresi, E., Barbatelli, G., and Cinti, S. (2000). Multilocular fat cells in WAT of CL-316243-treated rats derive directly from white adipocytes. Am J Physiol Cell Physiol *279*, C670-681.

Hoge, C.W., Auchterlonie, J.L., and Milliken, C.S. (2006). Mental health problems, use of mental health services, and attrition from military service after returning from deployment to Iraq or Afghanistan. Jama *295*, 1023-1032.

Hong, E.G., Ko, H.J., Cho, Y.R., Kim, H.J., Ma, Z., Yu, T.Y., Friedline, R.H., Kurt-Jones, E., Finberg, R., Fischer, M.A*., et al.* (2009). Interleukin-10 prevents diet-induced insulin resistance by attenuating macrophage and cytokine response in skeletal muscle. Diabetes *58*, 2525-2535.

Horbelt, T., Tacke, C., Markova, M., Herzfeld de Wiza, D., Van de Velde, F., Bekaert, M., Van Nieuwenhove, Y., Hornemann, S., Rodiger, M., Seebeck, N*., et al.* (2018). The novel adipokine WISP1 associates with insulin resistance and impairs insulin action in human myotubes and mouse hepatocytes. *61*, 2054-2065.

Hotta, K., Funahashi, T., Bodkin, N.L., Ortmeyer, H.K., Arita, Y., Hansen, B.C., and Matsuzawa, Y. (2001). Circulating concentrations of the adipocyte protein adiponectin are decreased in parallel with reduced insulin sensitivity during the progression to type 2 diabetes in rhesus monkeys. Diabetes *50*, 1126-1133.

Hotta, Y., Nakamura, H., Konishi, M., Murata, Y., Takagi, H., Matsumura, S., Inoue, K., Fushiki, T., and Itoh, N. (2009). Fibroblast growth factor 21 regulates lipolysis in white adipose tissue but is not required for ketogenesis and triglyceride clearance in liver. Endocrinology *150*, 4625-4633.

Hue, L., and Taegtmeyer, H. (2009). The Randle cycle revisited: a new head for an old hat. Am J Physiol Endocrinol Metab *297*, E578-591.

Hulver, M.W., Berggren, J.R., Cortright, R.N., Dudek, R.W., Thompson, R.P., Pories, W.J., MacDonald, K.G., Cline, G.W., Shulman, G.I., Dohm, G.L*., et al.* (2003). Skeletal muscle lipid metabolism with obesity. Am J Physiol Endocrinol Metab *284*, E741-747.

Hyysalo, J., Mannisto, V.T., Zhou, Y., Arola, J., Karja, V., Leivonen, M., Juuti, A., Jaser, N., Lallukka, S., Kakela, P*., et al.* (2014). A population-based study on the prevalence of NASH using scores validated against liver histology. J Hepatol *60*, 839-846.

IDF (2017). https://idf.org/aboutdiabetes/type-2-diabetes.html (International Diabetes Federation).

Inagaki, T., Dutchak, P., Zhao, G., Ding, X., Gautron, L., Parameswara, V., Li, Y., Goetz, R., Mohammadi, M., Esser, V*., et al.* (2007). Endocrine regulation of the fasting response by PPARalpha-mediated induction of fibroblast growth factor 21. Cell Metab *5*, 415-425.

Itani, S.I., Ruderman, N.B., Schmieder, F., and Boden, G. (2002). Lipid-induced insulin resistance in human muscle is associated with changes in diacylglycerol, protein kinase C, and IkappaB-alpha. Diabetes *51*, 2005-2011.

Izumiya, Y., Bina, H.A., Ouchi, N., Akasaki, Y., Kharitonenkov, A., and Walsh, K. (2008). FGF21 is an Akt-regulated myokine. FEBS Lett *582*, 3805-3810.

James, O.F., and Day, C.P. (1998). Non-alcoholic steatohepatitis (NASH): a disease of emerging identity and importance. J Hepatol *29*, 495-501.

Jelenik, T., Dille, M., Müller-Lühlhoff, S., Kabra, D.G., Zhou, Z., Binsch, C., Hartwig, S., Lehr, S., Chadt, A., Peters, E.M.J*., et al.* (2018). FGF21 regulates insulin sensitivity following long-term chronic stress. Molecular Metabolism *16*, 126-138.

Jelenik, T., Kaul, K., Sequaris, G., Flogel, U., Phielix, E., Kotzka, J., Knebel, B., Fahlbusch, P., Horbelt, T., Lehr, S*., et al.* (2017a). Mechanisms of Insulin Resistance in Primary and Secondary Nonalcoholic Fatty Liver. *66*, 2241-2253.

Jelenik, T., Kaul, K., Sequaris, G., Flogel, U., Phielix, E., Kotzka, J., Knebel, B., Fahlbusch, P., Horbelt, T., Lehr, S*., et al.* (2017b). Mechanisms of Insulin Resistance in Primary and Secondary Nonalcoholic Fatty Liver. Diabetes *66*, 2241-2253.

Jelenik, T., Sequaris, G., Kaul, K., Ouwens, D.M., Phielix, E., Kotzka, J., Knebel, B., Weiss, J., Reinbeck, A.L., Janke, L*., et al.* (2014). Tissue-specific differences in the development of insulin resistance in a mouse model for type 1 diabetes. Diabetes *63*, 3856-3867.

Jiang, N., Li, Y., Shu, T., and Wang, J. (2019). Cytokines and inflammation in adipogenesis: an updated review. Front Med *13*, 314-329.

Jiang, S.Z., and Eiden, L.E. (2016). Activation of the HPA axis and depression of feeding behavior induced by restraint stress are separately regulated by PACAPergic neurotransmission in the mouse. Stress (Amsterdam, Netherlands) *19*, 374-382.

Kadmiel, M., and Cidlowski, J.A. (2013). Glucocorticoid receptor signaling in health and disease. Trends Pharmacol Sci *34*, 518-530.

Kahn, B.B., and Flier, J.S. (2000). Obesity and insulin resistance. J Clin Invest *106*, 473-481.

Kajimura, S., Spiegelman, B.M., and Seale, P. (2015). Brown and Beige Fat: Physiological Roles beyond Heat Generation. Cell Metab *22*, 546-559.

Katz, J., and Tayek, J.A. (1998). Gluconeogenesis and the Cori cycle in 12-, 20-, and 40-h-fasted humans. Am J Physiol *275*, E537-542.

Kaur, J. (2014). A comprehensive review on metabolic syndrome. Cardiol Res Pract *2014*, 943162.

Keipert, S., Kutschke, M., Lamp, D., Brachthauser, L., Neff, F., Meyer, C.W., Oelkrug, R., Kharitonenkov, A., and Jastroch, M. (2015). Genetic disruption of uncoupling protein 1 in mice renders brown adipose tissue a significant source of FGF21 secretion. Mol Metab *4*, 537-542.

Kendrick, A.A., Choudhury, M., Rahman, S.M., McCurdy, C.E., Friederich, M., Van Hove, J.L., Watson, P.A., Birdsey, N., Bao, J., Gius, D.*, et al.* (2011). Fatty liver is associated with reduced SIRT3 activity and mitochondrial protein hyperacetylation. Biochem J *433*, 505-514.

Kershaw, E.E., Hamm, J.K., Verhagen, L.A., Peroni, O., Katic, M., and Flier, J.S. (2006). Adipose triglyceride lipase: function, regulation by insulin, and comparison with adiponutrin. Diabetes *55*, 148-157.

Kershaw, E.E., Morton, N.M., Dhillon, H., Ramage, L., Seckl, J.R., and Flier, J.S. (2005). Adipocyte-specific glucocorticoid inactivation protects against diet-induced obesity. Diabetes *54*, 1023-1031.

Kharitonenkov, A., Shiyanova, T.L., Koester, A., Ford, A.M., Micanovic, R., Galbreath, E.J., Sandusky, G.E., Hammond, L.J., Moyers, J.S., Owens, R.A.*, et al.* (2005). FGF-21 as a novel metabolic regulator. J Clin Invest *115*, 1627-1635.

Kim, K.H., Jeong, Y.T., Oh, H., Kim, S.H., Cho, J.M., Kim, Y.N., Kim, S.S., Kim, D.H., Hur, K.Y., Kim, H.K.*, et al.* (2013). Autophagy deficiency leads to protection from obesity and insulin resistance by inducing Fgf21 as a mitokine. Nat Med *19*, 83-92.

Kirk, C.J., Verrinder, T.R., and Hems, D.A. (1976). Fatty acid synthesis in the perfused liver of adrenalectomized rats. Biochem J *156*, 593-602.

Knebel, B., Fahlbusch, P., Dille, M., Wahlers, N., Hartwig, S., Jacob, S., Kettel, U., Schiller, M., Herebian, D., Koellmer, C.*, et al.* (2019). Fatty Liver Due to Increased de novo Lipogenesis: Alterations in the Hepatic Peroxisomal Proteome. Front Cell Dev Biol *7*, 248.

Knebel, B., Haas, J., Hartwig, S., Jacob, S., Kollmer, C., Nitzgen, U., Muller-Wieland, D., and Kotzka, J. (2012). Liver-specific expression of transcriptionally active SREBP-1c is associated with fatty liver and increased visceral fat mass. PLoS One *7*, e31812.

Koorneef, L.L., van den Heuvel, J.K., Kroon, J., Boon, M.R., t Hoen, P.A.C., Hettne, K.M., van de Velde, N.M., Kolenbrander, K.B., Streefland, T.C.M., Mol, I.M.*, et al.* (2018). Selective Glucocorticoid Receptor Modulation Prevents and Reverses Nonalcoholic Fatty Liver Disease in Male Mice. Endocrinology *159*, 3925-3936.

Kotzka, J., Knebel, B., Haas, J., Kremer, L., Jacob, S., Hartwig, S., Nitzgen, U., and Muller-Wieland, D. (2012). Preventing phosphorylation of sterol regulatory element-binding protein 1a by MAP-kinases protects mice from fatty liver and visceral obesity. PLoS One *7*, e32609.

Kovner, I., Taicher, G.Z., and Mitchell, A.D. (2010). Calibration and validation of EchoMRI whole body composition analysis based on chemical analysis of piglets, in comparison with the same for DXA. Int J Body Compos Res *8*, 17-29.

Krsek, M., Rosicka, M., Nedvidkova, J., Kvasnickova, H., Hana, V., Marek, J., Haluzik, M., Lai, E.W., and Pacak, K. (2006). Increased lipolysis of subcutaneous abdominal adipose tissue and altered noradrenergic activity in patients with Cushing's syndrome: an in-vivo microdialysis study. Physiological research *55*, 421-428.

Krssak, M., Falk Petersen, K., Dresner, A., DiPietro, L., Vogel, S.M., Rothman, D.L., Roden, M., and Shulman, G.I. (1999). Intramyocellular lipid concentrations are correlated with insulin sensitivity in humans: a 1H NMR spectroscopy study. Diabetologia *42*, 113-116.

Kuo, T., Harris, C.A., and Wang, J.C. (2013). Metabolic functions of glucocorticoid receptor in skeletal muscle. Mol Cell Endocrinol *380*, 79-88.

Kuo, T., McQueen, A., Chen, T.C., and Wang, J.C. (2015). Regulation of Glucose Homeostasis by Glucocorticoids. Adv Exp Med Biol *872*, 99-126.

Kyrou, I., and Tsigos, C. (2007). Stress mechanisms and metabolic complications. Horm Metab Res *39*, 430-438.

Kyrou, I., and Tsigos, C. (2009). Stress hormones: physiological stress and regulation of metabolism. Curr Opin Pharmacol *9*, 787-793.

Laeger, T., Baumeier, C., Wilhelmi, I., Würfel, J., Kamitz, A., and Schürmann, A. (2017). FGF21 improves glucose homeostasis in an obese diabetes-prone mouse model independent of body fat changes. Diabetologia *60*, 2274-2284.

Lampidonis, A.D., Rogdakis, E., Voutsinas, G.E., and Stravopodis, D.J. (2011). The resurgence of Hormone-Sensitive Lipase (HSL) in mammalian lipolysis. Gene *477*, 1-11.

Laskewitz, A.J., van Dijk, T.H., Bloks, V.W., Reijngoud, D.J., van Lierop, M.J., Dokter, W.H., Kuipers, F., Groen, A.K., and Grefhorst, A. (2010). Chronic prednisolone treatment reduces hepatic insulin sensitivity while perturbing the fed-to-fasting transition in mice. Endocrinology *151*, 2171-2178.

Lazarus, R.S. (1974). Psychological stress and coping in adaptation and illness. Int J Psychiatry Med *5*, 321-333.

Leal Vde, O., and Mafra, D. (2013). Adipokines in obesity. Clin Chim Acta *419*, 87-94.

Lee, D.V., Li, D., Yan, Q., Zhu, Y., Goodwin, B., Calle, R., Brenner, M.B., and Talukdar, S. (2014). Fibroblast growth factor 21 improves insulin sensitivity and synergizes with insulin in human adipose stem cell-derived (hASC) adipocytes. PloS one *9*, e111767.

Lee, J.H., Gao, Z., and Ye, J. (2013). Regulation of 11beta-HSD1 expression during adipose tissue expansion by hypoxia through different activities of NF-kappaB and HIF-1alpha. Am J Physiol Endocrinol Metab *304*, E1035-1041.

Leitner, D.R., Fruhbeck, G., Yumuk, V., Schindler, K., Micic, D., Woodward, E., and Toplak, H. (2017). Obesity and Type 2 Diabetes: Two Diseases with a Need for Combined Treatment Strategies - EASO Can Lead the Way. Obes Facts *10*, 483-492.

Lemke, U., Krones-Herzig, A., Berriel Diaz, M., Narvekar, P., Ziegler, A., Vegiopoulos, A., Cato, A.C., Bohl, S., Klingmuller, U., Screaton, R.A*., et al.* (2008). The glucocorticoid receptor controls hepatic dyslipidemia through Hes1. Cell Metab *8*, 212-223.

Leney, S.E., and Tavare, J.M. (2009). The molecular basis of insulin-stimulated glucose uptake: signalling, trafficking and potential drug targets. J Endocrinol *203*, 1-18.

Letteron, P., Brahimi-Bourouina, N., Robin, M.A., Moreau, A., Feldmann, G., and Pessayre, D. (1997). Glucocorticoids inhibit mitochondrial matrix acyl-CoA dehydrogenases and fatty acid beta-oxidation. Am J Physiol *272*, G1141-1150.

Lewis, G.F., Vranic, M., Harley, P., and Giacca, A. (1997). Fatty acids mediate the acute extrahepatic effects of insulin on hepatic glucose production in humans. Diabetes *46*, 1111-1119.

Li, H., Fang, Q., Gao, F., Fan, J., Zhou, J., Wang, X., Zhang, H., Pan, X., Bao, Y., Xiang, K.*, et al.* (2010). Fibroblast growth factor 21 levels are increased in nonalcoholic fatty liver disease patients and are correlated with hepatic triglyceride. J Hepatol *53*, 934-940.

Li, H., Gao, Z., Zhang, J., Ye, X., Xu, A., Ye, J., and Jia, W. (2012). Sodium Butyrate Stimulates Expression of Fibroblast Growth Factor 21 in Liver by Inhibition of Histone Deacetylase 3. Diabetes *61*, 797.

Li, Y., Wong, K., Giles, A., Jiang, J., Lee, J.W., Adams, A.C., Kharitonenkov, A., Yang, Q., Gao, B., Guarente, L.*, et al.* (2014). Hepatic SIRT1 attenuates hepatic steatosis and controls energy balance in mice by inducing fibroblast growth factor 21. Gastroenterology *146*, 539-549.e537.

Liang, Q., Zhong, L., Zhang, J., Wang, Y., Bornstein, S.R., Triggle, C.R., Ding, H., Lam, K.S., and Xu, A. (2014). FGF21 maintains glucose homeostasis by mediating the cross talk between liver and brain during prolonged fasting. Diabetes *63*, 4064-4075.

Lin, X., Liu, Y.B., and Hu, H. (2017). Metabolic role of fibroblast growth factor 21 in liver, adipose and nervous system tissues. Biomed Rep *6*, 495-502.

Liu, T., Zhang, L., Joo, D., and Sun, S.C. (2017). NF-kappaB signaling in inflammation. Signal Transduct Target Ther *2*.

Liu, X.X., Zhu, X.M., Miao, Q., Ye, H.Y., Zhang, Z.Y., and Li, Y.M. (2014a). Hyperglycemia induced by glucocorticoids in nondiabetic patients: a meta-analysis. Ann Nutr Metab *65*, 324-332.

Liu, Y.Z., Chen, J.K., Zhang, Y., Wang, X., Qu, S., and Jiang, C.L. (2014b). Chronic stress induces steatohepatitis while decreases visceral fat mass in mice. BMC gastroenterology *14*, 106.

Lo, K.A., and Sun, L. (2013). Turning WAT into BAT: a review on regulators controlling the browning of white adipocytes. Biosci Rep *33*.

Lotta, L.A., Gulati, P., Day, F.R., Payne, F., Ongen, H., van de Bunt, M., Gaulton, K.J., Eicher, J.D., Sharp, S.J., Luan, J.*, et al.* (2017). Integrative genomic analysis implicates limited peripheral adipose storage capacity in the pathogenesis of human insulin resistance. Nat Genet *49*, 17-26.

Ma, R., Zhang, W., Tang, K., Zhang, H., Zhang, Y., Li, D., Li, Y., Xu, P., Luo, S., Cai, W.*, et al.* (2013). Switch of glycolysis to gluconeogenesis by dexamethasone for treatment of hepatocarcinoma. Nature Communications *4*, 2508.

Macfarlane, D.P., Forbes, S., and Walker, B.R. (2008). Glucocorticoids and fatty acid metabolism in humans: fuelling fat redistribution in the metabolic syndrome. J Endocrinol *197*, 189-204.

Magomedova, L., and Cummins, C.L. (2016). Glucocorticoids and Metabolic Control. Handb Exp Pharmacol *233*, 73-93.

Marette, A. (2002). Mediators of cytokine-induced insulin resistance in obesity and other inflammatory settings. Curr Opin Clin Nutr Metab Care *5*, 377-383.

Marino, J.S., Stechschulte, L.A., Stec, D.E., Nestor-Kalinoski, A., Coleman, S., and Hinds, T.D., Jr. (2016). Glucocorticoid Receptor beta Induces Hepatic Steatosis by Augmenting Inflammation and Inhibition of the Peroxisome Proliferator-activated Receptor (PPAR) alpha. J Biol Chem *291*, 25776-25788.

Markan, K.R. (2018). Defining "FGF21 Resistance" during obesity: Controversy, criteria and unresolved questions. F1000Res *7*, 289-289.

Markan, K.R., Naber, M.C., Ameka, M.K., Anderegg, M.D., Mangelsdorf, D.J., Kliewer, S.A., Mohammadi, M., and Potthoff, M.J. (2014). Circulating FGF21 is liver derived and enhances glucose uptake during refeeding and overfeeding. Diabetes *63*, 4057-4063.

Maslov, B., Marcinko, D., Milicevic, R., Babic, D., Dordevic, V., and Jakovljevic, M. (2009). Metabolic syndrome, anxiety, depression and suicidal tendencies in post-traumatic stress disorder and schizophrenic patients. Collegium antropologicum *33 Suppl 2*, 7-10.

McEwen, B.S. (2017). Neurobiological and Systemic Effects of Chronic Stress. Chronic Stress (Thousand Oaks) *1*.

Meier, U., and Gressner, A.M. (2004). Endocrine regulation of energy metabolism: review of pathobiochemical and clinical chemical aspects of leptin, ghrelin, adiponectin, and resistin. Clin Chem *50*, 1511-1525.

Méndez-Lucas, A., Duarte, J.A.G., Sunny, N.E., Satapati, S., He, T., Fu, X., Bermúdez, J., Burgess, S.C., and Perales, J.C. (2013). PEPCK-M expression in mouse liver potentiates, not replaces, PEPCK-C mediated gluconeogenesis. Journal of Hepatology *59*, 105-113.

Merikangas, K.R., He, J.P., Burstein, M., Swanson, S.A., Avenevoli, S., Cui, L., Benjet, C., Georgiades, K., and Swendsen, J. (2010). Lifetime prevalence of mental disorders in U.S. adolescents: results from the National Comorbidity Survey Replication--Adolescent Supplement (NCS-A). J Am Acad Child Adolesc Psychiatry *49*, 980-989.

Mezuk, B., Eaton, W.W., Albrecht, S., and Golden, S.H. (2008). Depression and type 2 diabetes over the lifespan: a meta-analysis. Diabetes Care *31*, 2383-2390.

Mihaylova, M.M., Vasquez, D.S., Ravnskjaer, K., Denechaud, P.D., Yu, R.T., Alvarez, J.G., Downes, M., Evans, R.M., Montminy, M., and Shaw, R.J. (2011). Class IIa histone deacetylases are hormone-activated regulators of FOXO and mammalian glucose homeostasis. Cell *145*, 607-621.

Miller, G.E., Cohen, S., and Ritchey, A.K. (2002). Chronic psychological stress and the regulation of pro-inflammatory cytokines: a glucocorticoid-resistance model. Health Psychol *21*, 531-541.

Miller, W.L. (1988). Molecular biology of steroid hormone synthesis. Endocr Rev *9*, 295-318.

Moore, M.C., Coate, K.C., Winnick, J.J., An, Z., and Cherrington, A.D. (2012). Regulation of hepatic glucose uptake and storage in vivo. Adv Nutr *3*, 286-294.

Morgan, S.A., Sherlock, M., Gathercole, L.L., Lavery, G.G., Lenaghan, C., Bujalska, I.J., Laber, D., Yu, A., Convey, G., Mayers, R.*, et al.* (2009). 11beta-hydroxysteroid dehydrogenase type 1 regulates glucocorticoid-induced insulin resistance in skeletal muscle. Diabetes *58*, 2506-2515.

Morino, K., Petersen, K.F., and Shulman, G.I. (2006). Molecular mechanisms of insulin resistance in humans and their potential links with mitochondrial dysfunction. Diabetes *55 Suppl 2*, S9-s15.

Moro, C., Bajpeyi, S., and Smith, S.R. (2008). Determinants of intramyocellular triglyceride turnover: implications for insulin sensitivity. Am J Physiol Endocrinol Metab *294*, E203-213.

Morton, N.M., Holmes, M.C., Fievet, C., Staels, B., Tailleux, A., Mullins, J.J., and Seckl, J.R. (2001). Improved lipid and lipoprotein profile, hepatic insulin sensitivity, and glucose tolerance in 11beta-hydroxysteroid dehydrogenase type 1 null mice. J Biol Chem *276*, 41293-41300.

Naliboff, B.D., Cohen, M.J., and Sowers, J.D. (1985). Physiological and metabolic responses to brief stress in non-insulin dependent diabetic and control subjects. Journal of psychosomatic research *29*, 367-374.

Nguyen, K.D., Qiu, Y., Cui, X., Goh, Y.P., Mwangi, J., David, T., Mukundan, L., Brombacher, F., Locksley, R.M., and Chawla, A. (2011). Alternatively activated macrophages produce catecholamines to sustain adaptive thermogenesis. Nature *480*, 104-108.

NIH (2019). https://www.ptsd.va.gov/understand/common/common_adults.asp.

Nilsson, C., Jennische, E., Ho, H.P., Eriksson, E., Bjorntorp, P., and Holmang, A. (2002). Increased insulin sensitivity and decreased body weight in female rats after postnatal corticosterone exposure. Eur J Endocrinol *146*, 847-854.

Nishimura, T., Nakatake, Y., Konishi, M., and Itoh, N. (2000). Identification of a novel FGF, FGF-21, preferentially expressed in the liver. Biochim Biophys Acta *1492*, 203-206.

Niu, B., He, K., Li, P., Gong, J., Zhu, X., Ye, S., Ou, Z., and Ren, G. (2018). SIRT1 upregulation protects against liver injury induced by a HFD through inhibiting CD36 and the NFkappaB pathway in mouse kupffer cells. Mol Med Rep *18*, 1609-1615.

Nogueiras, R., Habegger, K.M., Chaudhary, N., Finan, B., Banks, A.S., Dietrich, M.O., Horvath, T.L., Sinclair, D.A., Pfluger, P.T., and Tschop, M.H. (2012). Sirtuin 1 and sirtuin 3: physiological modulators of metabolism. Physiological reviews *92*, 1479-1514.

O. Sullivan, I., Zhang, W., Wasserman, D.H., Liew, C.W., Liu, J., Paik, J., DePinho, R.A., Stolz, D.B., Kahn, C.R., Schwartz, M.W.*, et al.* (2015). FoxO1 integrates direct and indirect effects of insulin on hepatic glucose production and glucose utilization. Nat Commun *6*, 7079.

Ohshima, K., Shargill, N.S., Chan, T.M., and Bray, G.A. (1989). Effects of dexamethasone on glucose transport by skeletal muscles of obese (ob/ob) mice. Int J Obes *13*, 155-163.

Ohta, H., Konishi, M., and Itoh, N. (2011). FGF10 and FGF21 as regulators in adipocyte development and metabolism. Endocr Metab Immune Disord Drug Targets *11*, 302-309.

Okabe, K., Yaku, K., Tobe, K., and Nakagawa, T. (2019). Implications of altered NAD metabolism in metabolic disorders. J Biomed Sci *26*, 34-34.

Opherk, C., Tronche, F., Kellendonk, C., Kohlmuller, D., Schulze, A., Schmid, W., and Schutz, G. (2004). Inactivation of the glucocorticoid receptor in hepatocytes leads to fasting hypoglycemia and ameliorates hyperglycemia in streptozotocin-induced diabetes mellitus. Mol Endocrinol *18*, 1346-1353.

Ortenblad, N., Mogensen, M., Petersen, I., Hojlund, K., Levin, K., Sahlin, K., Beck-Nielsen, H., and Gaster, M. (2005). Reduced insulin-mediated citrate synthase activity in cultured skeletal muscle cells from patients with type 2 diabetes: evidence for an intrinsic oxidative enzyme defect. Biochim Biophys Acta *1741*, 206-214.

Ost, M., Coleman, V., Voigt, A., van Schothorst, E.M., Keipert, S., van der Stelt, I., Ringel, S., Graja, A., Ambrosi, T., Kipp, A.P.*, et al.* (2016). Muscle mitochondrial stress adaptation operates independently of endogenous FGF21 action. Mol Metab *5*, 79-90.

Ouchi, N., Parker, J.L., Lugus, J.J., and Walsh, K. (2011). Adipokines in inflammation and metabolic disease. Nat Rev Immunol *11*, 85-97.

Packard, A.E., Ghosal, S., Herman, J.P., Woods, S.C., and Ulrich-Lai, Y.M. (2014). Chronic variable stress improves glucose tolerance in rats with sucrose-induced prediabetes. Psychoneuroendocrinology *47*, 178-188.

Pasieka, A.M., and Rafacho, A. (2016). Impact of Glucocorticoid Excess on Glucose Tolerance: Clinical and Preclinical Evidence. Metabolites *6*.

Patel, R., Bookout, A.L., Magomedova, L., Owen, B.M., Consiglio, G.P., Shimizu, M., Zhang, Y., Mangelsdorf, D.J., Kliewer, S.A., and Cummins, C.L. (2015). Glucocorticoids regulate the metabolic hormone FGF21 in a feed-forward loop. Mol Endocrinol *29*, 213-223.

Patel, R., Williams-Dautovich, J., and Cummins, C.L. (2014). Minireview: New Molecular Mediators of Glucocorticoid Receptor Activity in Metabolic Tissues. Molecular Endocrinology *28*, 999-1011.

Patterson, Z.R., and Abizaid, A. (2013). Stress induced obesity: lessons from rodent models of stress. Front Neurosci *7*, 130.

Patterson, Z.R., Parno, T., Isaacs, A.M., and Abizaid, A. (2013). Interruption of ghrelin signaling in the PVN increases high-fat diet intake and body weight in stressed and non-stressed C57BL6J male mice. Frontiers in neuroscience *7*, 167.

Peckett, A.J., Wright, D.C., and Riddell, M.C. (2011). The effects of glucocorticoids on adipose tissue lipid metabolism. Metabolism *60*, 1500-1510.

Perez, A., Jansen-Chaparro, S., Saigi, I., Bernal-Lopez, M.R., Minambres, I., and Gomez-Huelgas, R. (2014). Glucocorticoid-induced hyperglycemia. J Diabetes *6*, 9-20.

Petersen, K.F., and Shulman, G.I. (2006). Etiology of insulin resistance. Am J Med *119*, S10-16.

Petersen, M.C., and Shulman, G.I. (2018). Mechanisms of Insulin Action and Insulin Resistance. Physiol Rev *98*, 2133-2223.

Pibernik-Okanovic, M., Roglic, G., Prasek, M., and Metelko, Z. (1993). War-induced prolonged stress and metabolic control in type 2 diabetic patients. Psychological medicine *23*, 645-651.

Pilkis, S.J., el-Maghrabi, M.R., and Claus, T.H. (1988). Hormonal regulation of hepatic gluconeogenesis and glycolysis. Annual review of biochemistry *57*, 755-783.

Pitman, R.K., Rasmusson, A.M., Koenen, K.C., Shin, L.M., Orr, S.P., Gilbertson, M.W., Milad, M.R., and Liberzon, I. (2012). Biological studies of post-traumatic stress disorder. Nat Rev Neurosci *13*, 769-787.

Polyzos, S.A., Kountouras, J., and Mantzoros, C.S. (2015). Leptin in nonalcoholic fatty liver disease: a narrative review. Metabolism *64*, 60-78.

Potthoff, M.J., and Finck, B.N. (2014). Head Over Hepatocytes for FGF21. Diabetes *63*, 4013.

Potthoff, M.J., Inagaki, T., Satapati, S., Ding, X., He, T., Goetz, R., Mohammadi, M., Finck, B.N., Mangelsdorf, D.J., Kliewer, S.A*., et al.* (2009). FGF21 induces PGC-1alpha and regulates carbohydrate and fatty acid metabolism during the adaptive starvation response. Proc Natl Acad Sci U S A *106*, 10853-10858.

Rahimi, Y., Camporez, J.P., Petersen, M.C., Pesta, D., Perry, R.J., Jurczak, M.J., Cline, G.W., and Shulman, G.I. (2014). Genetic activation of pyruvate dehydrogenase alters oxidative substrate selection to induce skeletal muscle insulin resistance. Proc Natl Acad Sci U S A *111*, 16508-16513.

Ramnanan, C.J., Edgerton, D.S., Kraft, G., and Cherrington, A.D. (2011). Physiologic action of glucagon on liver glucose metabolism. Diabetes Obes Metab *13 Suppl 1*, 118-125.

Randle, P.J. (1998). Regulatory interactions between lipids and carbohydrates: the glucose fatty acid cycle after 35 years. Diabetes Metab Rev *14*, 263-283.

Randle, P.J., Garland, P.B., Hales, C.N., and Newsholme, E.A. (1963). The glucose fatty-acid cycle. Its role in insulin sensitivity and the metabolic disturbances of diabetes mellitus. Lancet *1*, 785-789.

Rao, N.A., McCalman, M.T., Moulos, P., Francoijs, K.J., Chatziioannou, A., Kolisis, F.N., Alexis, M.N., Mitsiou, D.J., and Stunnenberg, H.G. (2011). Coactivation of GR and NFKB alters the repertoire of their binding sites and target genes. Genome Res *21*, 1404-1416.

Ray, P.D., Foster, D.O., and Lardy, H.A. (1964). Mode of Action of Glucocorticoids. I. Stimulation of Gluconeogenesis Independent of Synthesis De Novo of Enzymes. J Biol Chem *239*, 3396-3400.

Razzoli, M., and Bartolomucci, A. (2016). The Dichotomous Effect of Chronic Stress on Obesity. Trends in endocrinology and metabolism: TEM *27*, 504-515.

Rebrin, K., Steil, G.M., Mittelman, S.D., and Bergman, R.N. (1996). Causal linkage between insulin suppression of lipolysis and suppression of liver glucose output in dogs. J Clin Invest *98*, 741-749.

Reddy, T.E., Gertz, J., Crawford, G.E., Garabedian, M.J., and Myers, R.M. (2012). The hypersensitive glucocorticoid response specifically regulates period 1 and expression of circadian genes. Mol Cell Biol *32*, 3756-3767.

Reynolds, R.M., Labad, J., Strachan, M.W., Braun, A., Fowkes, F.G., Lee, A.J., Frier, B.M., Seckl, J.R., Walker, B.R., and Price, J.F. (2010). Elevated fasting plasma cortisol is associated with ischemic heart disease and its risk factors in people with type 2 diabetes: the Edinburgh type 2 diabetes study. The Journal of clinical endocrinology and metabolism *95*, 1602-1608.

Ritter, O., Jelenik, T., and Roden, M. (2015). Lipid-mediated muscle insulin resistance: different fat, different pathways? J Mol Med (Berl) *93*, 831-843.

Rizza, R.A. (2010). Pathogenesis of fasting and postprandial hyperglycemia in type 2 diabetes: implications for therapy. Diabetes *59*, 2697-2707.

Roden, M., and Bernroider, E. (2003). Hepatic glucose metabolism in humans--its role in health and disease. Best Pract Res Clin Endocrinol Metab *17*, 365-383.

Roden, M., Price, T.B., Perseghin, G., Petersen, K.F., Rothman, D.L., Cline, G.W., and Shulman, G.I. (1996). Mechanism of free fatty acid-induced insulin resistance in humans. J Clin Invest *97*, 2859-2865.

Romeo, S., Kozlitina, J., Xing, C., Pertsemlidis, A., Cox, D., Pennacchio, L.A., Boerwinkle, E., Cohen, J.C., and Hobbs, H.H. (2008). Genetic variation in PNPLA3 confers susceptibility to nonalcoholic fatty liver disease. Nat Genet *40*, 1461-1465.

Rose, A.J., Vegiopoulos, A., and Herzig, S. (2010). Role of glucocorticoids and the glucocorticoid receptor in metabolism: insights from genetic manipulations. J Steroid Biochem Mol Biol *122*, 10-20.

Rosso, C., Kazankov, K., Younes, R., Esmaili, S., Marietti, M., Sacco, M., Carli, F., Gaggini, M., Salomone, F., Moller, H.J*., et al.* (2019). Crosstalk between adipose tissue insulin resistance and liver macrophages in non-alcoholic fatty liver disease. J Hepatol *71*, 1012-1021.

Roth, T.L. (2014). How Traumatic Experiences Leave Their Signature on the Genome: An Overview of Epigenetic Pathways in PTSD. Front Psychiatry *5*, 93.

Rusli, F., Deelen, J., Andriyani, E., Boekschoten, M.V., Lute, C., van den Akker, E.B., Müller, M., Beekman, M., and Steegenga, W.T. (2016). Fibroblast growth factor 21 reflects liver fat accumulation and dysregulation of signalling pathways in the liver of C57BL/6J mice. Scientific Reports *6*, 30484.

Russell, C.D., Petersen, R.N., Rao, S.P., Ricci, M.R., Prasad, A., Zhang, Y., Brolin, R.E., and Fried, S.K. (1998). Leptin expression in adipose tissue from obese humans: depot-specific regulation by insulin and dexamethasone. Am J Physiol *275*, E507-515.

Saad, M.J., Folli, F., Kahn, J.A., and Kahn, C.R. (1993). Modulation of insulin receptor, insulin receptor substrate-1, and phosphatidylinositol 3-kinase in liver and muscle of dexamethasone-treated rats. J Clin Invest *92*, 2065-2072.

Saegusa, Y., Takeda, H., Muto, S., Nakagawa, K., Ohnishi, S., Sadakane, C., Nahata, M., Hattori, T., and Asaka, M. (2011). Decreased plasma ghrelin contributes to anorexia following novelty stress. American journal of physiology Endocrinology and metabolism *301*, E685-696.

Samuel, V.T., Petersen, K.F., and Shulman, G.I. (2010). Lipid-induced insulin resistance: unravelling the mechanism. Lancet *375*, 2267-2277.

Sanders, F.W.B., and Griffin, J.L. (2016). De novo lipogenesis in the liver in health and disease: more than just a shunting yard for glucose. Biol Rev Camb Philos Soc *91*, 452-468.

Sanghez, V., Razzoli, M., Carobbio, S., Campbell, M., McCallum, J., Cero, C., Ceresini, G., Cabassi, A., Govoni, P., Franceschini, P.*, et al.* (2013). Psychosocial stress induces hyperphagia and exacerbates diet-induced insulin resistance and the manifestations of the Metabolic Syndrome. Psychoneuroendocrinology *38*, 2933-2942.

Schaaf, M.J., and Cidlowski, J.A. (2002). Molecular mechanisms of glucocorticoid action and resistance. J Steroid Biochem Mol Biol *83*, 37-48.

Schakman, O., Kalista, S., Barbe, C., Loumaye, A., and Thissen, J.P. (2013). Glucocorticoid-induced skeletal muscle atrophy. The international journal of biochemistry & cell biology *45*, 2163-2172.

Schoneveld, O.J., Gaemers, I.C., and Lamers, W.H. (2004). Mechanisms of glucocorticoid signalling. Biochim Biophys Acta *1680*, 114-128.

Schwarz, J.M., Linfoot, P., Dare, D., and Aghajanian, K. (2003). Hepatic de novo lipogenesis in normoinsulinemic and hyperinsulinemic subjects consuming high-fat, low-carbohydrate and low-fat, high-carbohydrate isoenergetic diets. Am J Clin Nutr *77*, 43-50.

Scott, R.V., and Bloom, S.R. (2018). Problem or solution: The strange story of glucagon. Peptides *100*, 36-41.

Seale, P., Bjork, B., Yang, W., Kajimura, S., Chin, S., Kuang, S., Scime, A., Devarakonda, S., Conroe, H.M., Erdjument-Bromage, H.*, et al.* (2008). PRDM16 controls a brown fat/skeletal muscle switch. Nature *454*, 961-967.

Seckl, J.R. (2004). 11beta-hydroxysteroid dehydrogenases: changing glucocorticoid action. Curr Opin Pharmacol *4*, 597-602.

Sell, H., Habich, C., and Eckel, J. (2012). Adaptive immunity in obesity and insulin resistance. Nat Rev Endocrinol *8*, 709-716.

Shalev, A., Liberzon, I., and Marmar, C. (2017). Post-Traumatic Stress Disorder. N Engl J Med *376*, 2459-2469.

Shibli-Rahhal, A., Van Beek, M., and Schlechte, J.A. (2006). Cushing's syndrome. Clin Dermatol *24*, 260-265.

Shoelson, S.E., Lee, J., and Goldfine, A.B. (2006). Inflammation and insulin resistance. J Clin Invest *116*, 1793-1801.

Simoneau, J.A., and Kelley, D.E. (1997). Altered glycolytic and oxidative capacities of skeletal muscle contribute to insulin resistance in NIDDM. J Appl Physiol (1985) *83*, 166-171.

Sinclair, D., Fillman, S.G., Webster, M.J., and Weickert, C.S. (2013). Dysregulation of glucocorticoid receptor co-factors FKBP5, BAG1 and PTGES3 in prefrontal cortex in psychotic illness. Sci Rep *3*, 3539.

Smith, S.M., and Vale, W.W. (2006). The role of the hypothalamic-pituitary-adrenal axis in neuroendocrine responses to stress. Dialogues Clin Neurosci *8*, 383-395.

Stalmans, W., and Laloux, M. (1979). Glucocorticoids and hepatic glycogen metabolism. Monogr Endocrinol *12*, 517-533.

Stomby, A., Andrew, R., Walker, B.R., and Olsson, T. (2014). Tissue-specific dysregulation of cortisol regeneration by 11betaHSD1 in obesity: has it promised too much? Diabetologia *57*, 1100-1110.

Sukumaran, S., Dubois, D.C., Jusko, W.J., and Almon, R.R. (2012). Glucocorticoid effects on adiponectin expression. Vitam Horm *90*, 163-186.

Sul, H.S., and Wang, D. (1998). Nutritional and hormonal regulation of enzymes in fat synthesis: studies of fatty acid synthase and mitochondrial glycerol-3-phosphate acyltransferase gene transcription. Annu Rev Nutr *18*, 331-351.

Suzuki, S., Iben, J.R., Coon, S.L., and Kino, T. (2018). SIRT1 is a transcriptional enhancer of the glucocorticoid receptor acting independently to its deacetylase activity. Mol Cell Endocrinol *461*, 178-187.

Talbot, J., and Maves, L. (2016). Skeletal muscle fiber type: using insights from muscle developmental biology to dissect targets for susceptibility and resistance to muscle disease. Wiley interdisciplinary reviews Developmental biology *5*, 518-534.

Tamashiro, K.L., Nguyen, M.M., Ostrander, M.M., Gardner, S.R., Ma, L.Y., Woods, S.C., and Sakai, R.R. (2007). Social stress and recovery: implications for body weight and body composition. Am J Physiol Regul Integr Comp Physiol *293*, R1864-1874.

Tarantino, G., Savastano, S., and Colao, A. (2010). Hepatic steatosis, low-grade chronic inflammation and hormone/growth factor/adipokine imbalance. World J Gastroenterol *16*, 4773-4783.

Targher, G., Bertolini, L., Rodella, S., Zoppini, G., Zenari, L., and Falezza, G. (2006). Associations between liver histology and cortisol secretion in subjects with nonalcoholic fatty liver disease. Clinical Endocrinology *64*, 337-341.

Taylor, A.I., Frizzell, N., McKillop, A.M., Flatt, P.R., and Gault, V.A. (2009). Effect of RU486 on hepatic and adipocyte gene expression improves diabetes control in obesity-type 2 diabetes. Horm Metab Res *41*, 899-904.

Templeman, N.M., Skovso, S., Page, M.M., Lim, G.E., and Johnson, J.D. (2017). A causal role for hyperinsulinemia in obesity. J Endocrinol *232*, R173-r183.

Tilg, H., and Moschen, A.R. (2010). Evolution of inflammation in nonalcoholic fatty liver disease: the multiple parallel hits hypothesis. Hepatology *52*, 1836-1846.

Tomlinson, J.J., Boudreau, A., Wu, D., Abdou Salem, H., Carrigan, A., Gagnon, A., Mears, A.J., Sorisky, A., Atlas, E., and Hache, R.J. (2010). Insulin sensitization of human preadipocytes through glucocorticoid hormone induction of forkhead transcription factors. Mol Endocrinol *24*, 104-113.

Trayhurn, P., and Wood, I.S. (2005). Signalling role of adipose tissue: adipokines and inflammation in obesity. Biochem Soc Trans *33*, 1078-1081.

Tsigos, C., and Chrousos, G.P. (2002). Hypothalamic-pituitary-adrenal axis, neuroendocrine factors and stress. J Psychosom Res *53*, 865-871.

Turcotte, L.P., and Fisher, J.S. (2008). Skeletal muscle insulin resistance: roles of fatty acid metabolism and exercise. Phys Ther *88*, 1279-1296.

Turnbull, A.V., and Rivier, C.L. (1999). Regulation of the hypothalamic-pituitary-adrenal axis by cytokines: actions and mechanisms of action. Physiol Rev *79*, 1-71.

van Leijden, M.J., Penninx, B., Agyemang, C., Olff, M., Adriaanse, M.C., and Snijder, M.B. (2018). The association of depression and posttraumatic stress disorder with the metabolic syndrome in a multi-ethnic cohort: the HELIUS study. Soc Psychiatry Psychiatr Epidemiol *53*, 921-930.

Vandanmagsar, B., Warfel, J.D., Wicks, S.E., Ghosh, S., Salbaum, J.M., Burk, D., Dubuisson, O.S., Mendoza, T.M., Zhang, J., Noland, R.C*., et al.* (2016). Impaired Mitochondrial Fat Oxidation Induces FGF21 in Muscle. Cell Rep *15*, 1686-1699.

Vander Kooi, B.T., Onuma, H., Oeser, J.K., Svitek, C.A., Allen, S.R., Vander Kooi, C.W., Chazin, W.J., and O'Brien, R.M. (2005). The glucose-6-phosphatase catalytic subunit gene promoter contains both positive and negative glucocorticoid response elements. Mol Endocrinol *19*, 3001-3022.

Vegiopoulos, A., and Herzig, S. (2007). Glucocorticoids, metabolism and metabolic diseases. Mol Cell Endocrinol *275*, 43-61.

Vispute, S.G., Bu, P., Le, Y., and Cheng, X. (2017). Activation of GR but not PXR by dexamethasone attenuated acetaminophen hepatotoxicities via Fgf21 induction. Toxicology *378*, 95-106.

Vitali, A., Murano, I., Zingaretti, M.C., Frontini, A., Ricquier, D., and Cinti, S. (2012). The adipose organ of obesity-prone C57BL/6J mice is composed of mixed white and brown adipocytes. J Lipid Res *53*, 619-629.

Wang, B., Moya, N., Niessen, S., Hoover, H., Mihaylova, M.M., Shaw, R.J., Yates, J.R., 3rd, Fischer, W.H., Thomas, J.B., and Montminy, M. (2011a). A hormone-dependent module regulating energy balance. Cell *145*, 596-606.

Wang, C., Dai, J., Yang, M., Deng, G., Xu, S., Jia, Y., Boden, G., Ma, Z.A., Yang, G., and Li, L. (2014). Silencing of FGF-21 expression promotes hepatic gluconeogenesis and glycogenolysis by regulation of the STAT3-SOCS3 signal. The FEBS journal *281*, 2136-2147.

Wang, J.C., Gray, N.E., Kuo, T., and Harris, C.A. (2012). Regulation of triglyceride metabolism by glucocorticoid receptor. Cell Biosci *2*, 19.

Wang, Q., Zhang, M., Ning, G., Gu, W., Su, T., Xu, M., Li, B., and Wang, W. (2011b). Brown adipose tissue in humans is activated by elevated plasma catecholamines levels and is inversely related to central obesity. PLoS One *6*, e21006.

Wang, Q.A., Tao, C., Gupta, R.K., and Scherer, P.E. (2013). Tracking adipogenesis during white adipose tissue development, expansion and regeneration. Nat Med *19*, 1338-1344.

Wang, Z., Frederick, J., and Garabedian, M.J. (2002). Deciphering the phosphorylation "code" of the glucocorticoid receptor in vivo. J Biol Chem *277*, 26573-26580.

Wehrwein, E.A., Orer, H.S., and Barman, S.M. (2016). Overview of the Anatomy, Physiology, and Pharmacology of the Autonomic Nervous System. Compr Physiol *6*, 1239-1278.

Wei, W., Dutchak, P.A., Wang, X., Ding, X., Wang, X., Bookout, A.L., Goetz, R., Mohammadi, M., Gerard, R.D., Dechow, P.C.*, et al.* (2012). Fibroblast growth factor 21 promotes bone loss by potentiating the effects of peroxisome proliferator-activated receptor gamma. Proc Natl Acad Sci U S A *109*, 3143-3148.

Weinstein, R.S. (2012). Glucocorticoid-induced osteoporosis and osteonecrosis. Endocrinol Metab Clin North Am *41*, 595-611.

Weinstein, S.P., Wilson, C.M., Pritsker, A., and Cushman, S.W. (1998). Dexamethasone inhibits insulin-stimulated recruitment of GLUT4 to the cell surface in rat skeletal muscle. Metabolism *47*, 3-6.

Whitehead, J.P., Richards, A.A., Hickman, I.J., Macdonald, G.A., and Prins, J.B. (2006). Adiponectin--a key adipokine in the metabolic syndrome. Diabetes Obes Metab *8*, 264-280.

WHO (2018). www.who.int/news-room/fact-sheets/detail/diabetes (World Health Organisation).

Wolfe, R.R. (2006). The underappreciated role of muscle in health and disease. The American journal of clinical nutrition *84*, 475-482.

Woods, C.P., Hazlehurst, J.M., and Tomlinson, J.W. (2015). Glucocorticoids and non-alcoholic fatty liver disease. The Journal of Steroid Biochemistry and Molecular Biology *154*, 94-103.

Xu, C., He, J., Jiang, H., Zu, L., Zhai, W., Pu, S., and Xu, G. (2009a). Direct effect of glucocorticoids on lipolysis in adipocytes. Mol Endocrinol *23*, 1161-1170.

Xu, J., Lloyd, D.J., Hale, C., Stanislaus, S., Chen, M., Sivits, G., Vonderfecht, S., Hecht, R., Li, Y.S., Lindberg, R.A*., et al.* (2009b). Fibroblast growth factor 21 reverses hepatic steatosis, increases energy expenditure, and improves insulin sensitivity in diet-induced obese mice. Diabetes *58*, 250-259.

Yamauchi, T., Kamon, J., Waki, H., Imai, Y., Shimozawa, N., Hioki, K., Uchida, S., Ito, Y., Takakuwa, K., Matsui, J*., et al.* (2003). Globular adiponectin protected ob/ob mice from diabetes and ApoE-deficient mice from atherosclerosis. J Biol Chem *278*, 2461-2468.

Yan, H., Xia, M., Chang, X., Xu, Q., Bian, H., Zeng, M., Rao, S., Yao, X., Tu, Y., Jia, W*., et al.* (2011). Circulating fibroblast growth factor 21 levels are closely associated with hepatic fat content: a cross-sectional study. PLoS One *6*, e24895.

Yi, C.X., Foppen, E., Abplanalp, W., Gao, Y., Alkemade, A., la Fleur, S.E., Serlie, M.J., Fliers, E., Buijs, R.M., Tschop, M.H*., et al.* (2012). Glucocorticoid signaling in the arcuate nucleus modulates hepatic insulin sensitivity. Diabetes *61*, 339-345.

Yilmaz, Y., Eren, F., Yonal, O., Kurt, R., Aktas, B., Celikel, C.A., Ozdogan, O., Imeryuz, N., Kalayci, C., and Avsar, E. (2010). Increased serum FGF21 levels in patients with nonalcoholic fatty liver disease. Eur J Clin Invest *40*, 887-892.

Yu, C.Y., Mayba, O., Lee, J.V., Tran, J., Harris, C., Speed, T.P., and Wang, J.C. (2010). Genome-wide analysis of glucocorticoid receptor binding regions in adipocytes reveal gene network involved in triglyceride homeostasis. PLoS One *5*, e15188.

Yuan, X., Tsujimoto, K., Hashimoto, K., Kawahori, K., Hanzawa, N., Hamaguchi, M., Seki, T., Nawa, M., Ehara, T., Kitamura, Y*., et al.* (2018). Epigenetic modulation of Fgf21 in the perinatal mouse liver ameliorates diet-induced obesity in adulthood. Nat Commun *9*, 636.

Zhang, T., and Kraus, W.L. (2010). SIRT1-dependent regulation of chromatin and transcription: linking NAD(+) metabolism and signaling to the control of cellular functions. Biochim Biophys Acta *1804*, 1666-1675.

Zhang, X., Yeung, D.C., Karpisek, M., Stejskal, D., Zhou, Z.G., Liu, F., Wong, R.L., Chow, W.S., Tso, A.W., Lam, K.S*., et al.* (2008). Serum FGF21 levels are increased in obesity and are independently associated with the metabolic syndrome in humans. Diabetes *57*, 1246-1253.

Zhang, Y., Lei, T., Huang, J.F., Wang, S.B., Zhou, L.L., Yang, Z.Q., and Chen, X.D. (2011). The link between fibroblast growth factor 21 and sterol regulatory element binding protein 1c during lipogenesis in hepatocytes. Molecular and Cellular Endocrinology *342*, 41-47.

Zhao, L.F., Iwasaki, Y., Zhe, W., Nishiyama, M., Taguchi, T., Tsugita, M., Kambayashi, M., Hashimoto, K., and Terada, Y. (2010). Hormonal regulation of acetyl-CoA carboxylase isoenzyme gene transcription. Endocr J *57*, 317-324.

Zhou, C.C., Yang, X., Hua, X., Liu, J., Fan, M.B., Li, G.Q., Song, J., Xu, T.Y., Li, Z.Y., Guan, Y.F.*, et al.* (2016). Hepatic NAD(+) deficiency as a therapeutic target for non-alcoholic fatty liver disease in ageing. Br J Pharmacol *173*, 2352-2368.

Zierath, J.R., and Hawley, J.A. (2004). Skeletal muscle fiber type: influence on contractile and metabolic properties. PLoS biology *2*, e348.

APPENDIX

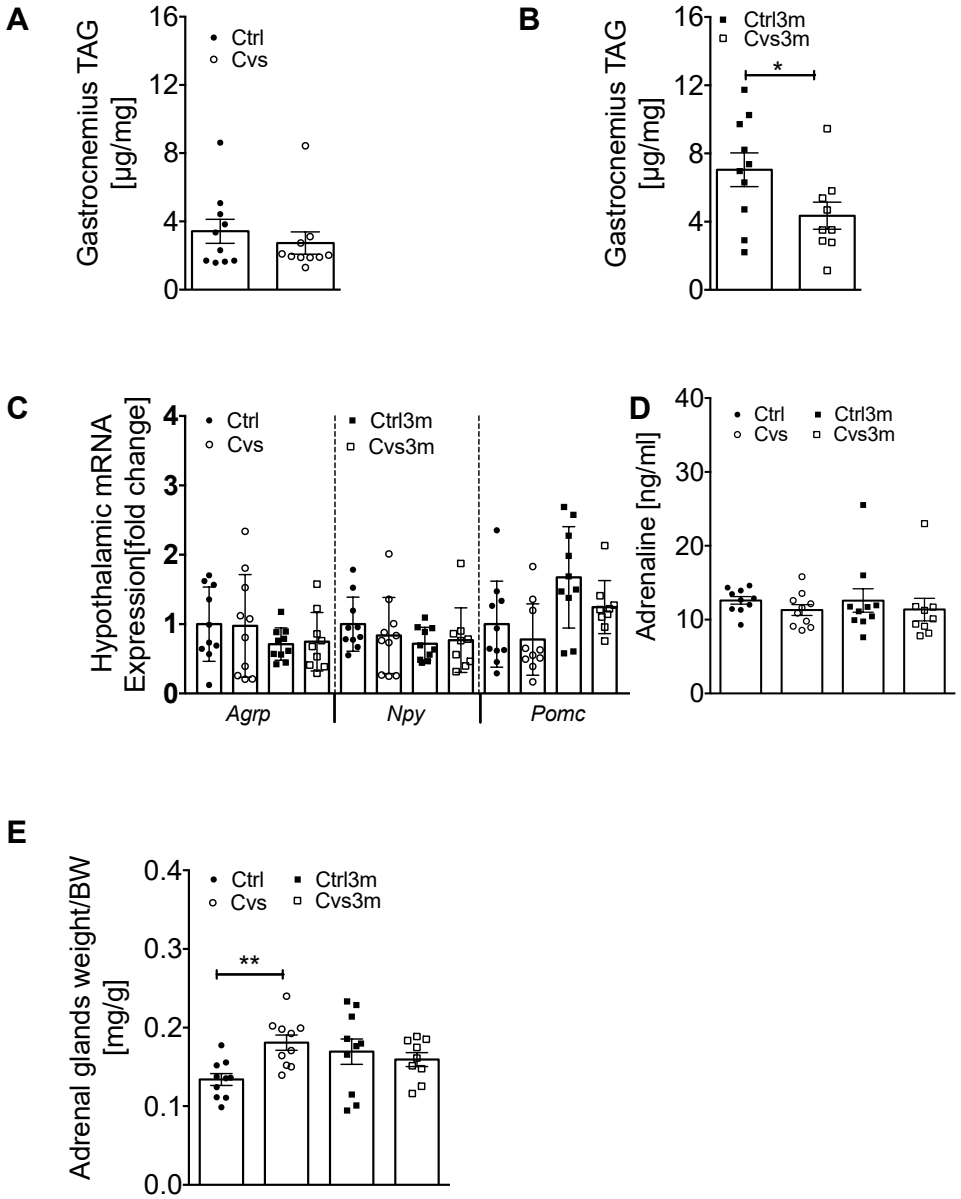

Supplemental Figure 1: Triglyceride content of *gastrocnemius* muscle from Cvs mice **(A)** and mice three months post Cvs (Cvs3m) **B)** compared to the age-matched controls (Ctrl and Ctrl3m, respectively). mRNA expression of hypothalamic neuropeptides **(C)**, plasma adrenalin level **(D)** and adrenal gland to body weight ration from Ctrl, Cvs , Ctrl3m and Cvs3m mice **(E)**. Data presented as means ± s.e.m. Statistical analyses were done by two-tailed unpaired Student's t-test **(A, B)** n=9-10 or by Two-Way ANOVA followed by Bonferroni **(C-E)** n=9-10. * $p < 0.05$, ** $p < 0.01$

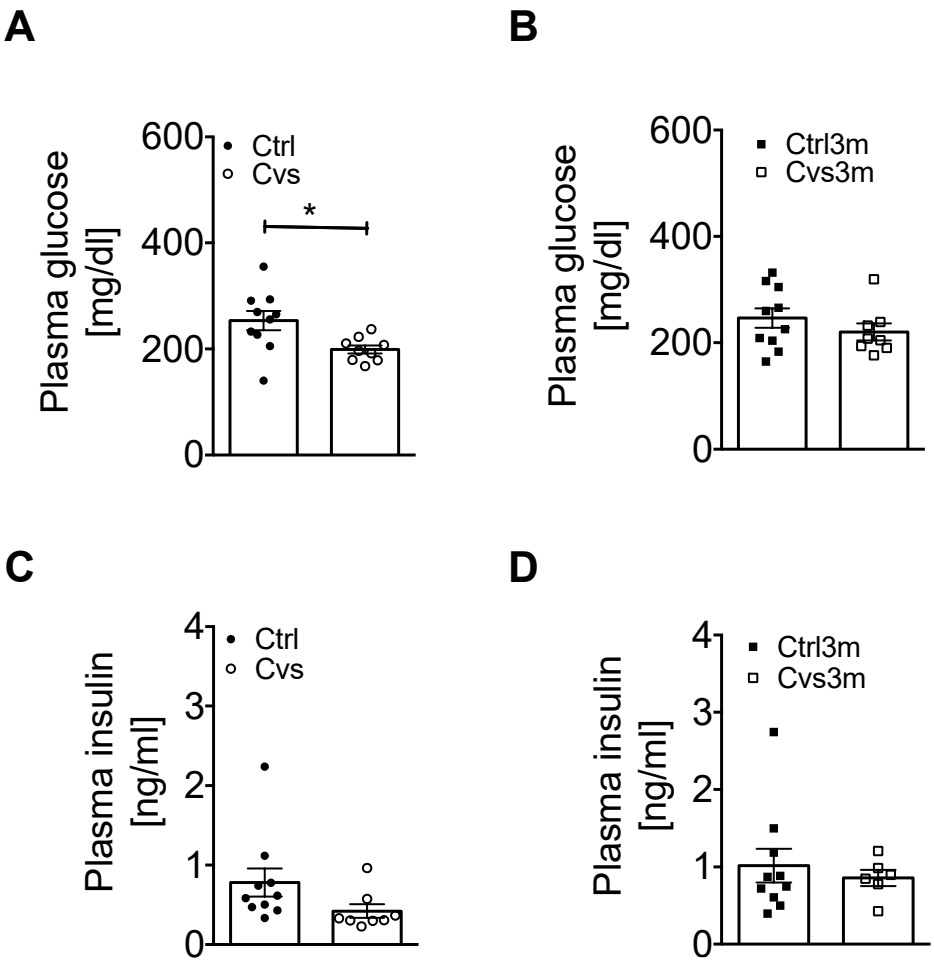

Supplemental Figure 2: Plasma glucose and insulin levels from Cvs mice **(A and C)** n=10 as well as mice three months post Cvs (Cvs3m) **(B and D)** n=9-10, compared to the age-matched controls (Ctrl and Ctrl3m, respectively)**.** Data presented as means ± s.e.m. Statistical analyses were done by two-tailed unpaired Student's t-test * $p < 0.05$

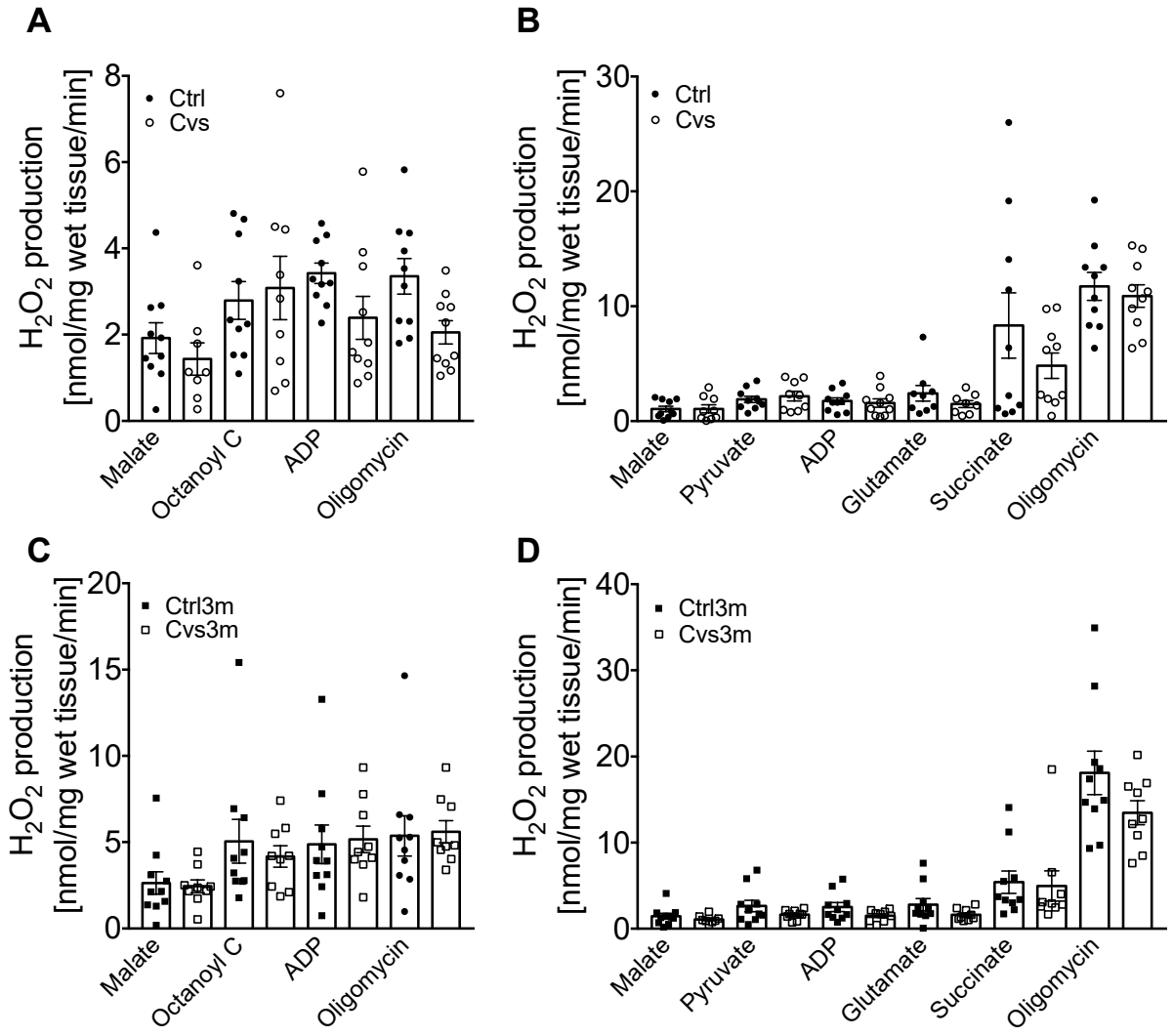

Supplemental Figure. 3: TCA-cycle-linked substrate-dependent mitochondrial H_2O_2 emission measured in permeabilized *Soleus* muscle from control **(A),** Cvs **(B),** Ctrl3m **(C)** and **(D)** Cvs3m mice**.** Data presented as means ± s.e.m. Statistical analyses were done by two-tailed unpaired Student's t-test. The experiments were conducted by Dr. Tomas Jelenik.

Supplemental Table 1. Analysis of plasma hormones post Cvs and diet intervention. Hormone analysis was done from final plasma after hyperinsulinemic-euglycemic clamps. Data presented as means ±s.e.m. Statistical analyses were done by two-tailed unpaired Student's t-test * $p < 0.05$, ** $p < 0.01$.

	Ctrl [ng/ml] (n=8-10)	**Cvs [ng/ml] (n=8-10)**		**Ctrl3m [ng/ml] (n=9-11)**	**Cvs3m [ng/ml] (n=9-10)**	
Leptin	1.13±0.06	1.44±0.15	p=0.07	1.60±0.23	1.07±0.14	p=0.07
Resistin	144.3±9.59	132.8±8.14	p=0.37	142.7±5.17	127.9±5.1	p=0.06
Adiponectin	8221±873.6	11520±1443	p=0.06	11290±138	5875±430	**p=0.00**
PAI-1	22.75±0.34	21.88±0.61	p=0.23	23±0.23	22.2±0.3	**p=0.05**
Ghrelin	12.41±0.9	9.85±0.63	**p=0.03***	15.78±1.6	16.21±2.6	p=0.89
GIP	0.25±0.02	0.22±0.02	p=0.18	0.26±0.03	0.22±0.02	p=0.30
GLP-1	0.051±0.004	0.045±0.002	p=0.22	0.053±0.00	0.043±0.0	p=0.21
Glucagon	0.31±0.02	0.24±0.1	**p=0.02***	0.27±0.04	0.24±0.03	p=0.52

Supplemental Table 2. Plasma cytokine levels post Cvs and diet intervention. Cytokine analyses were done from final plasma after hyperinsulinemic-euglycemic clamps. OOR: Out of range, cytokines abbreviations are explained in the corresponding material and methods section. Data presented as means ±s.e.m. Statistical analyses were done by two-tailed unpaired Student's t-test * $p < 0.05$.

Cytokines	**Ctrl [pg/ml] (n=8-10)**	**Cvs [pg/ml] (n=8-10)**		**Ctrl3m [pg/ml] (n=8-11)**	**Cvs3m [pg/ml] (n=7-10)**	
IL-1a	118.60±22.96	75.14±11.06	p=0.097	73.20±9.26	63.29±11.17	p=0.499
IL-1b	557±56.83	532±73.16	p=0.790	319.10±22.55	336.50±39.15	p=0.697
IL-2	58.05±14.26	59.90±13.19	p=0.925	---	---	OOR
IL-3	23.53±5.08	24.32±7.15	p=0.928	---	---	OOR
IL-4	---	---	OOR	---	---	OOR
IL-5	46.19±8.01	40.08±7.92	p=0.595	20.04±1.79	19.93±2.82	p=0.974
IL-6	118.90±24.81	127.80±30.04	p=0.820	66.43±14.07	87.07±28.75	p=0.514
IL-9	---	---	OOR	---	---	OOR
IL-10	212.20±19.12	300.40±37.67	**p=0.047***	113.90±16.10	136.2±28.96	p=0.509
IL-12(p40)	1057±242.5	718.7±154.3	p=0.245	1252±201.80	1723±385.20	p=0.280
IL-12(p70)	173.60±32.39	189.10±49.11	p=0.791	---	---	OOR
IL-13	623.30±131.30	631.50±151.7	p=0.967	157.30±16.95	163.90±28.71	p=0.840
IL-17	77.29±12.45	72.25±12.74	p=0.780	29.06±3.47	28.20±4.80	p=0.888
Eotaxin	656.2±12.45	418.0±70.74	**p=0.044***	---	---	OOR
G-CSF	3808±707.7	2885±745.60	p=0.391	4861±660.60	10231±2508	**p=0.045***
GM-CSF	346.30±43.59	298.90±48.61	p=0.477	---	---	OOR
IFN-g	28.14± 4.09	23.40±4.70	p=0.462	---	---	OOR
KC	454.10±62.77	515.30±85.38	p=0.565	597.60±55.10	504.90±86.59	p=0.369
MCP-1	938±171.90	1014±167.3	p=0.754	2137±365.90	1868±473.20	p=0.655

Cytokines	Ctrl [pg/ml] (n=8-10)	Cvs [pg/ml] (n=8-10)		Ctrl3m [pg/ml] (n=8-11)	Cvs3m [pg/ml] (n=7-10)	
MIP-1a	131.5±51.03	56.84±10.25	p=0.168	57.91±3.13	69.54±12.10	p=0.293
MIP-1b	204.50±18.82	144.50±21.01	p=0.054	131.3±18.46	155.6±42.96	p=0.597
RANTES	280.90±32.38	142.70±40.23	**p=0.020***	149.90±20.60	172.20±34.61	p=0.565
TNF-a	763.4±131.6	744.8±165.8	p=0.931	223.2±22.54	257.30±37.16	p=0.432

Supplemental Table 3. Cytokine levels in epididymal WAT post Cvs and diet intervention. OOR: Out of range; cytokines abbreviations are explained in the material and methods section. Data presented as means ±s.e.m. Statistical analyses were done by two-tailed unpaired Student's t-test * $p < 0.05$.

Cytokines	Ctrl [pg/ml] (n=7-10)	Cvs [pg/ml] (n=8-10)		Ctrl3m [pg/ml] (n=8-10)	Cvs3m [pg/ml] (n=5-7)	
IL-1a	82.95±9.54	78.86±12.49	p=0.802	76.29±18.88	52.40±13.69	p=0.357
IL-1b	368.80±31.34	332.6±38.70	p=0.477	240.8±25.03	196.90±28.07	p=0.273
IL-2	126.0±14.21	103.2±8.17	p=0.181	97.23±13.31	85.63±12.42	p=0.552
IL-3	11.17±0.63	12.74±1.10	p=0.220	7.98±1.02	6.97±0.89	p=0.491
IL-4	5.54±0.26	5.91±0.44	p=0.472	4.82±0.43	4.03±0.36	p=0.198
IL-5	12.97±0.97	14.61±1.26	p=0.260	10.41±0.96	8.23±0.88	p=0.126
IL-6	12.79±1.41	11.34±1.86	p=0.537	6.40±0.76	6.70±0.82	p=0.792
IL-9	311.4±73.89	346.1±92.43	p=0.783	210.6±56.73	---	OOR
IL-10	110.8±6.86	88.01±12.89	p=0.138	71.80±6.65	67.40±7.25	p=0.663
IL-12(p40)	12.03±0.79	12.07±1.52	p=0.984	7.40±0.53	6.36±0.79	p=0.278
IL-12(p70)	62.75±4.54	63.36±9.08	p=0.953	32.99±4.34	33.96±7.11	p=0.905
IL-13	648.30±64.54	506.70±63.83	p=0.136	428.3±34.05	398.7±51.63	p=0.625
IL-17	20.41±1.21	18.77±2.22	p=0.526	15.50±1.91	12.30±1.54	p=0.243
Eotaxin	639.00±54.55	584.00±73.81	p=0.556	417.5±37.71	376.1±60.56	p=0.554
G-CSF	25.75±1.56	36.76±4.22	**p=0.028***	20.64±1.60	22.97±3.28	p=0.502
GM-CSF	236.7±10.33	213.8±17.20	p=0.259	174.6±9.74	163.3±14.95	p=0.520
IFN-g	11.49±0.75	10.80±1.47	p=0.683	6.25±1.03	4.64±1.35	p=0.355
KC	17.47±1.47	17.85±1.32	p=0.850	12.96±2.34	9.96±1.55	p=0.333
MCP-1	120.5±5.72	132±9.53	p=0.303	97.30±4.25	80.33±5.25	**p=0.026***
MIP-1a	10.16±1.17	8.78±1.20	p=0.423	7.61±2.01	3.73±1.41	p=0.180
MIP-1b	43.17±2.63	45.86±4.54	p=0.610	30.20±1.85	26.57±2.83	p=0.291
RANTES	22.78±6.16	23.37±5.26	p=0.94	15.00±2.47	7.11±2.10	**p=0.054**
TNF-a	2405±299	1984±330.5	p=0.357	1602±162.3	1491±81.16	p=0.592

Table 15: Overview of persons who conducted experiments in the publication from 2018. List of figures and the respective experiments together with the person who realized these for the publication Jelenik*, Dille* et al. (2018; *shared first author). MD: Matthias Dille (Author of this thesis); TJ: Dr. Tomas Jelenik; ZZ: Dr. Zhou Zhou and SML: Dr. Sabrina Müller Lühlhoff.

	Experiments	**Performed by**
Figure 5:	A-H) Corticosterone measurements and body composition analyses	MD
Figure 6:	A-F) Hyperinsulinemic-euglycemic clamps	TJ
	G-I) Plasma analyses of glucose, NEFA and triglycerides	MD
Figure 7:	A,B,F,I) *Ex vivo* glucose uptake and FAO in EDL muscle	ZZ & SML
	C,D,E) Western blot analyses of AKT and AMPK	MD
	G,H,J,K) ß-oxidation-linked respiration and TCA-linked respiration in Soleus muscle	TJ
Figure 8:	A,B) *Ex vivo* glucose uptake in primary adipose cells	ZZ & SML
	C-K) Western blot and qPCR analyses in white and brown adipose tissue	MD
Figure 9:	A-G) Analyses of hepatic lipid content, qPCR and Western blot from liver	MD
Figure 10:	A-H) qPCR analyses of *Fgf21* along with FGF21 regulated genes in metabolic	MD
Supp. Figure 1:	A-E) Skeletal muscle lipid content, qPCR from hypothalamus, adrenal gland weight	MD
Supp. Figure 2:	A-D) Analyses of plasma insulin and glucose levels	MD
Supp. Figure 3:	A-D) Analyses of substrate-dependent mitochondrial H2O2 emission	TJ
Supp. Table 1:	Analyses of metabolic plasma hormones	MD
Supp. Table 2:	Analyses of plasma cytokine levels	MD
Supp. Table 3:	Analyses of gWAT cytokine levels	MD

DANKSAGUNG

Zuerst möchte ich mich bei Herrn Prof. Dr. Hadi Al-Hasani bedanken, dass er mir die Möglichkeit gegeben hat am DDZ zu promovieren und mich die letzten Jahre betreut hat. Weiter möchte ich auch Herrn Prof. Dr. Feldbrügge danken, dass er seitens der Heinrich-Heine-Universität als Gutachter meiner Arbeit zur Verfügung steht.

Besonderer Dank geht auch an Dr. Birgit Knebel und Dr. Jörg Kotzka, die mir trotz schwieriger Phasen in meiner Promotion immer zur Seite standen und mich bei allem unterstützt haben. Ebenfalls möchte ich hier auch Dr. Dhiraj Kabra erwähnen, von dem ich viel gelernt habe und der mir im Labor einiges beigebacht hat.

Großer Dank geht an alle meine Weggefährten während der Promotion und an alle Doktoranden am IKBP. Besonders bedanke ich mich bei den Jungs der „Ilf güldenen Zwölf“ für die tollen Freitagabende. Während meiner Zeit am DDZ sind auch aus vielen Arbeitskollegen großartige Freunde geworden. Besonderer Dank geht daher an Christian Binsch, Simon Göddeke, Tim Bennighoff, David Barbosa und Isabel Zeinert.

Ebenfalls gilt auch Tim Brecklinghaus und Natalie Wahlers besonderer Dank. Sie haben mir als Masterstudenten bei vielen Dingen geholfen und mich tatkräftig im Labor unterstützt. Viel Erfolg für Eure Zukunft. Andrea Cramer als technische Hilfe im Labor möchte ich auch noch ein großes Dankeschön aussprechen. Du hast mir in unserer gemeinsamen Zeit bei der Bewältigung des Laboralltags immer zur Seite gestanden, obwohl mein Herz Schwarz-Weiß-Grün und nicht Königsblau schlägt.

Riesen Dank geht an Giovanna, die mir seit zwei Jahren immer zur Seite steht und die mir neben der Arbeit immer Energie schenkt. Zuletzt möchte ich noch meinen Eltern, Schwestern, der Familie und Freunden danken für die großartige Unterstützung während des letzten Jahres. Danke, dass ich mich immer auf Euch verlassen kann.

EIDESSTATTLICHE ERKLÄRUNG

Ich versichere an Eides Statt, dass die Dissertation von mir selbständig und ohne unzulässige fremde Hilfe unter Beachtung der „Grundsätze zur Sicherung guter wissenschaftlicher Praxis an der Heinrich-Heine-Universität Düsseldorf“ erstellt worden ist. Die Dissertation wurde in der vorgelegten oder in ähnlicher Form noch bei keiner anderen Institution eingereicht. Ich habe bisher keine erfolglosen Promotionsversuche unternommen.

_____

Datum **Matthias Dille**